Electric Birefringence Studies of Biopolymer Systems

by Martin Isles, B. Tech.

a thesis submitted for the degree of -
doctor of philosophy

Brunel University,
Uxbridge.

June 1977

PAGE NUMBERING AS ORIGINAL

to my

MUM & DAD

AND DEDICATED IN HONOUR OF THE SILVER JUBILEE OF HER MAJESTY

Queen Elizabeth II

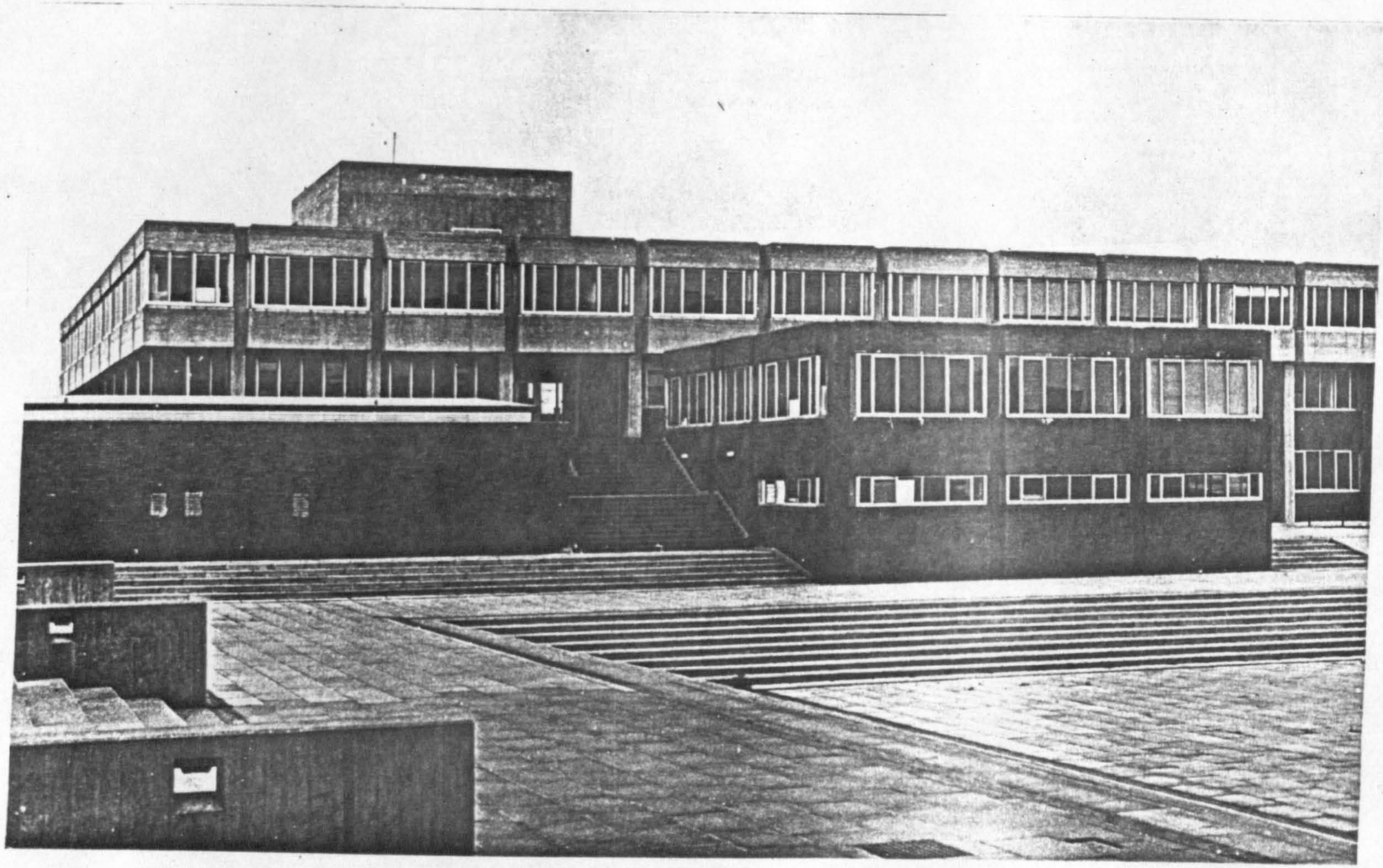

The Physics Department, Brunel University

INDEX

ABSTRACT

Important and novel electric birefringence measurements of immediate significance in the biomedical field are reported on a family of materials which form the major constituents of the cartilage connective tissue. Outstanding amongst the reported results is the confirmation of the Hardingham-Muir model for proteoglycan-hyaluronic acid aggregation, and the relative ease with which the technique was both able to substantiate the model, and, for the first time, to observe the gradual formation of the aggregate. The complex heteropolysaccharide, proteoglycan, has also been characterised by a wide ranging series of electric birefringence measurements.

Other conformational changes studied by the technique on other cartilage materials and reported herein are the effects of pH changes on hyaluronic acid conformation, the enzymatic degradation of hyaluronic acid and the thermal denaturation of collagen.

The work also considers aspects of the problems of application of theoretical models to flexible polymers and demonstrates what can be achieved on existing crude theories with the nitrocellulose in acetone system. Some exploratory measurements in the interfacial area between solute and solvent are reported for the bacterium E. coli and an aqueous suspension of PTFE particles.

A diverse range of materials was studied with particular reference to the values of particle rotary diffusion constants derived from dispersion of birefringence with frequency and analysis of birefringence relaxation time decay rates following the application of a pulsed DC field. Comparisons are drawn between these values and explanations of the discrepancies observed are considered.

Last, but not least, the design of an advanced and high sensitivity apparatus for the measurement of electric birefringence is reported. Unusually, the system adopts a vertical mode and the novel Kerr Cell design incorporated dispenses with end windows. The use of this new compact design is suggested as the basis for commercial applications.

CHAPTER 1

General Introduction

Novel applications of the electric birefringence technique and the design of a new and sensitive apparatus for its study are presented in this thesis. This chapter sets out to furnish the reader with a general background to the technique, its development and its application. Note that the S. I. system of units is used throughout.

1.1 Electric Birefringence: The Physics of the Technique

A dilute suspension of macromolecules is placed in a small cell, so designed that a light beam can pass through it, whilst an electric field can be applied at right angles to the light path. The light source is required to be of steady intensity, and the light entering the cell to be monochromatic, well collimated and polarised linearly, at a 45^{o} azimuth to the electric field direction. When the electric field is switched on, the molecules , hitherto in random array, orientate to align themselves with the applied field. (Fig. 1.1).

The orientation results from permanent dipole moments (due to fixed charge separation in the molecule) and/or induced dipole moments (arising from the ease with which charges separate in the presence of an electric field, i.e. the polarisability of the molecule). The partial alignment that occurs takes a finite time, and the degree of alignment is a function of the molecules' dipole moments and the applied field strength. When the field is switched off, the molecules return to a random array, again in a finite time. The rate of this field-free decay of ordering is a direct function of the molecules' rotary diffusion constant, and hence its size and shape.

Not surprisingly, polarised light interacting with an anisotropic molecule interacts differently according to the profile of the molecule which it encounters, and the subsequent order and number of bond types and their directions through which it has to pass. The speed which the light traverses the molecule is related to the refractive index of the material. When the molecules are aligned the anisotropy of the molecule, hitherto disguised by the random state of the medium, is now 'reflected' throughout the medium. Thus light polarised in two mutually perpendicular directions will now emerge from the solution having travelled at different speeds through it. The two vibrations will thus be out of phase as a result of the anisotropy of refractive index of the individual molecules which we

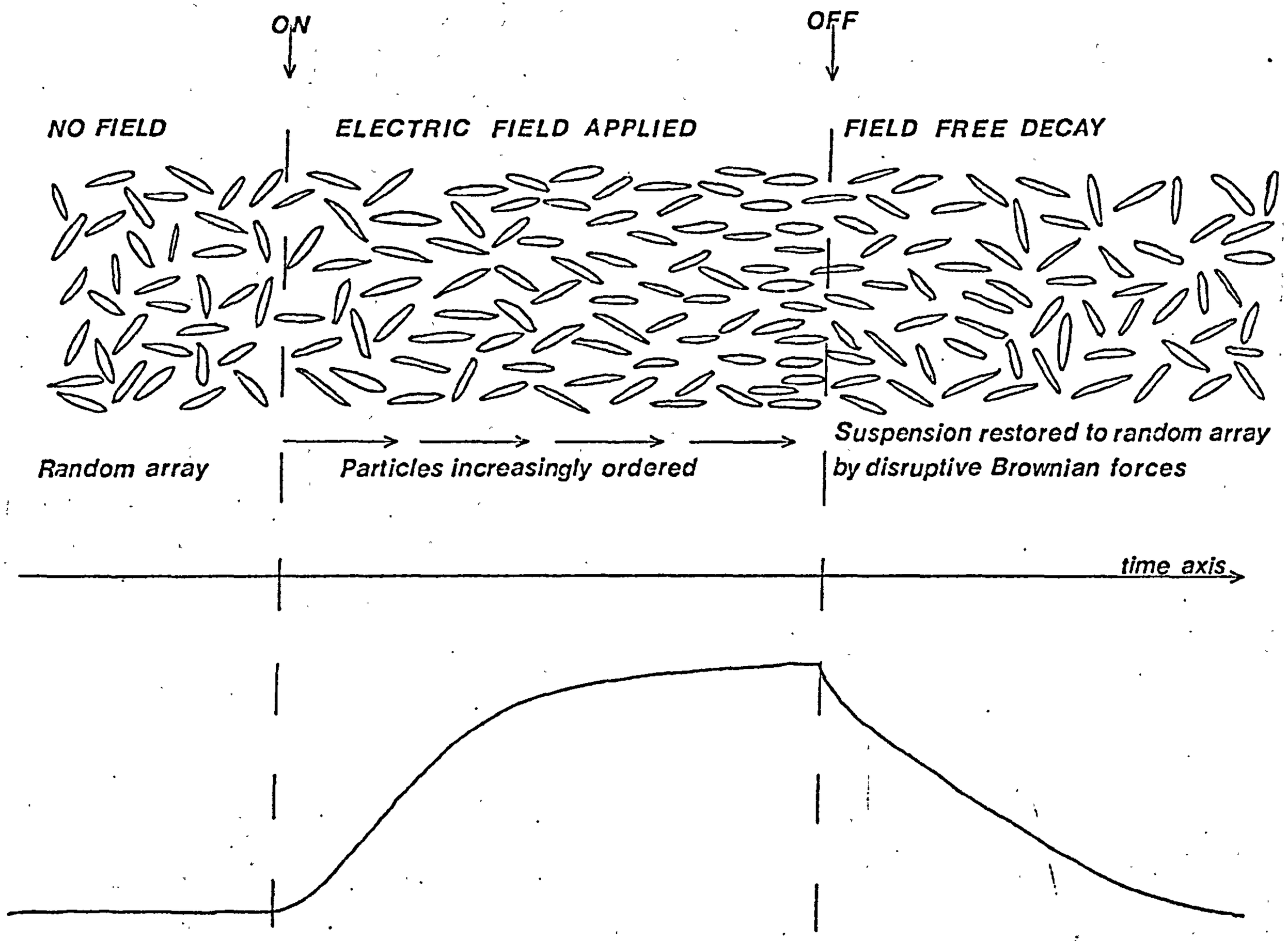

Fig. 1.1 Schematic representation of particle motion under the influence of an applied electric field compared to a typical transient response trace.

call birefringence or double refraction. Thus birefringence is not unique to the ordering of solutions by electric fields. It can result from any technique which is able to impart sufficient ordering of suspensions as all materials are birefringent to some degree. Electric birefringence describes the birefringence observed when the ordering results from the application of an electric field.

To measure electric birefringence, a dilute molecular suspension is placed between a crossed polarising prism system (polariser, P and analyser, A, Fig. 1.2), such that minimum light is transmitted with no field applied. On application of the field, the resulting [illegible] phase lag of light traversing the suspension, means that light emerges from the suspension elliptically polarised and thus penetrates the analysing prism. With a sensitive, light intensity monitoring system, these changes in the degree of elliptical polarisation can be followed and related in turn to the birefringence of the material, the rotary diffusion constants of the molecules and, in some circumstances, their electrical polarisability and dipole moments.

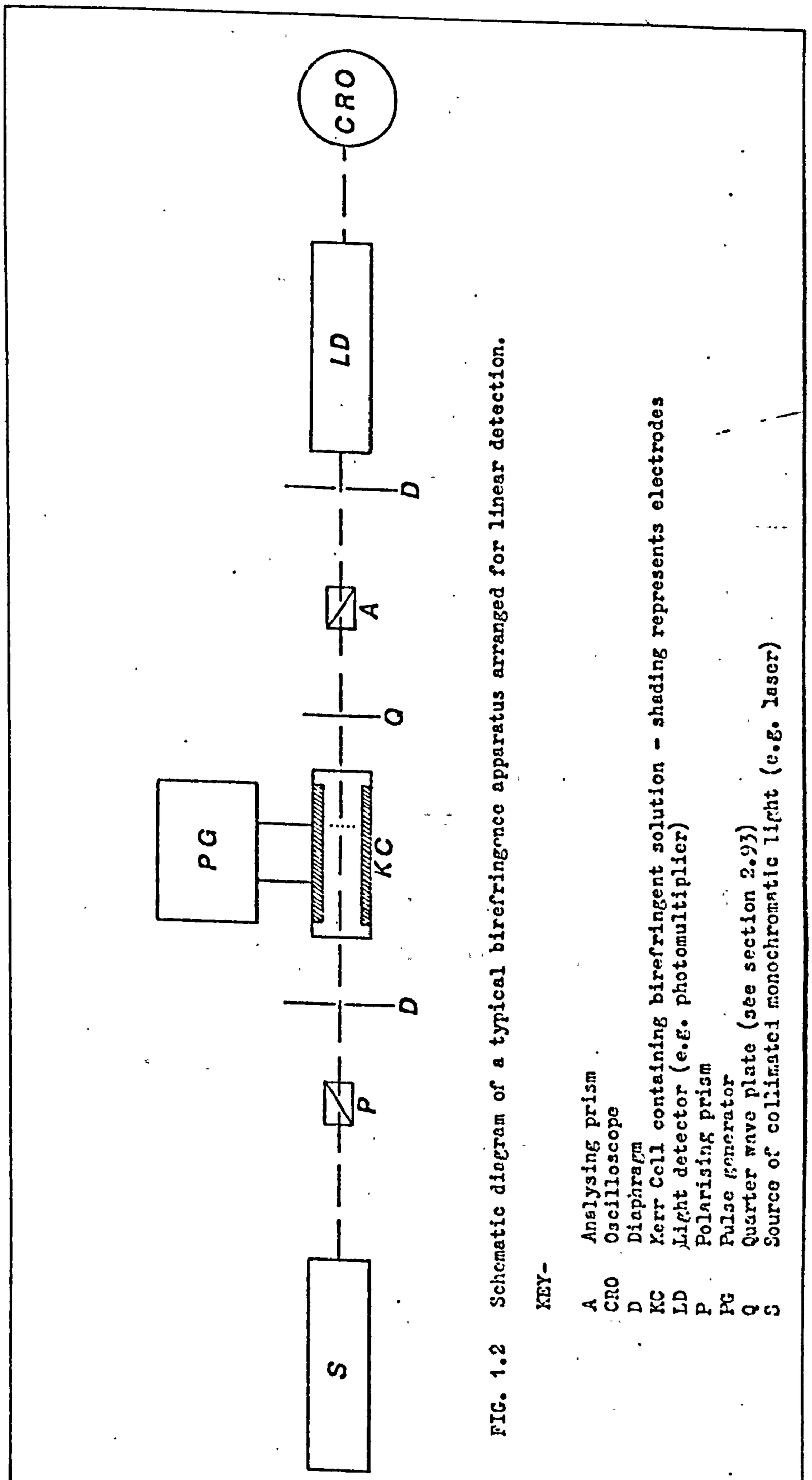

FIG. 1.2 Schematic diagram of a typical birefringence apparatus arranged for linear detection.

KEY-

A	Analysing prism
CRO	Oscilloscope
D	Diaphragm
KC	Kerr Cell containing birefringent solution - shading represents electrodes
LD	Light detector (e.g. photomultiplier)
P	Polarising prism
PG	Pulse generator
Q	Quarter wave plate (see section 2.93)
S	Source of collimated monochromatic light (e.g. laser)

1.2 Discovery of Electric Birefringence

It is over one hundred years since the Rev. Dr. John Kerr (1824 - 1909), a mathematics lecturer at the Free-Church Training College of Glasgow, first reported this birefringence phenomenon[11]. This was his first scientific paper at no less an age than fifty one! Inspired by the then recent electro-magnetic treatise of Maxwell, and the so far unsuccessful electro-optic researches of the now legendary Faraday, he proved to himself and the world his conviction "...that if a transparent and optically isotropic insulator were subjected to intense electrostatic force, it should act no longer as an isotropic body upon light sent through it..." Kerr reported his observations on glass plate, clear amber resin and quartz. Subsequent reports were on carbon disulphide, benzene, paraffin oil, kerosene, turpentine, olive oil and castor oil, observing both positive and negative effects. The liquids were placed in glass cells which he made himself, his light source was a paraffin candle and his experiments were conducted in his College laboratory, which was equipped largely at his own expense. Much of this original apparatus was preserved by Glasgow University.

1.3 Development of the Kerr Effect

Kerr's discovery became known, as it is today, as the Kerr Effect, and relates specifically to electrically induced birefringence.

Early twentieth century theoreticians studied the Kerr Effect, but its application to macromolecular suspensions in the manner used in this present study did not enter its formative period until the early post Second World War period, when three research groups, one led by O'Konski in America, another by Benoit in France and yet a third in Russia, independently began work on the pulsed DC electric birefringence technique. Pulsed, as opposed to continuous, field measurements offer the advantages of obtaining the transient data referred to earlier (rotary diffusion constants, etc.) as well as avoiding over heating of samples. Pulsed AC fields offer further improvements in this respect, but are best used at high frequency, when only induced moments produce orientation.

Benoit[12] himself derived the simple relationship between field free decay of birefringence and the rotary diffusion constant for molecules or particles. Linked with the preceeding theoretical work during the War years of Peterlin and Stuart[13] on molecular orientation in an applied field, this formed the basis for current theory.

Suspensions studied in these early days of pulsed electric birefringence were Tobacco Mosaic Virus,[12,14] D.N.A.[14] and Vanadium Pentoxide.[14]

Two important factors governing the range of studiable materials are their physical size and shape, and the value of their electric dipole moments. The former governs the rate at which the materials orientate or disorientate in solution : a compact molecule moves more quickly and therefore requires a short duration pulsed field to orientate it, an extended molecule - the opposite. The latter governs the magnitude of the field required to produce sufficient orientation : molecules with small dipole moments require a large field, and *vice versa* .

Many of the advances of the last twenty five years have come from improvements in the electronic equipment - as in so many other fields of research. Generators capable of delivering short pulses and sustaining high voltages have slowly brought more and more molecular systems within the scope of the technique. Improvements in sensitivity of the optic and detection systems have further added to the list. Moreover electronic data handling is leading to a speed up in the actual experimental procedure and analysis itself.

The use of the technique in conjunction with the related electro-optical techniques of light scattering, electric

dichroism, florescence and electrophoresis is providing useful comparisons of data - and the techniques can advantageously compliment each other. A significant advance in the birefringence technique itself was reported by these laboratories, appropriately on the hundredth anniversary of Kerr's first paper, namely the birefringence of pure liquids stressed by the electric field vector of a powerful laser beam.[15]

1.4 The advantages of Electric Birefringence over other techniques

For measuring molecular or particle sizes in solution, the electric birefringence technique offers a number of advantages compared with the existing and widely used techniques of molecular analysis : e.g. X ray crystallography, electron microscopy, sedimentation diffusion, gel chromatography. These advantages are:

1. The speed with which results can be obtained.
2. Normally elaborate sample preparation is not required.
3. Generally a small sample volume is all that is necessary (typically 5ml of a 1% suspension).
4. *In vivo* measurements are usually possible.
5. The technique is superficially simple to communicate.
6. The costs of establishing a suitable apparatus are by no means prohibitive.

7. The method is particularly sensitive to changes in size and conformation, typically dependent on the third power of the major dimension of the molecule or particle studied.

1.5 Problems confronting the wider application of the method

Currently the method is hampered by the lack of a rigorous theoretical base. Little real progress has been made on this front since Benoit's early work,[12] whilst experimental development has continued unabated. In particular, a study of the kinetics of semi-flexible molecules would allow the technique to realise its full potential. Nonetheless, this is not to belittle the present day applications which, even with existing crude theories, can offer valuable insight to molecular structure in terms of both size and shape. However, the method appears at its best when changes in conformation occur, and it is able to follow time dependent reactions with comparative ease.

It is disappointing that this potentially powerful tool has yet to become accepted and widely used in industry and research. It undoubtedly arouses interest in many fields and this is reflected in the financial support that the fundamental research receives from both Government and industry, even during a time of financial stringency.

pulsed electric field
Whilst birefringence has been used to study many different systems, its application with respect to its potential is still in its infancy. In particular, the biochemical and related medical fields, which are fundamentally concerned with macromolecular interactions, have had little contact with the technique. The author is certain that the method could ultimately help in solving many problems in these areas. However, before this is possible, the technique must be proved effective to the researchers involved and the technique has to be readily available to them rather than closeted in the hands of a few specialist research groups.

1.6 The aims of this treatise.

The aims of this work were therefore as follows:

1. To draw attention to the method's full potential, highlighting the fundamental problems - chiefly of a theoretical nature - which are currently holding it back.
2. To improve the sensitivity of existing apparatus and thereby broaden further the scope of the technique.
3. To design an apparatus which could be developed commercially and which could be readily used by non-physicists.
4. To open new areas of research in the bio-medical field designed to demonstrate the technique at its best, i.e. in studying changes in molecular conformation.

The work itself is thus presented in three sections, following a necessary theoretical resumé.

1.7 The programme of work

The first section of this work covers apparatus, describing the conventional instrumentation inherited by the author and the design of the novel *MINEO-1* instrument. This design set out to provide the increase in sensitivity sought, and to make an instrument which was easy to use as a standard laboratory tool.

The second section of the thesis looks at some major problems confronting the wider application of the method. The problems of semi-flexible molecules and the extent to which present theories can be used is well illustrated in a study of the polymer, nitrocellulose in acetone. The potential of the method and its sensitivity in investigating the fundamental problems of interfacial interactions is tackled. Precursory measurements showing the effect of additives on the suspensions of the bacterium *E.coli* and, separately, Poly tetra-floro-ethylene are reported. The section is completed with a study of a range of diverse materials. For each of these a comparison is drawn between the rotary diffusion constant derived from field free relaxations and that derived from a dispersion of birefringence with frequency. It has been observed hitherto that these values oddly rarely agree, and the

work herein attempts to find some correlation in the discrepancies.

The final section of this thesis reports extensive investigation of the members of a family of materials, namely the mucopolysaccharides, important in cartilage connective tissue. This area of research is chiefly the preserve of the biochemist and the medic, concerned as they are, with the problems of osteo-arthrosis. The experiments the author reports are designed to demonstrate the versatility of the technique, with particular attention drawn to its conformational sensitivity. The work reports changes in polyelectrolyte (potassium hyaluronate) conformation with pH, enzyme degradation (hyaluronidase on hyaluronate), formation of complex heteropolysaccharides (hyaluronic acid - proteoglycans complex) and the thermal denaturation of a polymer (collagen). The work is complimented by a wide ranging study of the essential cartilage tissue constituent, proteoglycans.

*** *** *** *** ***

The realisation of these aims and this work programme are contained in the ensuing pages.

SYMBOLS

A Constant in the Broersma Rod equation (section 2.811)

a Radius of polymer backbone in Worm Like Chain equation (section 2.823)

a_r Radius of a particle or molecule

a_1 Half rod length

$a_{\parallel} - a_{\perp}$ Segmental anisotropy factor as used by Tsvetkov[228]

B Zerr constant

b Radius of polymer backbone in Worm Like Chain equation (section 2.823)

C $0<C<1$ Light lost in optical components through absorption and reflection compared to initial intensity

c Concentration in g ml^{-1}

D Rotary diffusion constant

D_1 Initial slope value of D

D_2 Final decay value of D

D_{fd} Frequency dispersion derived value of D

D_{tr} Value of D derived from analysis of a transient reponse

D_p Peeled initial slope value of D

D_w Weight average value of D

D_z Z average value of D

D_{z+1} Z+1 average value of D

D_{e-g} Electron micrograph derived value of D

E Applied electric field

f Constant in Zimm-Stockmayer and Baur equation (section 2.821)

f_c Critical frequency of dispersion of birefringence

g	Optical volume polarisability
g_2	g along minor ellipse axis
g_1	g along major ellipse axis
* I_o	Light intensity incident on cell
I_θ	Light intensity transmitted by analyser offset by angle θ
I_δ	Light intensity received when field applied
ΔI_δ	$\lvert I_\delta - I_\theta \rvert$
K	Kerr Constant
K_m	Molar Kerr Constant
K_{sp}	Specific Kerr Constant
k	The Boltzman Constant
L	Extended hydrodynamic chain length
l	Length of Kerr Cell electrodes
l_e	Major dimension of ellipsoidal particle
M	Molecular Weight
$\overline{M}_N$	Number average molecular weight
$\overline{M}_W$	Weight average molecular weight
M_o	Molecular weight of a monomer unit
N_A	Avogadro's Number
n	Refractive index
$n_\parallel - n_\perp$	Anisotropy of refractive index, parallel and perpendicular to particle's major dimension. Birefringence.
Δn	Birefringence $(=n_\parallel - n_\perp)$
Δn_o	Steady component of birefringence
Δn_{alt}	Alternating component of birefringence
Δn_{min}	Minimum value of Δn_o during a reversing pulse
$\Delta n(t\to\infty)$	Steady state component of birefringence obtained at long time
$\frac{dn}{dc}$	Rate of change of refractive index with concentration

p Axial ratio of ellipse, $p<1$

q Persistence length as defined section 2.822

R The Universal Gas Constant

r Axial ratio

T Absolute temperature

* T (as used in Chapter 5) - Turbidity

t Time

t_{min} Time taken to reach Δn_{min} from steady value

V Volume of particle or molecule

x Stiffness parameter as defined section 2.822

* a Constant as used in Mark-Houwink equation

a_1-a_2 Electric polarisability anisotropy = Δa

$\beta = \frac{\mu'}{kT}$

$\gamma = \frac{a_1-a_2}{2kT}$

δ Phase difference

$[\eta]$ Intrinsic viscosity

η_o Solvent viscosity

θ Angle of analyser offset

Φ Orientation function

ϕ Phase angle

ω Frequency of electric field

μ Molecular permanent dipole moment

μ_o Permanent dipole moment of monomer unit

μ' Apparent molecular dipole moment (permanent)

$\bar{v}$ Partial specific volume

π 3.142

ρ $\frac{M}{L}$ mass/length for worm like chain/weakly bending rod

τ	Particle relaxation time
τ_1	Initial slope value of relaxation time
τ_2	Final slope value of relaxation time
*	Symbols I, T and a are defined differently in Chapter 5 (qv)

CHAPTER 2

Theoretical Background: A Resumé

2.1 Introduction

Besides the original theoretical work associated with the birefringence technique, numerous other workers have outlined and detailed the theory over the years. The reader is therefore referred to these in order to appraise himself of the complete treatise of the subject. Thus, in addition to the usual references at the end of this chapter a bibliography is presented, and the author gives a brief guide to the contents of each of the works listed. The theory outlined in this chapter is therefore only that pertinent to the work subsequently reported herein.

2.2 Basic experimental parameters

In a birefringent medium, the anisotropy of refractive index is embodied in the parameter, Δn, which is termed the 'birefringence' of the medium.

$$\Delta n = n_{\parallel} - n_{\perp} \qquad (2.1)$$

where $n_{\parallel}$ and $n_{\perp}$ are the principal refractive indices of the medium, parallel and perpendicular to the direction of the orienting electric field.

The phase difference arising from the birefringence is related to Δn as follows:

$$\delta = \frac{2\pi l}{\lambda}\Delta n \qquad (2.2)$$

where δ is the phase difference in radians, l the path length of the birefringent medium through which the light of wavelength, λ, travels. The parameter l is thus normally associated with the length of the electrodes with which the electric field is applied. Clearly, to produce the largest effect, l requires to be large and similarly, the blue end of the visible spectrum is to be favoured. The length of the birefringent medium is restricted by the attenuation of the light by the medium itself.

Kerr[21] established the quadratic field dependence of electric birefringence expressed by the Kerr Law. The law holds for gases, liquids and solutions of <u>low</u> molecular weight substances, viz:

$$B = \lim_{E\to 0}\left(\frac{\delta}{2\pi l E^2}\right) = \lim_{E\to 0}\left(\frac{\Delta n}{\lambda E^2}\right) \qquad (2.3)$$

where B is termed the Kerr Constant and E is the electric field strength.

Alternative expressions of the Kerr Constant have also found common usage:

(a) Kerr Constant as used by Debye[22] and others:

$$K = \frac{B\lambda}{n} = \lim_{E\to 0}\left(\frac{\Delta n}{nE^2}\right) \qquad (2.4)$$

where n is the medium's refractive index with no field applied.

(b) The Specific Kerr Constant, commonly used for suspensions:

$$K_{sp} = \lim_{E\to 0}\left(\frac{\Delta n}{cnE^2\bar{v}}\right) \qquad (2.5)$$

where c is the weight concentration of the suspension and $\bar{v}$ its partial specific volume in compatable units.

(c) The Molar Kerr Constant as defined by Otterbein[23] for molecules of molecular weight, M, at low densities:

$$K_m = \lim_{E\to 0}\left(\frac{2M\Delta n\bar{v}}{27E^2}\right) \qquad (2.6)$$

2.3 Outline of the theory of Molecular Orientation

This theory has only been developed rigorously for dilute solutions of rigid macromolecules. It is assumed that a macromolecule has a common axis of symmetry for its electric, optic and hydrodynamic properties and a permanent dipole moment along this axis. The assumption relating to the hydrodynamic axis of symmetry is only pertinent to the build-up and decay processes. It is further assumed that the dilution of the solution is such that there are no interactions between the solute molecules. The electric

birefringence is then given by Peterlin and Stuarts' equation:[24]

$$\Delta n = \frac{2\pi c\bar{\nu}}{n}(g_1-g_2)\Phi \qquad (2.7)$$

where (g_1-g_2) is the optical anisotropy factor and Φ is termed the orientation function. This latter function has been determined for arbitrary field strength by O'Konski *et al.*[25] At low fields their analysis shows:

$$\Phi = \frac{1}{15}(\beta^2 + 2\gamma) \qquad (2.8)$$

where $$\beta = \frac{\mu'}{kT} \qquad (2.9)$$

and $$\gamma = \frac{(a_1 - a_2)}{2kT} \qquad (2.10)$$

μ' being the apparent dipole moment of the macromolecule in solution, i.e. without regard to any internal field effects and $(a_1 - a_2)$ is similarly the electric polarisibility anisotropy of the molecule.

Thus expressed fully, the equation for the birefringence is

$$\Delta n = \frac{2\pi c\bar{\nu}}{15n}(g_1-g_2)\left\{\frac{\mu'^2}{k^2T^2} + \frac{(a_1-a_2)}{kT}\right\} E^2 \qquad (2.11)$$

Moreover at high fields, when $\Phi \rightarrow 1$, it can be readily seen that (g_1-g_2) can be obtained from equation 2.11. This equation is used widely by researchers engaged in electro-optical measurements, and is frequently used to characterise systems which do not accord with the basic assumptions upon which the theory is based. However, with the lack of more applicable theories, Eqn. 2.11 forms an acceptable basis for prognostication. It should be noted that the equations have been extended

to cover instances where $(a_1-a_2)<0$ [26] or where molecules are completely asymmetric with an arbitrarily orientated permanent moment.[27]

2.4 Quadratic Field Dependence of Birefringence

Equation 2.11 shows a quadratic dependence of the birefringence (Δn) on the applied field strength (E). To justify the application of this equation to any individual molecular system, measurements are first made to determine the region in which the quadratic dependence is true. All subsequent measurements are then normally made at a field strength at which the birefringence is a maximum whilst still linearly related to E^2. A typical set of such measurements is shown in Fig. 2.1. These results were obtained by the author for Heparin, a polyelectrolytic biopolymer important in the flow of blood and its clotting process.

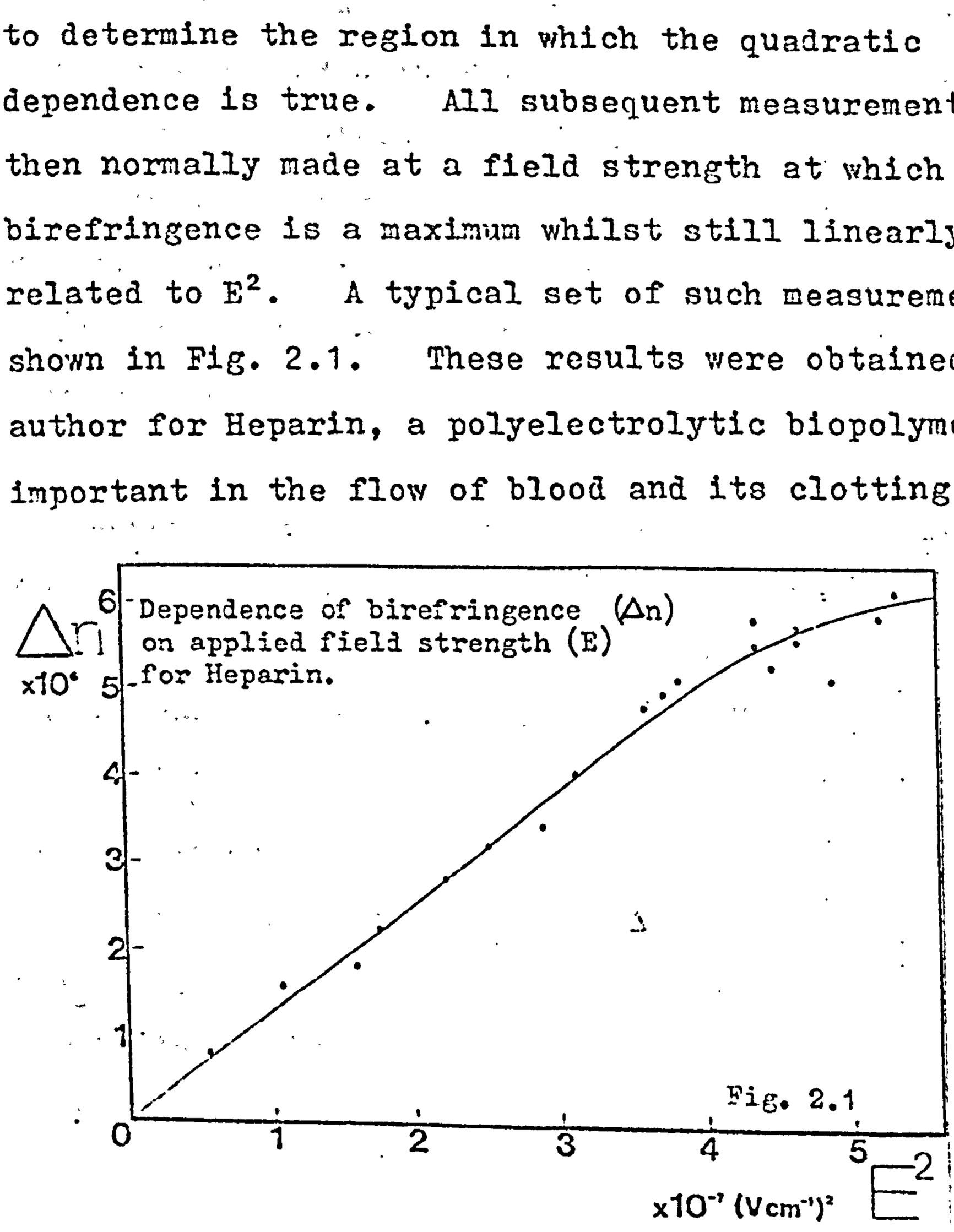

Fig. 2.1

2.5 Application of AC Field Pulses and Dispersion of Birefringence with Frequency

With an AC applied field, the permanent dipole of the molecule will change the orientation of the molecule so that it follows the alternating direction of the applied field. However, as the frequency of the applied field increases, so it becomes more difficult for the molecule to keep pace with the alternation and it eventually gives up. The induced moment, resulting from the displacement of charge, and usually of smaller value, simply follows the field by an alternating movement of charge associated with the molecule - as opposed to continually changing the molecule's orientation. One therefore expects to see a decrease in birefringence with increasing frequency, when the permanent moment ceases to orientate the molecule (cf dielectric dispersion).

The equations governing the value of birefringence under the influence of an AC electric field of frequency ω represented by the equation $E = E_o \sin\omega t$ have been derived by both Plummer and Jennings[28] and Thurston and Bowling[29] for equilibrium conditions. The birefringence can be represented as the sum of two terms as follows:

$$\Delta n = \Delta n_o + \Delta n_{alt} \cos(2\omega t - \phi) \qquad (2.12)$$

where Δn_o is the steady component and Δn_{alt} the magnitude of the double frequency alternating component having a phase angle, ϕ. The assumptions implicit and

the derivation of the equations is basically similar to that involved in the DC case (section 2.3). Consider the steady component:

$$\Delta n_o = \frac{2\pi c\bar{v}}{15n}(g_1-g_2)\left\{\frac{\beta^2}{\left(1+\frac{\omega^2}{4D^2}\right)}+2\gamma\right\}E_o^2 \quad (2.13)$$

Of particular interest is the critical frequency, f_c, at which the birefringence falls to half its maximum value over the complete range of frequencies. This condition is expressed by the equation:

$$\frac{\Delta n_o(\omega) - \Delta n_o(\omega\to\infty)}{\Delta n_o(\omega\to 0) - \Delta n_o(\omega\to\infty)} = \frac{1}{2} \quad (2.14)$$

which is satisfied when, in Eqn. 2.13, $\omega^2 = 4D^2$ or

$$D = \pi f_c \quad (2.15)$$

Thus the particle's rotary diffusion constant can be determined from a birefringence frequency dispersion. This can however be complicated by the polydispersity of the sample particle size. The polydispersity is reflected in the parameters μ, (a_1-a_2) and D, and a broadening of the frequency dispersion is the consequence. The contrast between a polydisperse sample and the more discrete curves obtained for theoretical monodisperse Debye dispersions is well illustrated in Fig. 4.4. Fig. 2.2 shows the two most common patterns of dispersion corresponding to permanent moments parallel and antiparallel to the induced moment direction. Examples of such dispersions can be found in Chapter 6.

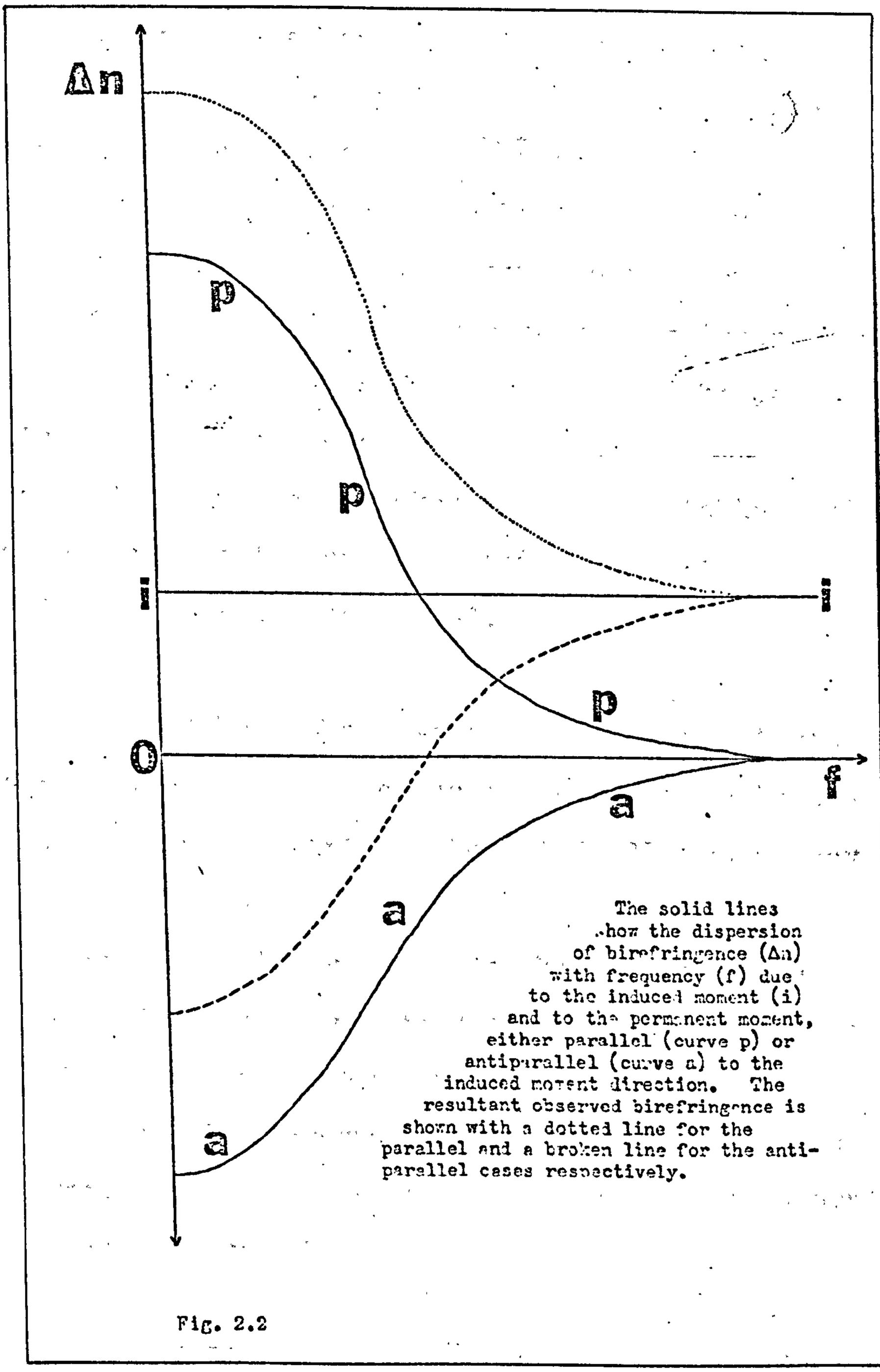

The solid lines show the dispersion of birefringence (Δn) with frequency (f) due to the induced moment (i) and to the permanent moment, either parallel (curve p) or antiparallel (curve a) to the induced moment direction. The resultant observed birefringence is shown with a dotted line for the parallel and a broken line for the antiparallel cases respectively.

Fig. 2.2

2.6 The Application of a Reversing Pulse

When the steady state value of birefringence has been reached within the region of quadratic field dependence for a given sample, reversal in sign of the applied DC field enables the distinction between permanent and induced dipole moments. A large molecule or macroparticle having a permanent moment will tend to reorientate through 180^{o} when the field is reversed producing a momentary decrease in birefringence. In the case of a pure induced moment the alternation of charge within the particle or molecule takes place so quickly that the molecule is not caused to reorientate and the birefringence remains unaltered.

Tinoco and Yamaoka[210] have theoretically investigated transient birefringence responses to reversing pulse fields. For a symmetrical elongated ellipsoid they have found:

(i) For a pure induced moment the steady state birefringence remains unchanged on field reversal.

(ii) If there is a permanent moment contribution a minimum is observed in the birefringence from which the ratio of permanent to induced moment can be found from:

$$\frac{\beta^2}{2\gamma} = \frac{1 - \frac{\Delta n_{min}}{\Delta n_o}}{0.1547 + \frac{\Delta n_{min}}{\Delta n_o}} \qquad (2.16)$$

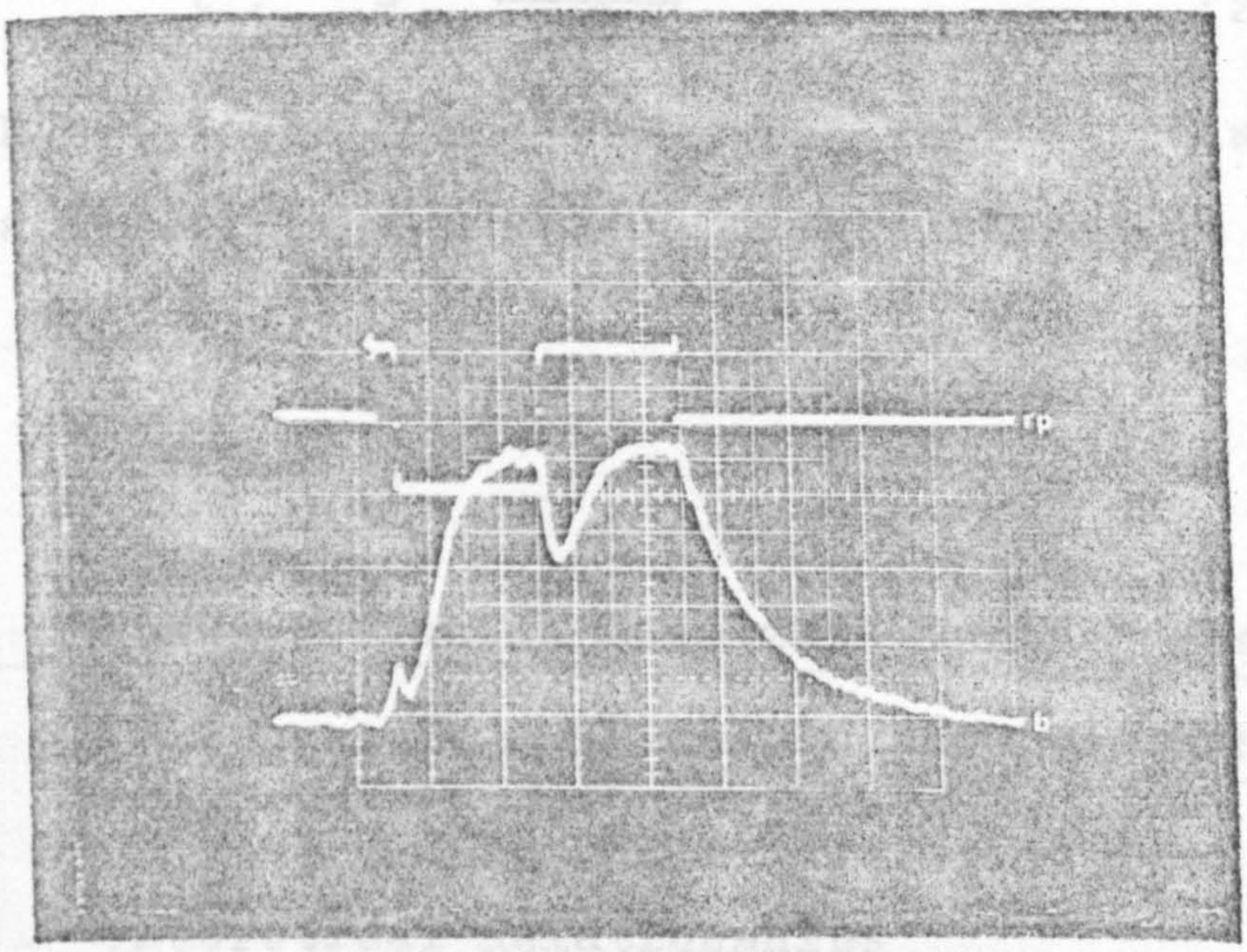

Fig. 2.3

A reversing pulse (trace rp) is applied to a solution of proteoglycans (see Chapter 8). The dip in the birefringence (trace b) should be noted at the point the field reverses. The dip indicates the presence of a permanent dipole moment.

Moreover the rotary diffusion constant can be calculated from the time taken to reach the minimum in response from the point at which the field is reversed, viz:

$$t_{min} = \frac{0.2747}{D} \qquad (2.17)$$

A typical transient showing a reversing pulse response for a material having a permanent moment is illustrated in Fig. 2.3.

2.7 Rotary Diffusion Constants derived from Transient Birefringence Responses

2.71 Theoretical Relationships

The most widely used and reliable method of determining the rotary diffusion constant is from analysis of the decay of a transient birefringent response to a pulsed electric field. Under the influence of an applied electric field, we have already seen that particles orientate and exhibit a steady birefringence once orientation, appropriate to the applied field strength, is complete. Upon removal of the field, the molecules now relax back under the influence of Brownian restoring forces to a completely random array. Benoit[211] has examined this process for solute molecules smaller than the wavelength of light used, monodisperse, in dilute solution and possessing an axial symmetry with electric, hydrodynamic and optic axes coincident. Benoit determined the birefringence at a time t after the removal of the applied field as:

$$\frac{\Delta n(t)}{\Delta n(t=0)} = \frac{\Delta n(t)}{\Delta n_o} = e^{-6Dt} \qquad (2.18)$$

This result is theoretically valid for arbitrary field strength and regardless of whether $\Delta n(t\rightarrow\infty)$ is attained during the pulse. For ellipsoidal molecules which do not possess either hydrodynamical or optical symmetry about their axis of electrical symmetry, Ridgeway[212] has shown that the decay is a function of two exponentials. Benoit also derived expressions relating birefringence as a function of time to particle rotary diffusion constants for the rise of a transient response.[211] Yoshioka and Watanabe have further developed Benoit's results by integration to relate the ratio $\beta^2/_{2\gamma}$ to areas defined by a transient response curve. The shape of the curved response thereby indicating the relative strength or simply the presence of a permanent moment.[213]

2.72 Relaxation Time

Frequently the term particle or molecular 'relaxation time' is used. The following relationship holds between this quantity (τ) and the rotary diffusion constant (D) for a rigid particle or molecule:

$$\tau = \frac{1}{6D} \qquad (2.19)$$

2.73 The Effect of Polydispersity on Transient Decays

For a monodisperse system, a plot of the natural logarithm of birefringence against time for a transient decay produces a linear relationship and the rotary diffusion constant can be calculated accordingly (Eq. 2.18)

For a polydisperse system, different size species result in a corresponding variety of rotary diffusion constants and a logarithmic plot, as described above, is no longer linear, (Fig. 2.4). A tangent to the curve at t = 0 corresponds to smaller particles which relax back to random array first. At long time, a tangent to the curve corresponds to larger particles. However, these two values of the rotary diffusion constant are not by any means representative of the smallest and largest particles present. Indeed, work by Schweitzer and Jennings[214,215] shows that the value obtained from the initial slope (t = 0) can be related to W, Z or Z+1 weight average rotary diffusion constants, according principally to the direction and presence of the particle's permanent dipole moment. Work within this research group[216] has recently progressed to linking the initial slope value of the rotary diffusion constant to an actual particle length distribution with the assumption of a specific particle shape model.

Results presented herein occasionally refer to the peeled values of the rotary diffusion constant (or corresponding relaxation time) obtained by subtracting the contribution of the long time rotary diffusion constant from the initial slope value. With this long time contribution removed from the overall decay, a fresh decay curve can be drawn and the process repeated as far as the data permit, to obtain a best possible value of the initial slope related diffusion constant.

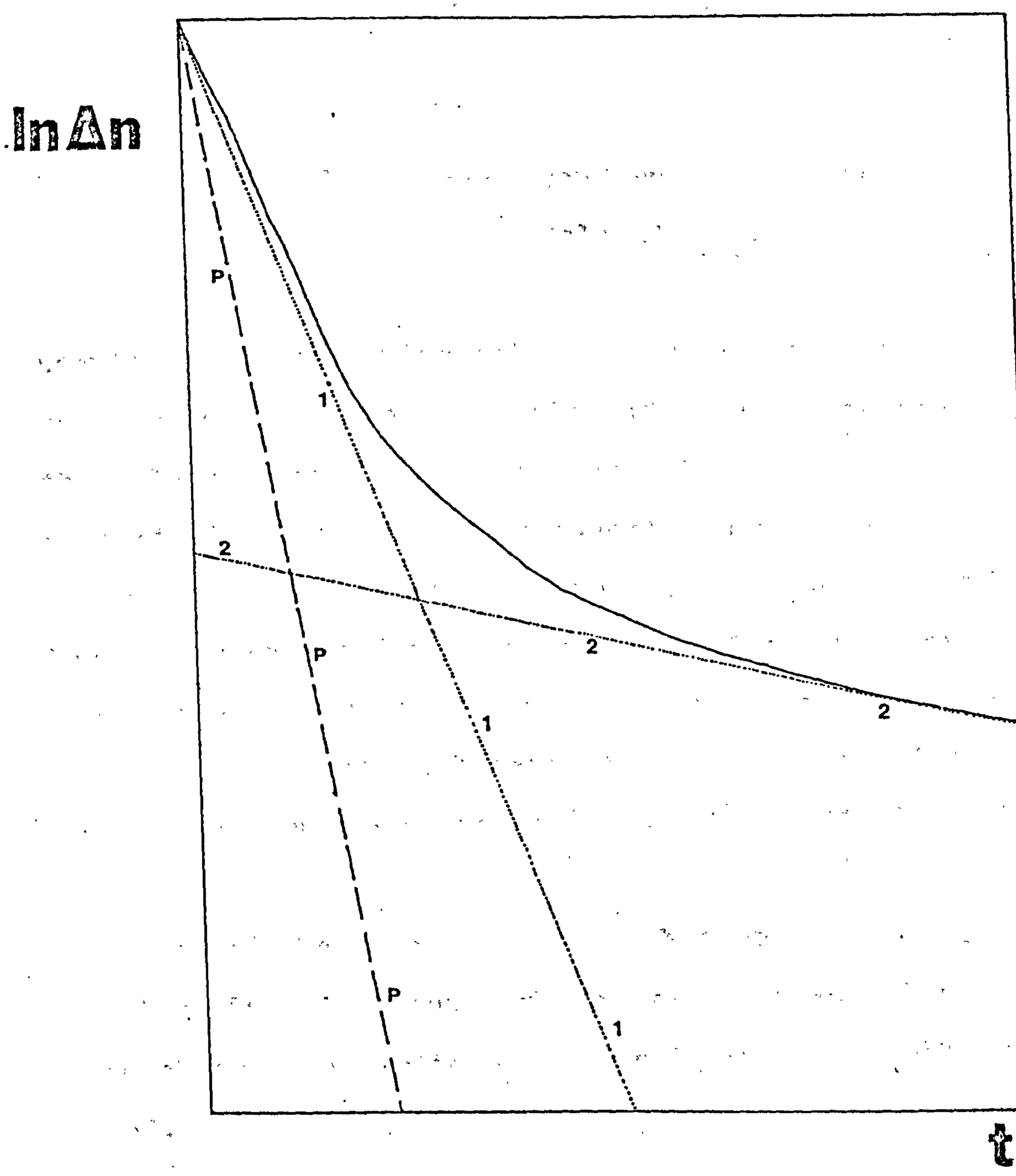

Fig. 2.4
DECAY ANALYSIS OF A BIREFRINGENCE TRANSIENT - PLOT OF LOGARITHM OF BIREFRINGENCE ($\ln \Delta n$) AGAINST TIME (t)
Tangent slopes yield rotary diffusion constants corresponding to the initial slope (1), the final slope (2) and the peeled value (P) obtained by subtracting the long time contribution (2) from the actual trace.

Unless stated otherwise, all results reported in this thesis refer to initial slope values of the rotary diffusion constant or relaxation time.

2.8 Relationships between Conformation, Size and Molecular Models

Knowledge of the conformation of a macromolecule in solution enables the evaluation of size parameters for the molecular system. Alternatively, a rough knowledge of particle sizes and other assorted parameters (e.g. direction of dipole moments, molecular weights) may lead to an evaluation of particle conformation, or at least an elimination of certain models for particular systems. The key link between conformation and model is quite often the rotary diffusion constant, D.

A resumé of the models used in this work follows, though the list is by no means exhaustive. The sensitivity of D to changes in particles' major dimensions should be noted.

2.81 Rigid Models

2.811 Rod (Broersma[217])

This is a refinement of a model originally proposed by Oseen and Burger.[218,219] Their result depended on deriving, mathematically, the force distribution in a moving object which produces a certain velocity at its surface.

Broersma took especial account of the effect of the ends of the uniform cylindrical model. The expression in both cases relates the rotary diffusion constant, D, to the third power of the rod's major dimension. Clearly D is thus a very size sensitive parameter:

$$D = \frac{3kT}{8\pi\eta_o a_1^3} (\ln 2r - A) \qquad (2.20)$$

where $A = 1.57 - 7 (\frac{1}{\ln 2r} - 0.28)$ (2.21)

r = Axial ratio of the rod

a_1 = Half length of the rod

η_o = Solvent viscosity

Note: The equation is not very sensitive to changes in the value of r.

2.812 Prolate Ellipsoid (Perrin[220])

Perrin has derived equations linking ellipsoidal particle dimensions with the rotary diffusion constant, viz:

$$D = \frac{3kT}{2\pi l_e^3 \eta_o} \left(\frac{1}{1-p^4}\right)\left\{\frac{(2-p^2)}{\sqrt{1-p^2}} \ln \left(\frac{1+\sqrt{1-p^2}}{p}\right) - 1\right\} \qquad (2.22)$$

where $p < 1$

p = Axial ratio of the ellipse

l_e = Major dimension of the ellipse

η_o = Solvent viscosity

The equation is not very sensitive to the value chosen for the minor ellipsoidal axis. The equation can also be used iteratively, knowing D, to improve l_e with updated values of p.

2.813 Oblate Ellipsoid (Perrin[220])

Perrin has similarly obtained an equation for an oblate ellipsoid, which can be expressed in the form:

$$D = \frac{3kT}{2\pi l_e^3 \eta_o}\left(\frac{1}{1-p^4}\right)\left\{\frac{(2-p^2)}{\sqrt{p^2-1}}\tan^{-1}(\sqrt{p^2-1}) - 1\right\} \quad (2.23)$$

where $p > 1$.

2.814 Disc

Equation 2.23 approximates a thin disc as when $p \gg 1$. The expression is then:

$$D = \frac{3kT}{32\eta_o a_r^3} \quad (2.24)$$

where a_r is the radius of the disc.

2.815 Sphere

Equation 2.23 can also be reduced to the Oseen and Burger equation for a cylindrical rod with the appropriate conditions, viz:

$$D = \frac{3kT}{8\pi\eta_o a_1^3}(\ln 2r - 0.8) \quad (2.25)$$

This reduces to the equation for a sphere:

$$D = \frac{kT}{8\pi\eta_o a_r^3} \quad (2.26)$$

2.816 Rigid Cylinders or Ellipsoids (Peterlin & Stuart[221])

This equation relates the magnitude of the molecular dipole moment (μ) to the Specific Kerr Constant (K_{sp}). In order that this can be done, a model has to be assumed for the system in question. Peterlin and Stuarts' model for a system of rigid, insulating, ellipsoidal particles predicted that:

$$K_{sp} = \frac{2\pi\bar{v}(g_1-g_2)\mu^2}{15n^2k^2T^2} \qquad (2.27)$$

where $\bar{v}$ is the system's partial specific volume

(g_1-g_2) the anisotropy of optical volume polarisability

and n the refractive index of the solvent

2.82 Flexible models

Molecular flexibility is a fundamental problem in the wider application of the birefringence technique. Birefringence decay, under the influence of Brownian restoring forces, has been studied by several workers, but only a few idealised models produce relatively stmightforward answers. The problem here lies in accounting for the relative motion of individual portions of a molecule, as well as the rotation of the molecule as a whole.

2.821 Random Coil (Zimm[222])

Zimm analysed the motion of a random coil in terms of the normal modes of motion, of which the first mode corresponded to rotation of the whole chain. Stockmayer and Baur [223] later extended his work to electric birefringence to show that:

$$D = \frac{RT}{3fM[\eta]\eta_o} \qquad (2.28)$$

where R = The Universal Gas Constant

M = The Molecular Weight of the Coil

$[\eta]$ = The Solution's Intrinsic Viscosity

η_o = The Solvent's Viscosity

and f = 1.21 or 0.85 for a free draining or non free draining coil, respectively.

2.822 Weakly Bending Rod (Hearst[224])

This model is defined in terms of a persistence length, q, seen as the projection of an infinitely long chain on the direction of the first segment of the chain. An alternative parameter is also quoted occasionally, namely the stiffness parameter, $x = \frac{L}{q}$, where L is the extended hydrodynamic chain length:

For a rigid rod values of $q \to \infty$ $(x \to 0)$
For a random coil values of $q \to 0$ $(x \to \infty)$

Values of q thereby enable evaluation of closeness to the extremes of rigidity and flexibility and a rough guide to the ordering of polymer chains according to the degree of flexibility. The equation for the weakly bending rod is:

$$D = \frac{kT\rho^3}{\pi\eta_o M^3}\left[3\ln\left(\frac{M}{2\rho b}\right) - 4.92 + 4\frac{b}{a} + \frac{M}{4\rho q}\left\{\frac{9}{2}\ln\left(\frac{M}{2\rho b}\right) - 10.2 + 4\frac{b}{a}\right\}\right] \quad (2.29)$$

where $\rho = \frac{M}{L}$ (2.30)

2.823 Worm Like Chain (Hearst and Stockmayer[225])

This system is essentially similar to the Weakly Bending Rod. The model itself is of a more flexible nature. Parameters q, x and ρ are as above:

$$D = \frac{2kT\rho^2}{\eta_o q M^2}\left\{0.126\sqrt{\frac{M}{q\rho}} + 0.159\ln\left(\frac{2q}{b}\right) - 0.387 + 0.16\frac{b}{a}\right\} \quad (2.31)$$

where a and b are the semi axes of the individual constituent segments of the chain, invariably assumed equal for circular cross-section models.

2.824 Polar Flexible Coils (Dows,[226] Peterlin & Stuart[227])

This equation relates the Molar Kerr Constant to the dipole moment of a monomer unit for a polar, flexible coil. As in section 2.816, a model has to be assumed to relate these quantities. Dows model theorised for flexible, polar, random coils in non-polar solvents and was based on a dilute gas model. He assumed the constituent polymer segments (taken here to be monomer units) to be orientated in an uncorrelated manner. Neglecting any contribution from induced dipole moments, Dows expression is as follows:

$$K_m = \frac{4\pi N_A}{405k^2T^2} \mu_o^2 \left(\frac{M}{M_o}\right) (a_{\parallel} - a_{\perp}) \qquad (2.32)$$

where M_o is the monomer molecular weight for the coil molecules and $(a_{\parallel} - a_{\perp})$ the segmental anisotropy factor as defined by Tsvetkov:[228]

$$(a_{\parallel} - a_{\perp}) = (g_1 - g_2) \frac{M_o \bar{v}}{N_A} \qquad (2.33)$$

The Dows' equation is essentially the same as that derived by Peterlin and Stuart for flexible polymers.

2.825 Rigid Frozen Coil (Dows[226])

Dows' alternative expression to that in the previous section is that for the Rigid 'Frozen' Coil in which all the dipolar segments are now considered to be orientated parallel to each other. The equation then has the form:

$$K_m = \frac{4\pi N_A}{405k^2T^2} \mu_o^2 \left(\frac{M}{M_o}\right)^3 (a_{\parallel} - a_{\perp}) \qquad (2.34)$$

2.9 Birefringence - Transmitted Intensity Relationships

The author has taken the reader through the various theoretical links appropriate to the work which follows. Before all this, however, a practical link has to be established, relating the birefringence to the practically measured parameter of transmitted light intensity, which itself is directly proportional to the voltage on the photomultiplier output. This relationship varies according to the manner of detection and various instances have been calculated by Fredericq and Houssier.[229] The results relevant to the three arrangements used in this thesis follow, and should be viewed in conjunction with Fig. 2.5. In this figure it can be seen that the quantities ΔI_δ and I_θ are measurable from a transient birefringent response, and it is the normalised ratio $\frac{\Delta I_\delta}{I_\theta}$ that is related to the birefringence via the phase difference, δ. The basic starting equation is that for the light intensity (I_δ) transmitted through an analyser offset from the crossed position by an angle θ and for a medium exhibiting a phase difference, δ, whence[229]

$$I_\delta = \frac{CI_o}{2}\left(1 - \cos 2\theta \cos\delta\right) \qquad (2.35)$$

where I_o is the light incident on the cell

and C is a factor between 0 and 1 taking care of light lost by absorption and reflection in the optical components.

Therefore in the absence of an electric field (no birefringence, $\delta = 0$)

$$I_\theta = \frac{CI_o}{2}\left(1 - \cos 2\theta\right) = CI_o\sin^2\theta \qquad (2.36)$$

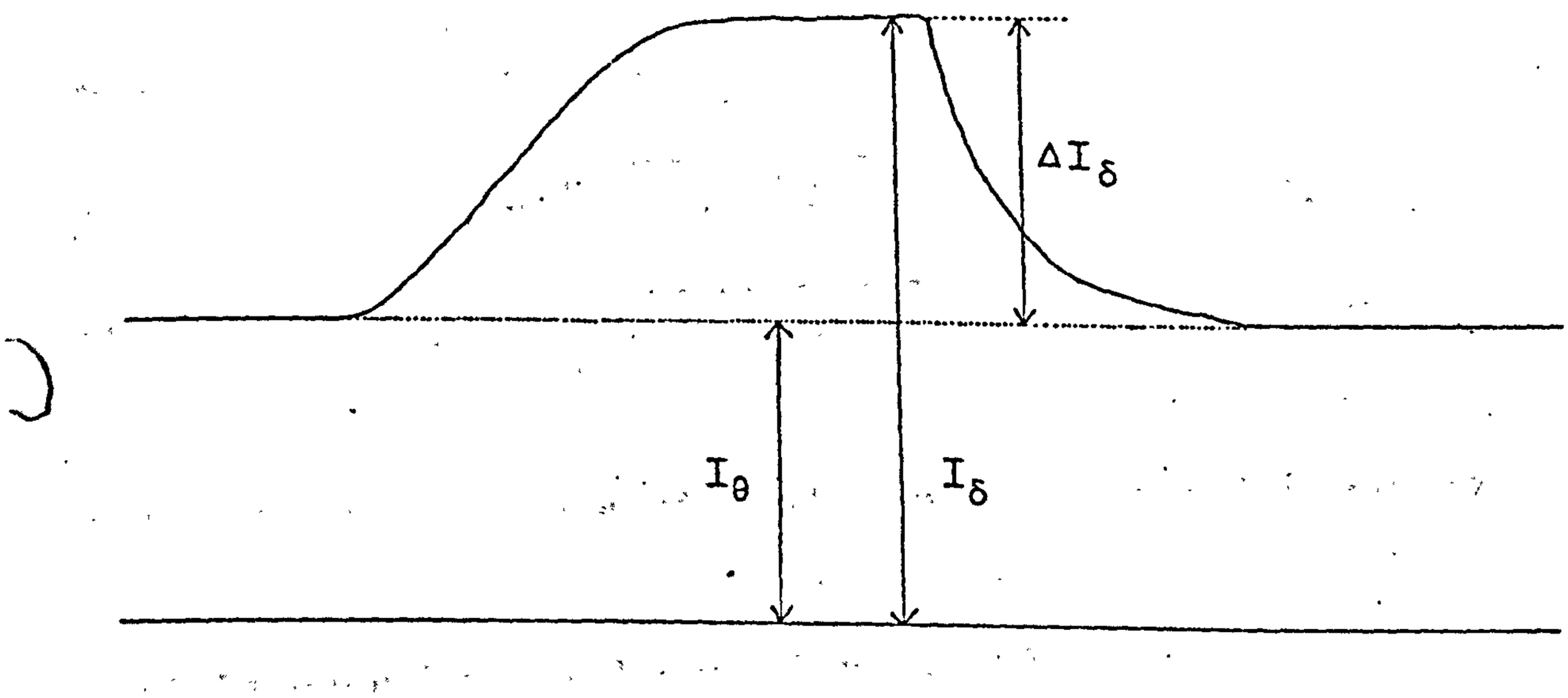

Fig. 2.5

Transient response, showing change in light intensity as seen on oscilloscope screen, consequent on a corresponding change in the sample's birefringence.

2.91 Quadratic Detection with Offset Analyser

The change in light intensity corresponding to the increased response of the photomultiplier to a transient birefringent response $\Delta I_\delta = |I_\delta - I_\theta|$ will be given by

$$\Delta I_\delta = \frac{CI_o}{2}(1 - \cos 2\theta \cos\delta) - \frac{CI_o}{2}(1 - \cos 2\theta)$$

$$= CI_o \sin^2(\delta/2) \cos 2\theta \qquad (2.37)$$

Then $$\frac{\Delta I_\delta}{I_\theta} = \frac{\sin^2(\delta/2)\cos 2\theta}{\sin^2\theta}$$

$$\therefore \quad \delta = 2\sin^{-1}\sqrt{\frac{\sin^2\theta}{\cos 2\theta}\left(\frac{\Delta I_\delta}{I_\theta}\right)} \qquad (2.38)$$

and $$\Delta n = \frac{\lambda}{\pi l}\sin^{-1}\sqrt{\frac{\sin^2\theta}{1-2\sin^2\theta}\left(\frac{\Delta I_\delta}{I_\theta}\right)} \qquad (2.39)$$

2.92 Quadratic detection with polariser and analyser crossed at 90°

In this case $\theta = 0$ and equation 2.35 becomes:

$$I_\delta = \frac{CI_o}{2}(1 - \cos\delta) = CI_o \sin^2\frac{\delta}{2} \qquad (2.40)$$

I_θ is now zero, so in order to obtain a value for CI_o a series of measurements has to be made to plot I_θ against $\sin^2\theta$ (equation 2.36), whence CI_o is the slope of the straight line obtained. (Law of Malus). The birefringence is then calculated thus:

$$\Delta n = \frac{\lambda}{2\pi l}\sin^{-1}\sqrt{\frac{I_\delta}{CI_o}} \qquad (2.41)$$

2.93 Linear detection with Offset Analyser

The presence of a quarter wave plate between the cell and the analyser will enable the differentiation between samples exhibiting positive and negative birefringence. The slow axis of the plate should be set at 135° with respect to the field direction. The plate also improves

the sensitivity of the arrangement.[230] The transmitted light intensity with the field applied is now:[229]

$$I_\delta = CI_o \sin^2(\theta + \delta/2) \qquad (2.42)$$

and $$\Delta I_\delta = CI_o \left\{ \sin^2(\theta + \delta/2) - \sin^2\theta \right\} \qquad (2.43)$$

Thus $$\frac{\Delta I_\delta}{I_\theta} = \frac{\sin^2(\theta + \delta/2) - \sin^2\theta}{\sin^2\theta} \qquad (2.44)$$

Hence $$\Delta n = \frac{\lambda}{\pi l} \left\{ \sin^{-1}\left(\sin\theta \sqrt{\frac{\Delta I_\delta}{I_\theta} + 1} \right) - \theta \right\} \qquad (2.45)$$

2.10 Conclusions and Bibliography

This concludes the theoretical resumé which has been designed to serve the work which follows. The opportunity has also been taken to pinpoint some of the weaker aspects of the currently available works in presentday applications. For further reading offering more details on both theory and application, the reader is referred to the following bibliography.

1. E. Fredericq and C. Housier. "Electric Birefringence and Electric Dichroism" Clarendon Press, Oxford, 1973.
An excellent text book covering both the theoretical and experimental aspects of electric birefringence in explicit detail.

2. K. Yoshioka and H. Watanabe in "Physical Principles and Techniques of Protein Chemistry" Part A, Chapter 7, p. 346, Ed. S. Leach. Academic Press, New York, 1969.
Presents a good theoretical background to the

technique which is easy to follow. Most of the treatise however discusses results of particular experimental work.

3. B. R. Jennings in "Advances in Polymer Science" Volume 22, pages 62 to 81, 1977.

This gives a simple review of the theory and technique and illustrates it with some of the most recent experimental data and observations. This article makes an excellent introduction to electric birefringence and also covers related electro-optic techniques.

SECTION I

APPARATUS

CHAPTER 8

Apparatus

3.1 Introduction

For most of this work, the apparatus used was that inherited from previous workers [31,32] though a number of modifications have been made as detailed further on. These modifications include the fabrication of a new cell designed for the easy circulation of solutions.

With the original apparatus now serving its third generation of research students, a completely new electric birefringence system has been designed and built, capable of very sensitive measurement. By directly incorporating recent advances in component design the complete system has been made simpler and much smaller with a view to making the apparatus available commercially as a laboratory tool. Moreover the cell used attempts to finally eliminate birefringence resulting from strain in the cell end windows by making the polariser and analyser prisms as integral parts of the cell. Full details of the design and performance of the new apparatus are given.

3.2 The Original Apparatus

The original apparatus is illustrated (Fig. 3.1) and detailed in Fig. 3.2. Completely enclosed in a light tight black box, it consists of an optical system producing a focused, collimated light beam which is directed through a polariser and into the Kerr Cell, following a path between the electrodes of the cell and emerging to pass through a second polarising prism, crossed with the first, to act as an analyser (quadratic detection) or through a quarter wave plate and analyser (linear detection). The light beam finally falls on to the end window of a photomultiplier, from which the electronic signal is displayed on an oscilloscope screen.

3.21 The Optical System

The focused, collimated light beam can be supplied by either a He Ne laser or an arc lamp.

(a) THE ARC LAMP This is a 500 W DC, high pressure mercury arc, powered by a highly stabilised voltage source developing 70 V $\pm$ 0.01% at 7 A. The light output was quoted by its builder (Rudd) as having a noise level of 1% and a short term stability of $\pm$ 3%. The light passes through a series of optical components to produce a suitable beam. Initially a heat absorbing glass (type HA3, Optical Works Ltd., Ealing), which shielded the other components from the intense heat of

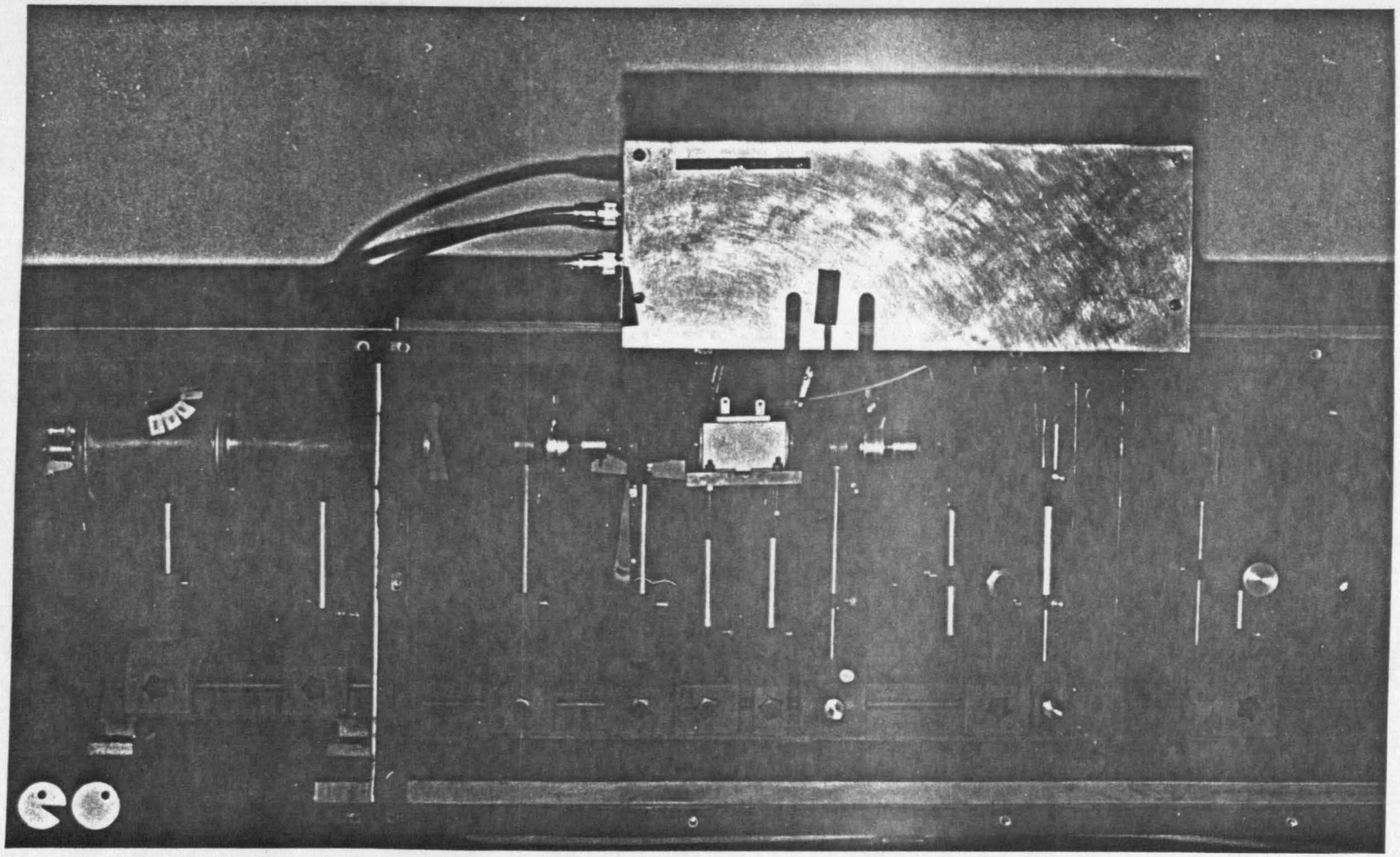

Fig. 3.1 The original apparatus - see Fig. 3.2 for key to components.

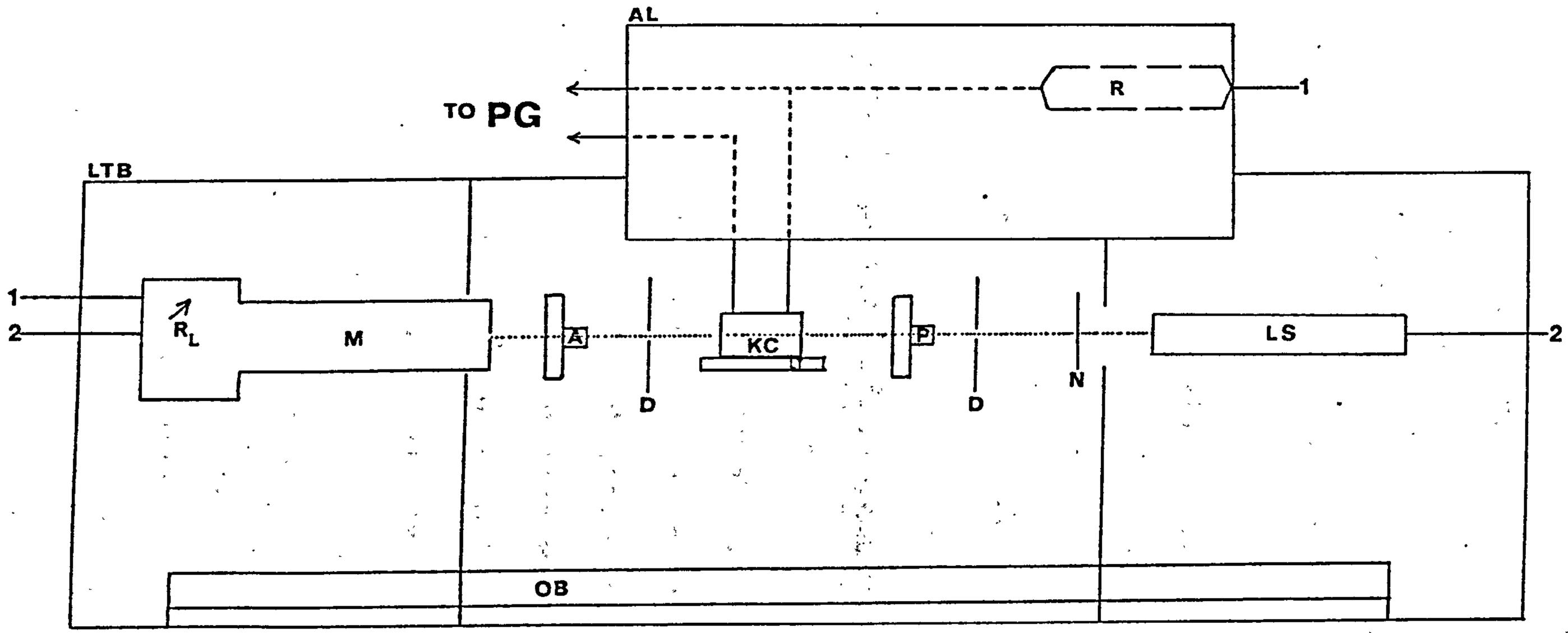

Fig. 3.2
Schematic diagram of the apparatus pictured in Fig. 3.1

KEY -

A	Analyser, mounted in a divided circle
AL	Access lid to Kerr Cell, etc. - linked to safety system
D	Diaphragm
KC	Kerr Cell
LS	Laser
LT	Adjustable level table
LTB	Light tight box
M	Photomultiplier tube
N	Neutral density filter
OB	Optical bench
P	Polariser, mounted in a divided circle
PG	Pulse generator
R	H.T. Probe
R_L	Variable load resistor

CONNECTIONS:

1	to oscilloscope
2	to appropriate power supply

the lamp is used, followed by an achromatic lens of focal length 8 cm, focusing the arc through a pinhole aperture at the focal point of a 10 cm focal length lens, which finally passes the light through an interference filter, chosen to select one wavelength from the mercury arc lamp's discrete spectrum. A narrow vertical slit is then included immediately before the cell to restrict the beam and obviate reflections along the electrodes.

(b) THE LASER A Coherent Radiation model 80 2 mW He Ne laser can be readily substituted for the arc. Its wavelength is 632.8 nm, the noise level is 1% and long term stability ± 5%. The particular laser head used in initial measurements, whilst quoted by the manufacturer as being linearly polarised, did in fact have a polarised beam that rotated its plane of polarisation to and fro with time. This head was later replaced with a head giving a fixed position polarised beam (Coherent Radiation model 80-2P). This head was coupled to a System Computors' power supply, which was further smoothed by a bank of six 'Visconol' 0.1 μF capacitors, rated at 5 kV. With both 2 mW lasers it was necessary to insert a neutral density filter to cut down the power of the beam before it entered the polariser and cell.

3.22 Polarisers and Quarter Wave Plate

Both polarising prisms (of the Glan-Thomson type) and the quater wave plate are mounted in rotatable divided circles manufactured by Messrs P.T.I. Ltd. These circles are adjustable to 0.05^{o} using a vernier scale. The polarising prism is set with its plane of polarisation at 45^{o} to the horizontal, i.e. at 45^{o} to the direction of the applied field. This procedure is described in section 3.33.

For linear detection, the quarter wave plate, a thin sheet of mica calibrated at 546.1 nm, is included, with its slow axis parallel to the direction of the incident polarised light. This can be set as follows, with the detection system set for maximum sensitivity and the polariser and analyser crossed to an accuracy of better than 0.05^{o}: The quarter wave plate should be positioned between the polariser and analyser and rotated to find the minimum in transmitted light intensity to within 0.05^{o}.

The analysing prism is crossed with the initial polarising prism for quadratic detection. This system of detection requires a knowledge of I_o (see section 2.92) this can be determined by a set of measurements of I_θ plotted against $\sin^2\theta$. For an optical system in which I_o is constantly changing, as with the arc lamp or laser with rotating plane of polarisation, this system of detection is unsatisfactory. With the arc lamp, the system of

linear detection was employed, enabling a direct measurement of I_θ (simply related to I_o) to be taken immediately before and after each birefringence measurement. The absence of a suitable quarter wave plate for the 632.8 nm He Ne laser radiation meant using the analyser offset from the crossed position, thus enabling a constant monitoring of I_o as required (section 2.91). The arrival of the highly stabilised, polarised Coherent Radiation 80-2P laser, permitted reliable I_o measurements to be made using the quadratic detection system.

3.23 Light Detection System

A pin hole aperture admits the light finally on to the photocathode of an E.M.I. 9816KB photomultiplier tube. Its spectral response is the E.M.I. designated "extended S20" which is particularly sensitive in the red, for use with He Ne lasers. Its housing, which was revised by the author, is described in detail in section 3.32. The tube is powered at 2.2 kV by an Isotope Developments EHT Unit, type 532/d. The signal from the scope is taken by a short coaxial cable (short: to minimise the time constant of the detection system, influenced by the capacitance of the cable) to the oscilloscope. The 'scope used is the Tektronix 585A 85 MHz dual beam model, the second beam being used to monitor the electric pulse applied to the birefringent

medium via a Tektronix P6013A 1000 to 1 probe (for large electric fields) or a P6006 10 to 1 probe as required. The exact attenuation of the probes is checked using a known signal, for example the 100 V peak to peak square wave signal generated by the 'scope's calibration unit.

In circumstances where the birefringence signal changes detected by the photomultiplier are too small to be seen against the background voltage from the photomultiplier output, a simple back-off unit, incorporating a battery and potentiometer is employed.

The pulsed electric field and transient electric birefringence response are thus displayed on the oscilloscope screen simultaneously, and photographed on Polaroid 46L film using a Tektronix C27 oscilloscope camera.

The transparencies thus produced are enlarged using a photographic enlarger, with the image projected on to graph paper for accurate assessment of field and birefringence amplitudes, and consequntly rates of intensity decay of birefringent responses.

3.24 Kerr Cells

The cells used in these experiments, with the exception of the onesdetailed in sections 3.34 and 3.45 were built by a previous worker (Rudd). They are designated A and B for future reference in the experimental chapters and their dimensions and details are as follows.

CELL A. This PTFE cell was designed with separately mounted, rotating, end windows, the object being to position them for minimum strain birefringence. However, clamping the window mounts in the preferred position reintroduced the strain in the glass microscope cover slip windows. Nonetheless, the performance of the cell was otherwise quite satisfactory, and incorporated a cooling jacket and solution flow facilities.

Electrode length:	4.979	$\pm$ 0.002 cm
Electrode separation:	0.264	$\pm$ 0.002 cm

CELL B. A simple cell having a PTFE body and circular microscope cover slip windows clamped in position against the cell body by PTFE end pieces. This cell has solution flow facilities too.

Electrode length:	4.984	$\pm$ 0.004 cm
Electrode separation:	0.272	$\pm$ 0.004 cm

The spectrophotometer cells of the previous author, made by Hellma of Westcliff-on-Sea, with inserts of Tufnol or PTFE holding the electrode assemblies were not used.

All were broken by virtue of Tufnol swelling in water, PTFE creeping with change in temperature, and - in the instance of the one glued in a perspex water jacket - forces exerted by the Araldite resin used. These appeared therefore to be expensive and short lived cells, and generally required large sample volumes compared to Cells A and B.

Both Cells A and B, which incorporated the solution flow facilities already mentioned, proved to be unsatisfactory in this respect. Two brass tubes were intended for passing solution in one end of the cell and out of the other. However, when the system was pressurised to induce flow, the seal around the 'plug', comprising the electrode insert, was inadequate. This prompted the new flow cell design (section 3.34).

3.25 Pulse Systems

The apparatus is arranged to be triggered from the oscilloscope. This enables the operator to apply the field pulse and 'instantaneously' record the reponse on the oscilloscope camera. The pulse is applied across the cell, which has a load resistor in parallel across it, so chosen to prevent too great a current flowing through the test solution. With the variety of materials studied in this work, a diverse range of pulses, both in amplitude and duration were required. A number of pulse generators was therefore used and

the characteristics of each are as follows:

PG1 This simple machine is one of the commercially available Lyons Instruments series of pulse generators, the PG21. It has to be used in the single pulse mode, triggered externally from the oscilloscope. Pulse width ranges from 0.2 μs to 200 ms but pulse amplitude is variable up to only 10 V. This system is only suitable for looking at clay suspensions and other similarly highly charged, large, anisotropic particles. However, this generator is more versatile in that its output can be used by other machines which can amplify the pulses up to kilovoltages. Delay circuitary in the PG21 can also be useful when using the machine on its own or in conjunction with the amplifiers. Finally, the PG21 has to be used to expand the spike trigger pulse from the oscilloscope, which on its own is inadequate to fire generator PG6.

PG2 For slightly higher voltages (up to 90 V) where little current will be drawn, a simple arrangement using reed relays and dry cell batteries can be utilised. The relay systems are triggered by the PG21.

PG3 Wareham power amplifier, type C646. This versatile machine is capable of amplifying DC, square wave or sinusoidal pulses. It has a 600 W capability. It is not inherently pulsed, though it is possible to pulse the system by either feeding in pulses (up to 1 V)

for amplification or chopping the output using a double relay system. Double relays are used to avoid the problems of bouncing, i.e. relays literally bouncing back on again, and thereby pulsing the solution a second time. The pulsed input system is easier to operate provided that the distortion that may occur in the pulse shape is not restrictive on measurements, and care is taken to ensure that any DC level is backed off and not applied continuously to the solution in the cell. The initial pulses fed into the amplifier are obtained from either the Lyons PG21 or by relay switching the output of a Levell Oscillator, type TG150DM, which can deliver sinusoidal or repetitive square wave output. The latter, switched correctly, can produce a reversing pulse (section 2.6). It is important to note that as the frequency of the output is increased, the voltage amplitude will decrease. This effect is particularly marked above 1 kHz. Therefore, the output should be constantly monitored, and the input adjusted accordingly if a constant voltage is required.

PG4 This is the most versatile of the DC generators used. It is capable of delivering 400 V to 10 kV at up to 10 A for between 50 μs and 1 ms. The initial shape and duration of the pulse is determined by amplification of the Lyons PG21 output. This pulse is applied to the grid of a set of valves which then conduct, discharging a large capacitor bank across the Kerr Cell. The system was originally designed by the

Electronics Department of Queen Elizabeth College, London, and is potentially lethal in that the high voltage is always present on the terminals and only for the duration of the pulse does one side of the output drop to earth potential.

The enclosed optical bench is wired to an alarm system, triggered via microswitches to remind the operator of the danger if he tries to gain access to the cell where the wires leading from the generator are laid bare. This system is far from satisfactory, and in consultation with Dr A R Foweraker of this research group and Mr G Ford of this University's Electronic Design Facility, modifications were made by Mr Ford to effectively take the voltage 'inside' the generator. A unit installed on top of the generator now enables the operator to arm the output for a period variable up to 10 minutes, i.e. sufficiently long to take one, or a sequence of measurements. The arming is accomplished by switching heavy duty relays installed on the line to the output terminals. When armed, the generator emits a warning note and shows a red light. The operator may cancel the armed state at any time.

PG5 This is another lethal machine capable of delivering up to 10 kV for up to 25 μs. It is a hard valve pulse generator, again driven by the Lyons PG21. Its output pulses are very square, but generator PG6 was used in preference, where possible, for safety reasons.

PG6 This consists of a 10 kV, 0.5 A hydrogen thyratron generator, coupled to a specially designed unit incorporating delay lines which can be charged up to 5 kV then discharged across the cell in 1, 3 or 5 μs pulses. The previous worker tested the new system, but faulted it on two particular aspects, namely pulse shape (which showed both droop and a time decay, particularly on the 5 μs pulse) and photomultiplier pick-up when the delay lines were discharged. The latter was overcome by screening the photomultiplier (see section 3.32). The former was taken into account when using the generator. If its time constant was too large then PG5 was available. Fields were recorded as at the drooped value of the pulse, corresponding to the field at saturation orientation. If transient reponses had shown signs of 'falling off' at saturation, then again PG5 could be used.

PG7 This is a low voltage thyristor pulse former, designed by a previous worker (Brown). It is capable of giving 350 V at 0.5 A continuously. The output can be chopped as required using reed relays in a similar manner to that mentioned previously.

3.3 Modifications to the Original Apparatus

Important modifications to the system are outlined as follows.

3.31 Photodiode Light Monitor

Using quadratic detection, with the polariser and analyser completely crossed, changes in the lamp output could suddenly occur, even half way through a measurement of I_o. This situation was difficult to tolerate and a means of constantly monitoring I_o via the lamp output was needed. The previous author had suggested a second photomultiplier in the manner of Orttung and Meyer[33]. A simpler and cheaper solution, not needing major modifications to the light tight housing of the apparatus, was to use a light sensitive diode. A suitable device was constructed by the University's Electronic Design Facility. The diode was fixed to the side of the enclosing box, and part of the beam from the lamp directed on to it using a half silvered mirror beam splitter. The response of the diode was then displayed on a meter with a scale in arbitrary units. The meter should be adjusted for maximum sensitivity. It incorporates an output via a BNC connector for continuous read out on a 'scope or chart recorder. In practice, the meter is placed on top of the apparatus where the scale can be clearly seen by the operator. The reading is

adjusted using the sensitivity control to a convenient value. Should this then alter during the course of an experiment, the lamp itself can be altered to restore the meter to its predetermined reading.

3.32 Modifications to the Photomultiplier Housing

The previous worker had had cause to change the photomultiplier tube from a Mullard 56AVP to an E.M.I. 9816KB. In so doing, the tube's housing was no longer light-tight. Pick-up from the pulse generator PG6 has been referred to, and on occasion, arcing in the vicinity of the dynode chain could be heard. On examination of the compartment, exposed solder joints were found, which could have arced to the side of the housing. The tube itself was found to have a serious fault, in that the photocathode was dislocated. This may have contributed to the pick-up and arcing problems. The opportunity was therefore taken to redesign the housing and to incorporate a set of variable load resistors for accurate determination of birefringence amplitudes (using large value resistors) and decay times (using smaller value resistances).

A larger compartment for the dynode chain was thus built, giving more room to keep exposed joints away from the sides, and to provide space for a wafer switch assembly to which the load resistors could attach.

Sockets were provided for the input and output leads, so that if in future the back needed to be removed for access to the dynode chain, no tension need be applied to these leads and the solder joints to which they attached. All leads within the compartment were screened, joints were taped over where possible, and wax used to separate components where necessary. The inside of the tube was lined with rubber sheeting to further obviate any possible shorting.

A mu-metal shield, to complete the screening, was incorporated, wrapped around the photomultiplier tube itself and maintained at the cathode's potential. A thick core of protective insulation was therefore employed to isolate the mu-metal shield from the photomultiplier housing.

The new housing was tested and measurements made of the time constants appropriate to the selection from the range of load resistors. Where only birefringence amplitude measurements are important a large resistor can be used. However, when seeking particle relaxation times, the load resistor must be selected such that the time constant of the detection system is less than that of the disorienting particle or molecule. To maximise the signal, the largest resistor compatible with this condition is used. To check the time constants of different resistors in the detection system, nitrobenzene is placed in the Kerr Cell. This exhibits a reasonable

birefringence, but being a pure liquid has a very fast relaxation time (~ns). Relaxation times measured are therefore those of the detection system. Values obtained for the load resistors of the new housing are set out below.

LOAD RESISTOR	TIME CONSTANT
500 kΩ	3.9 μs
50 kΩ	2.3 μs
5 kΩ	0.64 μs
500 Ω	0.35 μs
50 Ω	<0.3 μs

3.33 Specific Plane Polariser

The usual method prescribed for determining the plane of polarisation of a prism polariser is that of the 'pile of plates'. A pile of crown glass microscope slides are positioned so that light is reflected off them at Brewster's Angle. The pile has to be carefully positioned so that its face is normal to the incident light in the horizontal plane. During the course of the work it became necessary to remove both polarising prisms to have their faces repolished. (An explosion resulted in the cell windows being sputtered across them!). Moreover, the design of the new apparatus (section 3.4), and the prisms used therein required the determination of the plane of polarisation on several occasions. A simple 'pile of plates' holder was therefore designed,

holding the plates at the required Brewster angle and normal to the horizontal. It has a standard attachment for use on an optical bench.

Note: It is important to use clean, dust-free plates to minimise spurious reflections. When not in use the specific plane polariser is kept wrapped, undercover.

3.34 Use of the pH stat

For measurements undertaken in sections 7.1 to 7.5, an automatic titration system was used in conjunction with the new flow cell. This instrument is shown schematically in Fig. 3.3, and photographed with the apparatus in Fig. 3.4. The illustrations show that the instrument comprises the following units: a pH meter (PHM28), a titrator (TTT11), an automatic burette (ABU12) and chart recorder (SBR2), all supplied by Messrs. Radiometer Ltd., Copenhagen, Denmark. Combined in the manner shown in Fig. 3.3, the instrument is able to perform with the versatility indicated below.

1. The pH meter can detect changes of 0.1 in pH and is very stable.
2. The titrator, coupled with the pH meter, forms an automatic titrator, enabling the operator to predetermine an end point for an acid-base reaction by adjusting the titrator controls.
3. The titrator is then linked to control the automatic burette which will be made to add sufficient reagent

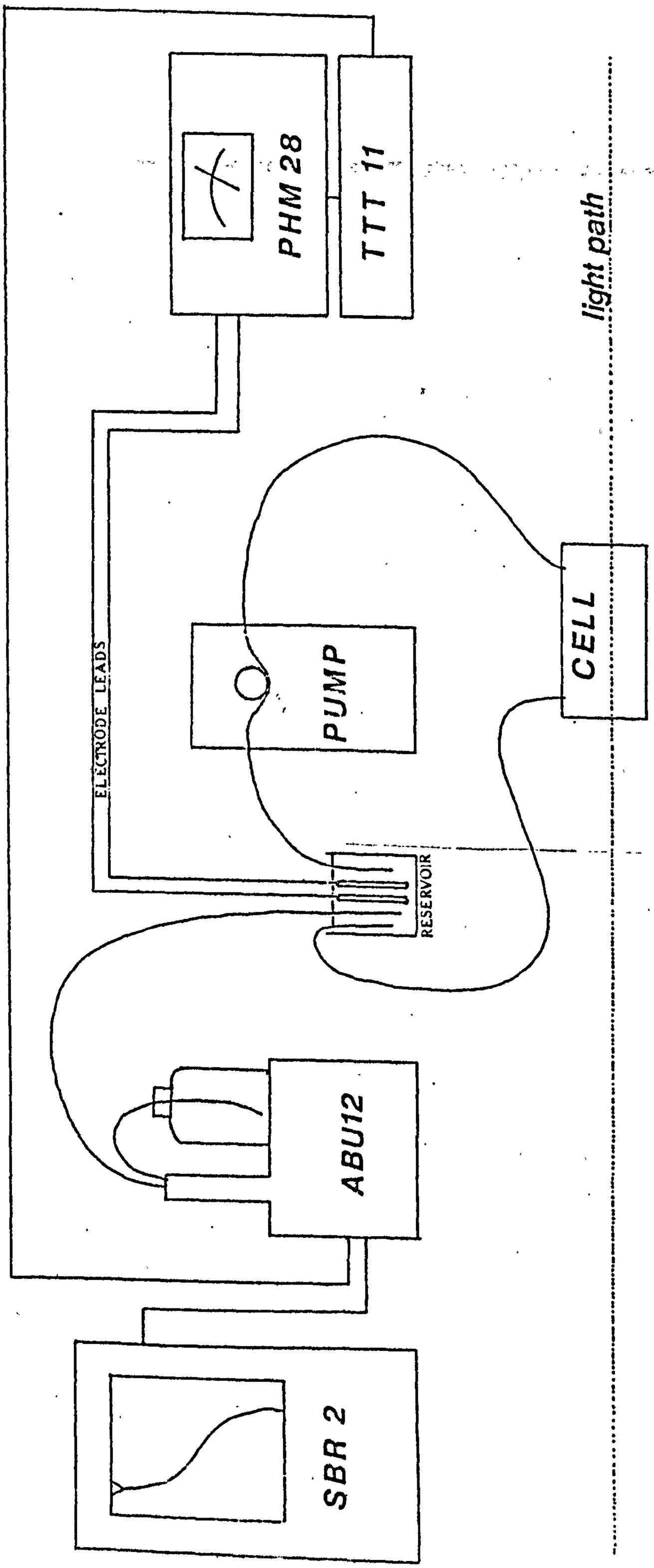

Fig. 3.3 Schematic diagram of pH stat as used with apparatus (see text for explanation of units)

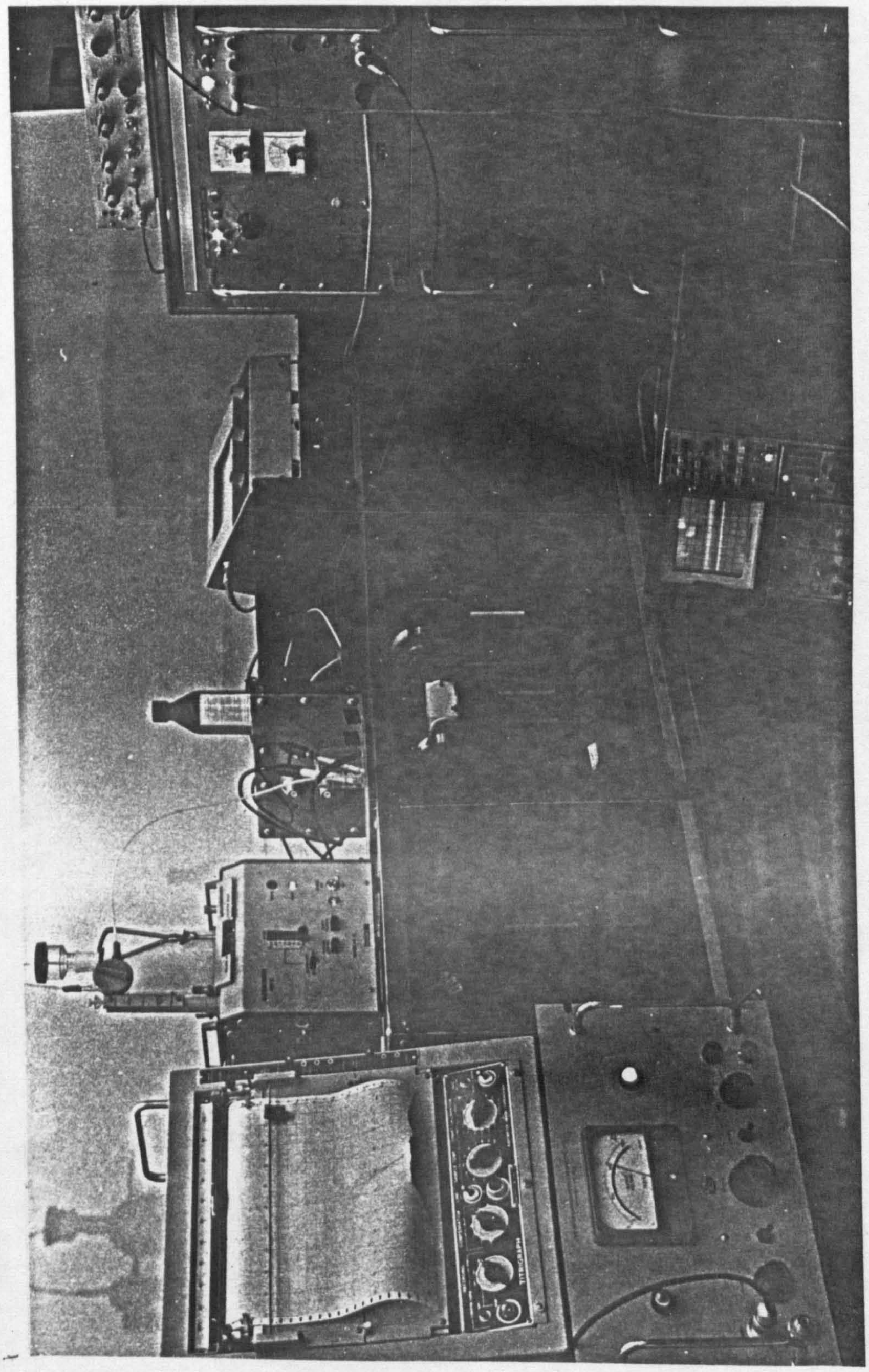

Fig. 3.4 The apparatus in use with the pH stat and generator PG6

to the solution to reach the required end point.

4. An important feature of the titrator is its 'proportional band setting' which controls the rate at which reagent is added to the solution, slowing this rate as the end point is approached, and thereby eliminating overshoot.

5. The ABU12 unit offers two sizes of burette, viz: 0.25 ml and 2.5 ml. The speed of the unit is widely variable, down to less than 1 μls^{-1} with the 0.25 ml burette.

6. The chart recorder may be used to record the amount of reagent added with time up to a period in excess of 33 hours. If time is not a parameter in an experiment, the burette unit incorporates a digital readout of volume of added reagent.

3.35 The Flow Cell

This new cell is illustrated in Fig. 3.5. To minimise the number of places where leaks might occur when the sample solution is induced to flow under pressure, the separate fixing of electrodes and cell windows is simplified. With most cells, such as A and B referred to earlier, the electrode assembly is removable, both for cleaning and for filling the cell with solution. In this design, the cell can be filled by flowing solution in at one end and out at the other via small diameter brass tubing. For cleaning

purposes, solvent can be readily circulated through the cell. If more abrasive cleaning of the interior is required, then access can be gained via one of the cell end windows.

Both windows, 2 cm diameter microscope cover slips, are recessed into both ends of the PTFE block (measuring 8 cm x 3.5 cm x 3.5 cm) against flat circular O-rings made of a thin synthetic skin to act as water-tight seals. The windows are each held in position by a PTFE plug which locates in the recess and is secured by four screws.

The electrode assembly is in the form of a tray. Two stainless steel electrodes are machined to be parallel and square edged. They are monted on a PTFE slider, the same length as the electrodes, thus serving as a 'tray' to hold the electrodes and keep them the set distance apart. This tray assembly slides neatly into a square channel cut through the centre of the solid PTFE block (Fig. 3.5). The electrode tray is then held firmly in position and given the required rigidity by two long screws which enter the electrodes via the top of the cell.

These screws simultaneously provide the electrical lead through to the cell. When embedded in the electrodes, a small washer and nut tighten at the point of entry of the screw into the cell as a further precaution against

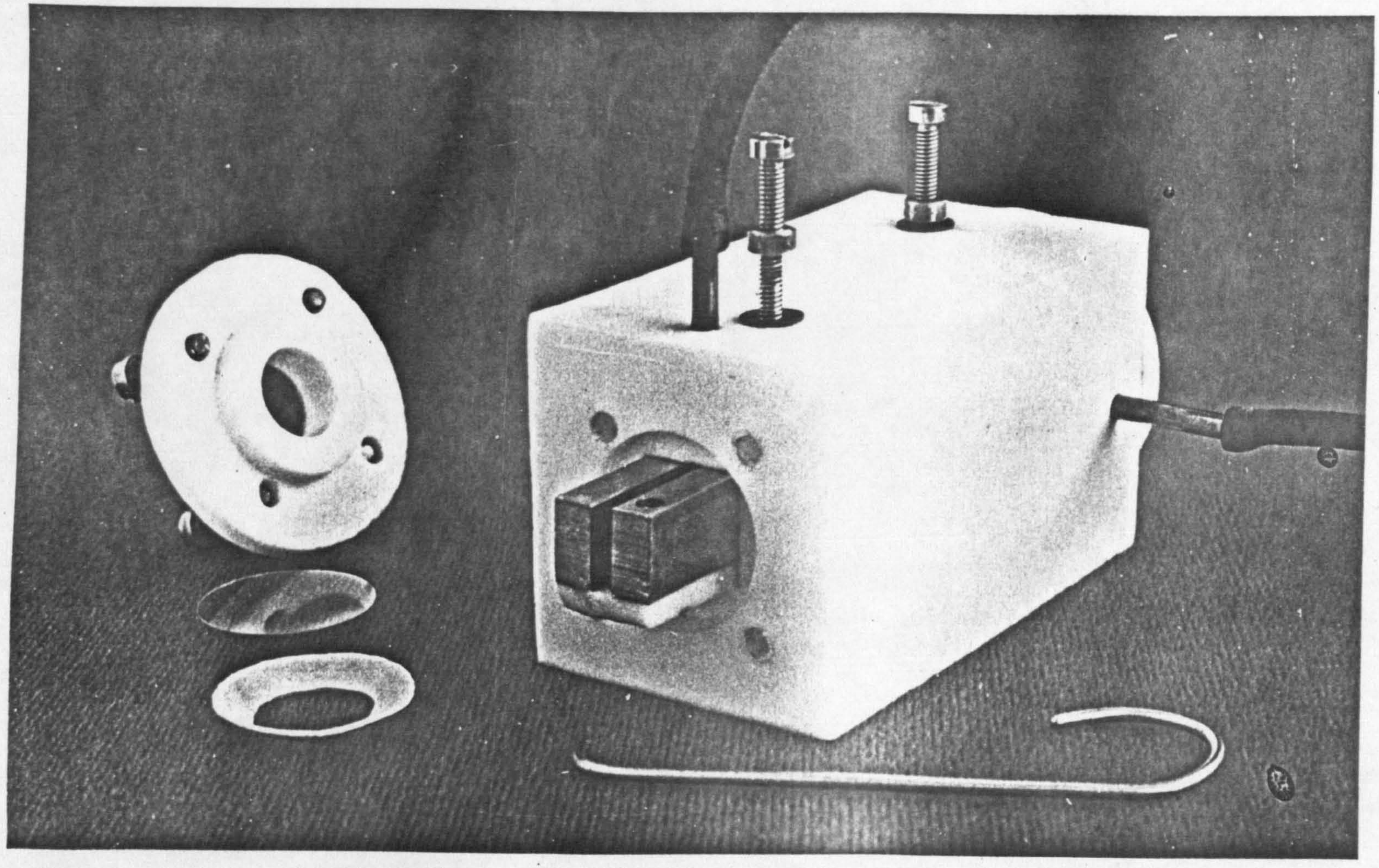

Fig. 3.5 The flow cell designed by the author, showing the end removed and the electrode 'tray' partly drawn out.

leakage.

The electrode tray can be readily removed for cleaning. In practice, the same cell window is always removed to gain access to the cell interior. The other window remains *in situ* unless in need of cleaning or replacement. An additional advantage of the electrode tray approach is that a variety of trays, offering different electrode lengths and separations could be readily accommodated in the same cell body.

The flow itself is induced by a Watson Marlow peristaltic 'HR Flow Inducer' type MHRE200. This is coupled to the cell via narrow bore brass tube inlets and outlets and 1 mm diameter neoprene tubing. Because many of the samples studied can be expensive or in limited supply, it is important to keep the total volume of solution as small as possible. Hence the use of narrow bore tubing and a compact electrode arrangement. Total volume of the cell, together with its tubing leading out of the apparatus and through the flow inducer to the external reservoir, is 4 ml. For practical measurements a certain amount of fluid must be additionally maintained in the reservoir, normally a small diameter 15 ml beaker. Only 2 to 3 ml are needed in the reservoir when the system is flowing. However, when used with the pH stat, which requires immersing the pH meter electrodes in the reservoir, a total sample volume of at least 10 ml is needed. A slightly larger electrode assembly could

reduce the sample volume a little more if necessary. The procedure for filling the system is as follcws. The sample is placed in the reservoir and the flow is started such that the liquid enters the cell by the side tube (at the rear, Fig. 3.5) and is removed via the top tube at the other end. If the front of the cell is now raised, any bubbles will be encouraged to flow up through the cell and be sucked up out through the top tube and subsequently discharged into the reservoir, (Fig. 3.6).

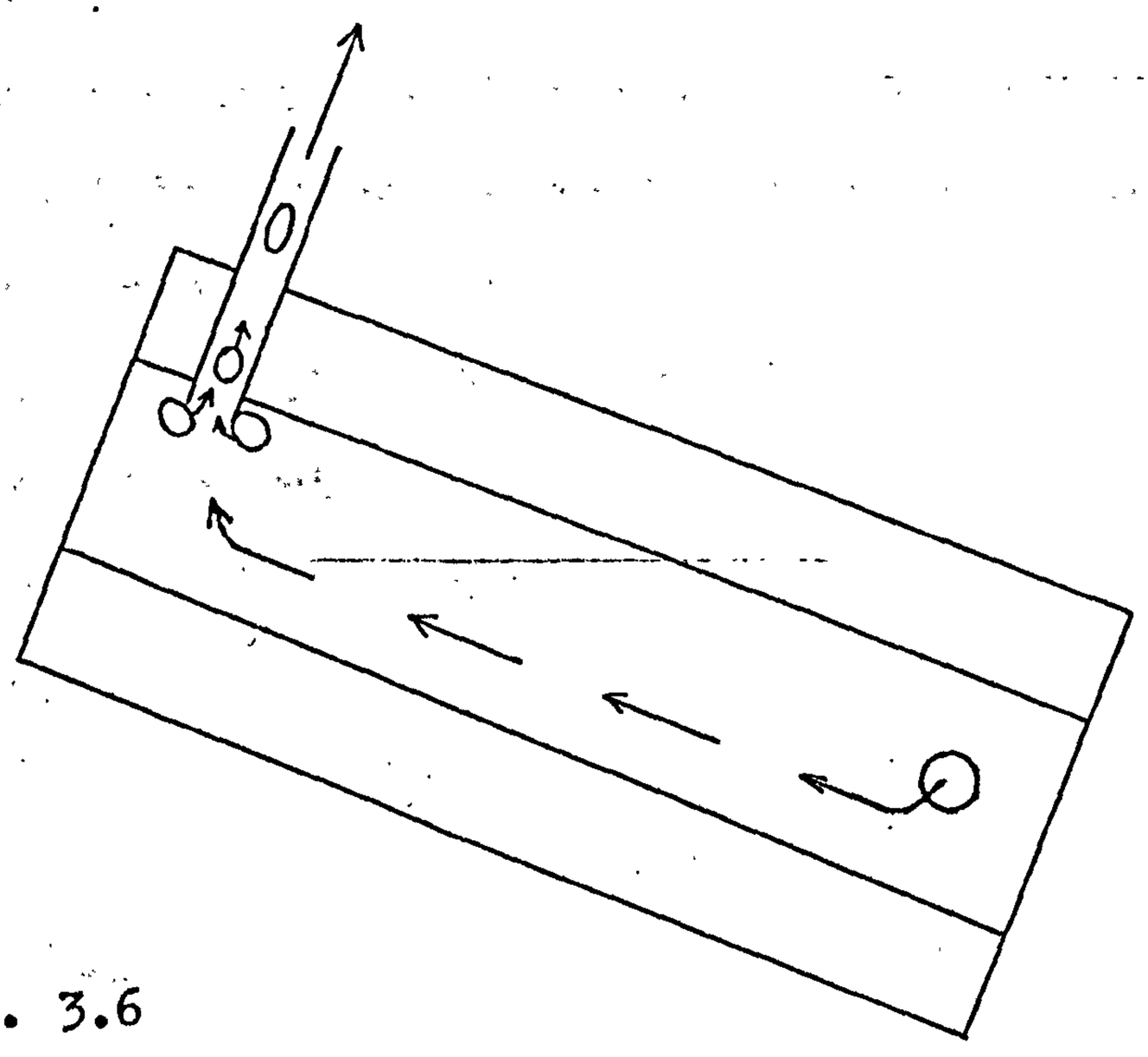

Fig. 3.6

Tilting the flow cell enables bubbles trapped in the cell to be removed with the flow of solution

3.4 The New Apparatus

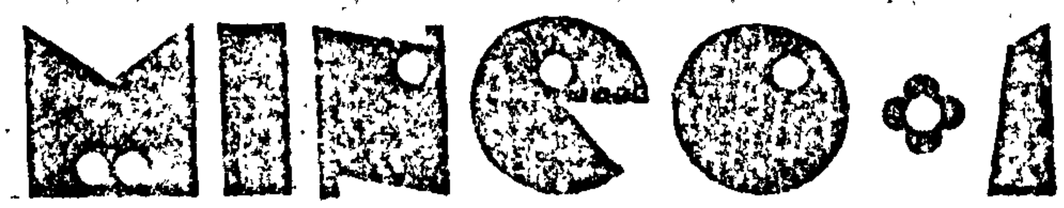

3.41 Design Objective

The primary aim in designing a new electric birefringence apparatus was to attempt an improvement on the sensitivity of the existing system. Moreover, since the construction of the existing laboratory equipment, improvements in component design and specification would enable a more compact apparatus to be built. This concept, coupled with the potential demand for a commercially available electric birefringence system for use as a standard laboratory tool, formed the objective for the final design.

3.42 Meeting the Objective

The main limiting factor for existing apparatus designs to the measurement of small birefringence changes is the strain birefringence of the glass windows of the Kerr Cell. The Cell A design of Rudd, mentioned earlier (section 3.24) was one attempt at minimising this handicap, albeit unsuccessfully. It was therefore decided to dispense with the cell end windows altogether and make the polarising prisms (polariser

and analyser) themselves the windows of the system. To minimise the problems of leakage from the cell, a vertical system was chosen. This meant that only the polariser, at the bottom of the cell, required a leak proof seal, with the analyser (or quarter wave plate for linear detection) dipping into the top surface of the sample solution. Additional advantages from adopting the vertical mode included simplified supports for most of the components (i.e. gravity assisting their retention) and, a considerable saving in laboratory space. This latter point is particularly useful should the apparatus be sold commercially.

This finished system thus fits flush to the wall with ancillary power supplies and monitoring equipment mounted on a small trolley. The accompanying figures show the apparatus in schematic form and as the fabricated prototype.

3.43 The Housing

The system is mounted in a light-tight box made from 0.8 mm 'Dural' of 11.5 cm square internal dimension and an overall length of 76.5 cm. This makes a frame for what is effectively a vertical optical bench. The box is not mounted directly on to the wall, but on to a 'Dural' plate. This plate is 1.5 m long, 20 cm wide and 1.25 mm thick. It has glued to its back a

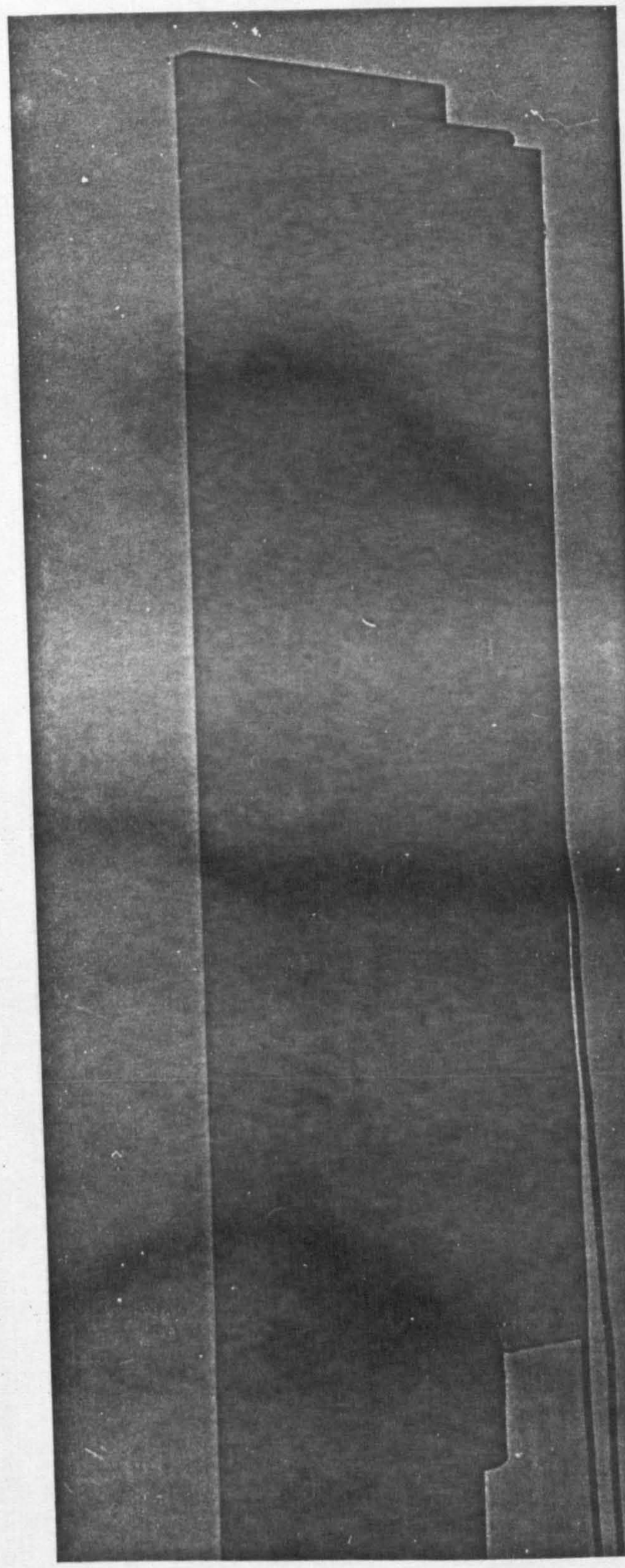

Fig. 3.7
The new apparatus attached to the wall.

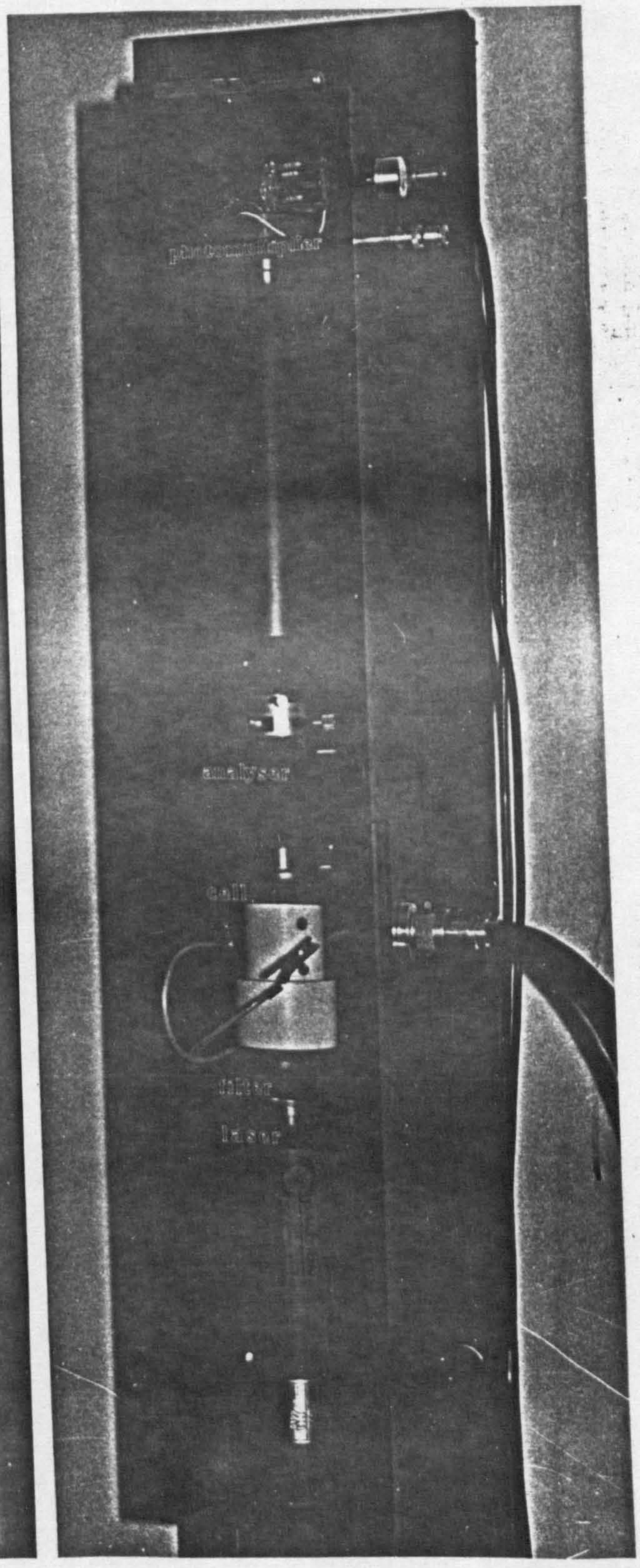

Fig. 3.8
A close-up of the apparatus with both front panels removed.

0.6 mm thick rubber sheet and is held flush to the wall with six heavy duty screws. The rubber backing forms an effective dampener of vibrations transmitted along the wall. The plate exceeds the length of the box considerably and this was to permit the mounting of any future ancillary equipment or modifications. In particular, the substitution of a larger laser light source of a different wavelength might be a distinct future possibility, or even the provision of a conventional arc lamp.

The box is held to the plate at three points. At the top is a central bolt on which the box can be pivoted and thus positioned with its vertical axis in a plane perpendicular to the wall. At the bottom of the box, the flange through which the two bolts pass have slots to allow the pivoting adjustment. Two nuts then clamp the bottom end in position against two springs. These are tightened until the box's axis is in a plane parallel to the wall.

With the box set in a true vertical position, all fittings are machined to align with the box and hence the vertical axis, centrally through it.

The box is divided into two sections, each separated by a 1.25 cm 'Dural' partition. The top section is 30 cm deep and houses the photomultiplier. Whereas

three of the sides are each in one piece, the fourth, front-facing side is in two, broken at the partition. The top half is held in place with screws (which are used throughout to hold the sections of the box together). Once the system is operational, there should be little need to gain entry to this upper compartment which contains the photomultiplier. The lower half is easily removable, locating on two studs and held by twist-locks. It provides access to the cell and optical components.

All the components are held in position, locating on suitably machined and centred recesses in 11.5 cm square sections of 1.25 cm thick perspex. In the lower half of the box these are able to slide in and out on runners which gives inherent flexibility for future adaptation.

In order to minimise the amount of stray light reflecting around inside the box, all the 'Dural' pieces were anodised in semi-matt black. Likewise, all the perspex sections were sprayed with matt black cellulose paint.

3.44 The Photomultiplier

To work in conjunction with the red light of the He Ne laser, the high gain, fourteen stage, red sensitive E.M.I. 9816KB tube was chosen. The dynode chain was based on the E.M.I. linear design[34] and a set of variable load resistors included, controlled by a

switch located on the side panel of the box. Similar values of load resistance were chosen to those used previously (section 3.32). The tube was powered by a Brandenburg 471/H Photomultiplier Power Supply, and the resulting signal fed out on to an oscilloscope with provision to record transient changes in the usual manner.

There is no separate housing for the photomultiplier tube as such. It is built directly into the upper compartment of the box. The photomultiplier base locates in a circular recessed hole in a square perspex section near the top. The space above being suitable for the necessary circuitary. The tube tightly push fits into the base and is thus held in its vertical inverted position. A 1.25 cm diameter hole in the 'Dural' partition dividing the two sections of the box allows the light to fall on the end of the photomultiplier tube. On top of this partition rests a square of perspex, partially recessed to hold the mu-metal shield around the tube. The perspex thus insulates the shield (held at cathode potential) from the rest of the box. Because there is no danger of the shield moving, it does not require H.T. insulation along its length, as with the horizontal apparatus.

Input and output connections are located externally on the side of the box.

3.45 The Laser

The initial model selected was the C W Radiation LS-1R with separate head. This 1 mW laser had a small 23 cm head, a highly stabilised power supply option giving a beam noise of 0.3% and beam ripple of less than 0.25%, together with a 1000 to 1 polarisation ratio. Disappointingly, when delivered, the laser nowhere near matched its specification. The output had considerable long time variation and when monitored with a chart recorder connected to a photomultiplier could be observed to drop to zero output on occasion! Consequently a substitute laser had to be found and the Spectra Physics model 136P was selected. This laser's head was 30 cm long and necessitated a small extension to the box, which results in the completed system losing a little of the flexibility inherent in the original design. The Spectra Physics laser works satisfactorily, it is one of a family of mass produced lasers purposely designed for use in commercial instruments of high or low volume production. Its specification is identical to a Coherent Radiation model designed for interavailability. The beam ripple and noise are less than 1% and the polarisation ratio is 200 to 1. The head on this particular option has two milled rings on it, machined concentric with the beam. Holders made from 1.25 cm thick perspex are thus mounted on these rings and locate in the box holding the laser and directing the beam up the box's vertical axis. By

releasing the tension on the upper perspex holder, the laser head can be rotated to optimise the direction of the beam's polarisation with that of the initial prism polariser.

Immediately above the laser is the first of the slidable perspex partitions. It has a central 0.5 mm diameter hole serving as a pin hole to cut down spurious laser light. Recessed into its upper side is a 5 cm diameter hole, capable of holding two to three neutral density filters to cut down the power of the laser beam as required.

3.46 The Cell, Prisms and Quarter Wave Plate

The cell is illustrated in Fig. 3.10. The body is made from the usual PTFE block of insulating material. With the initial polarising prism forming one of the end windows, ideally only the end face should be in contact with the solution. One of the prisms (Karl Lambrecht type MGT25E8) is first coated with a thin Magnesium Fluoride film by vacuum deposition. The author acknowledges the expertise of Mr K Schlacter of the department's vacuum section in this respect. The prism, thus protected against the corrosive action of mild solvents such as water, is now embedded in a leak proof, cylindrical PTFE shroud. A 3 mm diameter concentric hole admits the laser beam at one end,

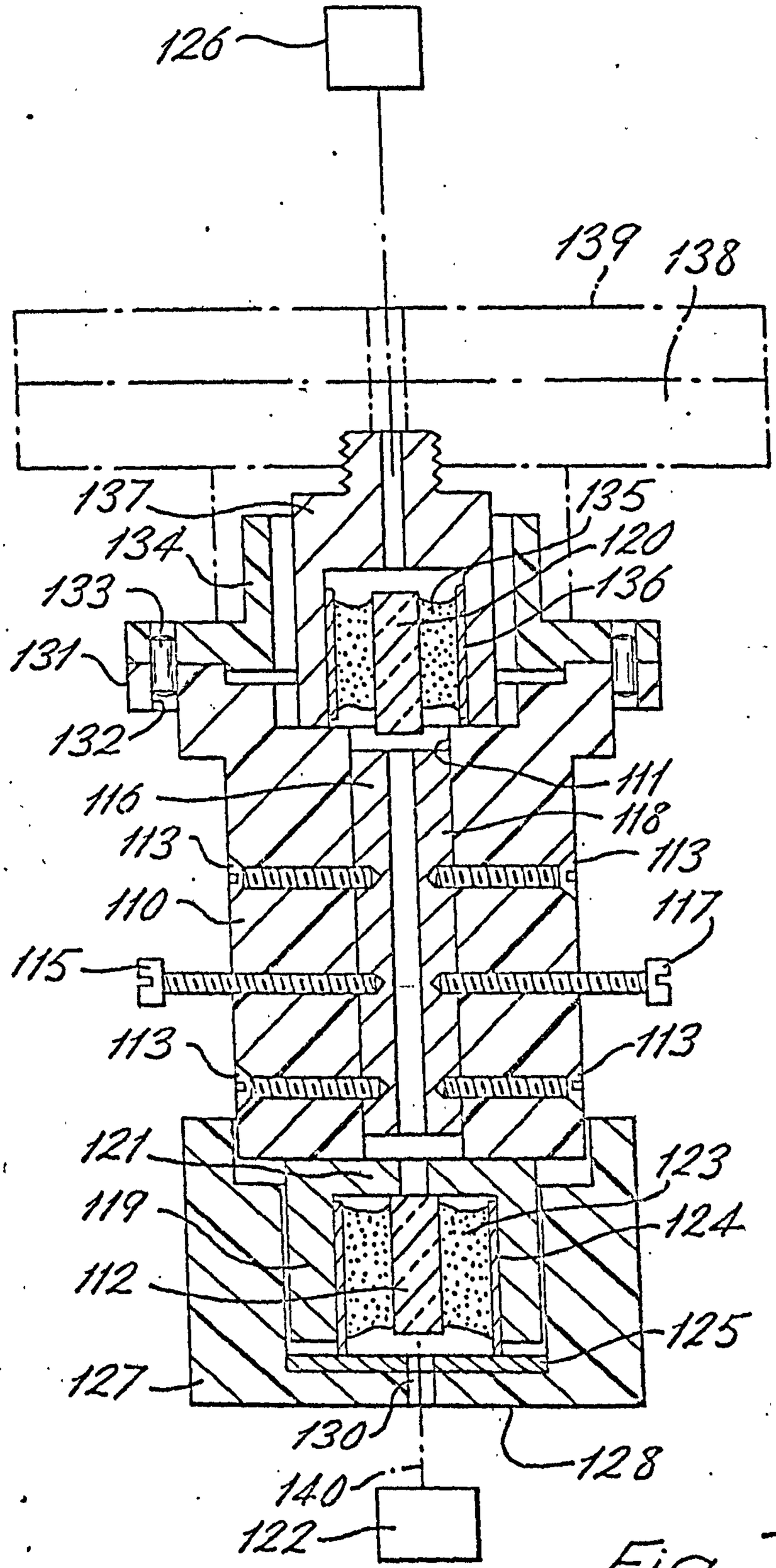

Fig. 3.9

courtesy of:

National Research Development Corporation

KEY - P.T.O.

110 PTFE Cell body
111 Cell filling area
112 Polarising prism
113 Screws holding electrodes in PTFE body
115, 117 Stainless steel screws enabling electrical connection to electrodes
116, 118 Stainless steel electrodes
119, 121 PTFE cap over prism
120 Analysing prism
122 Laser
123, 124 Polariser holder
125 Brass ring
126 Photomultiplier
127 PTFE shroud for polariser
128 Cell base
130 Hole for light to enter cell
131 Upper flange of cell body
132, 133 Locating stud
134 Flange for mounting analyser assembly on cell
135, 136, 137 Analysing prism holder threaded into divided circle
138, 139 Divided circle
140 Light beam

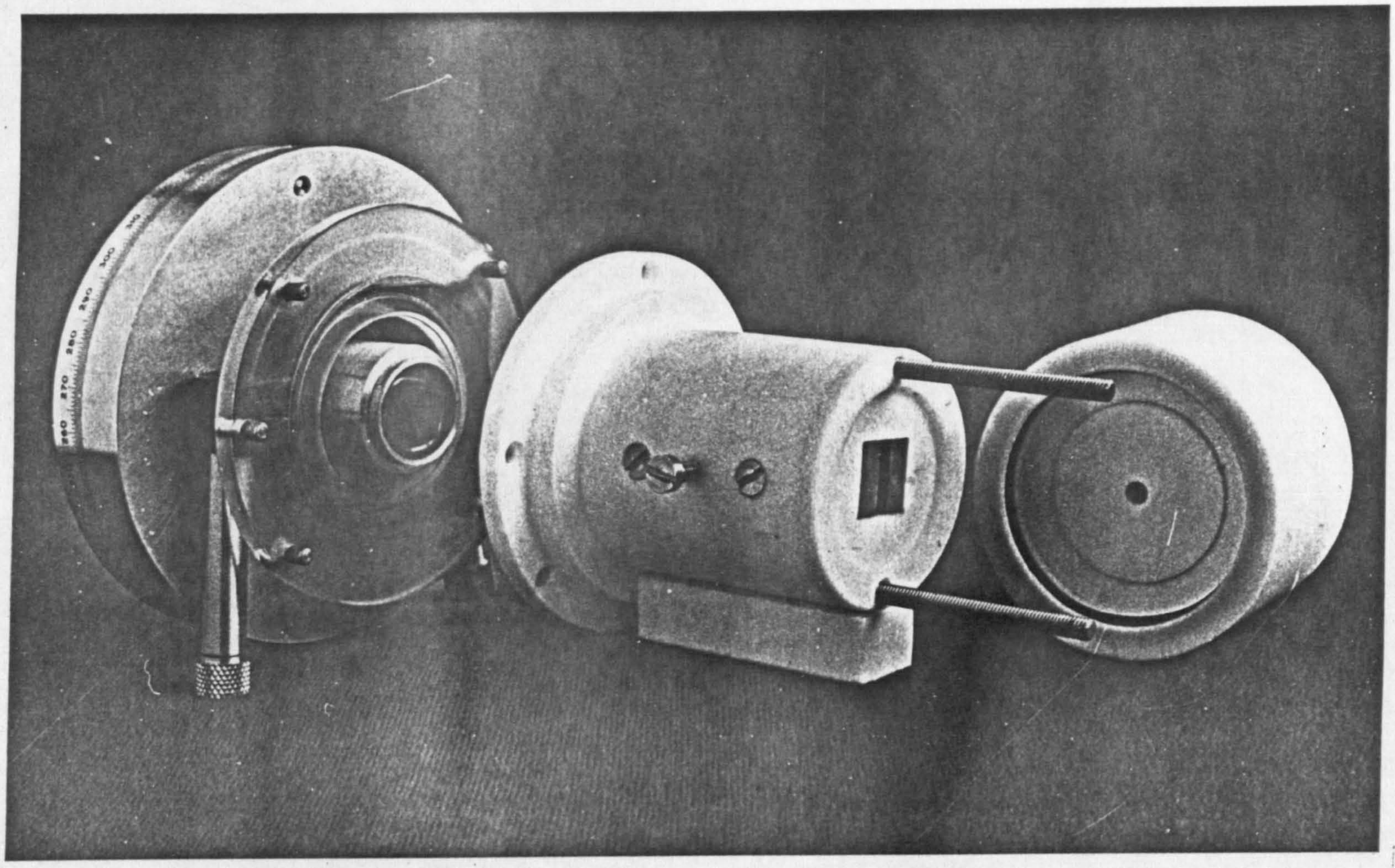

Fig. 3.10 An exploded view of the cell used in the new apparatus. On the right is the encapsulated polariser; supported in the centre is the section containing the electrodes. On the left, the analyser, mounted in its divided circle can be seen.

whilst a window of like diameter bares the upper face of the prism to the sample liquid. The particular arrangement chosen was tested for leaks before proceeding further. Using the specific plane polariser (section 3.33) the direction of polarisation of the prism within its shroud was determined and recorded, so that it could later be set at 45° to the direction of the field applied by the electrodes.

The main body of the cell has a 1.25 cm square hole through its centre to which a pair of stainless steel electrodes made to the normal specification are mounted. The electrode dimensions are:

Height	1.25 cm
Width	0.50 cm
Length	5.00 cm
Separation	0.25 cm

The top of the cell widens out to make a flange on which to mount the analyser prism or quarter wave plate. Locating pin arrangements determine a unique orientation of these components with respect to the initial polariser when it is bolted to the end of the cell. Above the electrodes, the cell widens out - within the flange - to permit the analyser or quarter wave plate to dip down into the solution.

The analyser is of the same type as the polariser and similarly coated with Magnesium Fluoride. It is mounted in a P.T.I. divided circle capable of

adjustment to half a minute of arc.

The quarter wave plate (Karl Lambrecht type WPM4L12) calibrated at 633 nm is mounted in its own specially fabricated holder which permits angular adjustment. Once set it should not require further adjustment. The plate is prevented from falling out of its mount by embedding it in soft wax.

For quadratic detection, the analyser is set crossed with respect to the initial polariser. The arrangement is such that rotation of the complete cell, with the analyser attached, maintains the quadratic set up. When changing to linear detection, the analyser locates in a perspex partition above the cell, and its orientation, with respect to the cell and initial polariser, is lost. The fixing on the quarter wave plate holder is therefore such that it only locates on the cell flange when the cell is orientated correctly for linear measurements.

Electric pulses from the generator are fed into the box via two H.T. terminals mounted on the outside, which lead via flexible connections to the cell.

3.47 Initial Measurements

A simple test has been made on a clay sample of Wyoming Bentonite. The first transient recorded on the apparatus is shown in Fig. 3.11. The relaxation time agrees with values obtained on the original horizontal apparatus. The quadratic field dependence is illustrated in Fig. 3.12. Note that these are the only measurements in this work which have been taken on the new apparatus.

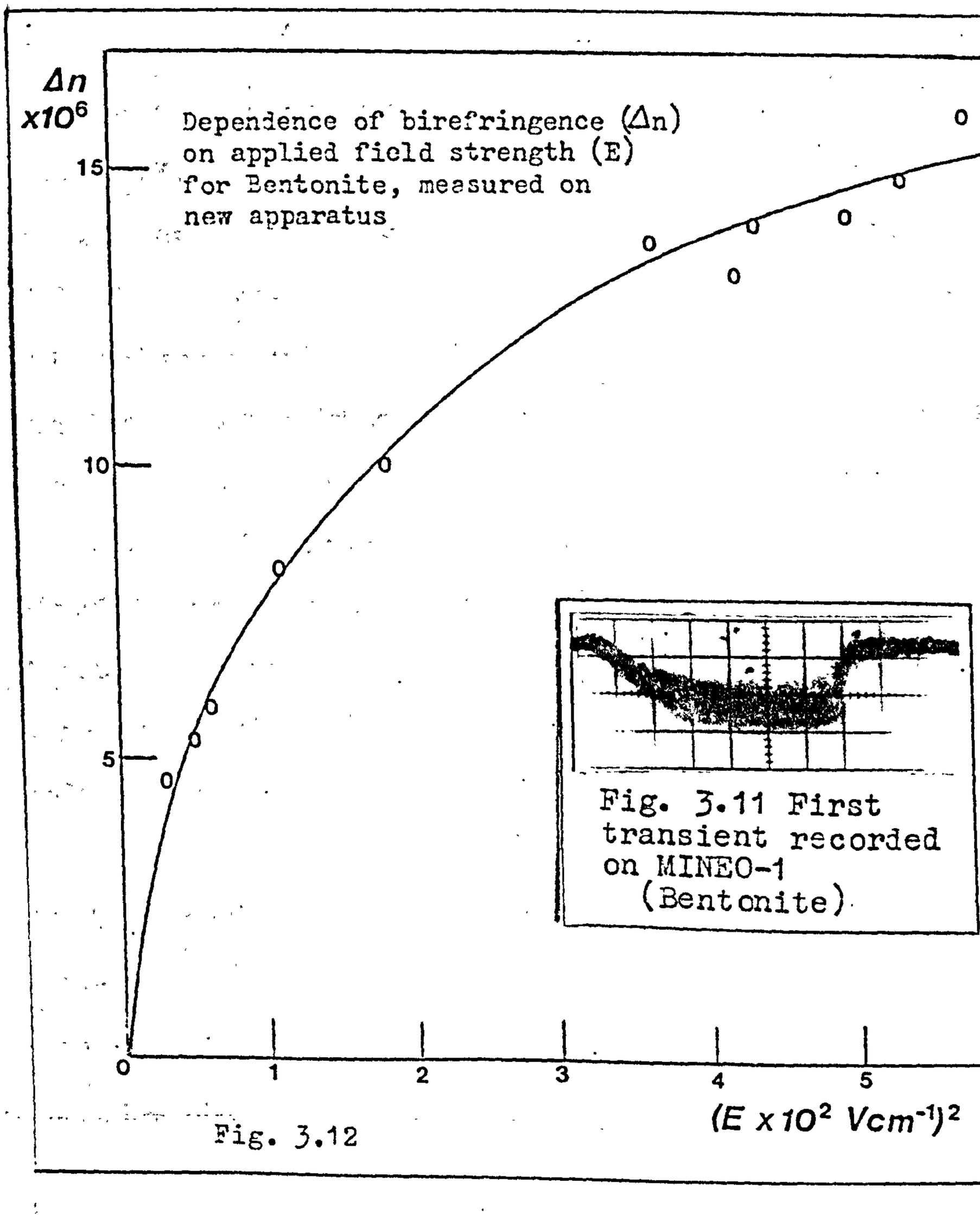

Fig. 3.11 First transient recorded on MINEO-1 (Bentonite)

Fig. 3.12

3.48 Sensitivity

The sensitivity of the system was determined by finding the smallest measurable voltage change which the apparatus was capable of detecting and relating this to a value of birefringence. The relationship between the sensitivity and voltage change can be obtained from a graph commonly used to measure I_o in quadratic detection (q.v. sections 2.92 and 3.22). From such a graph, the smallest measurable voltage can be read off in terms of a value of $\sin^2\theta$ and for small values $\delta \sim \frac{\theta}{2}$ whence

$$\Delta n = \frac{\delta\lambda}{2\pi l}$$

The graph obtained for the new apparatus is shown in Fig. 3.13. This was achieved with the detection and optical system set for maximum sensitivity, i.e. with the quarter wave plate inserted, the polariser and analyser crossed and maximum load resistance. The smallest change in measurable voltage observed on the oscilloscope screenwas noted as 1mV. Using the graph and above relationship, this yielded a value for the birefringence of less than 2×10^{-9}. This compares favourably with the value of 0.5×10^{-9} for the already sensitive original apparatus and commonly reported values from other workers.

It is probable that the value derived for this new apparatus could be improved further, though not with the compact laboratory designed *MINEO-1* apparatus. The following modifications are suggested in retrospect.

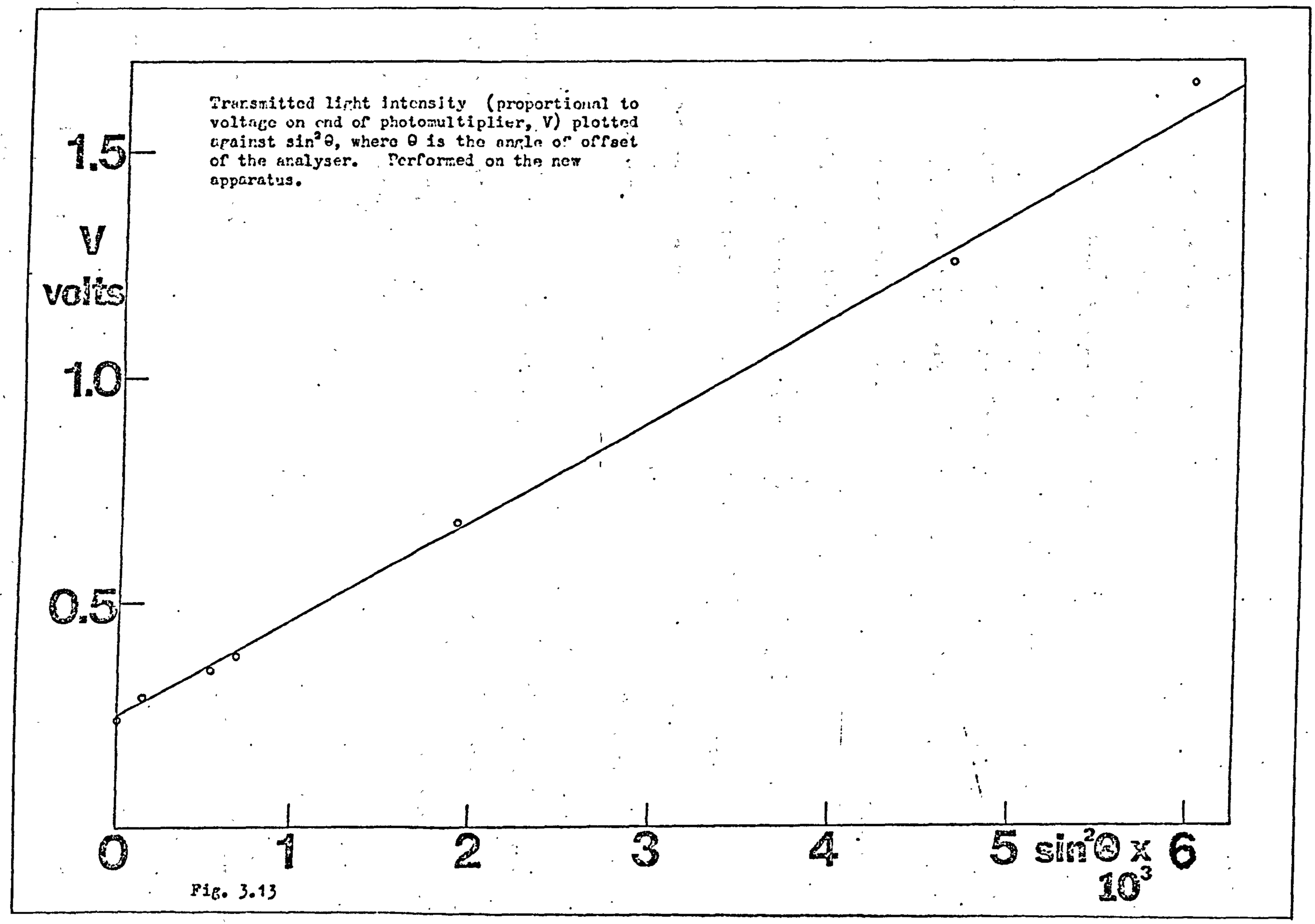
Transmitted light intensity (proportional to voltage on end of photomultiplier, V) plotted against $\sin^2\theta$, where θ is the angle of offset of the analyser. Performed on the new apparatus.
1.5
V
volts
1.0
0.5
0
1
2
3
4
5
6
$\sin^2\theta \times 10^3$

Fig. 3.13

1. The use of a blue laser (e.g. He Cd) would improve the sensitivity ($\Delta n \propto \lambda$).

2. Because in the existing *MINEO-1* the low power 2 mW laser beam has to be strongly attenuated by neutral density filters before entering the cell, it is evident that there is sufficient power to enable a longer cell length to be used, i.e. a greater length of solution for the beam to penetrate. Since $\Delta n \propto \frac{1}{l}$ this would improve the sensitivity too.

3. It should be possible to measure changes less than 1 mV, the inhibiting factor in this determination was the degree of noise. Improvements, such as cooling the photomultiplier base could help here, or using a more sensitive laser, such as the C W Radiation laser were it able to meet its specification.

These three factors together might result in as much as an order of magnitude or more, improvement in the sensitivity, if so desired, using the novel Kerr Cell design evolved in this work.

3.49 Conclusions and suggestions for further development

The new apparatus thus has the following advantages:

1. High sensitivity by virtue of the novel cell design.

2. Ease of use. It should require only simple adjustment. Most controls and connections are

accessibly mounted.

3. Compact, occupying only a minimum of laboratory space.

4. Relatively inexpensive. It is thought that similar instruments could be built and sold commercially at around £15,000 (1976 prices). A moderate cost when compared with X-ray machines and electron microscopes.

5. Durability. There is little that can be worn out in the apparatus, it has few moving parts. Most components are readily available and thereby replacable if necessary.

6. Adaptability. The design is readily adaptable and keyed to marketing on a modular basis. Choice of signal detector, cell and generator will be influenced by the application and the sensitivity required. Should the purchaser subsequently change his field of study alternative generators, detectors, etc. could be substituted on his existing apparatus.

In the light of experience, minor modifications to the original design are suggested by the author to further improve the ease of operation.

1. The provision of an automatic shutter to close over the hole leading into the photomultiplier compartment thereby protecting the tube from exposure to lighting in the room when the lower

compartment of the box is exposed.

2. Fabrication of the box from sections of ridged 'Dural' i.e. with a 'square wave' cross-section. Similarly aligned these would allow components to be slotted in anywhere in the length of the box.

The finished apparatus, readily suited to laboratory usage has been christened *MINEO-1*, short for *MIN*iature *E*lectro *O*ptics, with the numerical subscript in the hope of successors to the format.

SECTION 2

The work in this section is quite diverse in nature. The author has studied the application of theoretical models to flexible molecules in solution (Chapter 4). In Chapter 5, he has explored the interesting area of interfacial interactions on the well documented bacterium, E. coli, and the hitherto unstudied, yet fascinating material, polytetrafloroethylene. Chapter 6 examines an area of puzzlement in current research concerning the disagreement in values of the rotary diffusion constant derived from the two independent electric birefringent techniques of frequency dispersion and field free relaxation. Finally a possible solution to the problem of deciding between longitudinal and transverse dipole moments is offered.

CHAPTER 4

A Flexible Polymer: Nitrocellulose in Acetone

4.1 Objective of this Study

The conditions governing the applicability of current birefringence theory were discussed in Chapter 2. It will be recalled that these apply principally to rigid systems. Nonetheless, this has not inhibited the application of the theory to more flexible systems, and some of the equations derived for semi or completely flexible systems were also discussed earlier in Chapter 2. The objective of the work in this chapter was to choose a molecule known to be remote from the extremes of rigid and totally flexible conformation, and to see how far existing theories are able to describe it. The chosen molecule was the cellulose derivative, nitrocellulose, which is readily dissolvable in acetone. The importance of this polymer is now discussed.

4.2 Introduction to the Material

Cellulose is the main constituent of cell walls in the higher plants, and indeed accounts for one third of all vegetable matter in the world. The material consequently formed the nucleus for the study of organic chemistry and is still the object of intensive research as the most abundant and widely used organic chemical. It forms the raw material in many industries, with its derivatives used in the production of paper, cotton textiles, rayon, film, coatings, fuel and a myriad of other products.

It was in England in 1844 that John Mercer first used the process, now known as 'mercerising'. Cotton fibres are treated with caustic soda and nitrated to produce nitrocellulose and in 1846, the Swiss, Schönbein tried acid esterification techniques, which form the basis of the current commercial preparation.

Nitrocellulose has commercial applications in the lacquer, plastic and explosive industries. For the latter, a high degree of nitrogen content is required, approaching the theoretical maximum of 14.14%. In this state all six hydroxyl groups on the cellobiose unit are nitrated. The nitrated unit is shown in Fig. 4.1, esterification proceeding in the order 6, 6', 3, 3', 2, 2'.

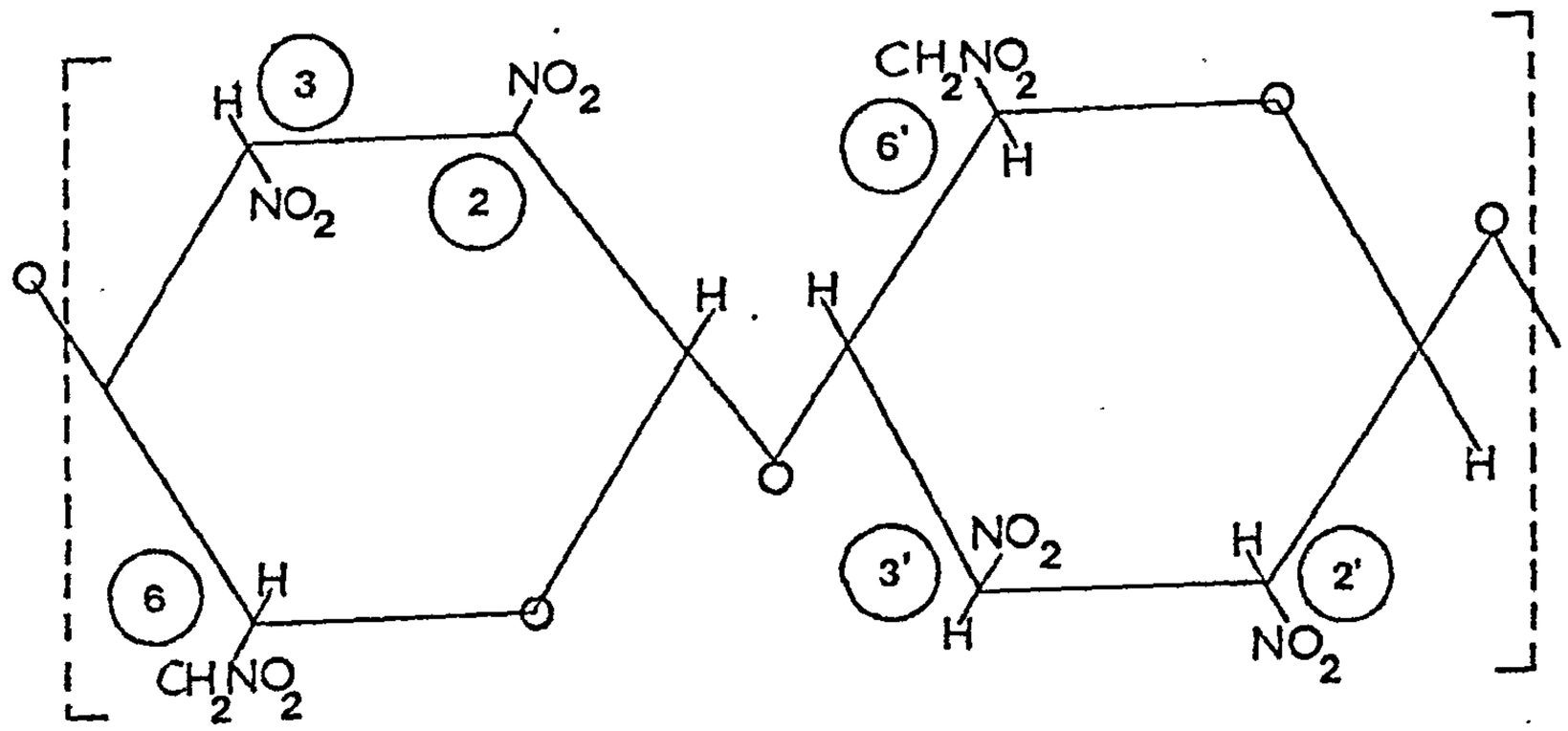

Fig. 4.1

The basic nitrated cellobiose unit.

Various techniques[41-43] have often been used to study nitrocellulose, of varying nitrogen content, in attempts to better understand the properties of cellulose and its derivatives. Recent electric field light scattering studies[44-46] have already shown the relatively large response of suitable solutions to electro-optic techniques.

4.3 Sample

The sample of nitrocellulose used was donated by Mr R Stadden of I.C.I. Ltd. The weight average molecular weight was 460,000 as previously determined by electric field light scattering.[46] The sample was the manufacturer's batch No. 245, stated to have a nitrogen content of 12 to 12.3% and prepared from cotton linters.

4.4 Sample preparation

Solutions were prepared by stirring for several hours in spectroscopically pure acetone (from Messrs B.D.H., Aristar brand) prior to filtration through Mitex 5μ Millipore filters (Type LS). A solution of concentration 7.68 $mgml^{-1}$ determined by evaporation to dry weight was used for these birefringence studies. It had a natural yellow-brown tinge.

4.5 Apparatus used

Cell A was used together with the He Ne laser and quadratic detection. DC measurements were made using generator PG4, with a 500 kΩ load resistor for amplitude measurements with pulses up to 0.5 ms duration. PG5 with a 50 Ω load resistor and 5 μs pulses was used for determining transient decay rates.

AC measurements used PG3 at 380 Vcm^{-1} (within the E^2 region), the 500 kΩ resistor and pulses ranging up to 0.3 s at low frequency, with the frequency range extending up to 35 kHz.

Independent determination of the solution's intrinsic viscosity, by the author, required the use of a Technico ASTMD 445 577 Ubberhölde Viscometer (nominal constant 0.01 cSs^{-1}). The capillary diameter was 580 μm corresponding to flow times of 80 s to 500 s. The temperature was controlled to 25.0 $\pm$ 0.5 °C.

4.6 Results

The solutions exhibited electrically induced birefringence which obeyed Kerr's E^2 Law (Fig. 4.2). The solvent contribution to the observed birefringence was negligible. From Fig. 4.2 a value of the Specific Kerr Constant, (section 2.2):

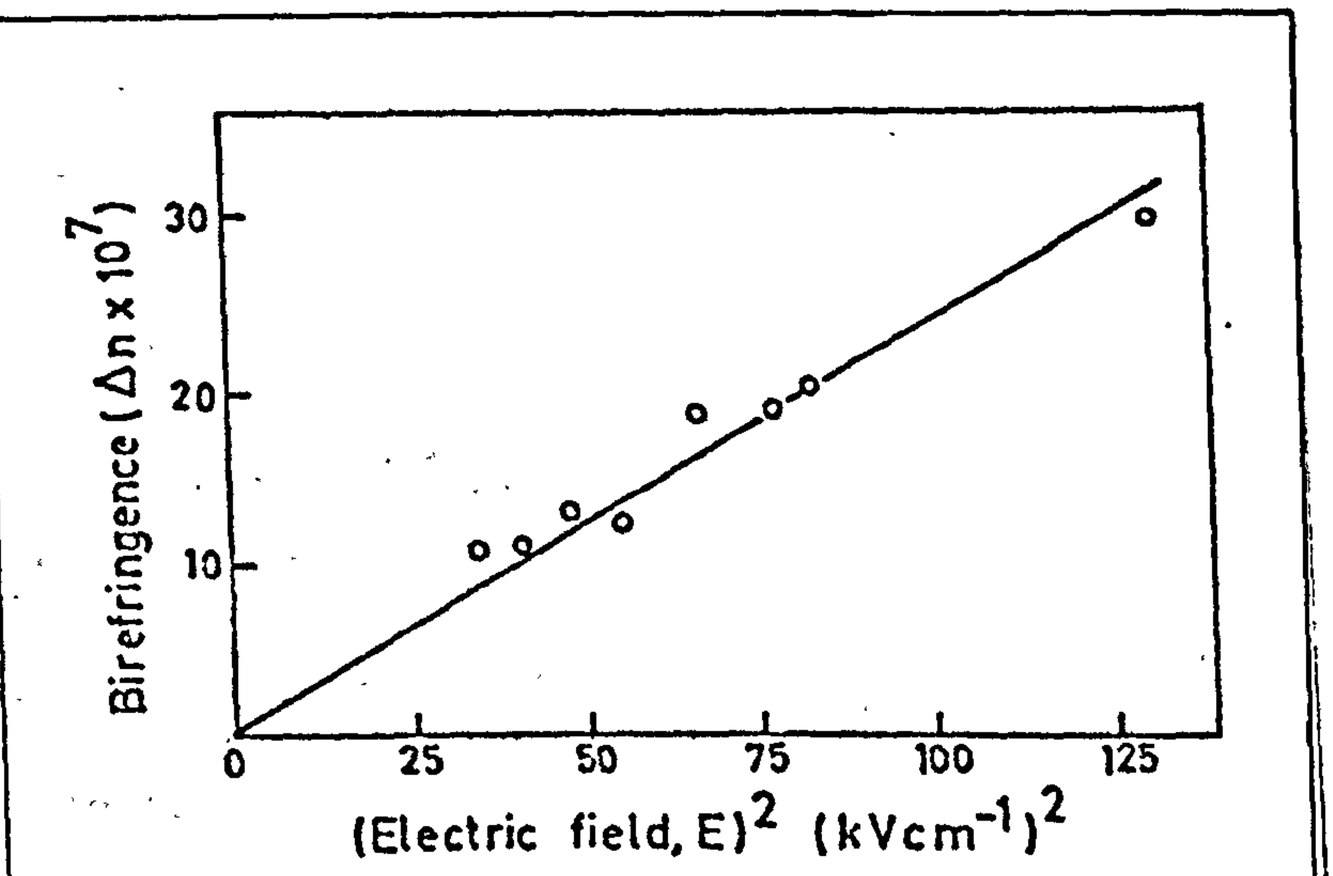

Fig. 42 Quadratic dependence of the birefringence on the electric field strength. Solution concentration of 7.7 mg. cm^{-3}, λ = 633 nm.

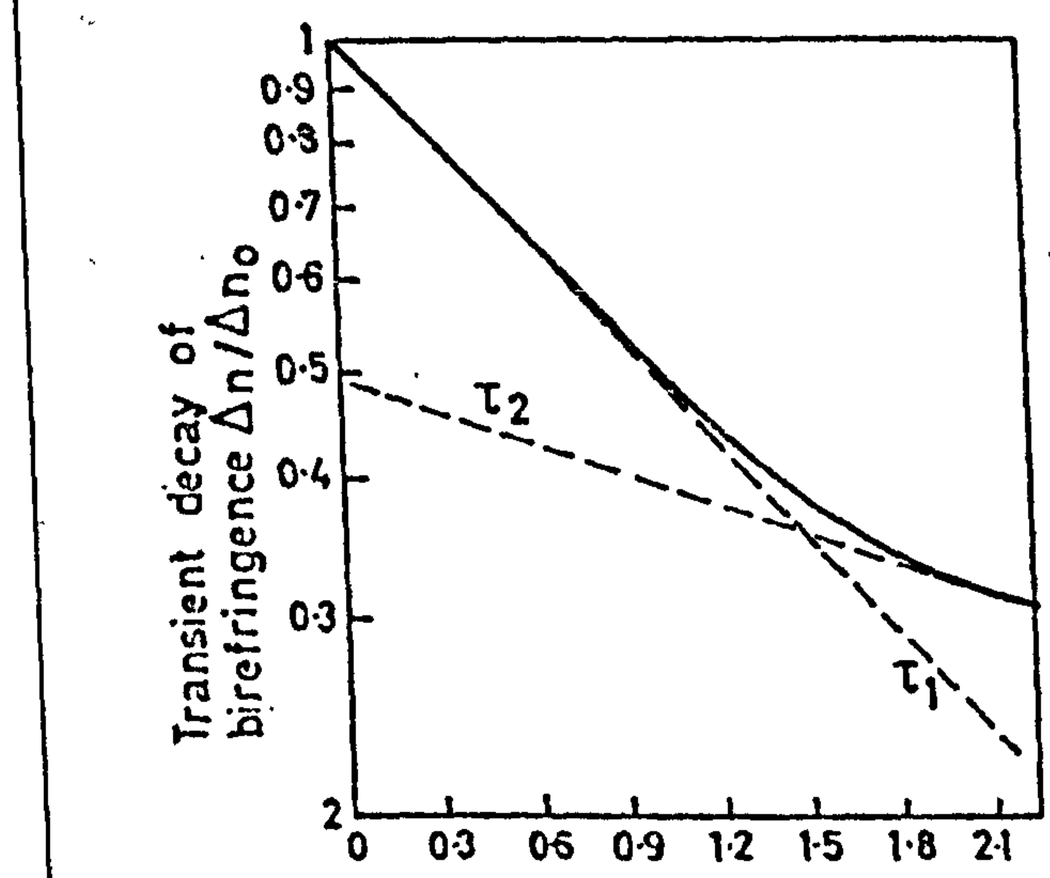

Fig. 43 Analysis of the transient decay of the birefringence. Data for c = 7.7 mg. cm^{-3} and E = 8.8 kV. cm^{-1} Tangents correspond to τ_1 = 1.6 μs and τ_2 = 5.0 μs respectively.

$$K_{sp} = \frac{\Delta n}{cnE^2\bar{v}} = 4.5 \times 10^{-16}\ V^{-2}m^2$$

was obtained.

The transient decay curves did not correspond to single component exponential decays (Fig. 4.3), but rather reflected the polydisperse nature of the sample. From Fig. 4.3, analysis of the decay data in terms of two contributions, indicates values of $\tau_1 = 1.6\ \mu s$ and $\tau_2 = 5\ \mu s$ corresponding to $3.3 \times 10^4\ s^{-1}$ and $10.4 \times 10^4\ s^{-1}$ for the respective rotary diffusion constants.

From the pulsed alternating frequency field experiments, the amplitudes of the induced birefringence could be analysed as a function of the frequency (Fig. 4.4) in much the same way as is customary in dielectric dispersion measurements. The critical frequency thus obtained leads to a value of $\tau = 5.7\ \mu s$ ($D = 2.9 \times 10^4\ s^{-1}$) treating the dispersion as Debye[47] type. This corresponds closely to the longer time component of the decay curve analysis. Whereas the breadth of the dispersion in Fig. 4.4 may display the polydisperse nature of the sample - as indicated by the theoretical Debye curves for single D values, encompassing the experimental data - the transient may indicate the polydisperse nature of the sample. The transient decay semi-logarithmic plot appears to be the more useful method for quantitative data on the polydispersity. Care should be taken not to treat τ_1 and τ_2 as

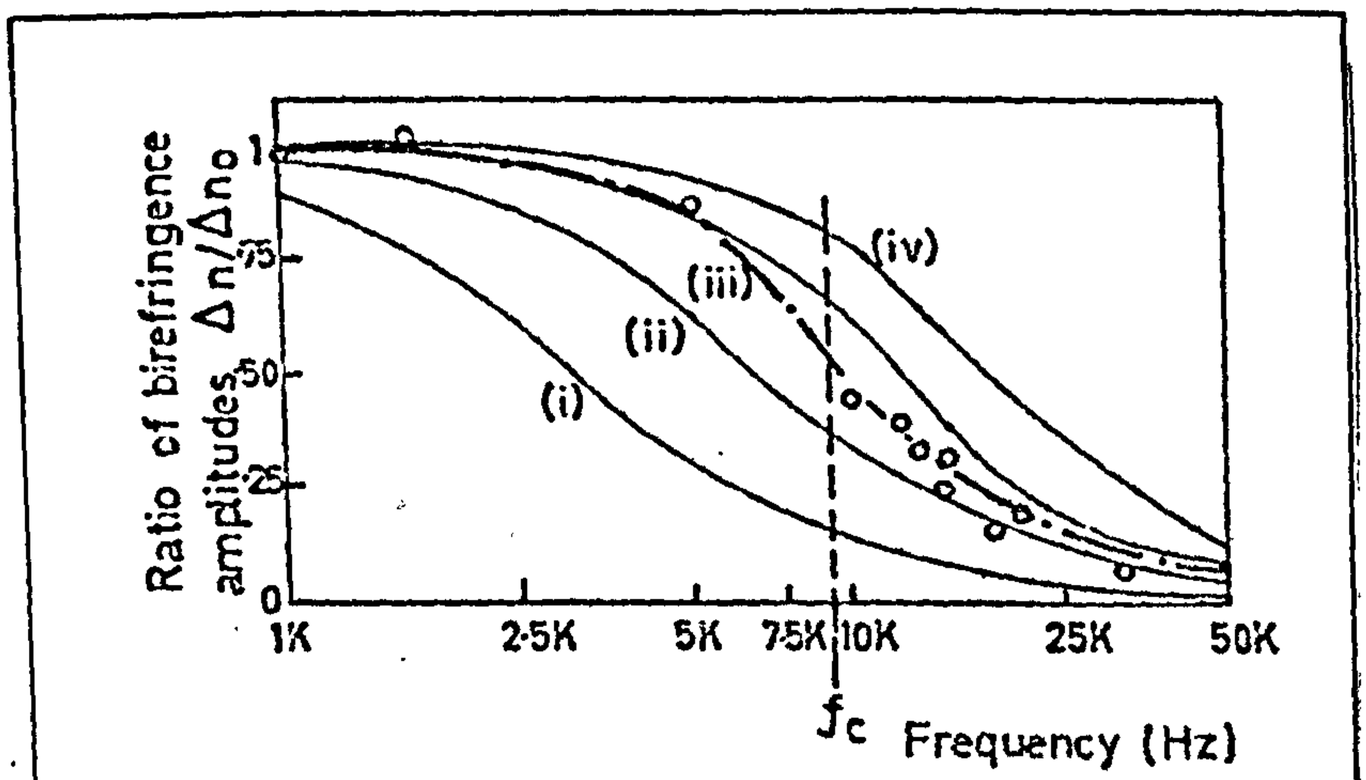

Fig. 44 Frequency dispersion of the birefringence amplitudes. Experimental data are for fields of root mean square strength 380 V. cm^{-1}. Theoretical curves are for single values of the rotary diffusion constant, D = 1, 2, 4 and 6×10^4 s^{-1} indicated by (i), (ii), (iii) and (iv) respectively. The critical frequency is indicated by f_c. Note that the monodisperse theoretical curves encompass the real data for the polydisperse sample

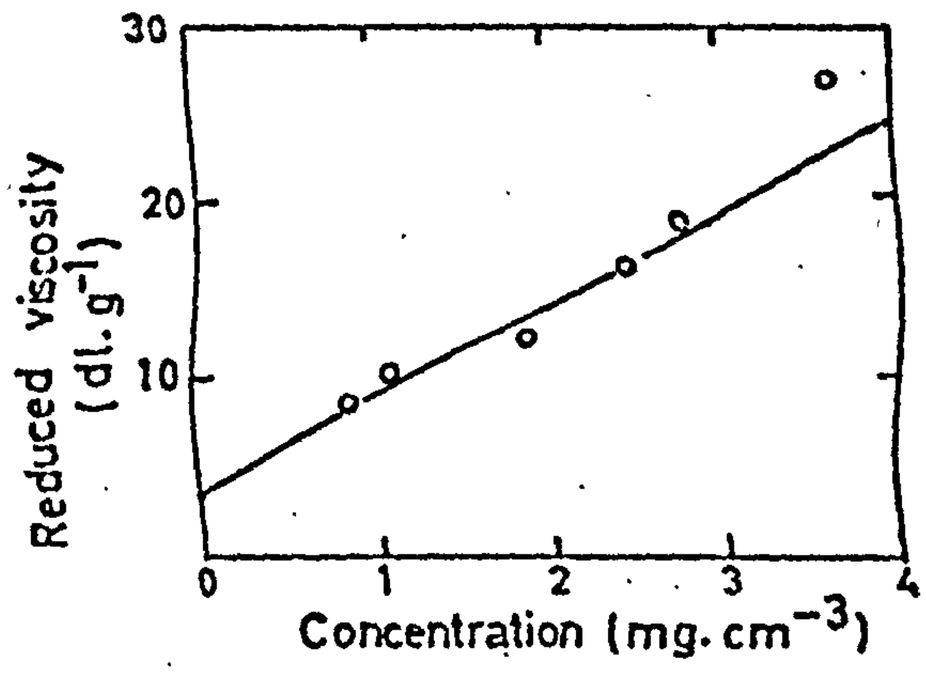

Fig. 45 Variation of the reduced viscosity with concentration. T = 25 (±0.5)°C.

representative of the largest and smallest particles present.[48]

Fig. 4.5 shows the plot of reduced viscosity varying with concentration. A value for the intrinsic viscosity of 3.5 dlg^{-1} was obtained from the measurements.

4.7 Discussion

4.71 Viscosity Data

The Mark Houwinck equation for molecular weight:

$$[\eta] = \kappa M^{a} \qquad (4.1)$$

is often used to evaluate M from measured $[\eta]$ and tabulations of the constants κ and a. κ is sometimes known as the Staudinger constant. There are over thirty different sets of values for the two constants for nitrocellulose in acetone (and equally as many for different solvents). The majority are listed in the 'Polymer Handbook'.[49] For the author's measured viscosity, they yielded values over the complete range $20,600 < M < 350,000$. The multiplicity of values is illustrated in Table 4.1, and clearly shows that great care must be taken in selecting values for the empirical constants κ and a. Values chosen at random could give wildly differing values for M. In this study, choice was narrowed by considering only those samples whose

A	κ.10²	a	[η]	T	%N	P	K	M
1	0.258	1	7.3-77	?	12.5	?	Osm	135 800
2	0.296	1	?	?	12.5	?	Osm	118 000
3	0.406	1	15-130	20	12-12.5	U	Osm	86 300
4	0.35	1	15-130	20	12-12.5	F	Osm	100 000
5	0.365	1	18.2-38.5	20	app 13.6	F	Osm	96 000
6	0.306	1	4.7-115.4	20	app 12.5	F	Osm	114 000
7	0.377	1	65-146	20	app 12.5	F	Osm	93 000
8	0.508	0.98	7.7-80	20	app 13.4	F	Osm	87 100
9	0.374	1	?	?	app 13.4	F	Osm	93 800
10	0.614	0.98	16.2-121	20	app 13.1	cotton U	Osm	70 800
11	0.722	0.98	17.6-120	20	app 13.1	pulp U	Osm	60 250
12	2.82	0.83	8-75	20	13.3-13.9	cotton F	Osm	85 100
13	4.37	0.82	10-70	20	app 13.5	pulp F	Osm	57 500
14	1.1	0.91	11.2-300	25	13.9	FU	Osm	89 125
15	0.42	1	11.2-68	25	13.9	FU	Osm	83 500
16	0.336	1	68-300	25	13.9	FU	Osm	104 000
17	105	0.516	35-65	?	13.8	F	Osm	72 450
18	0.378	1	62-245	25	13.8	F	Osm	92 700
19	1.12	0.91	12-285	20	13.8	?	Osm	87 100
20	0.713	0.933	10-150	25	14.1	F	Osm	107 150
21	0.62	0.948	10-180	20	13.8	F	Osm/SD	102 350
22	2.53	0.795	?	25	12.1	F	Osm	160 000
23	0.84	0.92	13.5-55.9	25	13.8	F	Osm	108 390
24	1.43	0.81	9.4-56.8	25	12.5	F	Osm	269 000
25	0.735	0.93	?	?	13.4	F	SD	107 150
26	0.863	0.91	39-502	?	13.8	F	SD	117 500
27	4.32	0.79	23.7-455	?	13.8	FU	SD	102 350
28	1.085	0.9	23.7-455	?	13.8	FU	SD	102 350
29	0.904	0.9	23.7-455	?	13.8	FU	SD	125 890
30	0.25	1	30-450	?	13.8	FU	SD	140 000
31	5.94	0.76	>120	?	13.8	FU	SD	22 900
32	0.282	1	<120	?	13.8	FU	SD	124 000
33	1.4	1	39-60	?	app 12	U	S	25 000
34	1.7	1	12.3-303	?	13.8	F	LS	20 600
35	0.377	0.95	9-180	25	13.8	F	LS-ba	175 000
36	1.66	0.86	17-52	?	13.8	F	LS	107 000
37	0.1	1	?	?	13.8	FU	LS	350 000

Table 4.1 Viscosity data for Nitrocellulose in acetone

KEY TO COLUMNS -

A Data set number
κ Staudinger constant
a Coefficient as defined in Mark-Houwinck equation
[η] Reduced viscosity range ($dl.g^{-1}$)
T Temperature (^{o}C)
%N Percentage Nitrogen content
P Technique of preparation resulted in:
F Fractionated sample
U Unfractionated sample
K Calibration method
Osm Osmometry
S Sedimentation
SD Sedimentation-Diffusion
LS Light scattering
LS-ba Light scattering in butyl acetate
M Resulting value for the MOLECULAR WEIGHT when combined with the author's data

degree of nitration was close to that of the sample used. These five are denoted in the table. In addition, data sets 7 and 33 were eliminated for having $[\eta]$ ranges an order of magnitude greater than the measured sample. Researching the original work of the denoted data sets showed the values quoted by Moore and Edge[410] (Data set 22) as appearing to be the most reliable, well documented and, moreover, representative of the majority of determinations.

Their equation involves a number average molecular weight, and with the experimentally determined value of $[\eta] = 3.5\ dlg^{-1}$ leads to a value of 160,000, denoted $\bar{M}_N$. Light scattering data from this laboratory have already established that the weight average molecular weight, $\bar{M}_W = 460,000$ for this sample.[46] A polydispersity of 2.9 : 1 is thus indicated for the sample.

From these viscosity data, three observations can be made. Firstly, had the parameters for κ and a suggested by Holtzer *et al*[43] been used, a weight average molecular weight of 230,000, half the true value, would have been indicated for polymer samples of the same nitrogen content. Thus their equation does not have the universal applicability that they claim. This is important as in the earlier electro-optic study on this particular sample, the measured value of $\bar{M}_W$ was used with the Holtzer *et al* data to obtain $[\eta]$ and use it in the analysis of τ values. The viscosity so used was

approximately twice the true value as measured in this work - the implications of this are discussed below. Finally, the exponent, $a = 0.8$, as determined by Moore and Edge,[410] is neither that for a rigid helix nor rod ($a = 2$) or for a freely flexible random coil ($a = 0.5$).[411] Some form of stiff coil is therefore indicated.

4.72 Relaxation Times

Broersma's equation for a rigid rod molecule (section 2.811) relates τ to the half rod length, a_1, viz:

$$a_1^3 = \frac{9kT\tau}{4\pi\eta_o} (\ln 2r - \Lambda) \qquad (4.2)$$

η_o, the solvent viscosity, is tabulated[412] at 0.324 cP. An initial value for a_1 of 100 nm was used and an iterative procedure used to obtain an ultimate value. This was used in conjunction with a rod diameter of 0.35 nm (from space filling models[46]) to obtain an approximate value for r, the axial ratio. Using

$$M = \frac{VN_A}{\bar{v}} \qquad (4.3)$$

where V is the rod volume and $\bar{v}$ the partial specific volume of this system has the value[413] 0.51 mlg^{-1} the largest relaxation time (smallest D) in this study is equivalent to a_1 = 61 nm and M = 14,000. This is clearly inappropriate and excludes this model for nitrocellulose in acetone.

For a free, flexible, polar random coil, the Zimm - Stockmayer and Baur equation (section 2.821) is considered, namely:

$$M = \frac{RT\tau}{f[\eta]\eta_o} \qquad (4.4)$$

Since the exponent of the Mark Houwinck equation suggests a non-free draining coil model as the most appropriate, f is taken as 0.85. Values of 5 μs and 1.6 μs for τ correspond to molecular weights of 128,000 and 41,000 respectively. Whereas these values are closer to the molecular weights ($\bar{M}_w$ = 460,000 and $\bar{M}_N$ = 160,000) of this sample than those obtained from the rod model equation, they are too small to be considered as appropriate. In addition, it should be noted that the apparent good agreement between experimental values of τ and the coil equation, 4.4, obtained in the previous electric field light scattering study,[46] was based on the data obtained from the Holtzer *et al*[43] viscosity relations. These have been shown, in the previous section, to lead to values of [η] and hence M, in equation 4.4, which are too large by a factor of two. It was therefore thought appropriate to study theories for models which are intermediate between the rigid rod and the flexible coil.

Two such models considered were the Weakly Bending Rod and Worm Like Chain, as detailed in sections 2.822 and 2.823, respectively. Using the values for the rotary diffusion constant (D) and molecular weight (M) obtained in this study, together with values of molecular weight per unit length (ρ) for nitrocellulose[41] of 5.56 x 10^{13} m^{-1} and assuming a circular molecular cross-section of radius 0.175 nm[46] the persistence length (q) as defined in

section 2.822 had values as follows. For the Worm Like Chain, q = 10.7 nm or 12 nm depending on whether $\bar{M}_w$ or $\bar{M}_N$ was used in the equations. The Weakly Bending Rod gave values of 1.5 nm and 11.2 nm using $\bar{M}_w$ and $\bar{M}_N$ respectively. It has not been possible to distinguish between these two models for nitrocellulose, but it has been noted that such values are always very low. Similar studies on other polysaccharides which are known to be stiff, but not rigid, coils, give q values of the same order of magnitude.[414,415]

It would appear that the relaxation times obtained from electro-optic experiments yield sensitive criteria which, in this particular study, enable one to reject the extreme assignments of the rigid rod on the one hand and the freely flexible coil on the other, to nitrocellulose of this molecular weight in acetone. Furthermore, they confirm the viscosity data and indicate the conformation of nitrocellulose in acetone is that of a stiff coil.

4.73 Dipole Moments

From Fig. 4.4, the birefringence amplitude reduces to zero at high frequency. This indicates that the molecules have a permanent dipole moment which at the lower frequencies tries to follow the field oscillations through a molecular tumbling motion. At sufficiently

high frequency, the viscosity of the medium and the molecular size prevent this. There is no significant induced dipolar mechanism as this would give rise to a non-zero higher frequency asymptote.

From space filling models, and the esterification of the cellobiose unit, it would appear that any resultant dipole moment from the nitro groups will act predominantly along the polymer backbone; the net dipole moment being greater the higher the degree of nitration.

Evaluating the magnitude of the molecular dipole moment is more difficult however, as a model and its related theory must be assumed. Three representative theories are conveniently available. These are for rigid cylinders or ellipsoids (Peterlin and Stuart, section 2.816), polar, flexible coils (Dows and Peterlin & Stuart, section 2.824) and rigid 'frozen' coils (Dows, section 2.825), respectively.

Jatkar and Sastry[416] have reported dielectric measurements on nitrocellulose of different degrees of nitration in a variety of solvents. They list dipole moments, that is of the cellobiose unit, of 4.0 and 4.7 debye (i.e. 13.2 x 10^{-30} and 15.5 x 10^{-30} Cm respectively) for polymer with 11.8% nitrogen content. The availability of these dielectric data provide an opportunity to evaluate the suitability of the three

models for this system.

For rigid, insulating, ellipsoidal particles, Peterlin and Stuart (section 2.816) predicted that:

$$K_{sp} = \frac{2\pi\bar{v}(g_1-g_2)\mu^2}{15n^2k^2\Phi^2} \qquad (4.5)$$

n is the refractive index of the solvent, tabulated as 1.362 for acetone.[412] (g_1-g_2) is the anisotropy of the optical volume polarisabilities (g) between the major (subscript 1) and minor (subscript 2) molecular axes for cylindrically symmetric or ellipsoidal molecules.

Tsvetkov[417] gives values of a segmental anisotropy factor $(a_{\parallel}-a_{\perp})$ for nitrocellulose, which he relates to (g_1-g_2) by the expression:

$$(g_1-g_2) = (a_{\parallel}-a_{\perp})\frac{N_A}{M_o\bar{v}} \qquad (4.6)$$

where M_o is the monomer molecular weight. From the value of the Specific Kerr Constant determined in this study, the molecular dipole moment, μ, is thus 2.7×10^{-30} Cm (815 debye). For a linear, extended or rod molecule, this corresponds to a monomer dipole moment, μ_o of 7.7×10^{-30} Cm (2.3 debye) or 2.6×10^{-30} Cm (0.8 debye) when M_N and M_W are used respectively. These are of the same order of magnitude as Jatkar and Sastry's dielectric values.

Dows' theory for flexible, polar, random coils in non-polar solvents (section 2.824) assumed that the constituent polymer segments (taken herein to be

monomer units in the first instance) experience uncorrelated freedom of rotation. His expression for the Molar Kerr Constant (see section 2.2), neglecting contributions from induced dipole moments, is

$$K_m = \frac{4\pi N_A}{405k^2T^2} \mu_o^2 \left(\frac{M}{M_o}\right) (a_{\parallel}-a_{\perp}) \quad (4.7)$$

Hence for such a flexible system, the theory predicts an observed birefringence which should be independent of concentration (within the limitations of the 'dilute gas' concept), molecular weight and polydispersity. Using 457 for M_o, this leads to a value of 1.5×10^{-28} Cm (44 debye) for μ_o. This is far too large for nitrocellulose.

Dows' alternative expression for the rigid 'frozen' coil, in which all the dipolar segments were considered as being orientated parallel to each other, has the form reported earlier in more detail (section 2.825):

$$K_m = \frac{4\pi N_A}{405k^2T^2} \mu_o^2 \left(\frac{M}{M_o}\right)^3 (a_{\parallel}-a_{\perp}) \quad (4.8)$$

Using $\bar{M}_N$ for M, a value of $\mu_o = 4 \times 10^{-31}$ Cm (0.13 debye) is obtained, whilst $\bar{M}_w$ would give a monomer dipole moment as small as 0.014 debye. Both of these results are far too small when compared with the dielectric data. It would therefore appear that the Peterlin and Stuart theory for the rigid ellipsoidal particle leads to values in closest agreement with the dielectric experiments, and is best able to account for the observed electric birefringence amplitudes, when a number average molecular weight is used in their equation.

A dipole moment per monomer unit of a few debye is in agreement with the previous electric field light scattering[46] and dielectric data.[416]

4.8 Conclusion

It is concluded that electric birefringence data indicate that nitrocellulose of high molecular weight and 12% nitrogen content, when dissolved in acetone, behaves as a very stiff, somewhat non-free draining, coiled polymer, whose monomer dipole moment is of the order of a few debye units. Transient electric birefringence measurements yield data on both the electric and geometric molecular data and appear to differentiate between rigid and flexible molecular systems. Whereas the experimental method is fast and sensitive, there is a need for theories better able to account for the region of intermediate flexibility between rigid rod and flexible chain extremes. More recent work[415] in these laboratories indicates an experimental method for classifying polymers in order of flexibility relative to each other. This work may lend further impetus to researching the theory required, but meanwhile serves as another useful tool in further exploring the grey area of intermediate flexibility.

The work in this chapter has been published in the Flory commemorative issue of the British Polymer Journal, and a copy appears in Appendix 1. (Brit Poly J, 6, 34-8, 1976).

CHAPTER 5

Interfacial Interactions

5.1 Turbidity Measurements of the Effect of Surfactant on the Bacterium, *E. coli.*

5.11 Introduction

Escherichia coli has been widely studied under the influence of electric fields[51-57] and is considered as a prolate ellipsoid of semi-major axis 2 μm and an axial ratio of 2 to 1.[58] As part of an investigative study on the effects of additives on bacteria by Dr V Morris of this group, the author was invited to study the effect of cetyltrimethylammonium bromide (CTAB) on *E. coli.*

Because of its size and resultant high scattering power, the bacterium is unsuitable for birefringence measurements[59] and light scattering is the study technique frequently employed. The author's birefringence apparatus can however be readily adapted to study the bacterium by the scattering related method of turbidity (conservative dichroism) and this is outlined later. Agreement between data derived from

electric field turbidity and light scattering has already been clearly shown.[510]

The measurements presented here demonstrate the extreme sensitivity of the induced dipole moment of the bacteria to the presence of small amounts of the additive, and possible explanations are discussed.

5.12 Experimental details

Dr Morris undertook the initial preparation of the sample : washing and centrifuging it, after warming it from its stored liquid nitrogen environment.[59] The encapsulated sample was supplied by the Microbiological Research Establishment, Porton Down. The prepared sample had an initial concentration of approximately 10^7 bacteria ml^{-1}. The concentration of the CTAB solution used was 0.698 mg μl^{-1}.

Four aliquots were prepared. The first, simply the initial bacteria solution, andthe other three with CTAB added in the ratios of 1 ml CTAB to 100 ml bacteria, 2 ml CTAB to 100 ml bacteria and 4 ml CTAB to 100 ml bacteria, respectively. Each preparation was looked at within ten to fifteen minutes of mixing.

Fields if 70 V cm^{-1}, known to be within the linear region of the quadratic field dependence of the sample's turbidity[511] were used throughout, supplied by generator PG3. The original He Ne laser, Cell B and a 500 kΩ load resistor on the photomultiplier completed the arrangement. However, both quarter wave plate and analyser were removed. Polarised light is therefore incident on the cell, is scattered by the solution, and that travelling in the forward direction ultimately falls on the photomultiplier.

5.13 Theoretical Background

The reduction in intensity, resulting from light being scattered out of the forward direction, is governed by the Beer Lambert Law, viz:

$$I = I_i e^{-Tl} \qquad (5.1)$$

where I is the light intensity incident on the photomultiplier, I_i that incident on the cell, l the length of the cell electrodes and T the turbidity of the solution.

With the field applied, these quantities can be represented:

$$I' = I_i e^{-T'l} \qquad (5.2)$$

Using the subscript 'o' to denote measurements made on bacteria with no added surfactant, the changes in turbidity on addition of the surfactant can be normalised with respect to the additive free condition, viz:

$$\frac{\Delta T}{\Delta T_o} = \frac{T' - T}{T_o' - T_o} = \frac{\ln (I'/I)}{\ln (I_o'/I_o)} \quad (5.3)$$

ΔT is proportional to the anisotropy of electrical polarisability (Δa) of the bacteria[510] and results are therefore presented in terms of the relative decrease of this quantity with increasing CTAB concentration.

5.14 Results and Discussion

The measured changes are shown in Fig. 5.1. They compliment the similar changes observed by Dr Morris in his electric field light scattering measurements using urea, alcohol and antibiotic additives. Dr Morris' measurements, which preceeded those of the author, are presented in the paper 'Electric Field Light Scattering as a Means of Studying the Effects of Additives on Bacteria' by Morris and Jennings in the Journal of Colloid and Interface Science, Volume 55, April 1976. The opportunity to include the present author's turbidimetric measurements in the report, was taken.

Measurements by both Dr Morris and the author followed the same observed pattern. As the concentration of additive was increased, there was an initial rapid decrease in $\frac{\Delta a}{\Delta a_o}$ tending to a limiting value at higher concentrations. Each additive resulted in a different limiting value for $\frac{\Delta a}{\Delta a_o}$. In the direct comparison drawn between the author's CTAB measurements and those of Dr Morris on urea and the antibiotics polymixin B

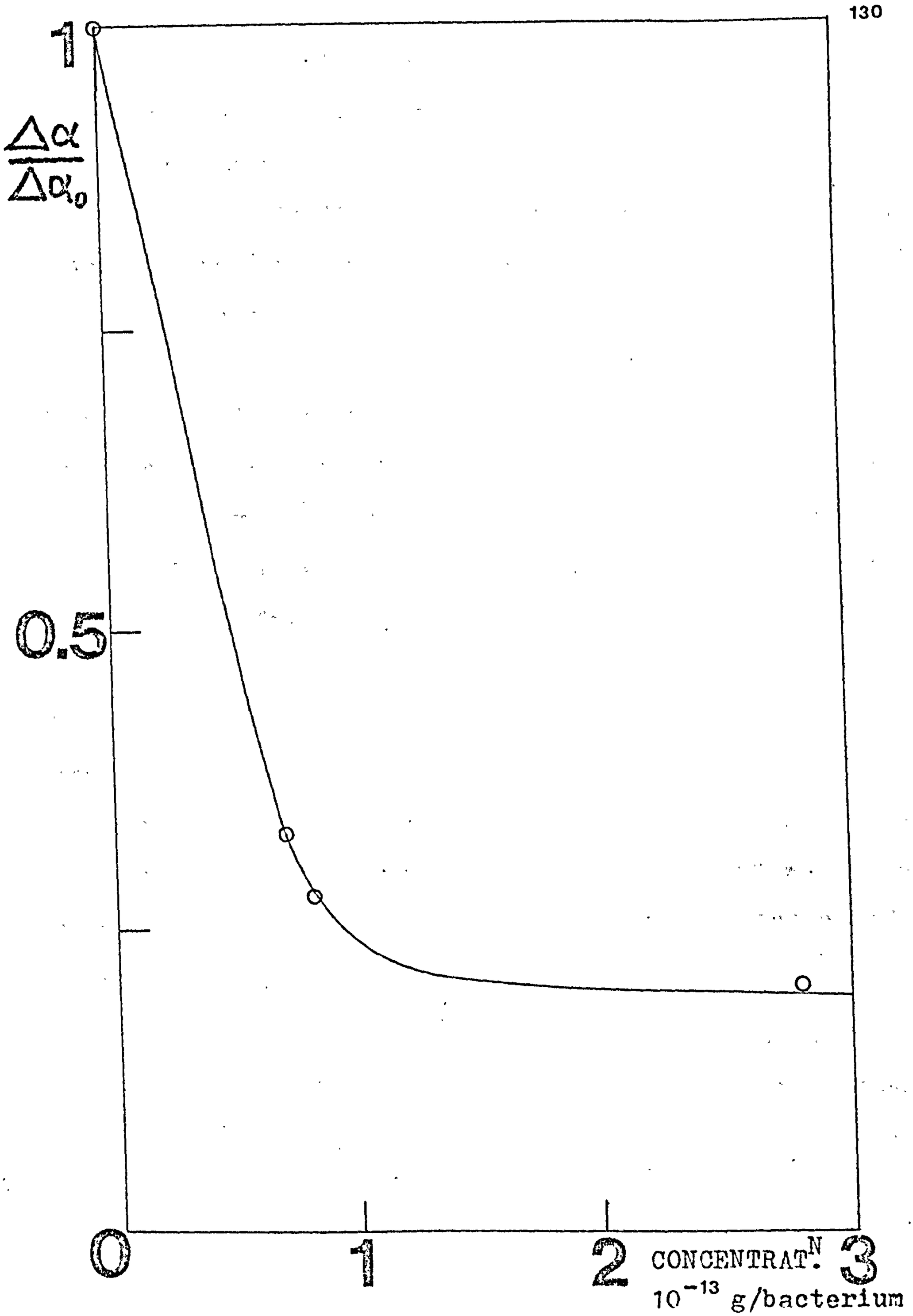

Fig. 5.1 Variation of relative electrical polarisability of E. Coli with concentration of CTAB.

and streptomycin, it was noted that a more rapid decrease in $\frac{\Delta a}{\Delta a_o}$ is observed with CTAB, even though its concentration was a factor of ten less at 10^{-14} g per bacterium. Note that in all measurements, Δa remains positive implying maximum polarisability is always along the major axis of the bacteria.

The family of curves for the different additives are similar to the Langmuir or monolayer isotherms of the physical chemist[512] which suggests that the changes in $\frac{\Delta a}{\Delta a_o}$ result from anaccumulation of CTAB molecules at the bacterial surface.

In their paper,[513] which also reports the action of fomaldehyde and sucrose on bacteria, Morris and Jennings suggest that Δa in aqueous solution arises from distortion of the counterion cloud associated with the bacterial surface from which three possible causes of the reduction in $\frac{\Delta a}{\Delta a_o}$ are deduced.

1. The effective neutralisation or a change in the number of ionised groups on the bacterial surface could lead to a reduction in the number of bound counterions.
2. The addition of tightly binding ions to the bacterial surface.
3. A reduction in the local dielectric constant.

For CTAB and other ionic additives, the data is currently insufficient to distinguish between changes in surface charge or changes in the dielectric constant.

The action of the additive itself could be one of two forms, either

1. Adsorption on to the surface (the limiting value of $\frac{\Delta a}{\Delta a_o}$ thereby implying a limited number of possible binding sites in each case).

2. Limited diffusion through the bacterial surface.

Both actions would result in a change in the local dielectric constant, and for a charged particle, the number of ionised groups would change. It is thought unlikely that CTAB would be able to penetrate the bacterial surface.

5.2 Exploratory Electric Birefringence studies on the Electrically Inert Material, PTFE

5.21 Introduction

Polytetrafloroethylene (PTFE) is well known and widely used as an insulating material. Indeed this property is put to good use by this research group in fabricating the variety of cells used for studying high field electro-optic effects. The material has strong internal bonding and is very dense; as such it is an unsuitable subject for study by electron microscopy or X-ray diffraction. It would be logical to think that a suspension of PTFE particles might also prove difficult to study by electric birefringence. There is the possibility, however, that in aqueous solution water dipoles are attracted to the environment of PTFE particles forming a charge layer within the vicinity of the particle's surface. Moreover, certain dipoles might actually locate on the PTFE surface. The expected random arrangement of these would not give rise to a permanent moment. The application of pulsed electric fields to such a suspension could therefore result in a birefringent response as the rTFE particles are oriented by the attached water dipoles and those influenced in the interfacial region. The suspected origin of this orientation mechanism could be verified by the addition of a surface active additive. An exploratory study is therefore reported.

5.22 Samples and Apparatus

Three samples were kindly supplied by Dr E Zichy of I.C.I. Plastics Division. These are designated A, B and N by the author. I.C.I. designated sample A as T30B and B as GP1. Sample N was a commercially prepared suspension called 'Fluon'. Each suspension contained about 60% solid, so diluted samples, approximately one part in 2,000 of distilled water, and exactly one part in 5,000 were used. B.D.H. Chemicals 'Analar' ethanol was used as an additive.

Generator PG4, delivering pulses of up to 12 ms duration, and resulting in a field of 4 kV cm^{-1} being applied across the electrodes of Cell A, the green line of the mercury arc lamp and quadratic detection made up the variables of the experimental apparatus.

5.23 Results and Discussion

At a concentration of one part in 5,000, typical transient responses of each of the three samples are shown in Fig. 5.2. Clearly the suspensions are birefringent, giving quite noise-free precise and discernable transient changes. Moreover, it is obvious that the method is able to differentiate between the three samples. The relaxation times are indicative of particle sizes in the range 0.1 μm

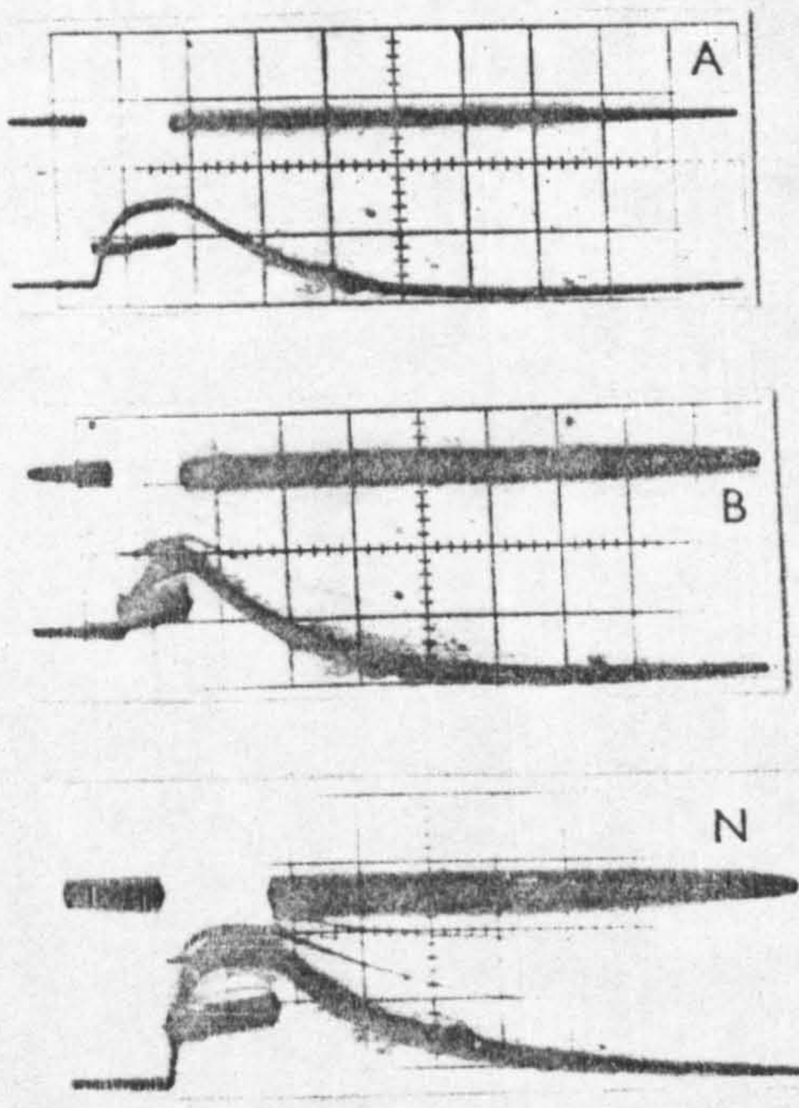

Fig. 5.2
The three PTFE suspensions: typical birefringent responses. Sample N behaving normally, but samples A and B exhibiting 'overshoot'. Scope settings for the three responses are:
A: 0.2 V/cm B and N: 0.05 V/cm

to 0.2 μm. It will be noted that samples A and B show 'overshoot' effects in their decay, i.e. the trace of the decay comes down below the base line, the condition when no field is applied. This could imply the formation of an agglomerate which changes the birefringence, and disrupts at a much slower rate than the disorientation of the isolated particles. However, in Fig. 5.3, it can be seen that the overshoot disappears from sample B on dilution by a further factor of ten. Therefore the overshoot could result from concentration effects.

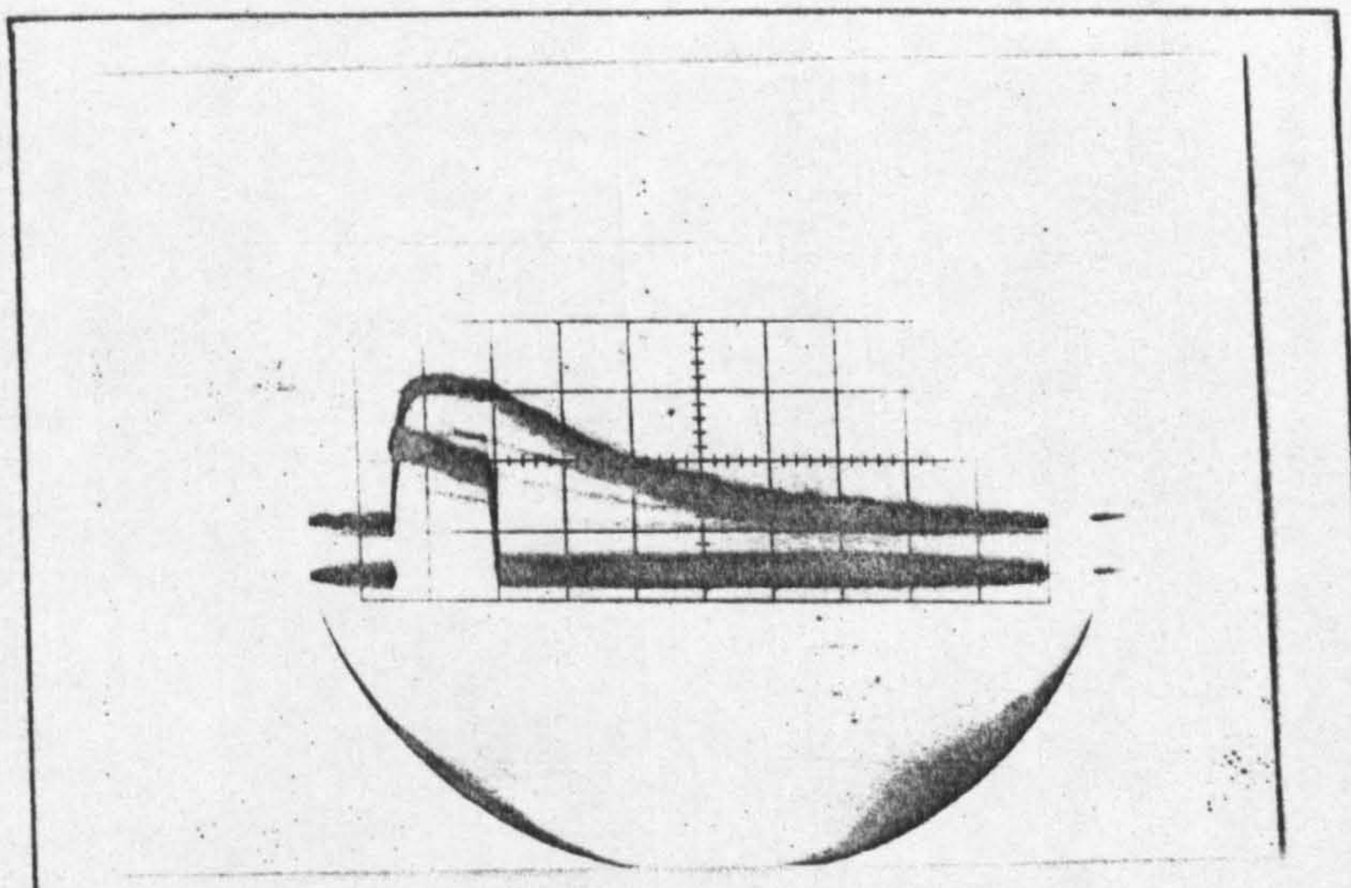

Fig. 5.3 PTFE sample B.
Dilution by a factor of 10
eliminates overshoot
(Scope setting for transient: 0.02 V cm^{-1})

Turning to the origin of the orientation, comparisons are made with the well-behaved responses obtained from sample N and the diluted sample B, (Fig. 5.4). The result of mixing sample N in equal parts with ethanol shows a four fold decrease in amplitude, where the change in concentration would only expect a halving of the effect. Diluting sample B with equal parts of water and ethanol, thereby obtaining a ten fold dilution of B as before, shows an approximate halving in amplitude consistent with the result obtained with N.

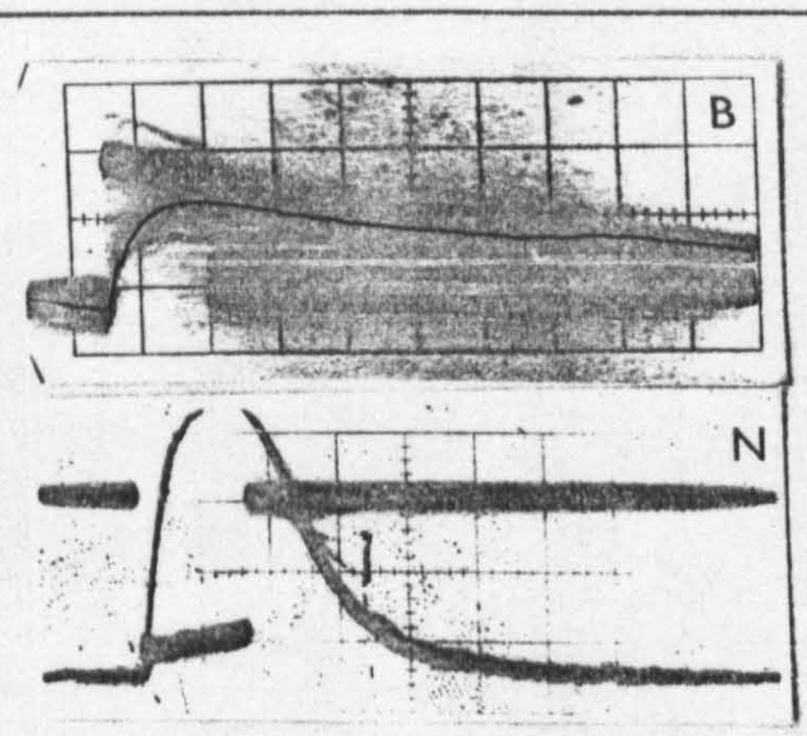

Fig. 5.4

The effect of alcohol on the birefringence of PTFE samples. Sample B is diluted by a factor of 10 in a 50:50 ethanol:water solution. (Scope setting for transient: 0.02 V/cm, cf Fig. 5.3) Sample N is diluted 50:50 with ethanol. (Scope setting for transient: 0.01 V/cm, cf Fig. 5.2 N).

A satisfactory explanation is as follows. The water dipoles attach to the PTFE surface and are oriented on application of an electric field. In turn, their alignment causes the motion of the PTFE particle as a whole and thereby giving rise to the observed birefringence. Surplanting the water dipoles with alcohol molecules absorbing to the particles' surfaces would explain the corresponding decrease in birefringence which occurs.

This proposal has subsequently been further substantiated by measurements observing decreases in birefringence consequent on the addition of flexible polymers to PTFE suspensions.[514] These polymers, in turn, would be expected to upset the attached water dipoles by similarly rivalling them for sites on the PTFE particle surface. The results were consistent with this hypothesis.

5.3 Conclusion

From the data on both *E. coli* and PTFE, it is evident that a powerful tool exists for studying the interfacial region of particles, macromolecules and bacteria in aqueous suspension. The author is pleased to record that an intensive investigation over a number of years is now started by Dr Morris in conjunction with I.C.I., using the electric birefringence technique.

CHAPTER 6

Attapulgite

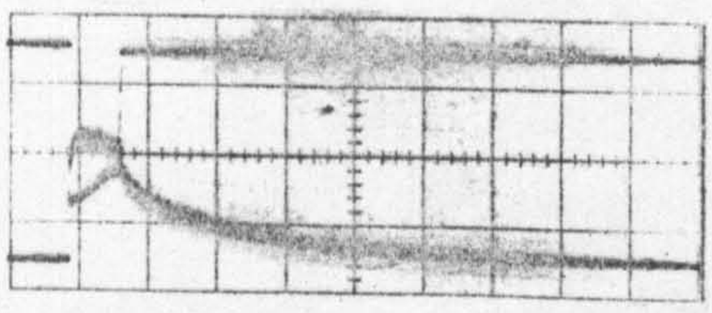

PBLG

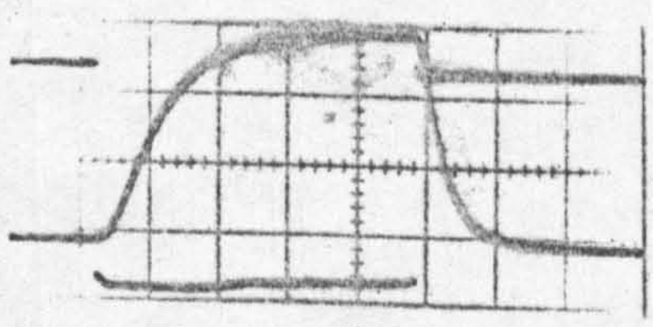

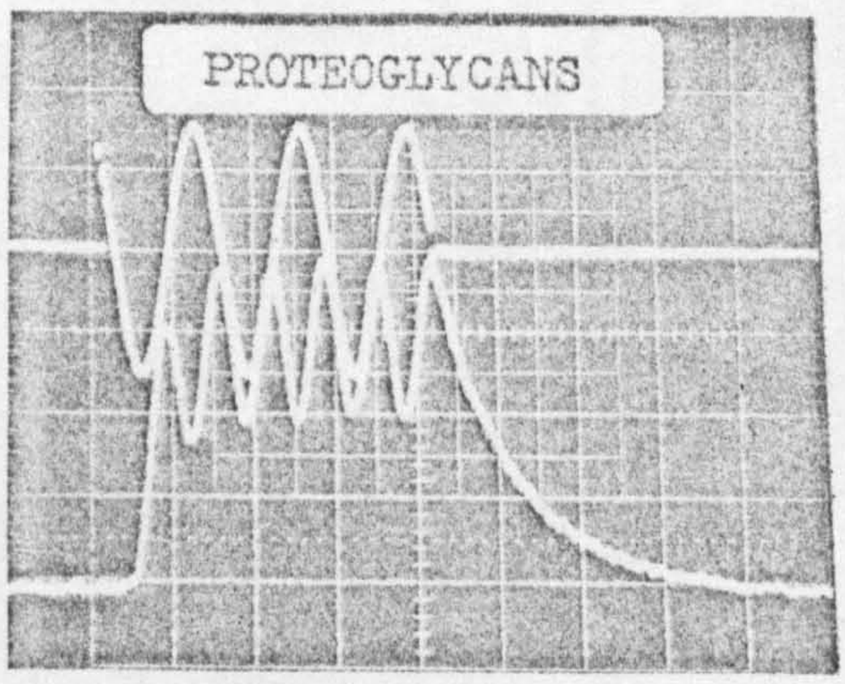

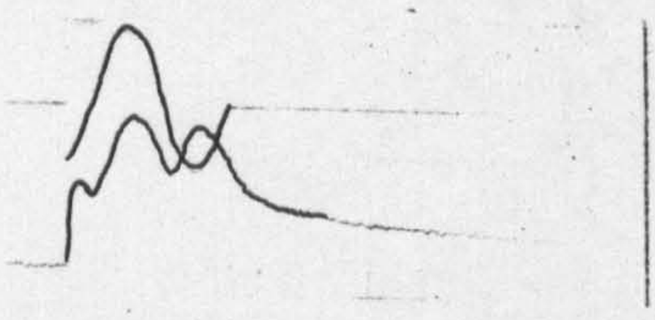

Kaolinite

Benzopurpurine

Comparisons of Independently Derived Values of the Particle Rotary Diffusion Constant

6.1 Introduction

The Rotary Diffusion Constant, D, is commonly derived from electric birefringence measurements by either or both of two methods, viz:

1. The decay time of a transient response resulting from the application of a DC or AC field, denoted herein as D_{tr}.
2. The critical frequency of an AC Debye type frequency dispersion of birefringence, denoted herein as D_{fd}.

Both methods have been used in this thesis. Attention is drawn to the discrepancy between the two values for both Nitrocellulose in Acetone (section 4.6) and proteoglycans in water (section 8.47). The author has therefore attempted to investigate a number of aqueous suspensions of a variety of materials to determine and then compare the rotary diffusion constants, D_{tr} and D_{fd}. In addition, the non-polar system, poly-benzyl-L-glutamate (PBLG) in dichloroethane,

has been studied for comparison.

6.2 Materials studied

Details of these are presented in Table 6.1

6.3 Experimental

The original He Ne laser is used for all materials except the blue coloured Copper phthalocyanine. To obviate absorption in the red by this sample, the blue, 436 nm line of the mercury arc lamp is used. Also, throughout the measurements, generator PG3 is used for all AC work. The pulse length is varied such that at high frequency the pulse is sufficiently long enough to achieve saturation orientation for the material concerned, i.e. of equivalent duration to the typical applied DC pulse. At low frequency the pulse duration is increased considerably to permit a minimum of one complete cycle AC to be applied to the suspension. All measurements pertinent to the calculation of the D_{tr} and D_{fd} values of the rotary diffusion constant are made in the region of linear dependence of birefringence on the quadratic field. Where this has not been known, the field dependence of the sample has been evaluated by the author.

MATERIAL	STRUCTURE	SHAPE	SIZE	ORIGIN	COMMENT
Laponite	Synthetic clay based on hectorite	Disc shaped particles	0.25μ-0.85μ diam. Ref 61	Dr B Neumann (Laporte)	Batch No EP5/CP
Kaolinite *	Alternate tetrahedral sheets of silica and octahedral sheets of alumina	Hexagonal flakes	0.3μ-4μ 0.05μ thick Ref 62	Dr Neumann, Laporte Industries, Redhill	Stabilised in solution with 0.0364% CTAB
Halloysite *	Alternate layers of Kaolinite and water. Maximally hydrated	Cylindrical Ref 63	Up to 1μ long Outer diam 0.07μ Ref 62	Dr Neumann (Laporte)	$(OH)_8 Si_4 Al_4 O_{10}.4H_2O$
Attapulgite *	Double silica chains oxygen linked at longitudinal edges	Elongated laths	Many microns long, 5-10nm wide Ref 62	Dr Neumann (Laporte)	
Tobacco Rattle Virus	Cultivated in tobacco leaves	Straight cylinders	Two size species, in size ratio 2 to 1. Smaller are 43μ-114μ Ref 64	Dr Dixon, Scottish Agricultural Research Institute	Dispersed in pH 7.1 phosphate buffer
E. coli	SEE CHAPTER 5				
Benzopurpurine	Red crystallite	-	-	B.D.H. 4B	Batch No 574700
Copper + phthalocyanine	Blue crystallite	Needle shaped	Several μm long Ref 65	Ref 65	Dispersed in water using a surfactant
Vanadium ▪ pentoxide	Yellowish crystallite	Rod	1μ (from emg)	Hopkins and Williams Ltd	
PTFE	SEE CHAPTER 5				
PBLG	Synthetic	α helix	150nm long (from emg)	-	Dissolved in BDH Analar 1,2 Dichloro-ethane (synonymous with ethylene dichloride)
Proteoglycans	Measurements and details drawn from Chapter 8				
Nitrocellulose	Measurements and details drawn from Chapter 4				

Table 6.1

Details of materials used in this study

KEY -

* Sample kindly prepared by Mr M L Bhanot
\+ Sample kindly prepared by Dr A R Foweraker
▪ Sample kindly prepared by Dr H J Coles
emg Electron micrograph

The varying experimental conditions for different samples are tabulated in Table 6.2.

To afford further comparison between D_{tr} and D_{fd}, the author is indebted to Mr R K Banerjee of this department for electron micrographs of some of the materials. For exact calibration of the magnification of the JEM7 microscope, polystyrene spheres of known radius are added to the suspension being so studied. From a micrograph, a value for the rotary diffusion constant (D_{emg}) can be obtained from the dimensions indicated and the use of the appropriate equation for the conformation of the particle (e.g. Perrin ellipsoid, Broersma rod, etc.).

D_{fd} is calculated from the critical frequency dispersion. This is the frequency at which the birefringence of the sample is half the difference of its maximum and minimum values (section 2.5). The rotary diffusion constant is then simply given by

$$D_{fd} = \pi f_c \qquad (6.1)$$

D_{tr} is calculated from a transient response resulting from the application of a DC field pulse of the same field strength as that at which the frequency dispersion is measured. The decay is analysed as indicated in Chapter 2 (section 2.7).

MATERIAL	CELL USED	DC PULSE GENERATOR USED	WITH OR WITHOUT ANALYSER OFFSET	MAX. PULSE LENGTH FOR DC PULSES	MAX. DC FIELD (Vom^{-1})	FIELD USED IN FREQUENCY DISPERSION RMS (Vom^{-1})	ORIGIN OF QUADRATIC FIELD DEPENDENCE OF SAMPLE'S BIREFRINGENCE IF NOT FOUND AS PART OF THIS WORK
Lepotilo	A	PG7	With	100ms	700	200	
E. Coli+	B	PG7	With	4ms	80	70	
Kaolinite	A	PG7	With	40ms	160	42.5	Ref 610
PTFE	B	PG7	With	10ms	42.5	42.5	
Tobacco Rattle Virus	A	PG7	With	30ms	83	83	Ref 611
Halloysite	B	PG7	With	30ms	1350	280	
Proteoglycans	B	PG3	With	10ms	635	350	Section 8.47
PBLG*	B	PG4	Without	1ms	7000	300	
Nitrocellulose*	A	PG4	Without	0.5ms	11500	380	Section 4.5
Attapulgite	B	PG4	Without	1ms	8000	DC only	
Benzopurpurine	B	PG4	With	1ms	4600	89	
Copper phthalocyanine	B	AC only	Without	100ms(AC)	AC only	600	Ref 65
Vanadium Pentoxide	B	PG4	With	1ms	1000	DC only	Ref 612

Table 6.2 Experimental variations with the different materials used in this study

KEY -
* non aqueous suspensions
+ turbidimetric measurements, fields correspond to those used by Rudd et al[68] and Morris et al[69]

6.4 General Observations and Discussion

Problems were encountered with certain materials in the study and are discussed below.

6.41 Indistinct dispersions

Certain materials in the study proved unsuitable for analysis as part of the D_{tr} and D_{fd} comparisons. The biggest problem occurs when the AC critical frequency of the Debye type dispersion is close to DC, i.e. less than about 5 Hz. When this occurs it is difficult to accurately determine the critical frequency anywhere in the range up to 5 Hz. This correspondingly puts no lower limit on the value of the rotary diffusion constant. This was evident for solutions of Kaolinite, and moreso for *E.coli*, Benzopurpurine and Copper phthalocyanine. For the latter, no dispersion could be found at all. Its response was very small at the 600 V maximum output of PG3 and remained unchanged throughout the range 1.5 Hz to 30 kHz.

6.42 The Field Dependence of Benzopurpurine

It is interesting to note that at low voltages, relaxation times of the order of 100 ms are apparent whilst above about 4 kV cm^{-1} relatively larger responses occur with a relaxation time of about 2 ms. This could indicate some form of disaggregation in the

field and the material is obviously worth closer investigation, but this does not form the object of the present study.

6.43 Solution Conductivity

With Vanadium pentoxide, DC measurements showed a high conductivity (as noted by a previous worker[612]) which put the system outside the voltage range of generator PG3 for AC measurements.

6.44 Observations on Attapulgite

Due to circumstances irrelevant to the object of this study, it was necessary to abandon the study of attapulgite at an early stage, and the halloysite clay was studied in lieu. The following observations on the birefringence of attapulgite are made:

1. From an approximate set of field dependence measurements, the birefringence is observed to continue increasing at fields approaching 10 kV cm^{-1}.
2. A typical transient response indicates a relaxation time of about 1 ms.
3. The transient decay indicates a polydisperse sample with a bias towards larger particles.
4. These results concur with light scattering data[611].

6.45 Laponite: Reversing Pulse application and Irregular Transients.

For Laponite, a reversing pulse applied to the suspension, revealed the presence of a permanent as well as an induced dipole moment, and an approximate value of D is obtained (section 2.6) from

$$D = \frac{0.2747}{t_{min}} \qquad (6.2)$$

which gives $D = 115\ s^{-1}$.

Transients of Laponite did not display the characteristics of 'blip' or 'droop' reported by Scweitzer and Jennings[612] and Jennings *et al*,[61] respectively.

6.46 Unusual Double Frequency Component with PTFE Suspensions

AC pulses applied to suspensions of PTFE produced an unusual form of the double frequency component on birefringent responses. Alternate peaks of the double frequency ripple on the transient varied in amplitude. A similar effect has been noted by Coles and Watanabe[613] on some liquid crystal solutions and Tobacco Mosaic Virus - they suggest that these may be field dependent in origin when outside the region of quadratic field dependence.

6.47 High Frequency Anomalies with PBLG

An unexpected increase in birefringence of PBLG was observed above 80 kHz i.e. after the normal frequency dispersion. No reasonable molecular interpretation can be given, though the effect was reproducable. This could be some facet of the instrumentation at these high frequencies. For example, a change in the amplitude of output voltage could account for the observed effect. This was, however, recorded as constant throughout.

6.5 Quadratic Field Dependence of Materials and Their Frequency Dispersions

Figures 6.1 to 6.12 illustrate the field dependence of the materials for which definitive measurements were made as part of this study, together with a complete set of frequency dispersions.

6.6 Results Pertinent to the Required Rotary Diffusion Constant Comparisons

In Table 6.3, the results and other parameters considered relevant to drawing comparisons between D_{tr} and D_{fd} are collated.

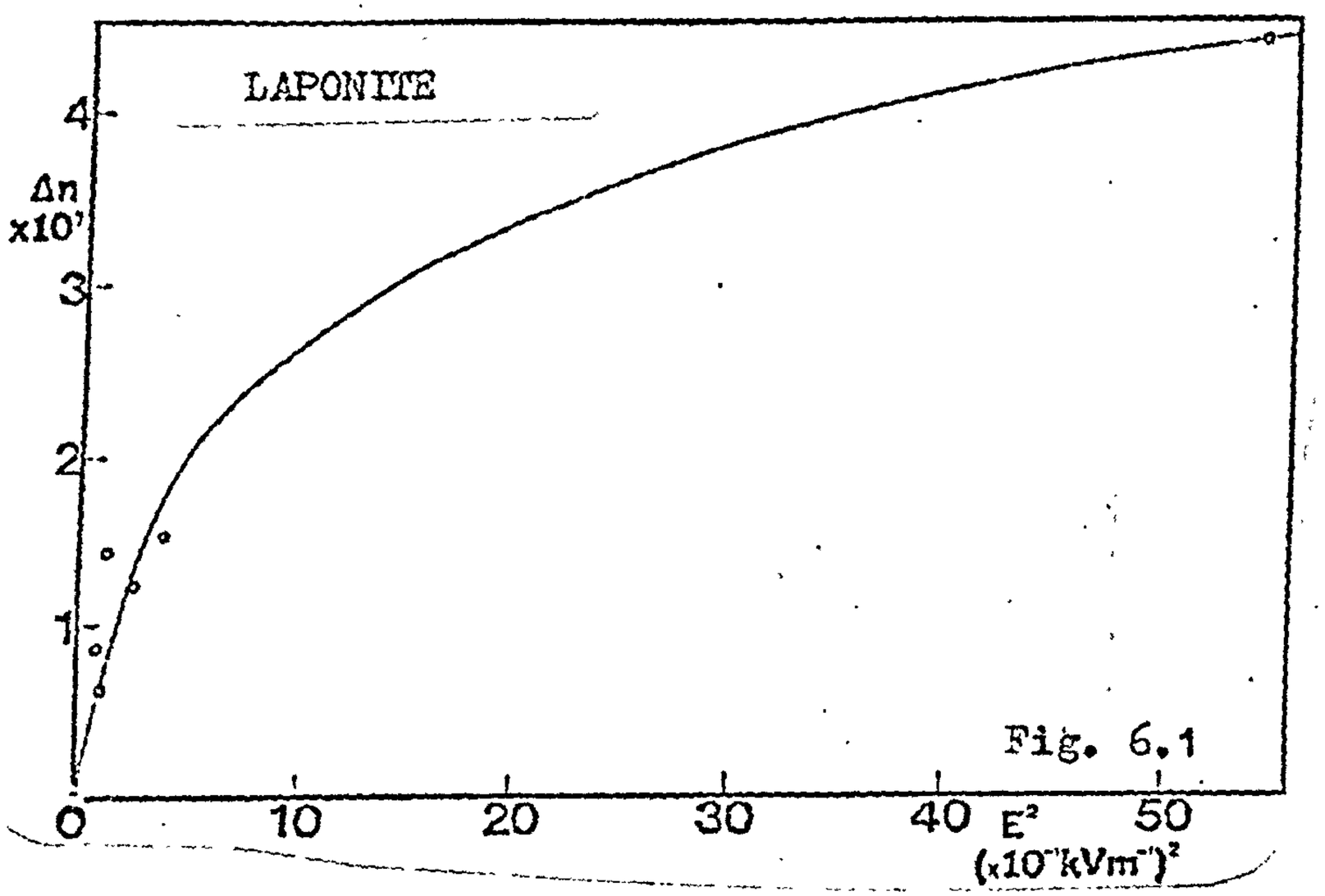

Fig. 6.1

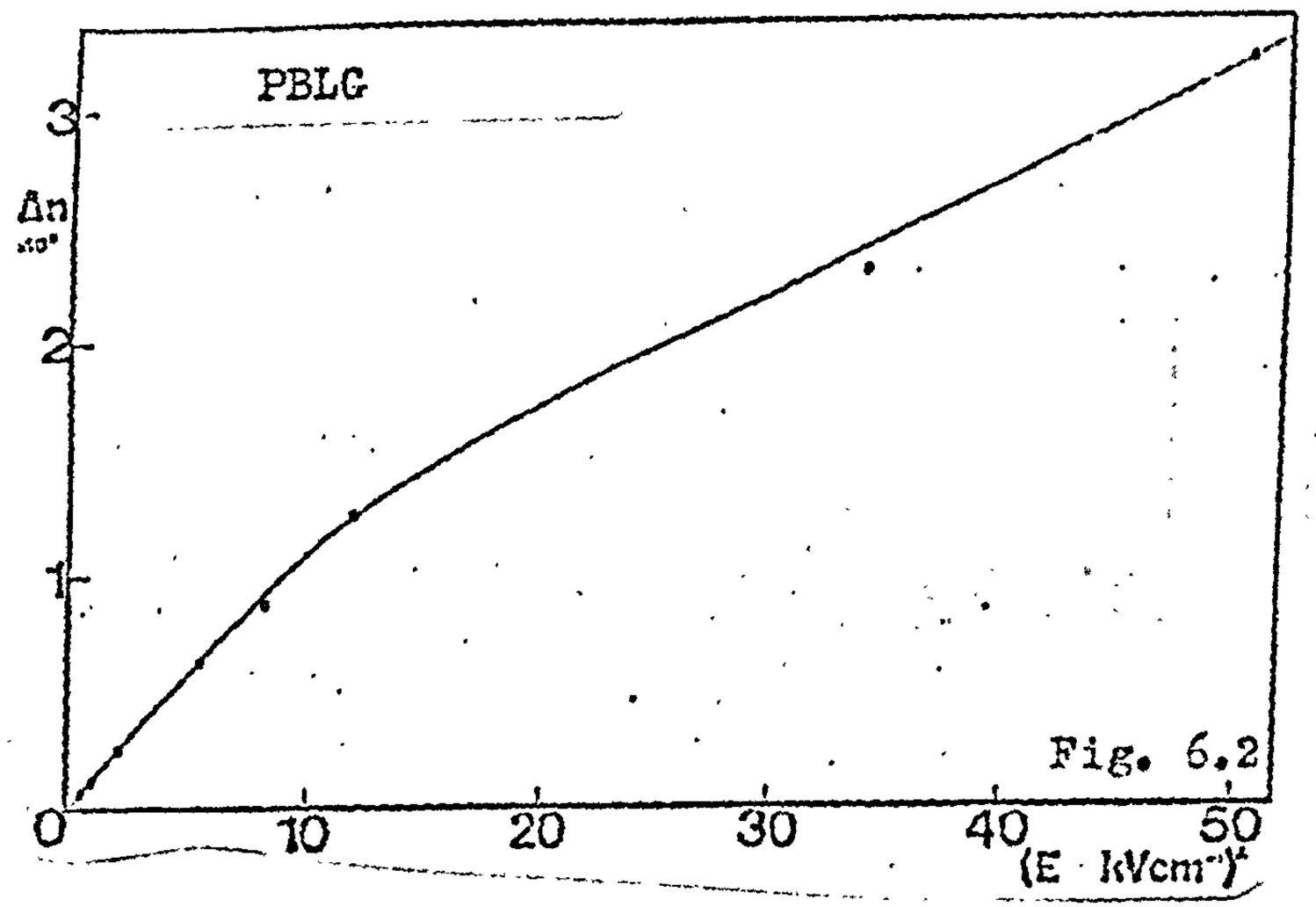

Fig. 6.2

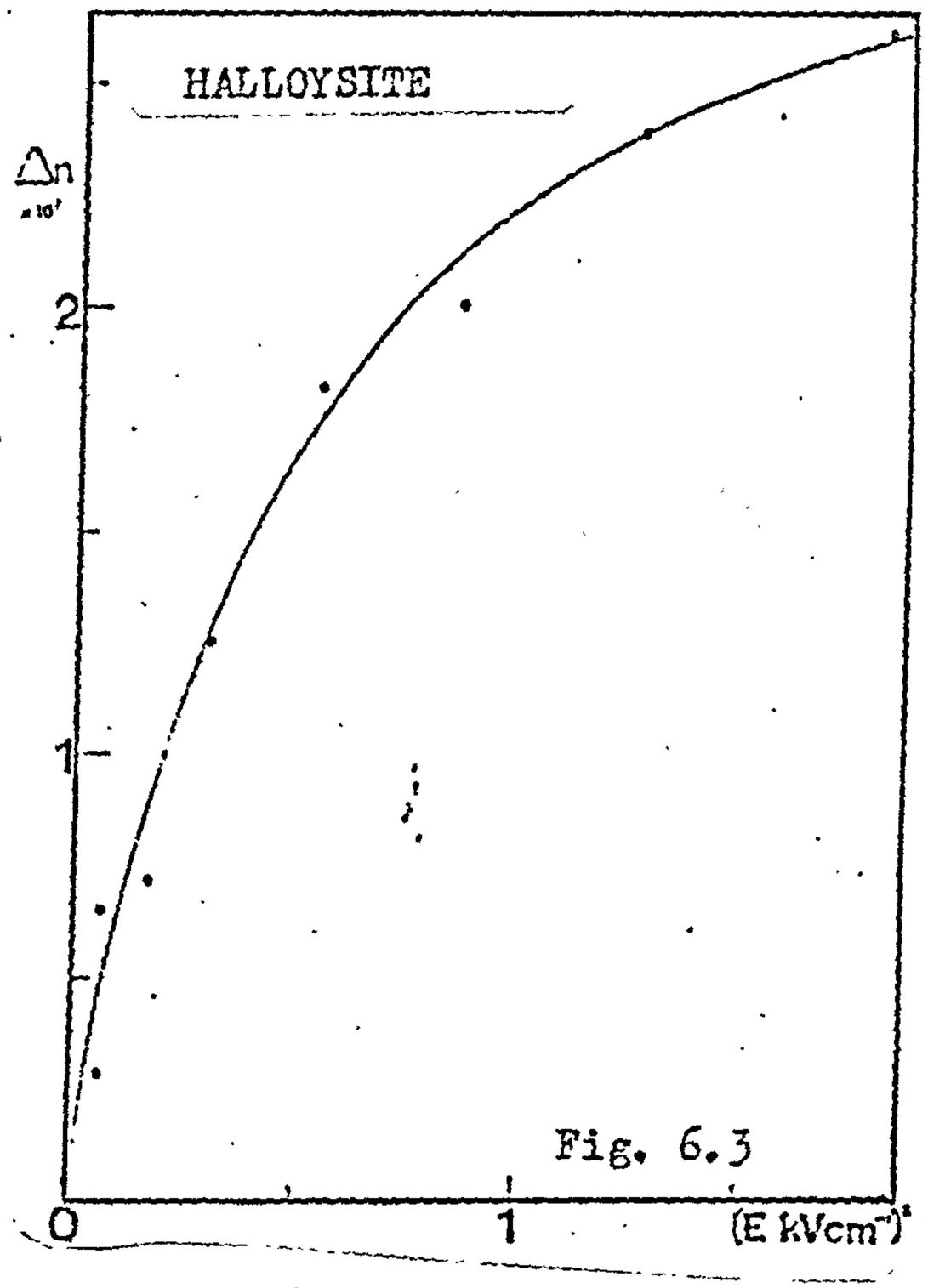

Fig. 6.3

Figs. 6.1 - 6.3

Dependence of birefringence (Δn) on applied field strength (E)

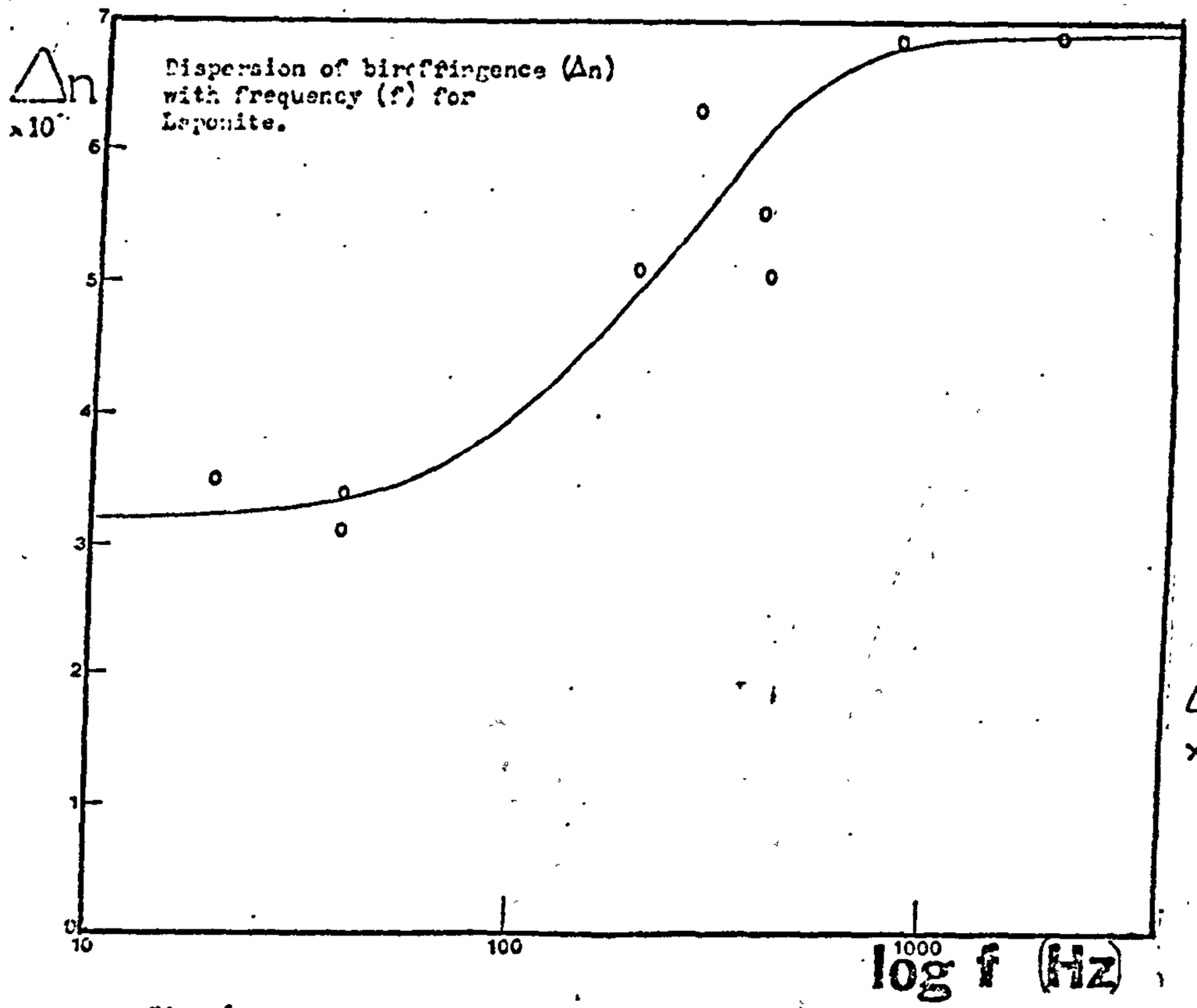

Fig. 6.4

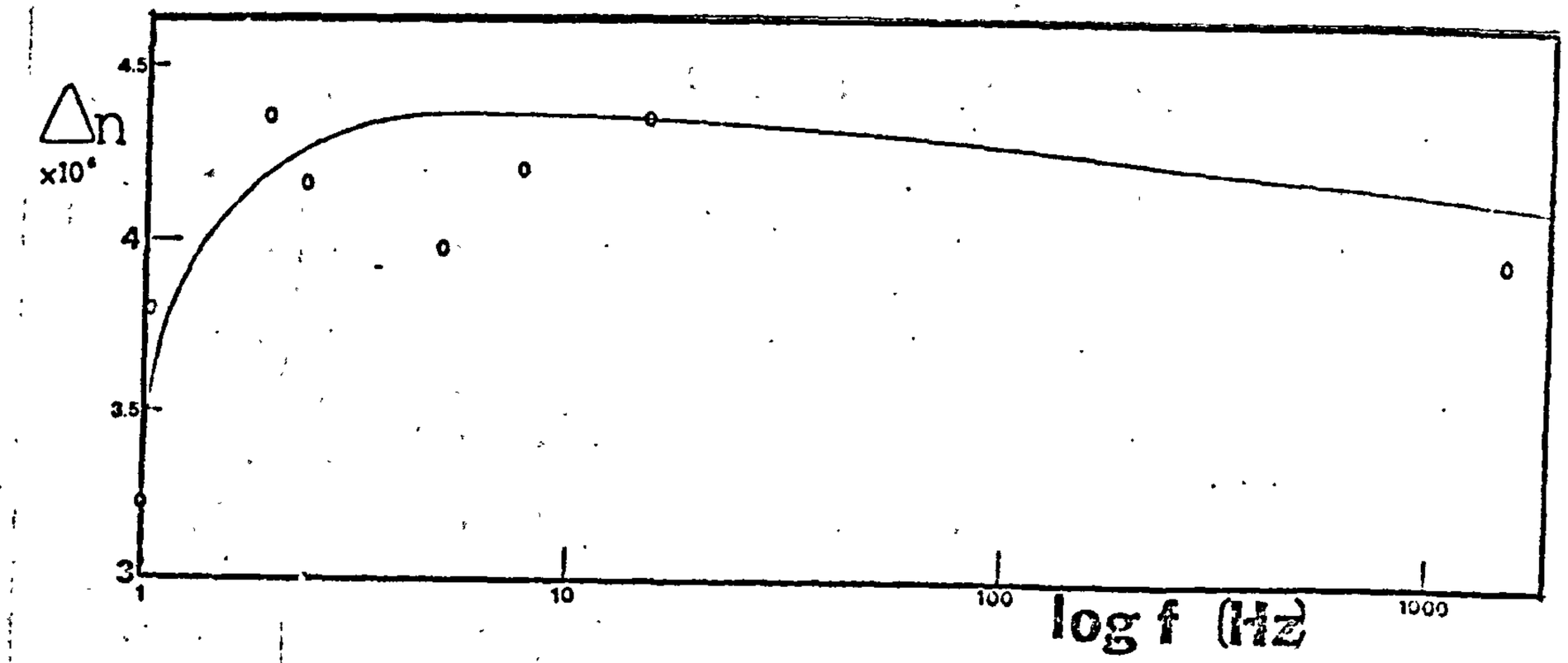

Fig. 6.5 Dispersion of birefringence (Δn) with frequency (f) for E. coli.

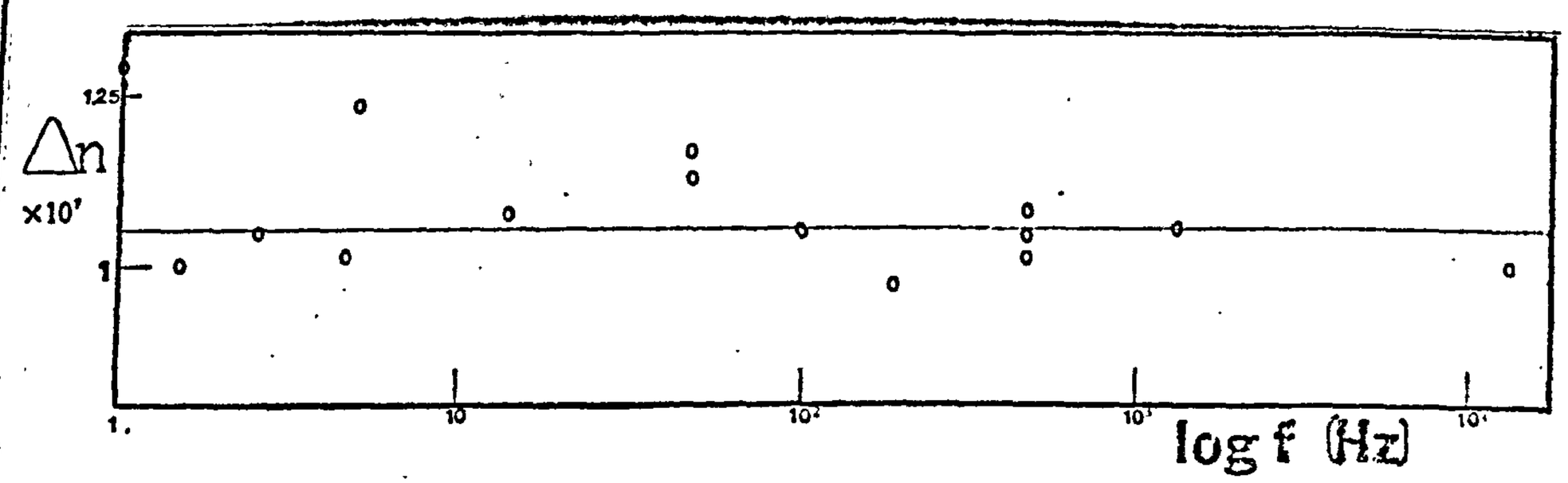

Fig. 6.6 Dependence of birefringence (Δn) on frequency (f) for Kaolinite

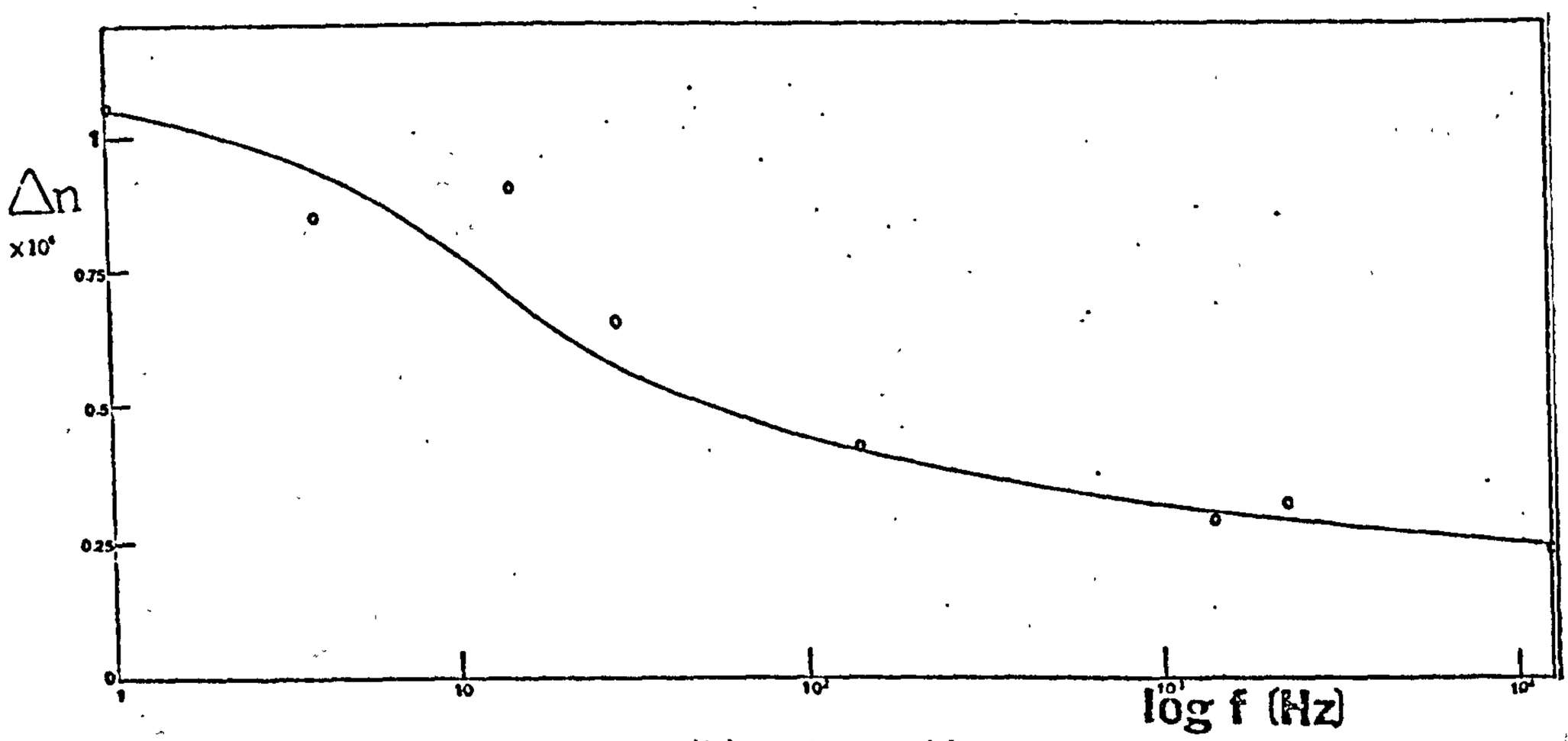

Fig. 6.7 Dispersion of birefringence (Δn) with frequency (f) for PTFE.

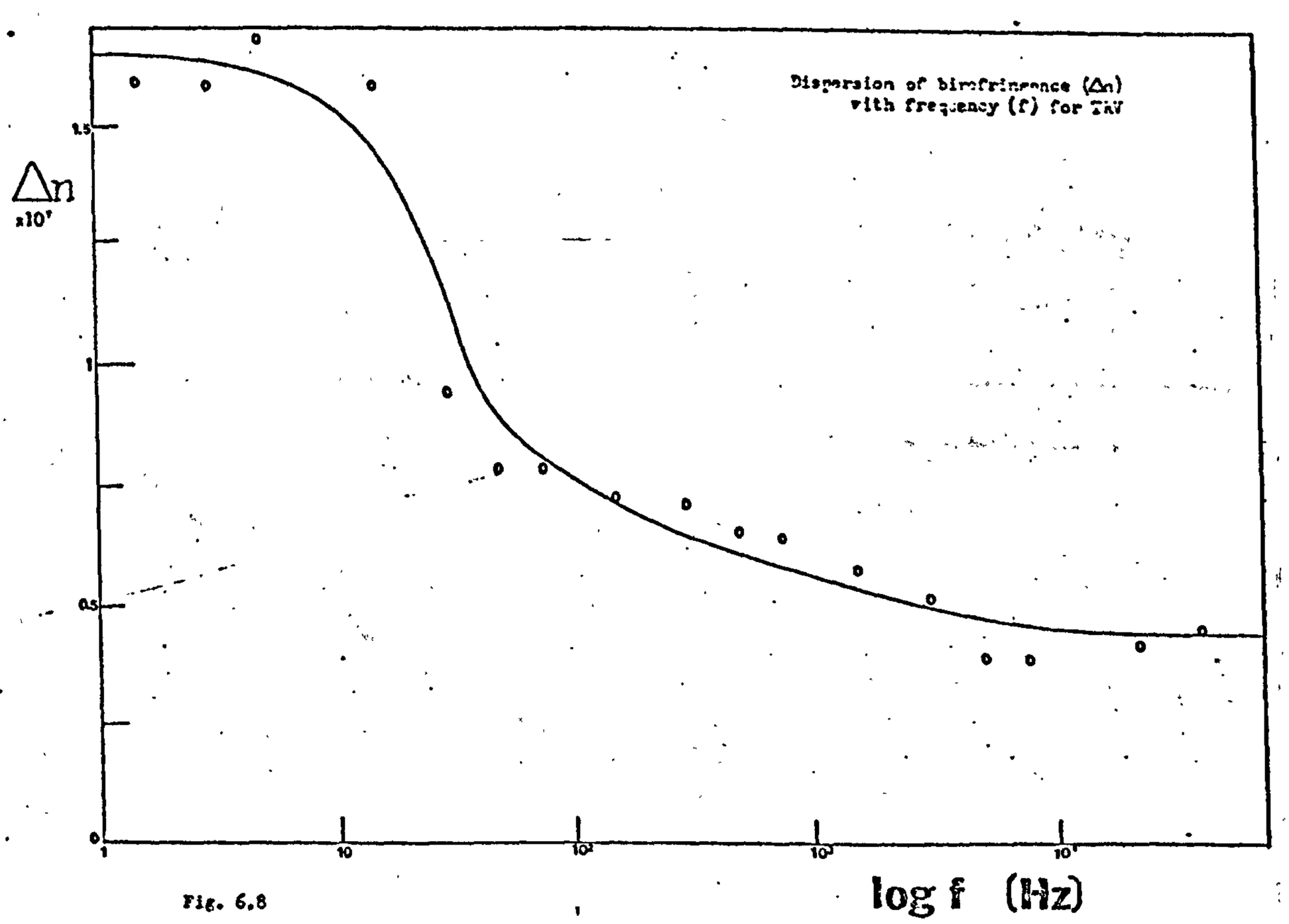

Fig. 6.8

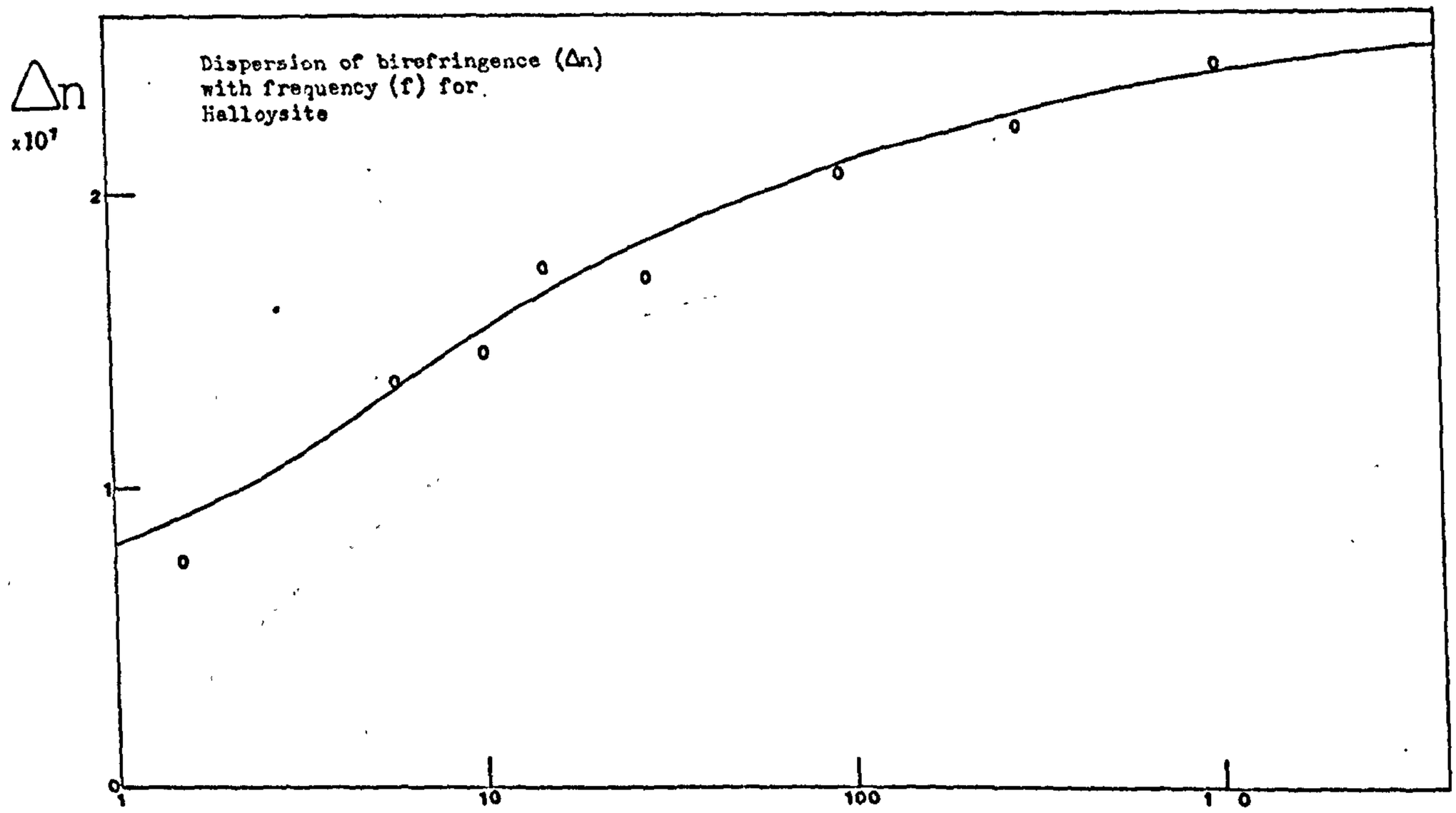

Fig. 6.9

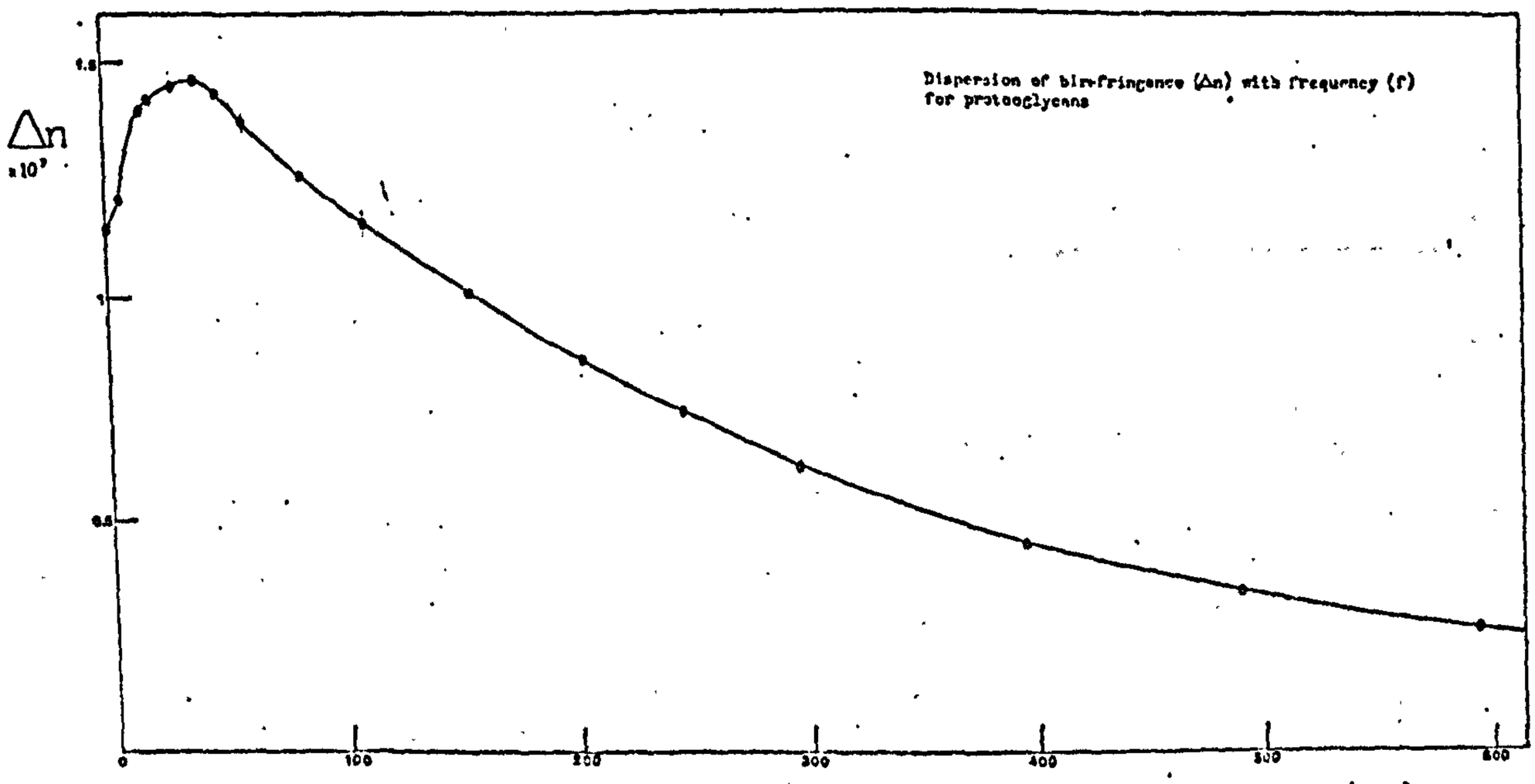

Fig. 6.10

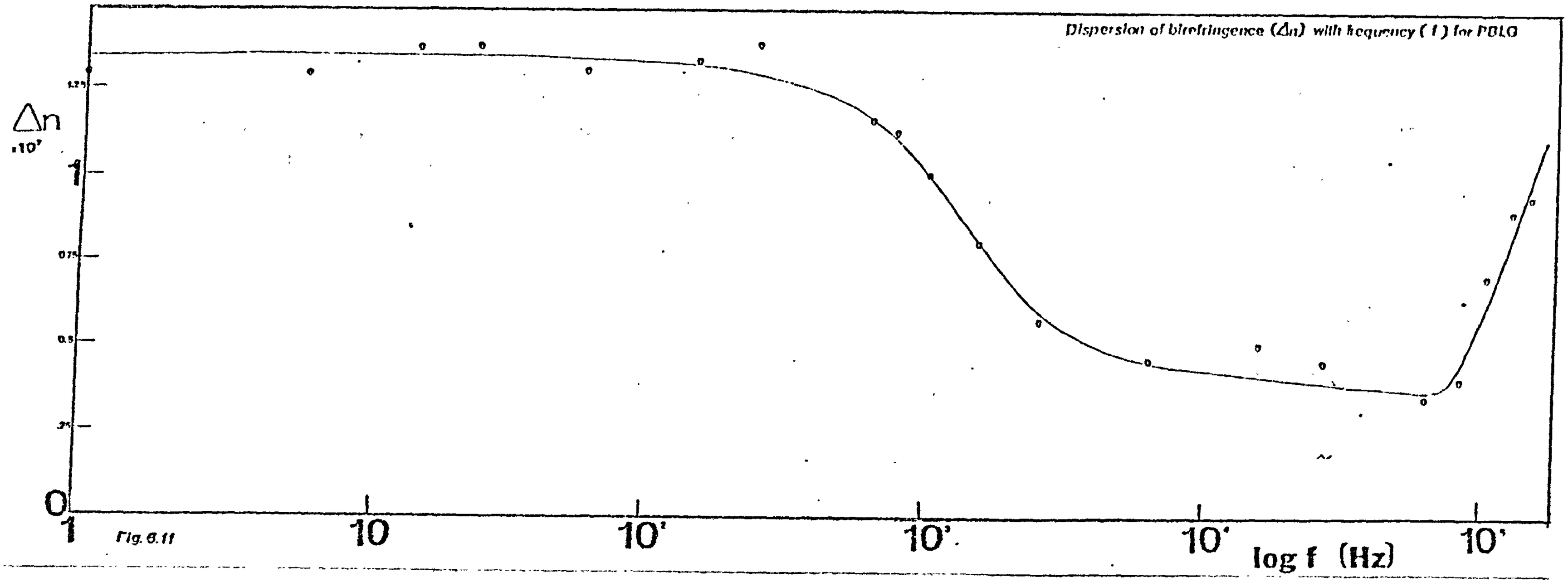

Fig. 6.11

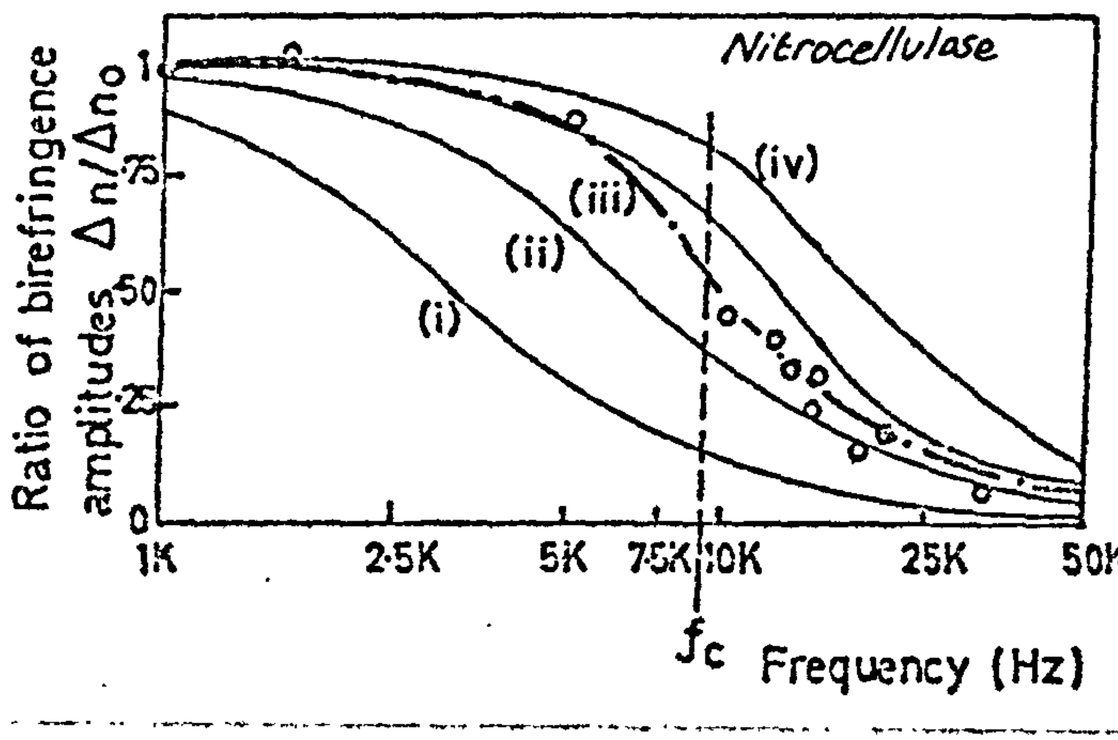

Fig.6.12 Frequency dispersion of the birefringence amplitudes. Experimental data are for fields of root mean square strength 380 V. cm^{-1}. Theoretical curves are for single values of the rotary diffusion constant, D = 1, 2, 4 and 6×10^4 s^{-1} indicated by (i), (ii), (iii) and (iv) respectively. The critical frequency is indicated by f_c.

A MATERIAL	$0_{:r}$ s^{-1} B D_1 initial slope of DC transient	C D_2 long time slope of DC transient	D D_p peeled slope of DC transient	K D_{fd} corresponding to critical frequency s^{-1}	F D_{emg} from electron micrograph s^{-1}	G model used to calculate D_{emg}	H f_c close to DC?	I D_1 or $> D_{fd}$ D_p	J shape of dispersion
Laponite	1185	47	a	912	92	DISC	?	YES	
E. coli	0.293	0.204	1	<4.7	0.015-b	ELLIPSE	YES	-	
Kaolinite	5.54	0.145	a	c	35-d	ELLIPSE	YES	-	-
PTFE	100	1	150	40	3.7	ELLIPSE	YES	YES	
TMV	53	11.4	a	80	5	ROD	YES	YES	
Halloysite	39	8.5	77.5	125	10	ROD	YES	NO	
Proteoglycans	46	107	70	110-700 - e	133-f	ELLIPSE	NO	NO	
PBLG in ethylenedichloride	1500	850	2520	4400	1800-g	ROD	NO	NO	
Nitrocellulose in acetone	104000	33100	222000	29300	-	(COIL)	NO	YES	

Table 6.3 Rotary diffusion constant comparisons and relevant data

KEY TO NOTES.-

a The nature of these results is such that the application of the peeling technique introduces too great an error. The value of D_1 should therefore be taken for D_p in these cases.

b Derived from measurements made by MRE, Porton Down (Ref 614).

c No dispersion is apparent from DC up to 50 kHz though independent measurements in these laboratories suggest $D_{\frac{1}{2}}$ = 10 Hz. It is likely however that the sample studied herein had aggregated, thereby suggesting an even smaller D value

d Derived from sample known not to have aggregated.

e Corresponds to the range of values appropriate to the higher frequency dispersion (see section 8.47).

f Derived from measurements made by Rosenberg et al (Ref 515).

g Derived from measurements by Jennings (Ref 67).

6.7 Discussion of the Comparisons between D_{tr} and D_{fd}

Studying Table 6.3, it is possible to cite some agreement between D_{tr} (D_p or D_1) and D_{fd}. The agreement is particularly good for Laponite, TRV and Halloysite, yet these three have seemingly nothing else in common.

6.71 The DC Phenomena

It has been noted [616] that for large colloidal particles, permanent moments deduced from low frequency measurements involving dielectric properties are 'apparent' rather than 'true' and a number of suggestions to support this hypothesis are put forward. It is suggested that for DC fields, electrode polarisation and space charge effects result in a field, lower than that measured, actually being applied to the molecules in the suspension. As the frequency increases these effects themselves relax out, and the actual field experienced by the molecules increases, resulting in the corresponding increase in the birefringence observed.

There is also the possibility of ions or dust particles in solution being electrophoretic within the field and inhibiting ordering of the solute at DC and low frequencies, until they too can no longer keep pace with an AC field, and their disordering effect is nullified.

6.72 The DC Phenomena and D_{tr}, D_{fd} Comparisons

From Table 6.3 it can be seen that in many instances, the critical frequency is below 40 Hz. These values correspond to those associated with the DC phenomena. Column H in Table 6.3 lists those materials for which $f_c \leq 40$ Hz, thus excluding only proteoglycans, Laponite and the two non-aqueous solutions. It is possible that Laponite would also be influenced by the DC phenomena, but the effect would be masked by the dispersion of the Laponite itself.

Of the materials denoted in column H, TRV and PTFE have dispersions of a different shape to the rest (column J, Table 6.3). This shape is not compatible with the DC phenomena, suggesting, therefore, that these are dispersions of the materials themselves. Proteoglycans exhibits this shape too, however, at very low frequencies, the dispersion exhibits an additional dispersion of the shape compatible with DC phenomena, (Fig. 6.10). It may be that TRV and PTFE might also display similar low frequency dispersions, but because their critical frequency is lower than that of proteoglycans, the two dispersions may coalesce to result in the observed effect.

The frequency dispersion of proteoglycans is discussed in fuller context in section 8.4.

6.73 Comparison with Electron Micrograph derived values, D_{emg}

In suspension many of the materials, particularly clays, swell and attract ionic clouds to hinder their rotary motion. They thus appear larger than they are, when measured in suspension, by birefringence. One would expect the value of the electric birefringence relaxation time to be larger and hence for the rotary diffusion constant (D_{tr} or D_{fd}) to be smaller, than values of D_{emg}. This is a consequence of the sample preparation technique for electron microscopy which results in dessication. This might even suggest a method for determining the relative water absorption of clays.

Studying Table 6.3, however, all the materials, except Kaolinite (see Table 6.3, note d) and proteoglycans (see section 8.47) behave contrary to expectation.

This observation thus supports the idea that the true frequency dispersion for these materials is masked in some way - for example, by the DC phenomena already discussed.

6.74 Molecular and Particle Conformations

Agreement between D_{tr} and D_{fd} values (Table 6.3) is poor, even for the non-aqueous suspensions. Whilst

a factor of nearly two for PBLG is not bad, this is nearly ten for nitrocellulose. The importance of particle conformation should not be neglected. PBLG is approximated as a rod, albeit a helical molecule, and the other two rod-like materials - Halloysite and TRV - also show closest agreement between D_{tr} and D_{fd} values.

Schweitzer and Jennings[617] have shown that for rods, initial slope values of D_{tr} (i.e. D_1, Table 6.3) are analagous to discrete distribution averages. Similarly, basic birefringence theory is in terms of rod like particles. Clearly, the relative simplicity of a rod geometry is advantageous for demonstrating simple, fundamental relationships, so perhaps it is not surprising that the rod conformations give the best agreement in this study.

6.75 Unaccounted Factors in this Study

Whilst Schweitzer and Jennings[617] can point to discrete averages for rod geometries and ultimately to the polydispersity of the sample, polydispersity is not a factor accounted for in this study. It is however important, being reflected in both the differences between D_1, D_p and D_2 values of D_{tr} and in the breadth of the AC frequency dispersion (The latter is discussed with reference to nitrocellulose in Chapter 4).

It should also be noted that all measurements were conducted using quadratic detection, and all values of D_{tr} calculated from responses to DC pulses.

6.8 Conclusion

Interpretation of the data presented in this study is not possible beyond that discussed so far. A better understanding of DC phenomena may help in investigating these results further at a later stage. The development of the electric birefringence theory in terms of non-rigid systems would also assist in a deeper understanding of these problems.

It is important that in any future studies to verify or investigate, experimentally, the D_{tr}, D_{fd} comparison, materials should be carefully selected with particular regard to molecular conformation and polydispersity. Care should also be taken to avoid any overlap with the frequency band in which the DC phenomena are likely to be present.

6.9 Corollary: A Study of the Clay, Halloysite, with Particular Reference to the Direction of the Dipole Moment.

Schweitzer and Jennings[617] have shown that for a rod-like macroparticle, discrete averages of the rotary diffusion constant can be obtained. The particular average, thought to be dependent chiefly on the particle's dipole moment and whether the moment is permanent or induced.

Bhanot and Jennings[618] have studied the rod like clay, Halloysite, and their study is inconclusive with regards to the permanent moment. Whilst their results indicate a transverse, permanent moment, they find it difficult to reconcile this with the particle's geometry.

As a corollary to the preceeding work on frequency dispersions, the author has proceeded to further investigate the clay, Halloysite, and the results offer further evidence on the dipole's direction.

The sample was precisely that used and detailed earlier in this chapter. In addition to the field dependence and frequency dispersion measurements, each individual transient response in the frequency dispersion was analysed, and the rotary diffusion constant, corresponding to the initial slope obtained. These values are presented graphically in Fig. 6.13.

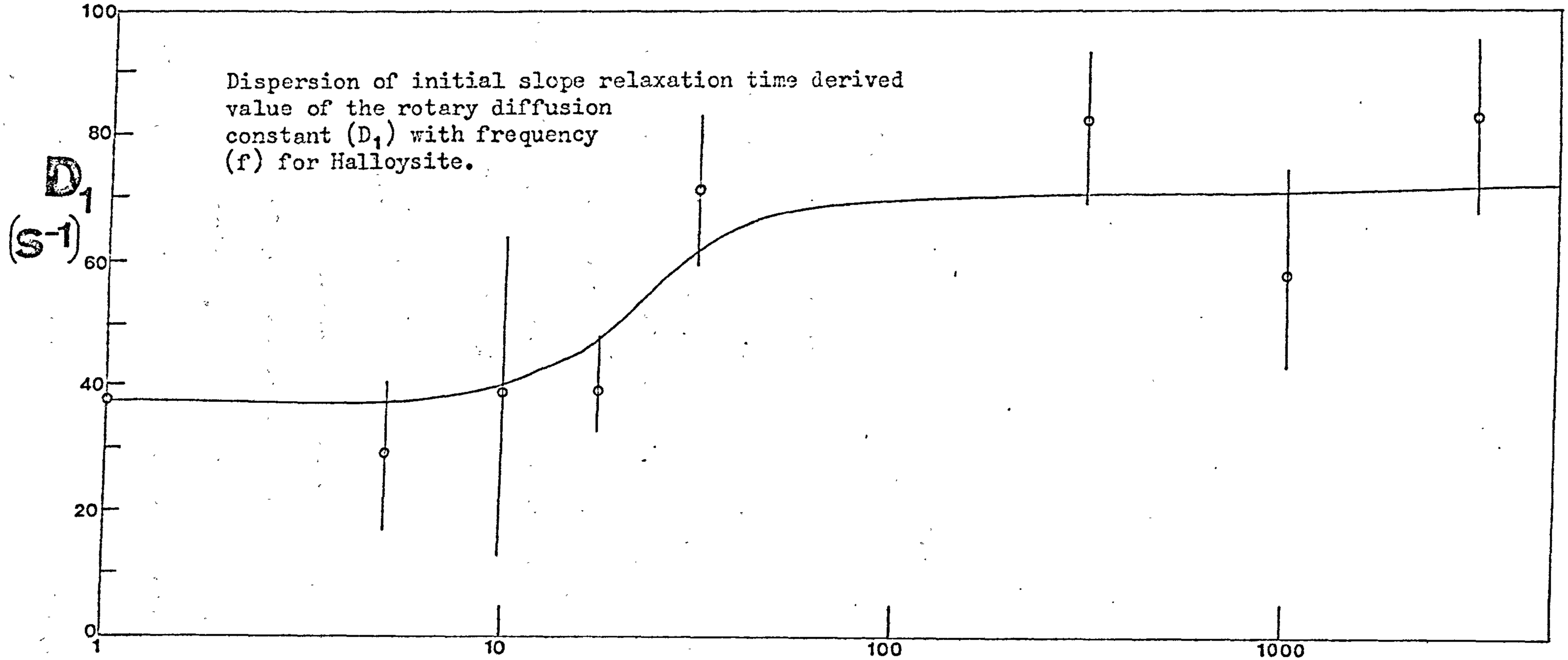
Dispersion of initial slope relaxation time derived value of the rotary diffusion constant (D_1) with frequency (f) for Halloysite.
D_1 (S^{-1})
100
80
60
40
20
0
1
10
100
1000
log f (Hz)

Fig. 6.13

Examining this dispersion, it can be seen that the high frequency value is greater than that at DC.

According to Schweitzer and Jennings, at high frequency, when orientation is due solely to the induced moment of the sample, the appropriate discrete average is the Z average. The corresponding rotary diffusion constant can be denoted D_z.

At DC two possibilities arise:

1. A permanent dipole moment along the longitudinal axis.

2. A permanent transverse dipole moment.

The latter case is implied by Bhanot and Jennings' pulsed electric field light scattering data. However, Schweitzer and Jennings' calculations suggest a weight average rotary diffusion constant (D_w) for this possibility. The results herein would therefore imply $D_z > D_w$, which is impossible.

If the possibility is now considered in (1) above, i.e. a longitudinal permanent moment, then Schweitzer and Jennings results suggest a Z+1 average rotary diffusion constant, D_{z+1}. Now D_{z+1} can be greater than D_z, and this fits the experimental evidence of Fig. 6.13. Therefore a permanent moment could exist along the longitudinal axis of a Halloysite clay particle.

It may be that the transverse moment suggested by Bhanot and Jennings is not so, and the origin of their frequency dispersion, in common with many of the birefringence dispersions reported earlier, could be the consequence of the proposed DC phenomena discussed earlier.

The results reported herein should be treated with caution until they can be substantiated, or otherwise, on other materials. In particular, current work within this research group is examining distributions and their related discrete averages, which may lead to a reappraisal of the Schweitzer and Jennings work. It would, nonetheless, be of value if comparison of a high frequency transient decay, yielding a value of D_z, with a DC (zero frequency) transient decay would indicate a transverse or longitudinal permanent moment as suggested herein:

EITHER D_w (at DC) > D_z (at high frequency)$\Longrightarrow$transverse

OR D_{z+1} (at DC) < D_z (at high frequency)$\Longrightarrow$longitudinal

It should be noted that Schweitzer and Jennings' original paper limits the application to particles with rod geometries, and measurements made within the region of quadratic field dependence as their theory is unable to differentiate between rod geometries with transverse moments and particles or molecules at saturation orientation regardless of dipole direction.

SECTION 3

Cartilage Mucopolysaccharides and Conformational Changes

The previous section demonstrated an area in which electric birefringence may become of increasing importance and value in the near future. By contrast the chapters of this section present work of immediate and profound significance. The measurements are those in which dramatic changes in the size of birefringence responses and relaxation times of effects are readily interpretable in terms of conformational changes.

A family of biomedical macromolecules is studied to demonstrate a variety of conformational changes and, at the same time, the opportunity has been taken to characterise some of the materials involved, particularly those novel to the electric birefringence technique.

CHAPTER 7

Hyaluronic Acid: Its Characterisation, Changes with pH and Enzymatic Degradation

7.1 Introduction to Hyaluronic Acid

7.11 Origin and Source

Meyer and Palmer[71] first discovered hyaluronic acid in bovine vitreous humour in 1934 and two years later in the umbilical cord.[72] The molecule associates with large quantities of water to form a jelly like matrix between cells. Hyaluronic acid solutions are highly viscous and serve as a lubricant in the synovial fluid. As a major constituent of the vitreous humour, the acid forms an optically transparent, low refractive index gel, which maintains the precise shape of the eyeball. Other sources include adult skin tissue, the sexual skin of apes, rooster comb, normal urine and streptococcal cultures.

It is one of the family of connective tissue polysaccharides (mucopolysaccharides), though it is the only one which contains no ester sulphate groups. The others are chrondroitin-4-sulphate, chrondroitin-6-

sulphate, dermatan sulphate, heparan sulphate, keratan sulphate and heparin. Heparin, however, is not found extracellularly, but has the same basic structure as the others. They are all regular, linear, unbranched biopolymers, and in the case of hyaluronic acid, this has been shown by electron micrographs.[73] These materials are often referred to as glycosaminoglycans, glycosaminoglucurons or, simply, glycans. Hyaluronic acid is made up of the repeating unit $(-N-G-)_n$ where N is the N-acetyl glucosamine and G is glucuronic acid : n can range up to 10^4. The basic unit is shown in Fig. 7.1.

7.12 Conformation and Structure

Chain conformation of these polysaccharides is considered important in determining their biological function[74] though precise relations between conformation and function are still wanting. Hyaluronic acid, in gel form, acts to exclude other macromolecules from its domain.[75] When isolated, its conformation is such that it supports large amounts of water in an open, porous, gel or gel-like structure.[76-78]

Sedimentation and viscosity measurements[79,710] have implied an expanded, random coil conformation for hyaluronic acid in solution. This has been confirmed[711]

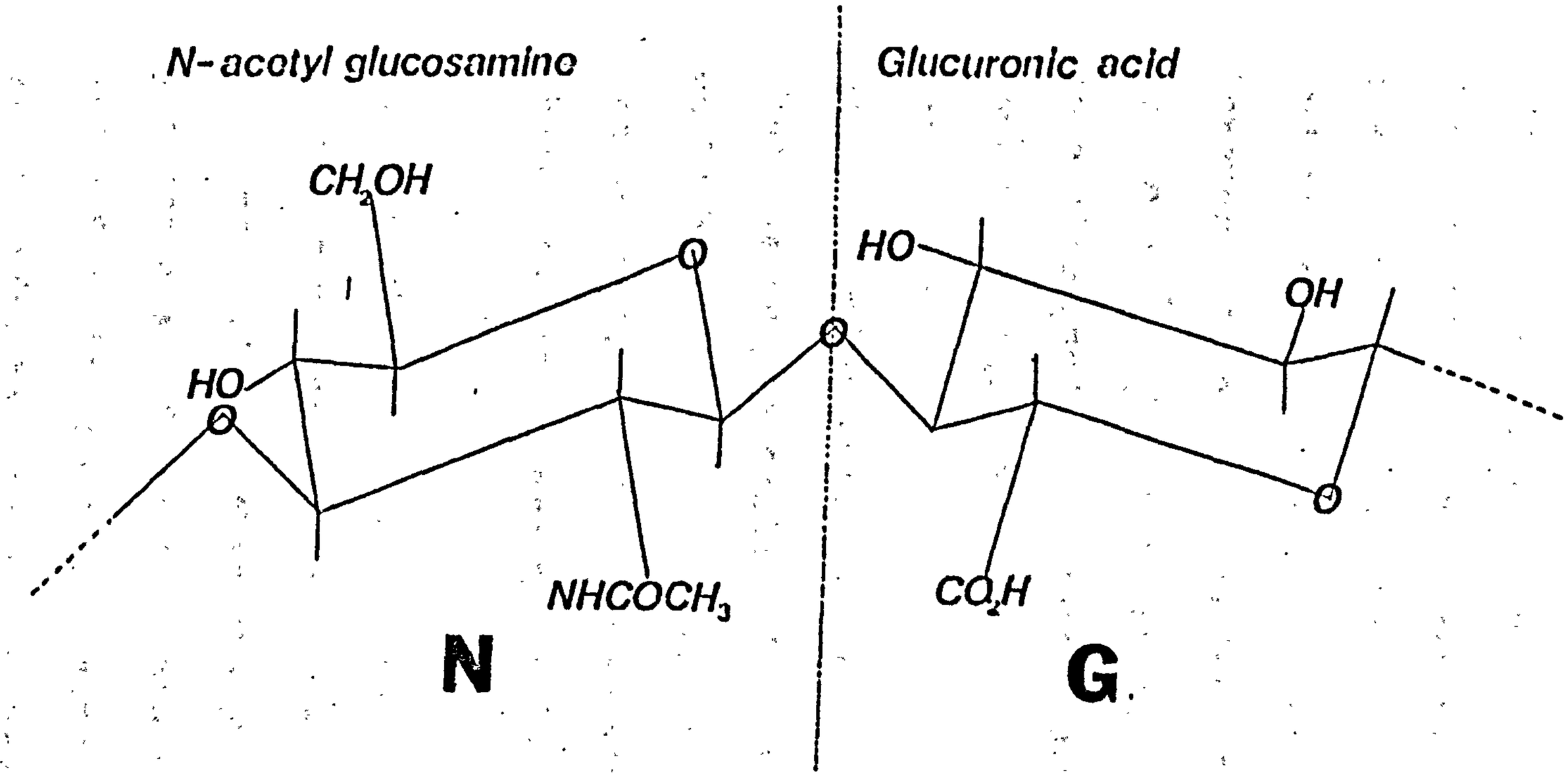

Fig. 7.1 The basic monmer unit of hyaluronic acid.

by light scattering measurements indicating a somewhat stiff, random coil and Preston *et al*[712] have equated their scattering data to a sphere of radius 200 nm.

In common with other connective tissue polysaccharides, hyaluronic acid, when oriented in films and fibres for X-ray diffraction measurements, has been observed to have a two or three fold helical form.[713] Dea *et al*[714] and Atkins and Sheehan[715] also report a double helix. However, these conformations find no favour with Guss *et al.*[716] Their X-ray studies, coupled with new molecular modelling techniques lead them to the conclusion that the structure consists of single left hand chains. A double helix in any condensed phase is ruled out. Also, it is thought unlikely that the double helix exists in solution where it would be stable to changes in ionic strength, pH and temperature, yet fail to survive mild crystallisation. These properties are not observed experimentally.

Guss *et al*s' results are supported further by nuclear magnetic resonance work done by Darke *et al.*[717] Their findings indicate that the chain molecule is formed of alternate stiff and flexible regions with between 55 and 70% of the molecule being stiff. These proportions are thought to remain the same regardless of pH, ionic strength, temperature or denaturation by, for example, urea. Sugar residues in the stiff section can be made conformationally mobile by the action of enzyme

(hyaluronidase) or alkali and this indicates approximately sixty disaccharide residues per stiff domain. This points to a chain consisting of a small number of stiff chain segments defined by minor covalent features, connected by flexible chain sections. Such a model would appear similar to the stiff, random coil when studied by light scattering, sedimentation and viscosity.

Darke *et al*[717] further postulate that their model could explain the visco-elasticity of the material in terms of a dynamic three dimensional network formed by fleeting associations of the stiff segments.

7.13 The effect of pH

Because the polysaccharide carries one carboxyl group per disaccharide unit (Fig. 7.1) this group is dissociated at physiological pH and the polymer thus behaves as a polyanion in solution.

At alkaline pH therefore, the negative charges are to an extent unscreened by the hydrogen ions in aqueous solution, and thus expand the molecular coil as a result of mutual charge repulsion. As the pH is lowered, so hydrogen ions screen the charge and the coil slowly collapses. This change has been seen by Preston *et al*[712] using both light scattering and viscosity.

Electric birefringence has already been used to monitor conformation changes on a number of biological systems with pH.[718,719] The globular protein, bovine plasma albumin for example shows sizeable changes in the relaxation time of its electric birefringence response as it dissociates into its subunits.[718] This present study is intended to find how sensitive the birefringence technique can be in following the continuous changes with pH of a relatively weak and coiled polyelectrolyte.

7.2 Characterisation and pH changes of Hyaluronic Acid: Experimental

For all these measurements, a commercial preparation of the potassium salt of hyaluronic acid is used. This was purchased from Messrs Koch Light Ltd., Colnbrook and formed part of their batch, No. 69131, extracted from human umbilical chord.

The hyaluronate was dissolved in distilled water, by slowly shaking, by hand, in preference to using a mechanical stirrer (see later). Concentrations of 0.2% were used throughout. The pH of solutions prepared in this manner was approximately 6.4 to 6.5. For measurements at alkaline pH, the hyaluronate was dissolved in a very weak solution of potassium hydroxide (one pellet dissolved in 2.5 l). Earlier

measurements using a more concentrated preparation were unsatisfactory (see later).

All measurements were made starting at alkaline pH and working towards acidic environments by adding hydrochloric acid. Charges on the polysaccharide, screened by hydrogen ions at acid pHs, are reluctant to detach from the molecule when the pH is again made alkaline.[712]

When not being used, solutions were stored frozen in the ice compartment of a refrigerator.

The pH stat used was illustrated in Fig. 3.3 and Fig. 3.4, together with the flow cell specially designed for these experiments. For the initial measurements Cell B was used. Pulse generator PG6, delivering 5 μs pulses up to 3.5 kV (14 kV cm^{-1}), the original He Ne laser and a 5 kΩ load resistor on the photomultiplier completed the arrangement. Itwas not possible to use a larger load resistor for amplitude measurements as the increased time constant prevented saturation of the transient response within the 5 μs pulse length.

7.3 Characterisation and pH changes of Hyaluronic Acid: Results and Discussion

7.31 Conventional Birefringence Measurements

The polysaccharide was shown to exhibit electric birefringence according to the Kerr Law. The value of the Kerr Constant calculated from the graph (Fig 7.2) is

$$K = \lim_{E \to 0} \left(\frac{\Delta n}{n E^2} \right) = 4.3 \text{ cm}^2 \text{ kV}^{-2}$$

The asymmetry of the birefringence response suggests a permanent dipole moment.

During the course of exploratory measurements, a value of the variation of refractive index with concentration was found, viz:

$$\frac{dn}{dc} = 0.146 \text{ cm g}^{-1}$$

7.32 Changes with pH

A preliminary set of measurements of variation with pH was made. From these data, it became obvious that fine control of the pH was needed, that would not unduly effect either the concentration of the initial solution or its ionic strength. The relative strengths of the hydrochloric acid and alkaline hyaluronate solutions were adjusted such that

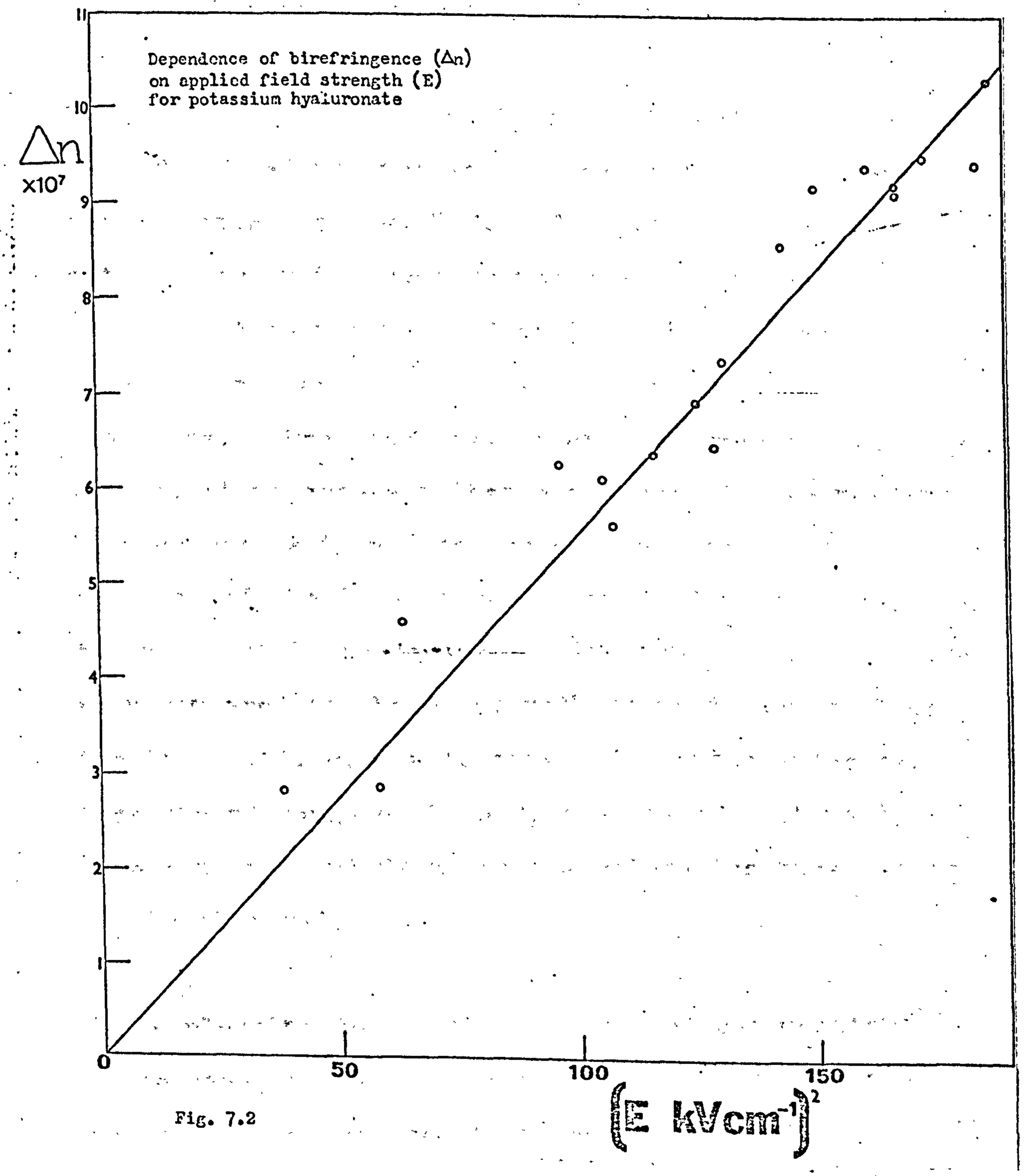
Dependence of birefringence (Δn)
on applied field strength (E)
for potassium hyaluronate
Δn
×10⁷
10
9
8
7
6
5
4
3
2
1
0
50
100
150
(E kVcm⁻¹)²

Fig. 7.2

changes of 0.1 pH could be achieved by the addition of less than 0.1 µl of acid. A large proportional band setting (5) was thus used on the titrator, to avoid overshooting the required pH value (see section 3.34).

The sensitivity of the environmental conditions for both the birefringence and the relaxation times are clearly shown in Fig. 7.3. The data in this graph satisfactorily incorporate measurements taken from two initial solutions. Each individual point on the graph is an average of three separate transient responses. From the scatter on the experimental points, it is apparent that a minimum of five readings is necessary within a change of 1 pH to fix the position of the line of the graph. But, even so, the technique still possesses its inherent speed advantage when compared to the other methods mentioned earlier, (section 7.1), e.g. viscosity and light scattering. Over the pH range of 5 to 8, changes of 115% in the birefringence and 82.5% in the relaxation time can be easily observed.

It is pleasing to see that the method can monitor these changes, particularly when one considers the conformational changes that these represent. It will be noted in the next section that no exact model can be found to fit the hyaluronate molecule, but from section 2.8, it will be remembered that Perrin and Broersma models show an approximate cubic dependence

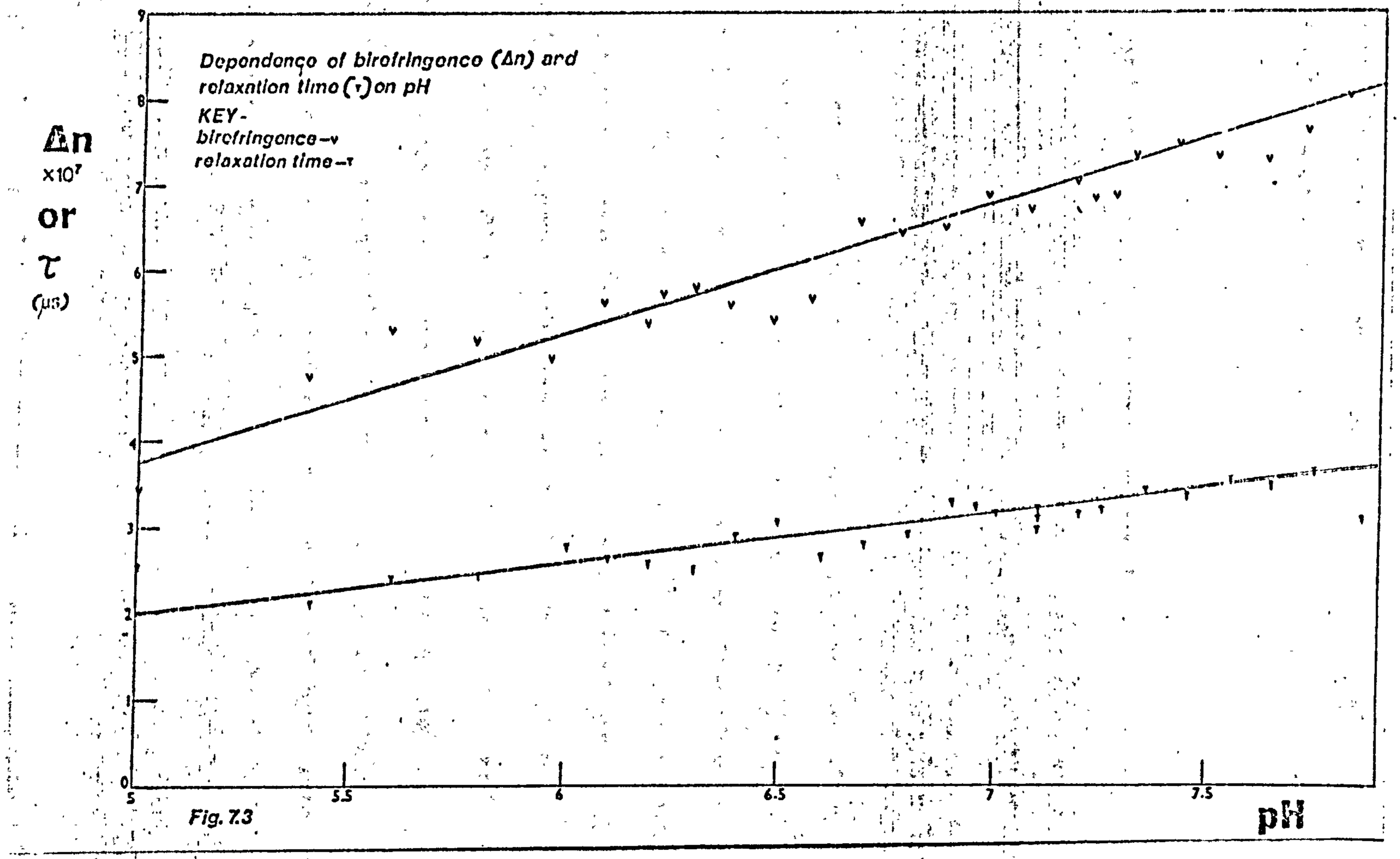
Dependonço of birefringonco (Δn) ard
relaxation time (τ) on pH
KEY-
birefringonce–v
relaxation time–τ
Δn
×10⁷
or
τ
(μs)
9
8
7
6
5
4
3
2
1
0
5
5.5
6
6.5
7
7.5
pH

Fig. 7.3

of the major molecular dimension on the relaxation time. Thus the 82.5% change in the hyaluronate's relaxation time corresponds to only about 4.5% change in its major dimension.

7.33 Conformation of hyaluronic acid

(a) RIGID ROD. Turning to the actual conformation of the molecule in the suspension used in this study, it is firstly noted that at neutral pH no agreement can be found with Broersma's rigid rod equation (section 2.811). It will be recalled that this equation is somewhat insensitive to the value chosen for the rod diameter. Therefore the same value (0.35 nm) as used for the polysaccharide, nitrocellulose (section 4.62) was employed, since both appear to be chain like molecules of broadly similar construction. A rod length of 60 nm was thus found, corresponding to the neutral pH relaxation time of 2.85 μs. This compares with the extended chain length of hyaluronic acid, generally accepted to be typically about 1000 nm.

(b) FLEXIBLE COIL. The Zimm, Stockmayer and Baur random coil model (section 2.821) was considered, and the molecular weight value suggested from the use of their equation with the author's data was compared with the viscosity average molecular weight kindly determined by Dr T E Hardingham of the Kennedy Institute

of Rheumatology under the same conditions as used by Cleland and Wang[720] in 0.2 M NaCl. The value thus obtained by Dr Hardingham was 351,000.

The author measured an experimental value of the sample's intrinsic viscosity of 101 dl g^{-1} at neutral pH. Because of the hydration of the hyaluronic acid, the constant for a non-free draining coil was used in the Zimm, Stockmayer and Baur equation. A molecular weight of 78,800 was thus obtained. Comparing this with the viscosity value of 351,000, it is clear that the randcm coil model is not suited to hyaluronic acid.

7.4 Conclusion

It therefore appears that the conformation of the molecule is similar to that of nitrocellulose (see Chapter 4), and likewise awaits the development of rigorous flexible or semi-flexible theories of molecular kinetics before the birefringence method can be used to its full potential in this instance. General concord with the restrained flexible single strand coil model suggested by other workers (section 7.12) can be thus concluded. Moreover the technique's sensitivity to changes in this conformational state is well established in this study.

7.5 Corollary: Comparison with Laser Induced Birefringence results

It is interesting to compare the relaxation times found in this study with those found by Coles and Jennings[721] using the new laser induced birefringence technique. Their value was as large as 0.3 ms. Subsequent to this initial observation, all suspensions were prepared as indicated in section 7.2, to counteract suggestions[722] that the polysaccharide chain could have been broken by the action of the mechanical stirrer used. Suspensions prepared according to the method of section 7.2, continued to exhibit microsecond relaxation times throughout this study.

It is suggested that the laser induced value of 0.3 ms derives from the time constant of the applied laser field which Coles[722] quotes at 0.2 ms. The 0.3 ms is calculated by considering the 'long term' decay (as opposed to initial slope) of the birefringent response relative to the applied laser field. Clearly it would be difficult to detect a microsecond effect masked by these longer-millisecond relaxation values.

It is unlikely that the discrepancy was due to the samples themselves, which were both from the same source, and were similarly prepared. A note of caution is therefore offered in respect of fast laser induced changes.

7.6 Introduction to Hyaluronidase

Enzymes which degrade hyaluronates include Bacterial Hyaluronate Lyase, Leech Hyaluronate Hydrolase and Testicular Hyaluronate Hydrolase. The latter, which is classed as an endohexosaminidase is the subject of this study and it specifically attacks alternate symmetric oxygen bonds of the hyaluronate chain (Fig. 7.1), degrading the polymer into oligosaccharide units. Its activity is a maximum in the presence of NaCl[723,724] and the optimum pH[725] (in the absence of NaCl) is 6.0.

Outside of the testes, hyaluronidase has been found in the spleen, ciliary body, iris and skin.[725] Mature mammalian testes though are by far the richest source of the enzyme. Its presence here is due to the important role it plays in the fertilisation process.[725] It assists in the removal, or possibly completely removes, the layers of cumulus cells and the corona of the female ovum and thus permits the ovum's penetration by the male sperm. Elsewhere in the body it is known to be involved in the temporal control of cell migration and differentiation in embryonic tissues.[726] The enzyme promotes diffusion of inert substances through the dermis of both living and dead animals. It has found medical uses in assisting the absorption of fluids in the treatment of dermal clysis in children,[727] in allergy tests on the skin[728] and in

reducing swelling associated with plastic surgery operations on the nose.[729]

This set of results presents data showing the degradation of the hyaluronate substrate by the hyaluronidase enzyme. The use of the technique for studying this and other enzyme-substrate interactions is clearly demonstrated.

7.7 Hyaluronidase Degradation of Hyaluronate:

Experimental

7.71 Materials

The sample used was purchased from B.D.H. Chemicals of Poole. It was an extract from ovine testes with a stated activity of 350 - 500 W.H.O. units mg^{-1}. (Batch No. 2180800). The hyaluronic acid salt sample was the same as that used earlier (section 7.2).

7.72 Apparatus and Procedure

The apparatus was similar to that used in the hyaluronate pH measurements, without the pH stat. The reservoir of the flow cell was used to add the enzyme to the substrate and the system was allowed to circulate for a period in order to mix. The enzyme was in powdered

form and measurements were made by adding pre-weighed amounts directly, or by first dissolving the enzyme in distilled water and adding the resulting solution.

Testicular hyaluronidase readily adsorbs on to glass surfaces[730] and consequently plastic containers were thus used throughout. It was not possible to avoid the use of the glass end windows of the cell, so these were changed after each set of measurements.

7.73 Determination of the Relative Concentration of Enzyme and Substrate

The concentration of hyaluronidase, relative to the substrate was determined by a series of preliminary measurements, based initially on the work of Meyer and Rapport,[731] though the activity of their enzyme and extract of their substrate were different to those in this study. Using a hyaluronate solution prepared in distilled water (initial pH 5.6) and adding 10 mg of hyaluronidase to 10 ml of this substrate, no change in birefringence or relaxation time was noted up to 48 hours. A second substrate solution prepared in the dilute potassium hydroxide solvent (initial pH 5.8) became too cloudy cn addition of 57 mg of enzyme to 10 ml of substrate. This solution was then diluted through a range of concentrations and electric field pulses applied to each. A satisfactory concentration

was thus determined at 13 mg enzyme to 10 ml substrate.

Field strengths were then kept constant at 20 kV cm^{-1} and 5 μs duration throughout.

7.8 Hyaluronidase Degradation of Hyaluronate: Results and Discussion

The enzymic degradation with time of the hyaluronate substrate is shown in Fig. 7.4. The degradation is reflected in the decreases observed in both birefringence and relaxation times.

No measurements are recorded in the first 2 - 3 minutes as, during this time, the enzyme was stirred into the substrate suspension. It was only after 7 - 10 minutes that a definite trend could be detected in the responses, the preceeding period being characterised by erratic variation in response, particularly in the relaxation time values. This parameter is particularly sensitive to conformational changes in the same way as viscosity and turbidity measurements. These too have been noted to vary erratically during hyaluronidase activity.[732]

It can be seen that Δn decreases more rapidly than τ. This is accentuated by the field dependence of birefringence. As the enzyme is successively

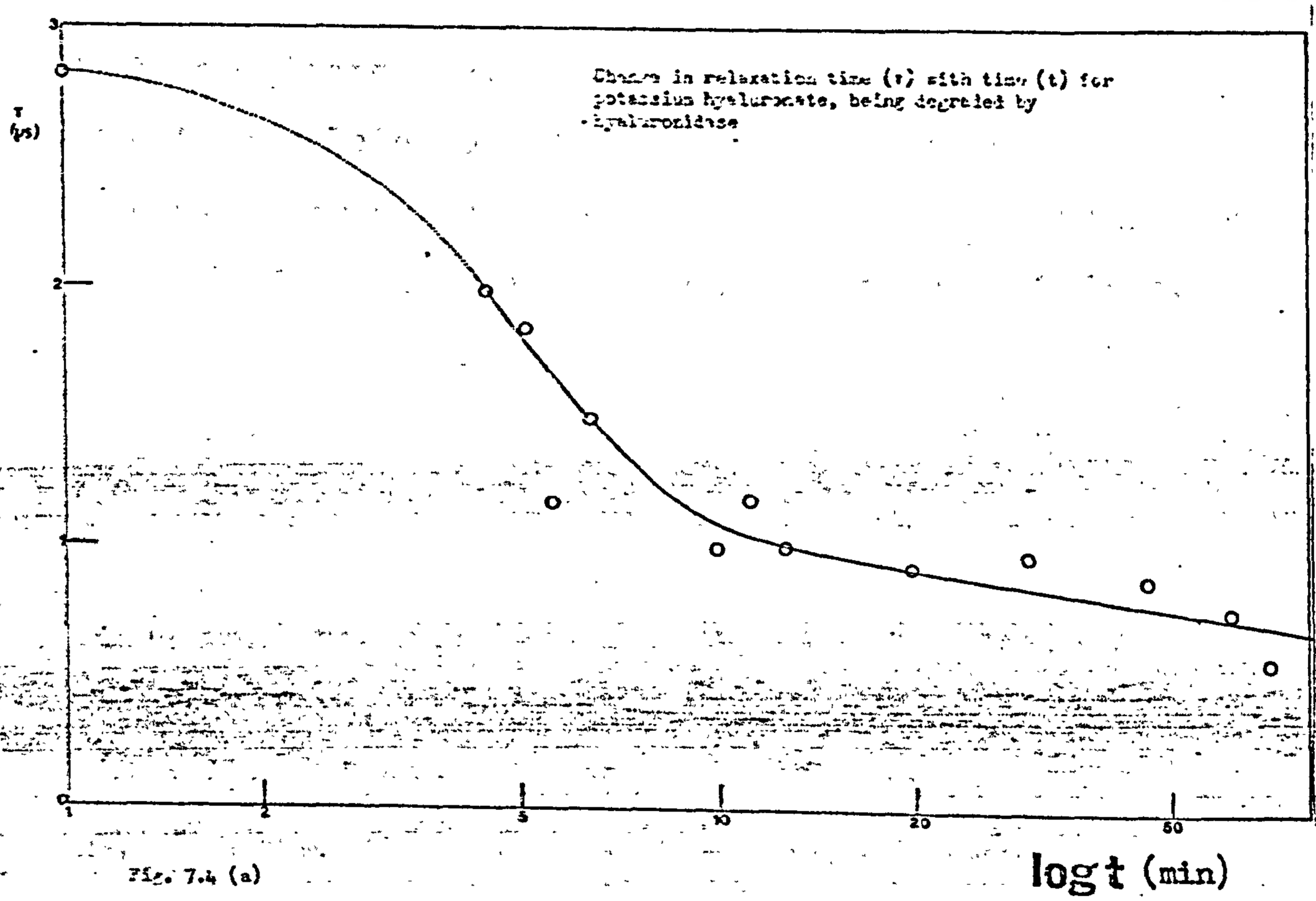

Fig. 7.4 (a)

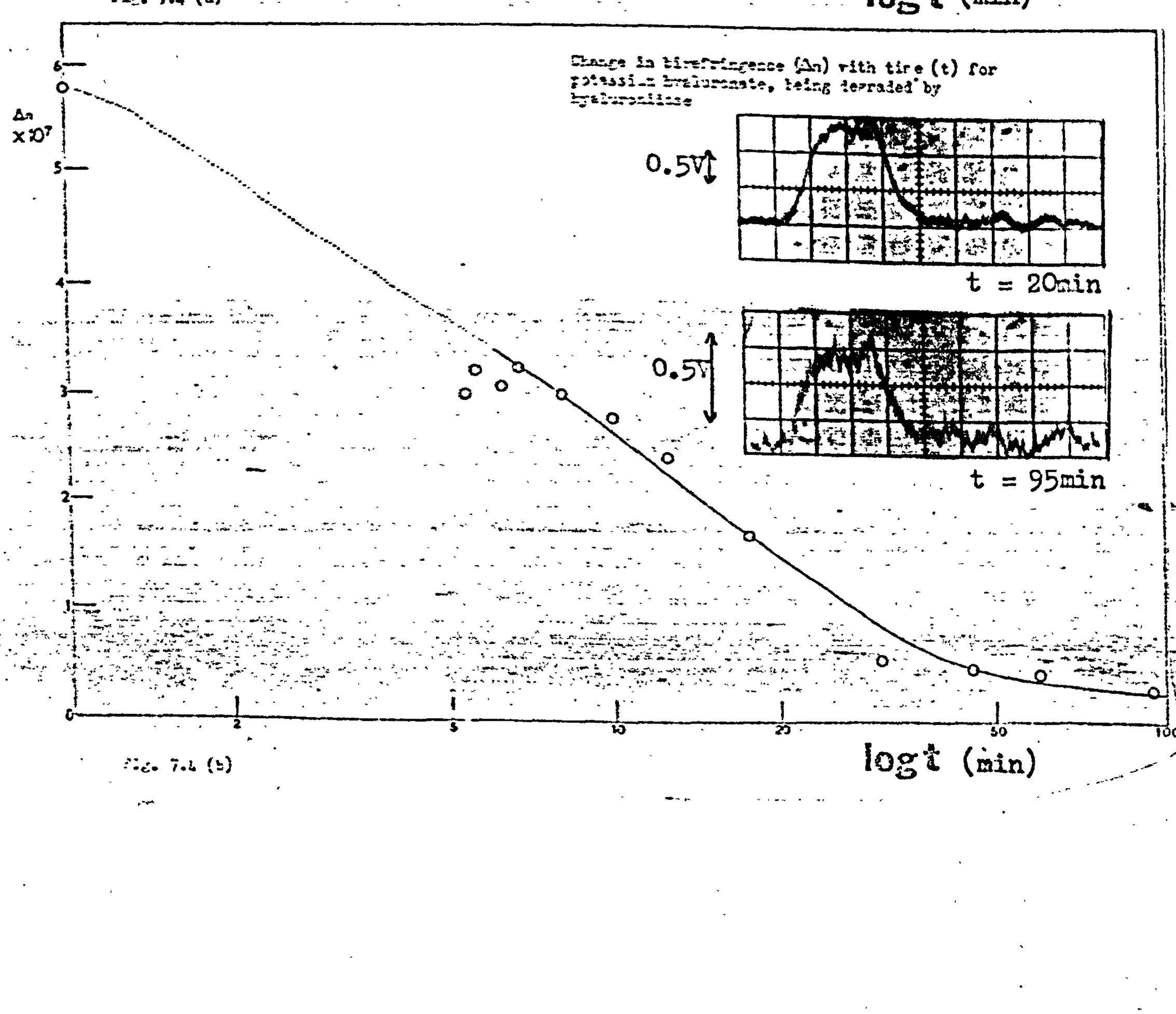

Fig. 7.4 (b)

degraded so the field required to orientate the fragments increases. In a more rigorous study, were it possible to monitor the field dependence at intervals throughout the degradation, the measurements could be normalised with respect to this variation.

7.9 Conclusion: Hyaluronidase Activity.

These measurements demonstrate another area, i.e. enzyme action, in which the birefringence technique could prove a useful tool in laboratory studies. They confirm the results of the more laborious methods already mentioned.

CHAPTER 8

Cartilage Proteoglycans: A Wide Ranging Exploratory Study

8.1 Introduction

Proteoglycans are complex heteropolysaccharides. Each consists of[81] a protein core about 400 nm long with approximately 100 sidechains, each about 40 nm long, extending radially outwards along its length. These sidechains are predominantly chondroitin sulphate, though there are also a number of the shorter polysaccharide, keratan sulphate.

The role of proteoglycans within the body is primarily to transport water, which it holds in its dense ionic structure. Proteoglycans found in cartilage differ from those found elsewhere in the body in that they have a specific affinity for binding to hyaluronic acid.[81] At one end of a cartilage proteoglycan molecule is a globular protein, and it is this region of the proteoglycan which binds it to hyaluronic acid. This binding can be broken by chemical degradation or pH changes. There is however a 'protein link'[81] which reinforces the bond and makes it stable against

these environmental changes.

The proteoglycan - hyaluronic acid complex has a similar structure to an individual proteoglycan with proteoglycans arranged radially about the linear polysaccharide, as the sulphate sidechains of a proteoglycan molecule are similarly arranged about its protein core. The proteoglycan and its aggregate are shown schematically in Fig. 8.1.

The role of the aggregate and its biomedical investigation are discussed in the following chapter (9).

The measurements reported in this chapter are on proteoglycans and its major constituent, chondroitin sulphate. These measurements, and those in Chapter 9, were made jointly with Dr A R Poweraker of this research group and in collaboration with Dr T E Hardingham of the Kennedy Institute of Rheumatology, Bute Gardens, Hammersmith, London.

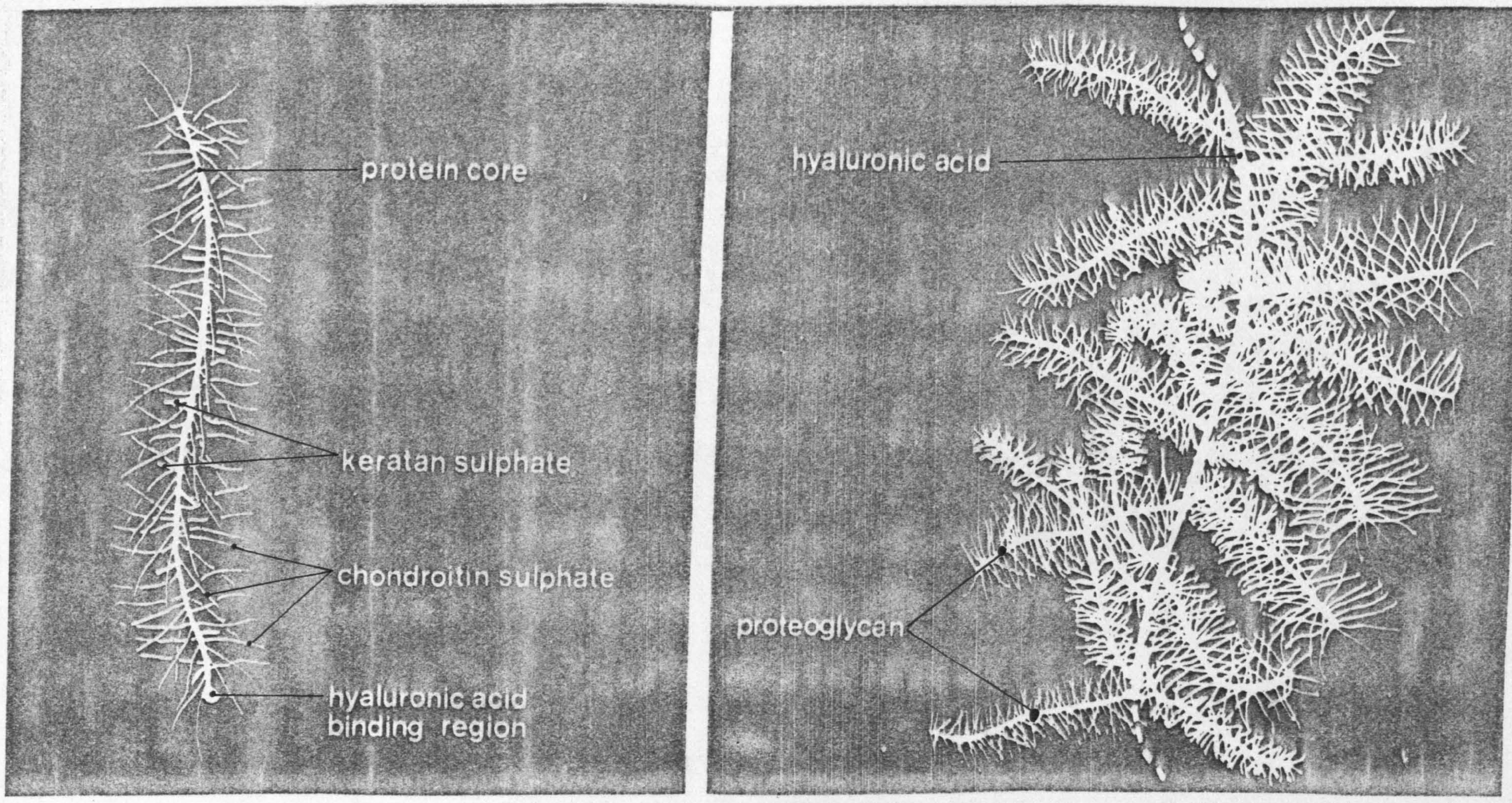

Fig. 8.1 Schematic representation of proteoglycans and the proteoglycan-hyaluronic acid complex.

8.2 Materials

All the samples used were supplied by the Kennedy Institute. The proteoglycans were prepared[82] from a fresh pig's larynx, kindly supplied to the Institute by T Walls and Sons. All materials were suspended in distilled water, their concentrations being quoted in micrograммes of Uronic Acid per millilitre, (μgUA/ml) determined using an automated analyser for assaying their uronic acid contents. For comparison with normal concentration units it should be noted that proteoglycans have ~2.6% UA content. The initial stock solution had a concentration of 240μgUA/ml. Samples were stored in a frozen condition.

8.3 Apparatus

Unless otherwise stated, the apparatus used was Cell B, generator PG3 for both AC and DC measurements, the fixed plane polarised He Ne laser and all the transients were recorded on a Tektronix storage oscilloscope, model 7623A. Transients requiring detailed analysis were photographed on to Polaroid 107C film, which produced prints. Transient decays were analysed by tracing the responses from the prints, superimposing the tracing on to graph paper and thus accurately reading off values along the decay.

8.4 Characterisation of Proteoglycans: Results and Discussion

8.41 High Field Anomalous Transients

The complexity of this molecule with its radial and linear geometry of chain formations naturally calls for care in interpreting results. An initial field dependence set of measurements showed peculiar anomalies at fields in excess of only 450 V cm^{-1}. The transient responses began to exhibit a sudden increase, immediately after the applied field ceased, and then followed the same rate of decay as exhibited at lower field strengths. The effect is shown in Fig. 8.2, which also displays the clarity of signals common throughout the measurements. Two probable causes of these atypical responses are considered.

8.42 Interpretation of Anomalous Effects in terms of the Independent Motion of Sidechains

The effect could be interpreted as a birefringence of opposite sign to that of the individual bulk of a proteoglycan molecule, assumed to be responsible for the initial rise and the final decay. Orientation of the chondroitin sulphate sidechains independent of the overall proteoglycan orientation could cause this secondary high field effect. The hypothesis is

illustrated in Fig. 8.2.

A value for the supposed relaxation time of the sidechains, when evaluated from an enlarged scale transient photo is 180 μs. This compares with a theoretical value of 1.8 μs, treating the sidechain as a rigid rod of 40 nm length and diameter 0.35 nm. This though is a poor model as the sidechains are hydrated and sterically hindered by attachment to the protein core at one end and by neighbouring chains all round. The effect of this hindrance is not readily estimable, and whether it could reconcile the two values is a matter for conjecture. This problem is considered again in section 8.7.

8.43 Considerations of the Effect of Concentration on the Observed Anomalies

The concentration of the solution was considered as a possible cause of the anomalous transients. Although the concentration was only about 0.1%, the suspension was noticeably viscous : the high degree of hydration of the strong ionic structure would explain this. The result of a series of measurements on the variation of the proteoglycan's birefringence with concentration show that the birefringence, normalised with respect to concentration, varies linearly in the range up to 210 - 220 μgUA/ml.

---------- proteoglycan, independent response

---------- sidechain, independent response

resultant transient

Fig. 8.2 (a) Transient response of proteoglycan to applied DC field
(b) Schematic interpretation of possible mechanism to explain the observed response.

Beyond this, non-linearity was evident, indicating a high degree of molecular interaction. A convenient concentration of 209 μgUA/ml was thus used throughout subsequent measurements, thereby giving near maximum birefringence within the linear region of concentration dependence.

The anomalous after-pulse effects now disappeared. Similar concentration dependent effects have been seen by other workers on other systems, both during[83] and after[84] pulse applications. Nonetheless, the model of a two component birefringent system is not discounted entirely as will be seen from the further measurements which follow.

8.44 Quadratic Field Dependence of Proteoglycans

Presented in Fig. 8.3 are birefringence field dependence measurements, for DC pulses. The field dependence is atypical. At fields greater than about 500 V cm^{-1} there is a change in the slope just when the effect appears to reach conventional saturation. This set of measurements should be considered in conjunction with three other sets of data as reported in sections 8.45, 8.46 and 8.47.

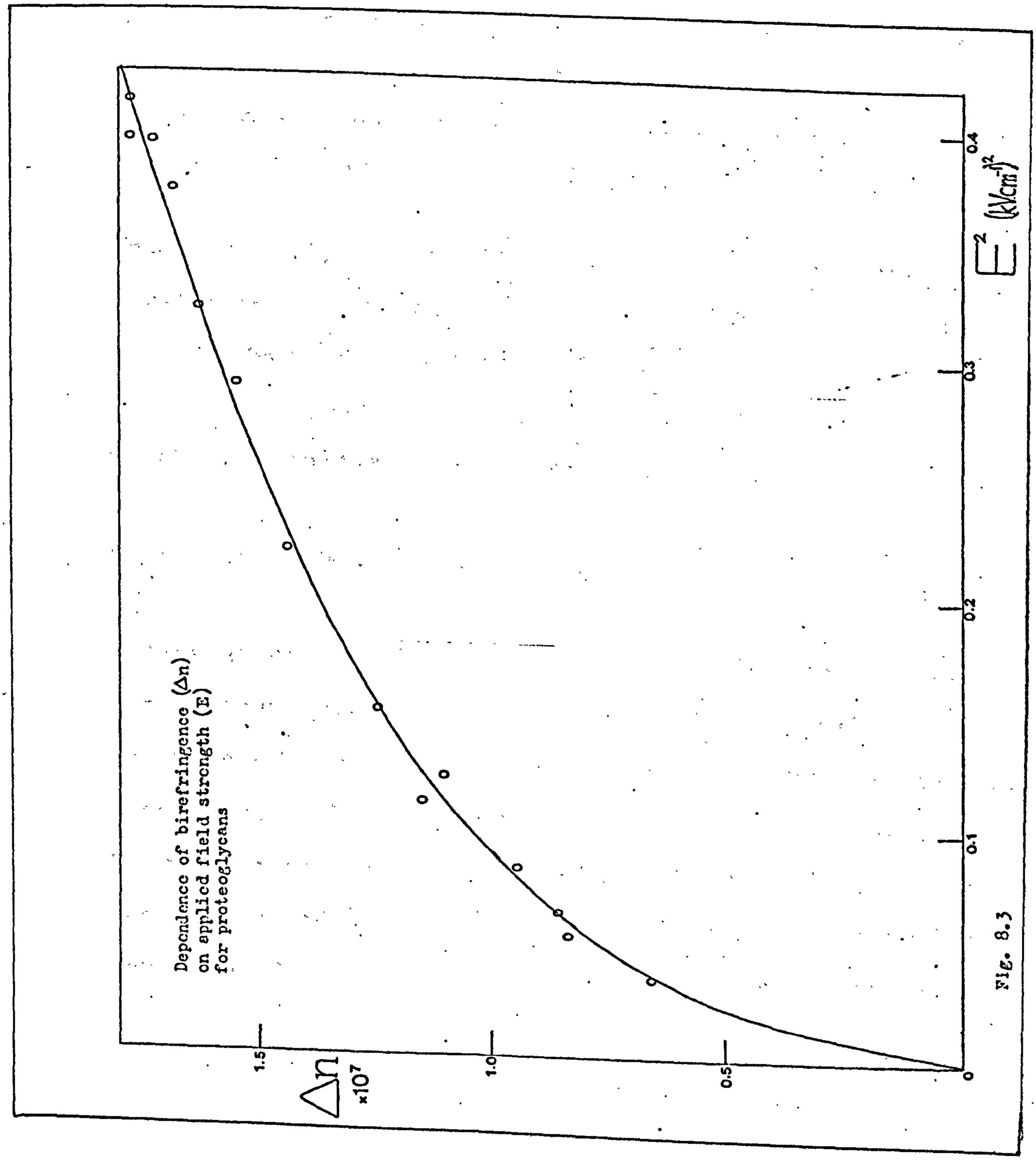

Dependence of birefringence (Δn) on applied field strength (E) for proteoglycans

Fig. 8.3

8.45 Application of a Reversing Pulse

A reversing pulse at low field strength, applied to the suspensions (see section 2.6) indicated a permanent dipole moment and a ratio of apparent permanent to induced dipole moment for proteoglycans such that:

$$\frac{\beta^2}{2\gamma} = \frac{2}{15}$$

from Fig. 8.4. As will be recalled from section 2.6, a value for the rotary diffusion constant can also be deduced from this response, viz:

$$D = 68.5 \pm 17\ s^{-1}$$

which corresponds to $\tau = 5.85 \pm 1.45$ ms.

8.46 Field Free Decay Analysis

A more accurate value for the relaxation time, τ $(= \frac{1}{6D})$ can be found from the second set of data, namely analysis of the decay rates of the transient birefringent responses. These give $\tau = 3.6 \pm 0.3$ ms. Using Perrin's equation for a prolate ellipsoid of 40 nm semi-minor axis, the value of τ relates to a molecular length of 380 ± 20 nm which is in good agreement with previous estimates.[85]

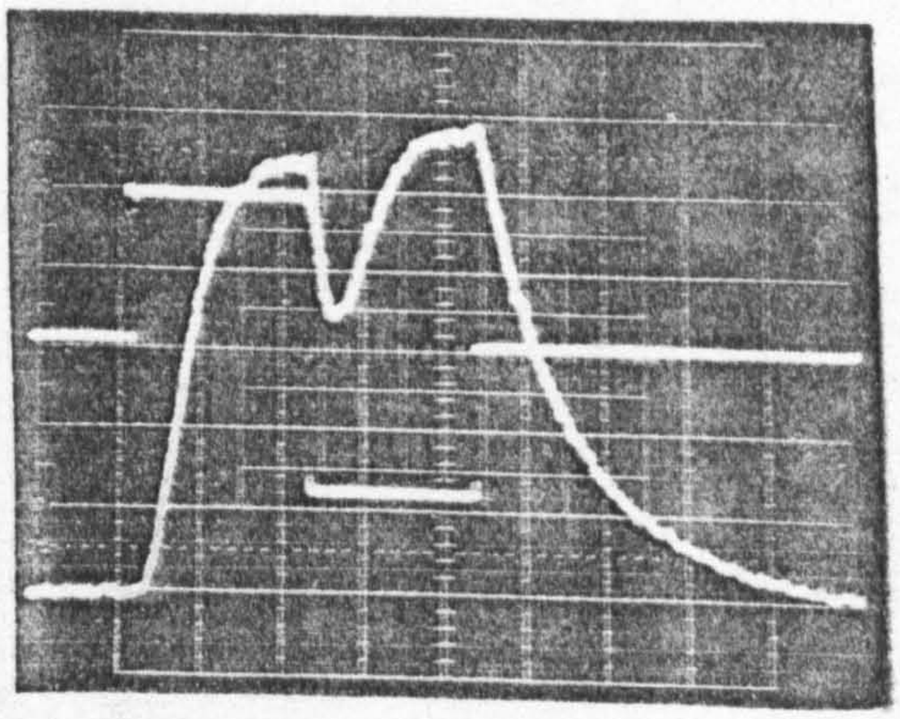

Fig. 8.4

Reversing field pulse response of proteoglycan suspension demonstrating a permanent moment.

8.47 Dispersion of Birefringence with Frequency

Thirdly, the birefringence dispersion with frequency is presented (Fig. 8.5). These measurements were conducted at a constant field strength of 350 V cm^{-1}, corresponding to a voltage at the higher end of the first region of linear dependence of birefringence with the square of the field strength (Fig. 8.3). The dispersion shows a sudden rise to a peak value at 35 Hz followed by a conventional decrease in birefringence with frequency. This pattern of behaviour was noted in two initial sets of measurements on separate suspensions, in addition to the data presented in Fig. 8.5. Therefore whilst being atypical it cannot be regarded as spurious. It is considered that two relaxation processes are taking place through the frequency range and Fig. 8.6 illustrates a combination which would result in the effect seen. With such a combination, the critical frequency of each of the two contributing dispersions is not exactly determinable, but a range of possible values is. Clearly the lower frequency dispersion must occur between the perceived dispersion (Fig. 8.5, f_{c1} = 8 Hz) and the frequency for maximum birefringence (f_{max} = 35 Hz). Analysis of transient decay times in this region still yield the value as at DC for the relaxation time, τ, of 3.6 ms, which in turn corresponds to an equivalent critical frequency of 14.2 Hz. This value of 14.2 Hz falls conveniently

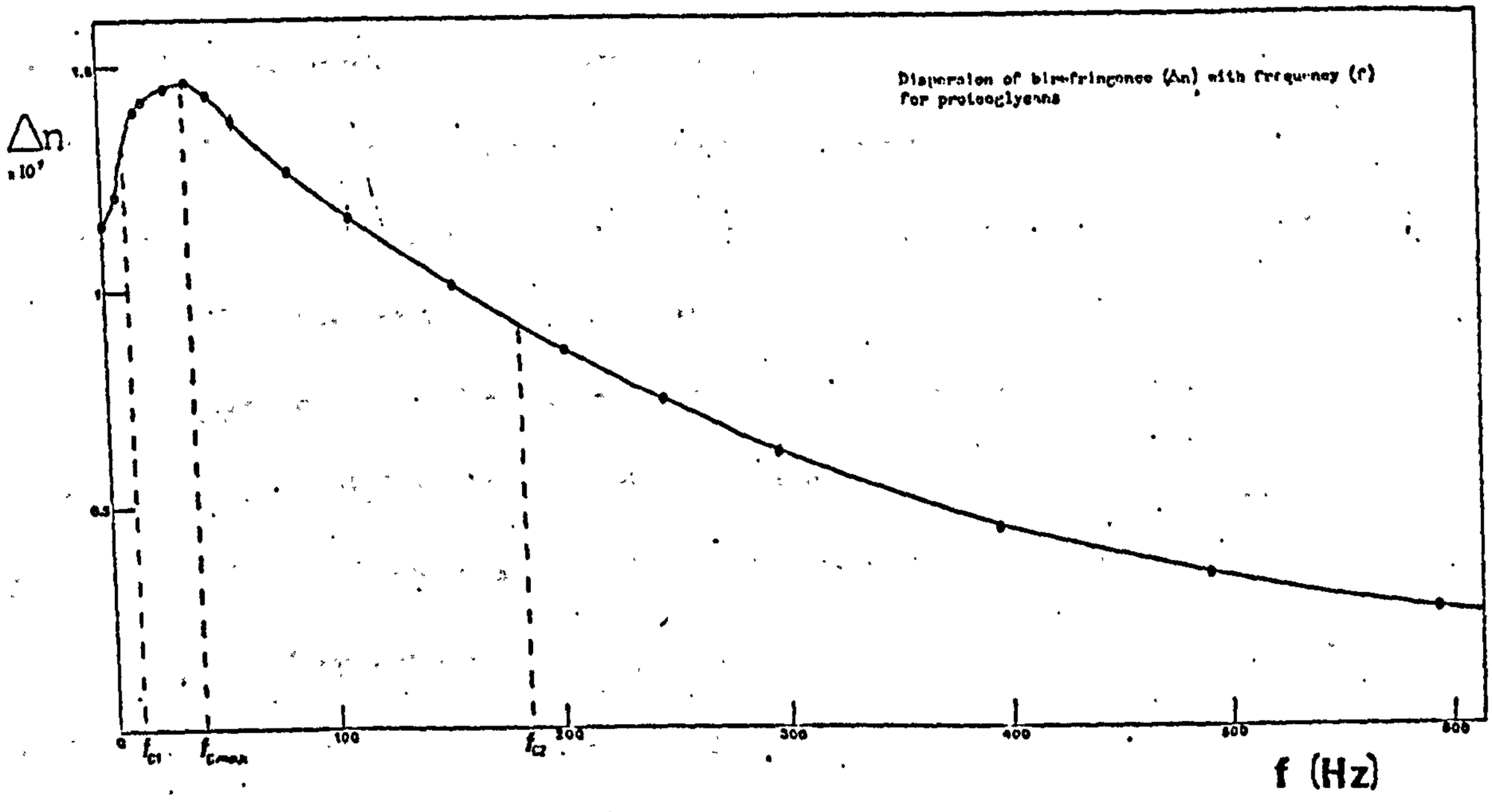

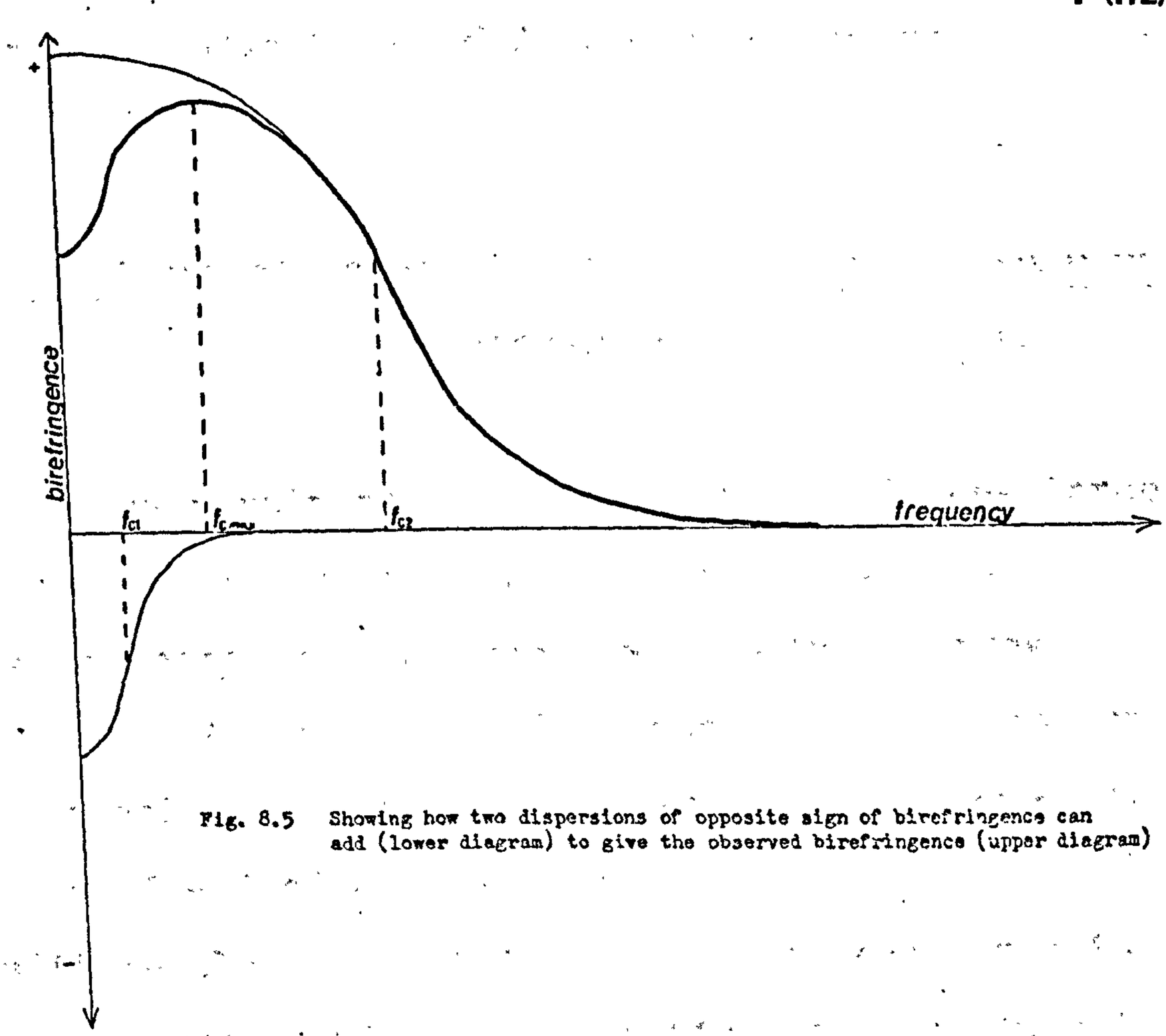

Fig. 8.5 Showing how two dispersions of opposite sign of birefringence can add (lower diagram) to give the observed birefringence (upper diagram)

in the range of values suggested for the lower frequency dispersion.

Thus, if the proteoglycan relaxes out at 14.2 Hz this implies that the proteoglycan molecule itself is not contributing to the overall birefringence much above 50 Hz and the question remains : 'What causes the higher frequency dispersion?' Again the critical frequency of this dispersion must lie between f_{max} and f_{c2}. f_{c2} corresponds to a relaxation time of 0.22 ms. Moreover the second mechanism is indicated to have a birefringence of opposite sign to the phenomenon associated with the lower frequency dispersion.

8.48 Correlation of anomalies in E^2 and frequency dispersion measurements.

It is now pertinent to examine the field dependence results shown in Fig. 8.3 more closely. The DC measurements are in concord with a two component system. At the lower field strengths orientation of the complete proteoglycan molecule is suggested and at higher field strengths, the molecule's sidechains are sufficiently orientated along the molecule's axis to further contribute to the birefringence, Fig. 8.6. Measurements on isolated sidechains (section 8.8) support this model. They show a continual increase in birefringence with field strength which does not

saturate, even at very high fields.

If this is so, then clearly the sidechains cannot be responsible for the higher frequency dispersion for two reasons. Firstly, the field dependence measurements indicate that the proteoglycan molecule and the sidechains have birefringence of the same sign, contrary to the conclusions drawn from the frequency dispersion. Secondly, the dispersion was carried out at a field strength below that at which the field dependence suggests that the sidechains are capable of contributing to the overall birefringence.

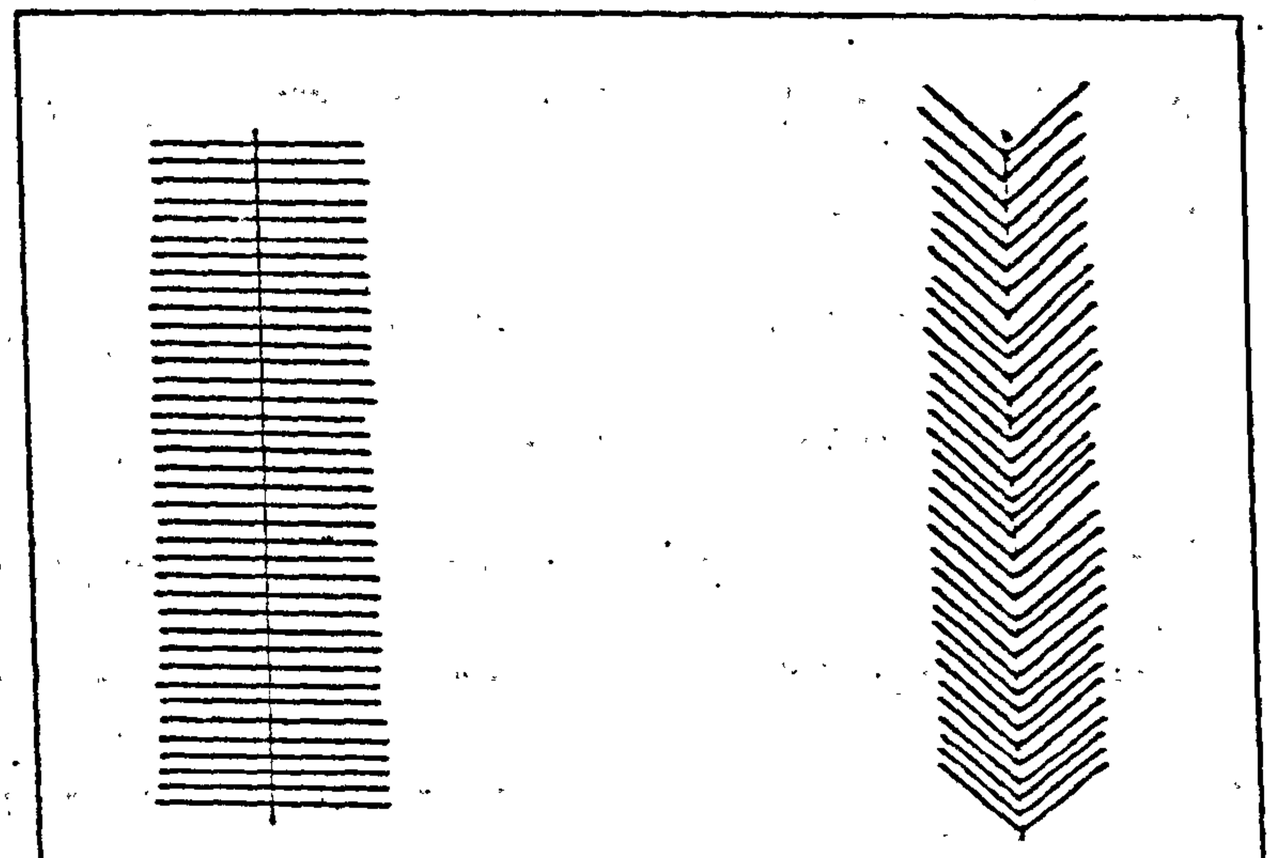

-Fig. 8.6

Schematic representation of suggested mechanism for sidechain orientation.

3.49 Conclusion

It is therefore concluded that the higher frequency dispersion is the proteoglycan molecule itself relaxing. The agreement between the DC relaxation time, τ = 3.6 ms, and the frequency dispersion is regarded as coincidental, and indeed misleading. Studies by the author (presented in Chapter 6), and other workers, have shown many occasions, using polar solvents, in which the value of the relaxation time obtained from pulsed DC transients and from AC frequency dispersions, via the critical frequency, do not agree. Chapter 6 reports differences as large as 10 to 1. Thus the DC value of 3.6 ms could relate to the higher frequency range dispersion which corresponds to τ values from 0.22 ms up to 1.52 ms. This leaves the lower frequency dispersion without explanation, and the reader is referred back to the discussion in Chapter 6 on DC phenomena as a possible explanation for this. Until a better understanding of DC phenomena, such as electrophoresis, is obtained, the actual mechanisms involved will continue to be conjecture. Albeit on other materials, many workers are having difficulty in reconciling data from low frequency dispersions with other measurements, so whilst not definitive, the DC phenomena offer plausible explanations for the shape of the proteoglycan dispersion reported herein, and for the difficulties experienced by others.

8.410 Summary

This section has discussed and presented data on the proteoglycan molecule in aqueous suspension. Solutions to the problems posed by the atypical data have been proposed, with the object of forming a basis for a more detailed study.

In the next few sections, the author expands the basis for future study further by examining specific properties of proteoglycans and its components before, in the next chapter, looking at the dramatic process of aggregate formation with hyaluronic acid.

8.5 Investigation of a Proposed Mechanism for Bonding in the Protein Core

8.51 Proposal of Wells and Serafini-Fracasini

Equilibrium sedimentation and gel filtration measurements by Wells and Serafini-Fracassini[86] suggest that proteoglycan molecules may be formed from a number of subunits, with a very strong aggregating tendency. They believe the subunits are held together by hydrophobic bonds within the protein core, possibly reinforced with crosslinks. In order to dissociate the subunits, they added a non-ionic detergent, "Triton X-100" (from Messrs. Rohm and Haas, Croydon)

to proteoglycan solutions and observed approximately four fold decreases in molecular weight.

Wells and Serafini-Fracasinis' model is not generally favoured by biochemists researching in this field of study, and the existence of the hydrophobic bonds is doubted.[87]

8.52 Investigation of the Proposed Bonding using Electric Birefringence

With the electric birefringence technique, the effect of Triton X-100 on proteoglycans, were it as dramatic as suggested by Wells and Serafini-Fracasini[86] would be readily observable. Assuming the molecules are roughly quartered when the hydrophobic bonds are broken (corresponding to Wells and Serafini-Fracasinis' molecular weight decrease) then one would expect the relaxation time to decrease by 4^3 (i.e. 64). This is derived from Perrin's equation (section 2.812) which proportions τ to the cube of the major axis of the ellipsoidal model, ignoring the change in axial ratio. In reality quartering the proteoglycan would imply spherical geometry and the use of Perrin's equation for a sphere : nonetheless, the change in relaxation time would still be roughly of the same order.

8.53 Results and Discussion

A suspension of proteoglycan was therefore treated with the addition of 0.1% Triton X-100 solution, supplied by the.Kennedy Institute, at the same concentration as used by Wells and Serafini-Fracasini. Changes in the relaxation time and birefringence amplitude occur, but were not as large as predicted. The value of τ decreased by less than a factor of two implying (via Perrin's ellipsoid equation) a ratio of 'before and after' lengths of 1 to 0.87. The birefringence, similarly, halved in value. Clearly the hydrophobic bonds were not broken as suggested. It is likely that the detergent acted to screen the proteoglycan in some way from its ionic environment resulting in a slight coiling of the molecule and the reduction in length intimated by the changes in τ. It should be noted that the previous workers conducted their measurements in 1 M potassium acetate at pH 4.0, an environment that might be more inducive to the action of Triton X-100 on proteoglycans.

8.54 Conclusion

To rigorously establish the existence or otherwise of the subunit structure and hydrophobic bonding, electric birefringence offers the ideal straight-forward and sensitive technique. The interaction could be

investigated further in a variety of solvents, at different pH and different concentrations of detergent, and indeed, with different detergents which should lead to a definitive solution to the question posed by Wells and Serafini-Fracasini.

8.6 Variation of the Ionic Strength of Proteoglycan Solutions

Even small changes in the ionic strength of the proteoglycan suspension result in significant changes in transient respose. The effect is even visible to the naked eye in that the viscosity of the suspension can be seen to change between distilled water and 2 mM NaCl solvents.

With the existing pulse generators it is not possible to make measurements at 2 mM NaCl with negative going pulses (i.e. reversing pulses and AC pulses are clipped in the negative phase). The contrast showing the change in birefringence response with positive DC pulses in 2 mM NaCl is illustrated in Fig. 8.7. An ionic environment is clearly to be preferred from a biomedical viewpoint, as it more closely resembles the *in vivo* state. With higher power pulse generators, it may be possible to approach the *in vivo* condition, but with the duration of pulses required for proteoglycan

suspensions, it is likely that electrophoretic and heating effects would pose severe problems

From Fig. 8.7, it can be seen that both the birefringence and relaxation time have halved in value as a result of the change in the ionic environment (Δn : 7.4×10^{-8} to 3.7×10^{-8}, τ: 4.75 ms to 2.55 ms). This is indicative of the molecules' native charge being screened by the extra ions and a resultant decrease in the extension of the proteoglycans in solution.

8.7 Trypsin digested Proteoglycans

8.71 The action of Trypsin

Trypsin attacks the protein core of proteoglycan molecules effectively leaving a solution of portions of the protein core, with attached sidechains.

8.72 Simulation of Sterically Hindered Sidechains

Under an applied electric field, each individual portion might well act in a similar fashion to the sterically hindered sidechains on a normal proteoglycan. The relaxation times and field responses of these portions

would therefore be useful in assessing any contribution from sidechain orientation in addition to that from the overall proteoglycan molecule.

8.73 Experimental

A solution of trypsin digested proteoglycans was therefore studied. Generator PG6, applying 5 μs pulses at voltages up to 12 kV cm^{-1} was required to obtain birefringent responses.

8.74 Results and Discussion

Relaxation times of a few microseconds were observed but were not consistent one with another. Likewise, the size of the overall birefringence varied eratically from pulse to pulse. This may be a concentration effect resulting from interaction of the digested proteoglycan portions.

The original concentration of the sample was unknown, but believed to be of the same order as that of the proteoglycans studied earlier. Dilution did not improve the consistency of the responses, and dilution by more than a factor of ten diminished the response beyond the power of the pulse generator.

8.75 Consideration of Conformation

The relaxation times lie between two values derived from plausible models of the digested proteoglycans, namely the rod and disc models. Taking a typical value for a sidechain of 40 nm then an 80 nm Broersma rod model implies a value of 14.4 μs for the relaxation time, and a 40 nm radius Perrin's disc model implies a 0.262 μs relaxation time. A Perrin ellipsoid of semi-major axis gives an approximate value of 50 μs and is therefore not appropriate in this instance (see section 2.8 for details of these models).

8.76 Conclusion

The relaxation times observed are consistent with the sort of model one would expect for portioned proteoglycan molecules, lying as they do between the values for rod and disc models. The erratic behaviour of the birefringence is not so readily understandable, and may first require the application of stronger electric fields and a better understanding of the proteoglycan anomalies mentioned earlier. Whether the variations result from fleeting associations of digested portions, the random adoption of different molecular alignments, or other possible causes, is currently a matter for further research or conjecture.

8.8 Chondroitin Sulphate Sidechains

8.81 Introduction

Compared to its fellow mucopolysaccharide, hyaluronic acid, chondroitin sulphate is much shorter, with a consequent lower molecular weight range, and it is highly charged.[88] It follows from the latter that its conformation in aqueous solution will be more rod like.

8.82 Sample and Apparatus

A sample of chondroitin sulphate of approximately 15,000 molecular weight was prepared for study by the Kennedy Institute. Molecular weights of this size are at the limits of observable experimentation with the birefringence technique and it was initially doubted whether any measurements could be recorded.

Nonetheless, it proved possible to detect birefringence in the suspension supplied, using generator PG6 to deliver pulses of 3 μs duration.

8.83 Results and Discussion

It can be seen that it was not possible to saturate the effect at high fields, but a clear E^2 dependence is evident as can be seen from the graphical representation of the sample's quadratic field dependence of birefringence, Fig. 8.8.

A typical transient is indicated in Fig. 8.9. That the effect can be seen at all is an indication of the high charge and consequent large dipole moment associated with the molecule. It also confirms the notion of an extended rod formation.

Assuming the chondroitin sulphate to be a rigid rod of 40 nm length, Broersma's equation (section 2.811) gives a corresponding value for τ as 1.8 μs. This is close to the experimental value of 0.9 μs equivalent to a Broersma rod length of 32 nm. However, it should be noted that with the 5kΩ photomultiplier load resistor - the smallest that could be used to obtain a measurable pulse - the time constant of the signal detection system is 0.64 μs. This implies that the relaxation time measured might be larger than the true relaxation time of the molecule.

Dependence of birefringence (Δn) on applied field strength (E) for chondroitin sulphate

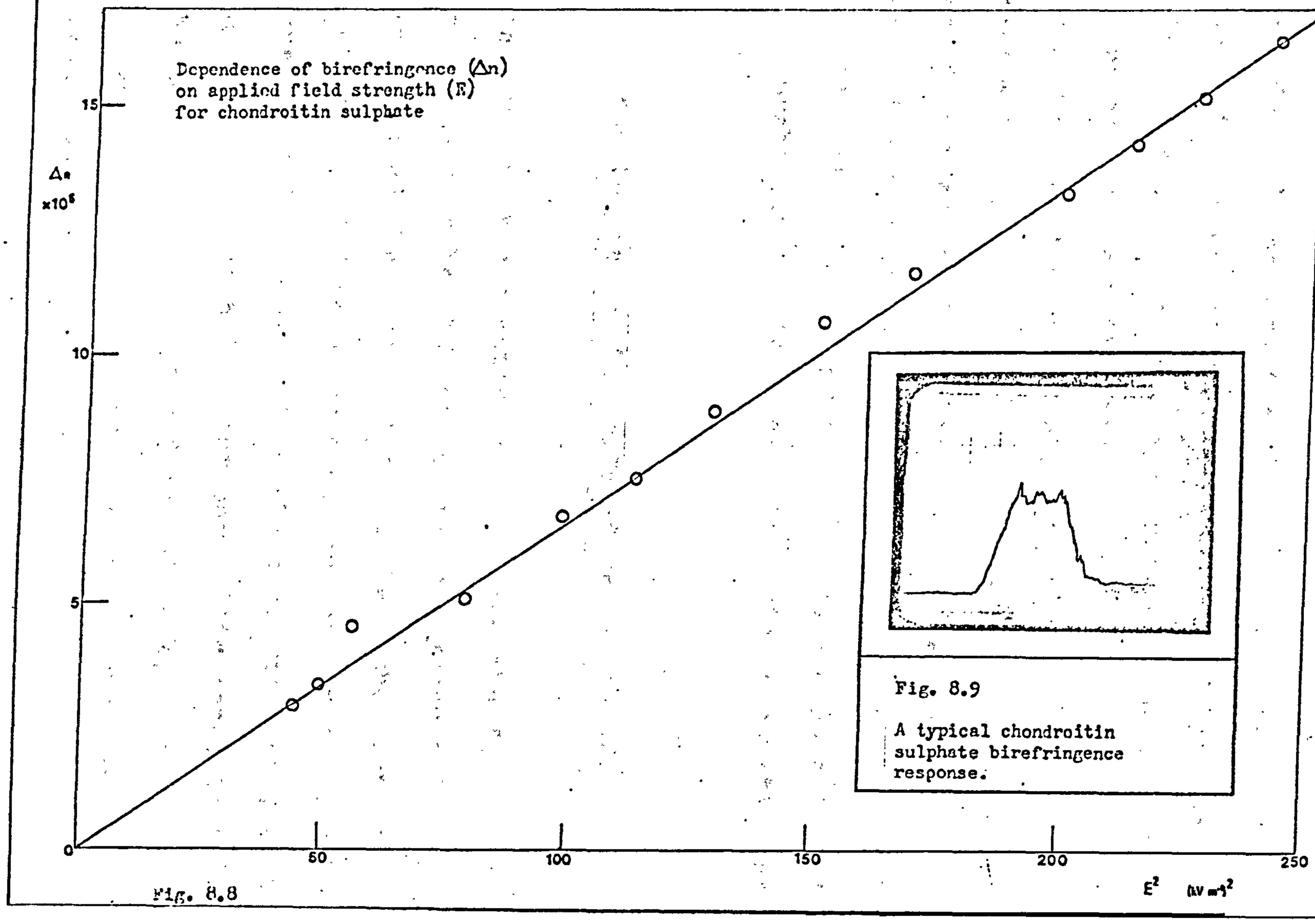

Fig. 8.8

Fig. 8.9

A typical chondroitin sulphate birefringence response.

8.84 Conclusion

Because of the molecule's size and charge, an extended rod conformation has been suggested. The theoretical Broersma rod model shows good agreement with the observed molecular relaxation times. It is therefore unlikely that the true relaxation time is much short of that measured. It is thus possible, that with a little care, the birefringence technique could be used to study this major proteoglycan constituent on its own. This is an important consideration in envisaging the technique as a tool for a comprehensive study of cartilage tissue constituents.

8.9 Conclusion to the study of Proteoglycans

The work in this chapter has presented the first electro-optic data to be obtained on proteoglycans and has demonstrated the ease with which the method can and could be applied to a range of problems in the further general study of this vital molecule, important, as it is, in the research into osteoarthritic conditions. The next chapter presents detailed work, suggesting an insight into proteoglycans' role in the onset of osteoarthrosis.

CHAPTER 9

Formation of the Proteoglycan–Hyaluronic Acid Aggregate

9.1 Introduction

The binding of proteoglycans to the polyelectrolyte, hyaluronic acid, has already been mentioned in section 8.1. This chapter reports data on the formation of the proteoglycan - hyaluronic acid aggregate. The aggregation is simultaneously followed stage by stage by two independent techniques.

The aggregates themselves are known to exist as such in cartilage tissue, together with free proteoglycans. Their exact physiological role is unknown, though there is some evidence that the proportion of aggregates may vary with age,[91] with development and maturity[92] and in pathological states.[93,94] For these reasons a great deal of research has gone on in recent years to fully characterise proteoglycans, their aggregates and their interactions, much of the work involving techniques requiring intricate sample preparation, tedious measurements or both. The various techniques include gel chromatography,[95] viscosity,[95] electron microscopy[96]

and X-ray diffraction.[97] It is from these tedious labours, nonetheless, that the models already outlined have been deduced, and their sizes determined. For example, by controlled hyaluronidase degradation of hyaluronic acid, it has been shown that the minimum size to which a proteoglycan molecule will bind is a decasaccharide of hyaluronate.[98] This is roughly equivalent to one per 10,000 molecular weight units. Thus a typical aggregate will have about forty proteoglycans attached to one hyaluronic acid chain.

By varying pH conditions, it has been deduced that the proteoglycan bonding has nothing to do with hyaluronic acid's carboxyl groups[95] yet it has also been shown that the binding is specific to hyaluronic acid with no aggregation being observed in respect of other polyanions, particularly from the mucopolysaccharide family: dextran sulphate, chondroitin sulphate, DNA, sodium alginate.[95]

To further aid researches into this aggregate, which is at the centre of the biochemical research into the osteoarthritic condition, the following report is presented. In reading this report, the reader should bear in mind the rapidity with which these results are obtainable and the sensitivity of the technique to the conformational changes seen.

9.2 Experimental

To facilitate the addition of the hyaluronic acid to the proteoglycans, the flow cell was employed in a similar manner to that used in the hyaluronidase measurements, (section 7.72). The proteoglycan solution was the same as that used in Chapter 8 (section 8.2) with an initial concentration of 209 μgUA/ml. The hyaluronic acid was a commercial preparation supplied to the Kennedy Institute by Messrs B.D.H. Ltd., Poole.

Initially hyaluronic acid of concentration 20 μgUA/ml ($\sim$60μg ml^{-1}) was added, via the reservoir, in steps of 0.05 ml, using a fine pipette to a total volume of 10 ml of proteoglycans. In later measurements (section 9.35) a more concentrated solution of hyaluronic acid was used and added to the reservoir using a Finnpipette graded from 5 - 50 μl. After each aliquot of acid was added to the sample, it was circulated through the system to allow dispersion. It was then allowed to stand for some fifteen minutes, to enable the proteoglycans to interact with the hyaluronic acid before a pulsed electric birefringence transient was recorded.

Using the system of quadratic detection with offset analyser, the level of the transmitted light intensity was monitored throughout the readings.

Electric fields of 360 V cm^{-1} were used throughout, initially with pulses of 10 ms duration, and later of 160 ms.

9.3 Results and Discussion

9.31 Proteoglycan Solutions

A typical birefringence transient for proteoglycans is shown in Fig. 9.1. The following points are noted:

1. The birefringence appears positive, indicating that the molecules' optical polarisability is greatest along the major geometric axis.

2. An initial slope relaxation time of 3.6 ± 0.3 ms is indicated, as reported in section 8.46

3. Using a Perrin ellipsoid model (section 2.812), and taking a value of 40 nm for the semi-minor axis (the length of a chondroitin sulphate sidechain[99]), a value of 380 nm is found for the length of a proteoglycan molecule. Comparing this with Hardingham and Muirs' value[99] of 300 to 400 nm, this suggests that the molecule was maximally extended at these low conditions of ionic strength.

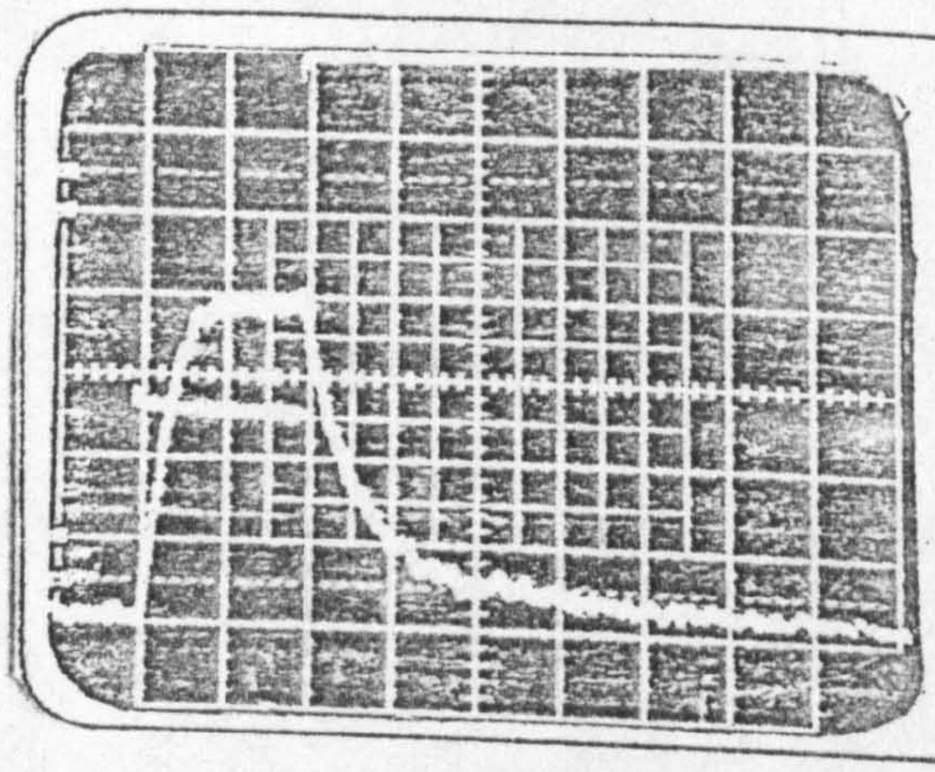

No added HA

amplitude ~ 7.8 v

$n = 6.4 \times 10^{-8}$

$\tau = 3.6$ ms

Fig. 9.1

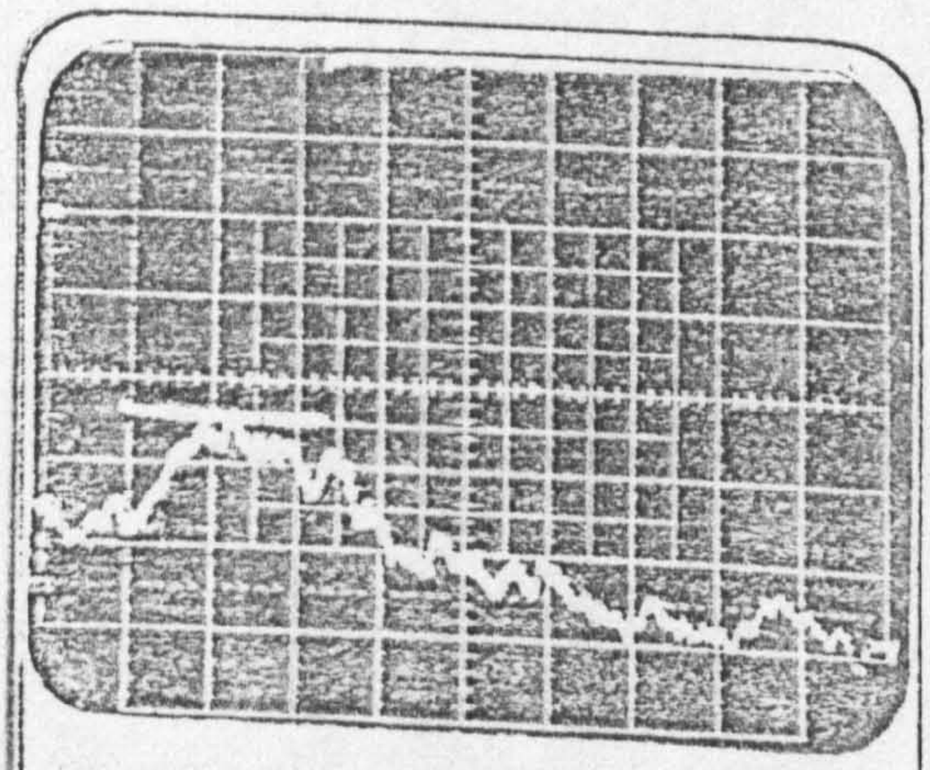

Fig. 9.2

'Fast' contribution

with 0.67% HA

amplitude ~ 0.1 v

$n = 9.8 \times 10^{-9}$

$\tau = 3$ ms

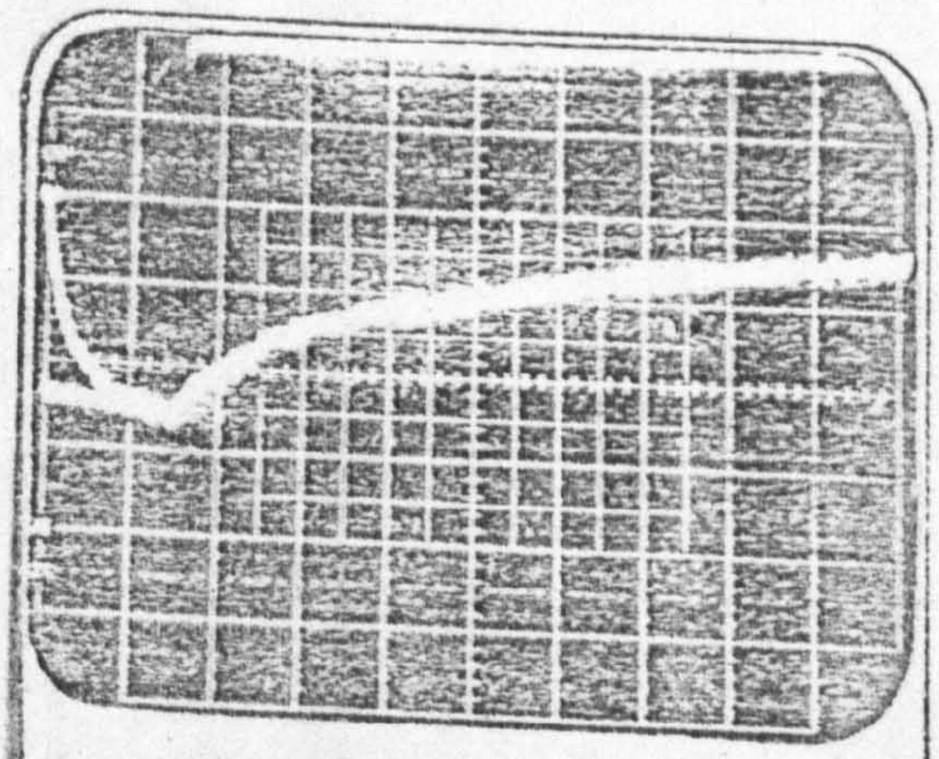

Fig. 9.3

'Slow' contribution

with 0.77% HA

amplitude ~ -1.3 v

$\tau = 650$ ms

9.32 Proteoglycan - Hyaluronate Complex

As the hyaluronic acid was progressively added to the proteoglycan solution, the birefringence changed. Under fields of 360 V cm^{-1} and 10 ms duration, the following points were noted:

1. The positive amplitude of the birefringence progressively and continuously decreased, as shown in Fig. 9.4.
2. Analysis of decay curves revealed the same initial slope, i.e. the same relaxation time through the complete range of added hyaluronic acid measurements.
3. For concentrations of acid greater than 0.57% the transients exhibited an increasing tendancy to overshoot the base line at the end of the decay process, (Fig. 9.2).

The final point appears due to the presence of a second rotary process with apparent birefringence of opposite sign and of a much longer relaxation time. In an attempt to study this additional contribution, the field duration was increased to the 160 ms value. A typical response is seen in Fig. 9.3. The characteristic relaxation time of this response, a slow negative contribution, was 650 $\pm$ 30 ms. It was noted that as the hyaluronic acid content was increased, the positive, fast contribution diminished, and the negative, slow process became increasingly dominant. These will

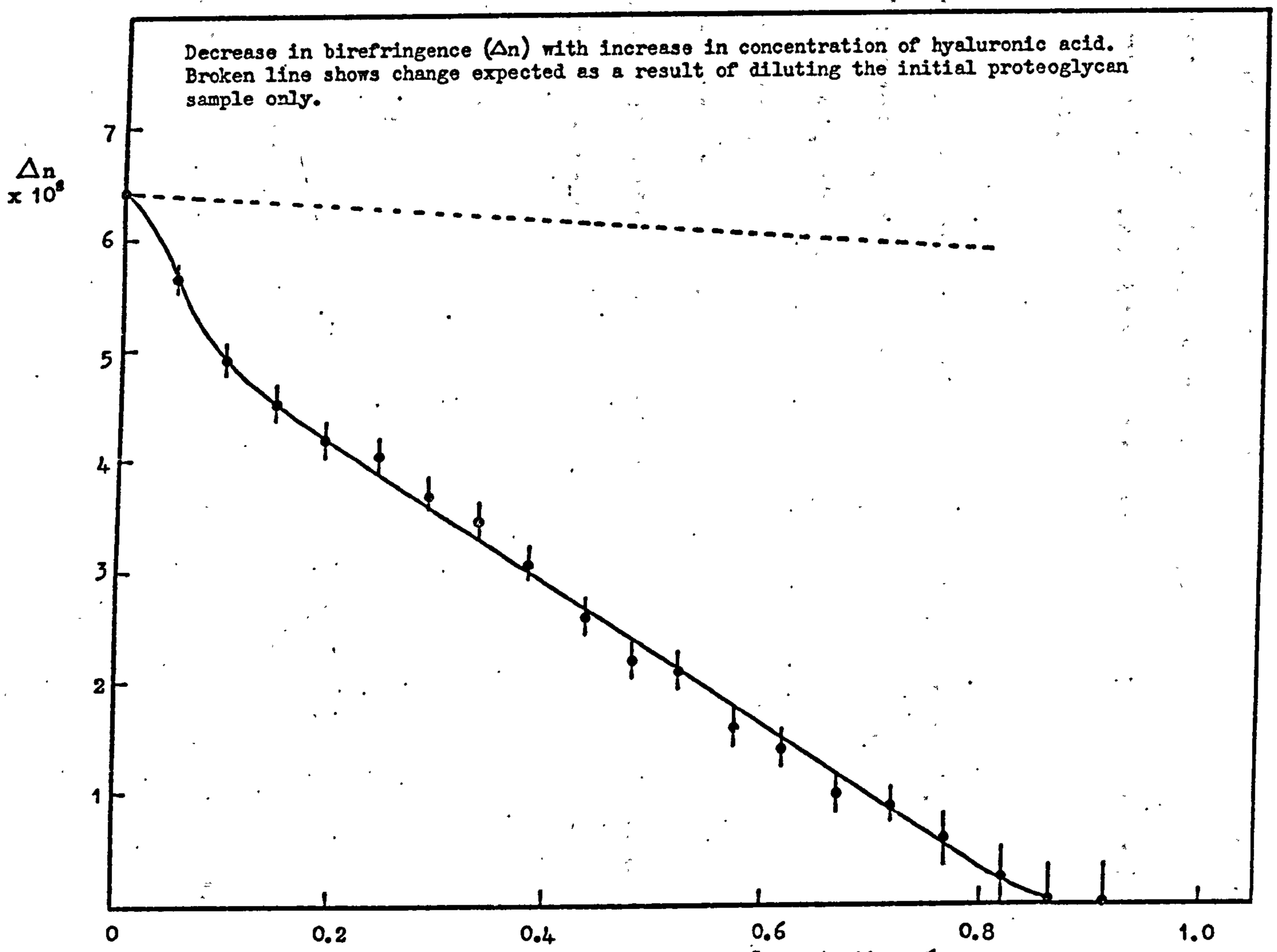
Decrease in birefringence (Δn) with increase in concentration of hyaluronic acid. Broken line shows change expected as a result of diluting the initial proteoglycan sample only.
Δn x 10⁸
7
6
5
4
3
2
1
0
0.2
0.4
0.6
0.8
1.0
Concentration: % Uronic acid of HA to proteoglycan

Fig. 9.4

subsequently be referred to as the 'fast' and 'slow' contributions respectively.

In addition to these electric birefringence measurements and their changes with addition of hyaluronic acid, Fig. 9.5 illustrates the concurrent changes in optical density measured as its reciprocal, i.e. the background transmitted light intensity.

The increase in optical density which Fig. 9.5 illustrates, suggests that as the hyaluronic acid was added, the scattering power of the solution increased, thereby depleting the light flux penetrating the medium. Thus the growth in scattered intensity pointed immediately to a growth in solute particle size.

9.33 Interpretation of the Data so far

The constant value of the fast component relaxation time and its identification with the value obtained for the proteoglycan molecules in section 8.46 indicates the retention of free proteoglycan molecules in solution when small quantities of hyaluronic acid are added. Fig. 9.4 thus provides an indication of the declining quantity of free proteoglycans in the

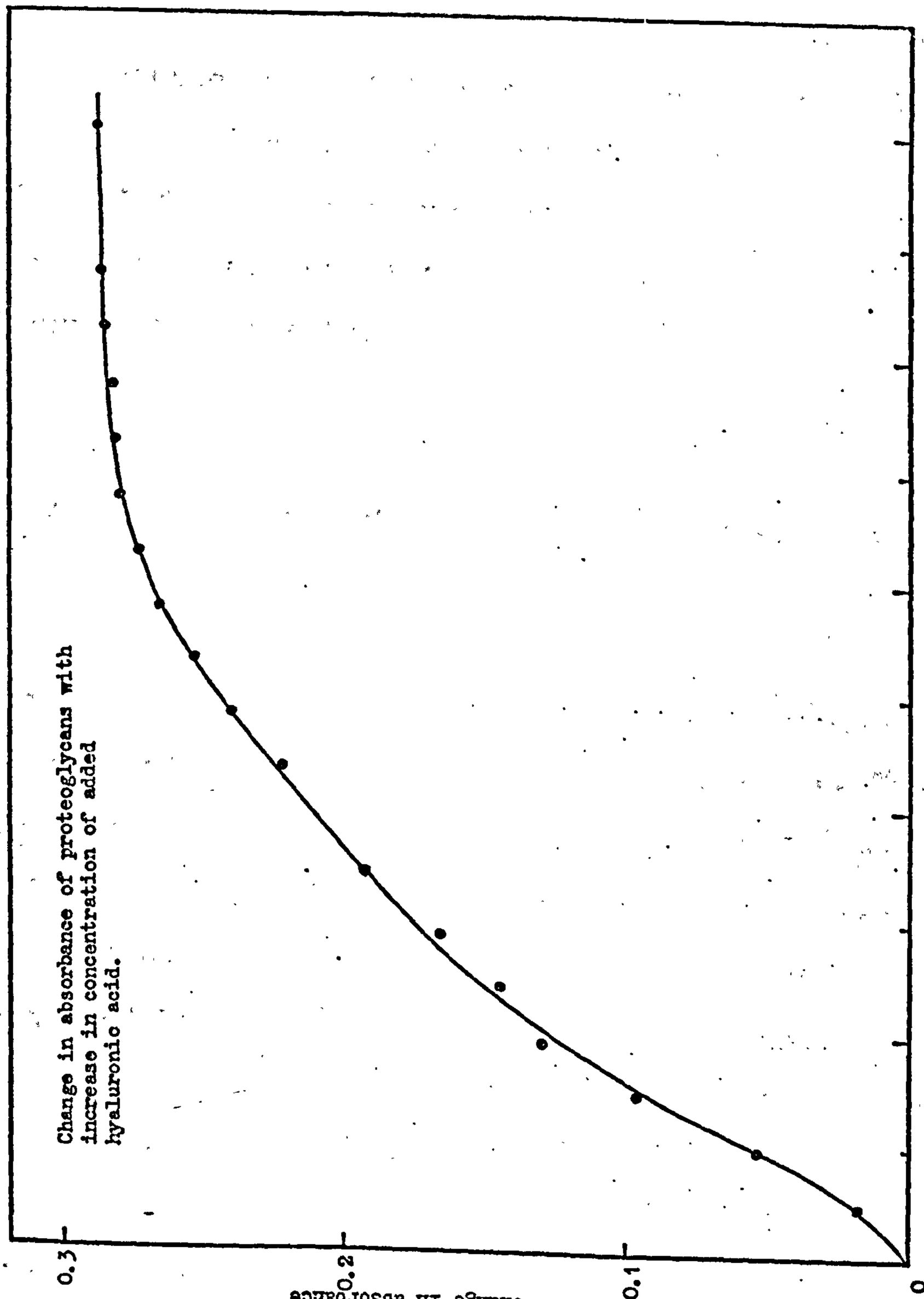
Change in absorbance of proteoglycans with increase in concentration of added hyaluronic acid.
Change in absorbance
0.3
0.2
0.1
0
0.2
0.4
0.6
0.8
1.0
Concentration: % Uronic acid of HA to proteoglycan

Fig. 9.5

component became increasingly important as the fast component suffered its decline. The much greater, but constant, value of τ for the slow component was some 180 times the value of the fast component. This, coupled with the corresponding increase in optical density and the accompanying change in the sign of the birefringence, all suggest that a highly specific molecular aggregation was present in ever increasing quantity.

9.34 Agreement with the Proposed Hardingham-Muir Model

Furthermore, the data offer excellent confirmation of the model described by Hardingham and Muir [99] for the complex aggregate formed between proteoglycans and hyaluronic acid. In essence the model consists of proteoglycan molecules which are attached to the extended hyaluronic chains in a radial manner. Fig. 9.6 illustrates the aggregate with a photograph of a model built by the author. The proteoglycan molecules are seen to be attached with an approximate regular spacing. The attachment results from a specific interaction with a globular protein head located at the end of each proteoglycan molecule.

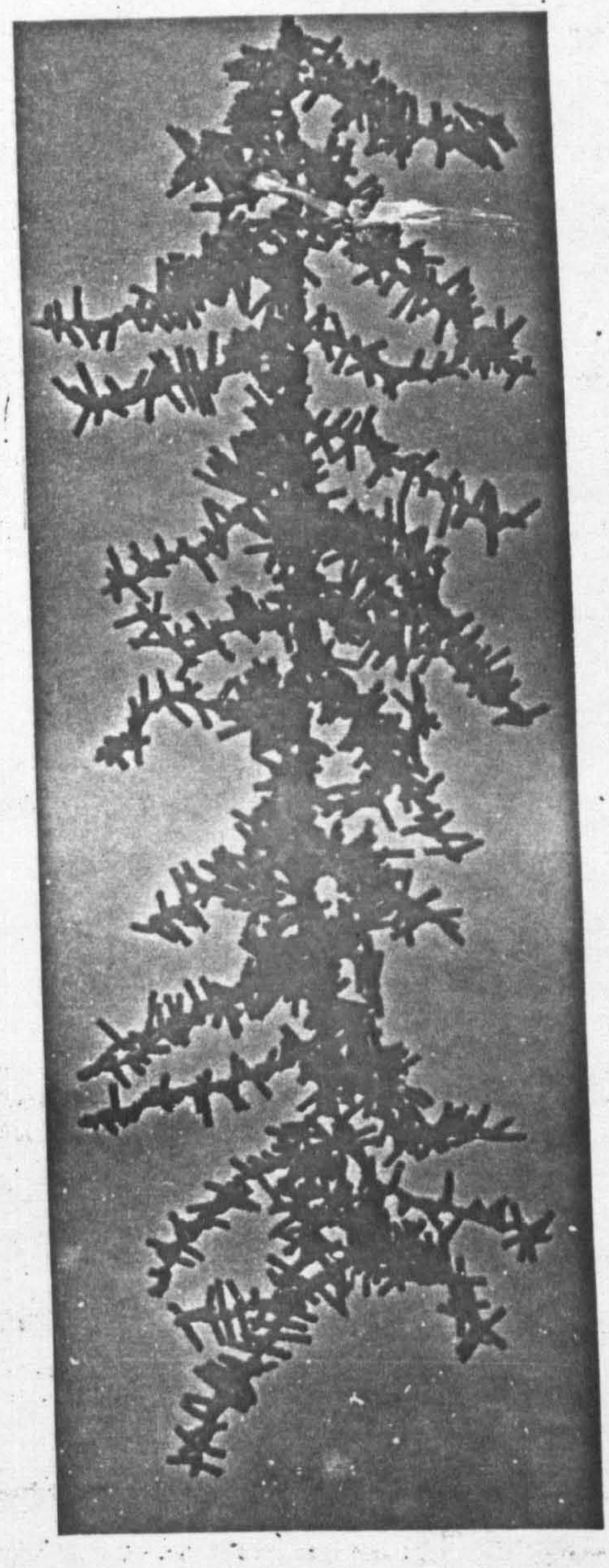

Fig. 9.6
The proteoglycan aggregate model.

The electric birefringence data enable quantitative discussion of the model. Firstly, note that the *major* axes of the proteoglycan molecule, in the model, form the transverse or ***minor*** axes of the aggregate. Hence the birefringence of the aggregate should be of the opposite sign to that of the individual proteoglycan molecules. This was observed experimentally, (cf Fig. 9.1 and Fig. 9.3).

Secondly, to an initial approximation, the aggregate may be considered as a prolate ellipsoid, with the major axis defined by the length of the extended hyaluronate chain, Fig. 9.6.

Taking the previous value of 380 nm for the length of an individual proteoglycan (section 9.31) this is equivalent to the semi-minor axis of the ellipsoidal aggregate. Coupling this information with the slow relaxation time of 650 ms and the Perrin equation

(section 2.812) an overall length of 1.8 ± 0.1 μm is indicated for the aggregate. This is in remarkably close agreement with the length of 1.6 μm estimated for the individual hyaluronic acid molecules from viscosity data obtained by the Kennedy Institute. In addition it supports the suggestion that the aggregate too exists in a highly extended state at the low ionic strengths used in this study.

Thirdly, from Fig. 9.4, the birefringence is observed to decrease to zero when the hyaluronic acid concentration has risen to 0.86% of the total uronic acid content. If the positive birefringence is taken as indicative of the unaggregated proteoglycans in solution, then this particular value for added hyaluronic acid corresponds to the condition where all the proteoglycans is used up in the formation of aggregates. From this condition, and assuming molecular weights of 2×10^6 and 6.7×10^5 for proteoglycans and hyaluronic acid respectively, the experimental data indicate a packing of one proteoglycan molecule every 29 nm along the hyaluronic acid chain. This agrees well with previous estimates, Table 9.1

Spacing of Proteoglycans along Hyaluronate chain	Workers	Reference
every 29 nm	This work	-
every 24 nm	Hardingham & Muir	98
every 24-48 nm	Hascall & Heinegård	910
every 20-30 nm	Rosenberg et al	96

Table 9.1 **Proteoglycan Spacing: Comparison with Data From Other Workers.**

9.35 Further Evidence of Aggregation: Reduced and Alkylated Proteoglycans

It is possible to treat the globular protein head of a proteoglycan molecule in such a way that it is no longer able to attach to a hyaluronate chain. By reduction, the disulphide bonding in the protein head is broken, and the protein unfolds. Alkyl groups are then attached to the free bonds preventing the reformation of the head.[911] This expanded bonding region is unable to form an association with hyaluronic acid. Proteoglycans so treated are known as 'reduced and alkylated' proteoglycans, and electric birefringence measurements were correspondingly made on such a sample. Solution concentrations were identical to those of 'normal' proteoglycans and fields of 240 V cm^{-1} and 6 ms duration used. Data were recorded in the absence of and presence of various amounts of hyaluronic acid. Typical transients are shown in Fig. 9.7 from which the following observations are made:

1. In the absence of hyaluronic acid for a solution of 209 μgUA/ml, the magnitude of birefringence was 8×10^{-8} and the relaxation time was 2.6 ms. These should be compared with 6.8×10^{-8} and 3.6 ms respectively for the 'normal' sample used in the first study. The small difference in these two parameters simply reflects minor differences in the molecular sizes between the two

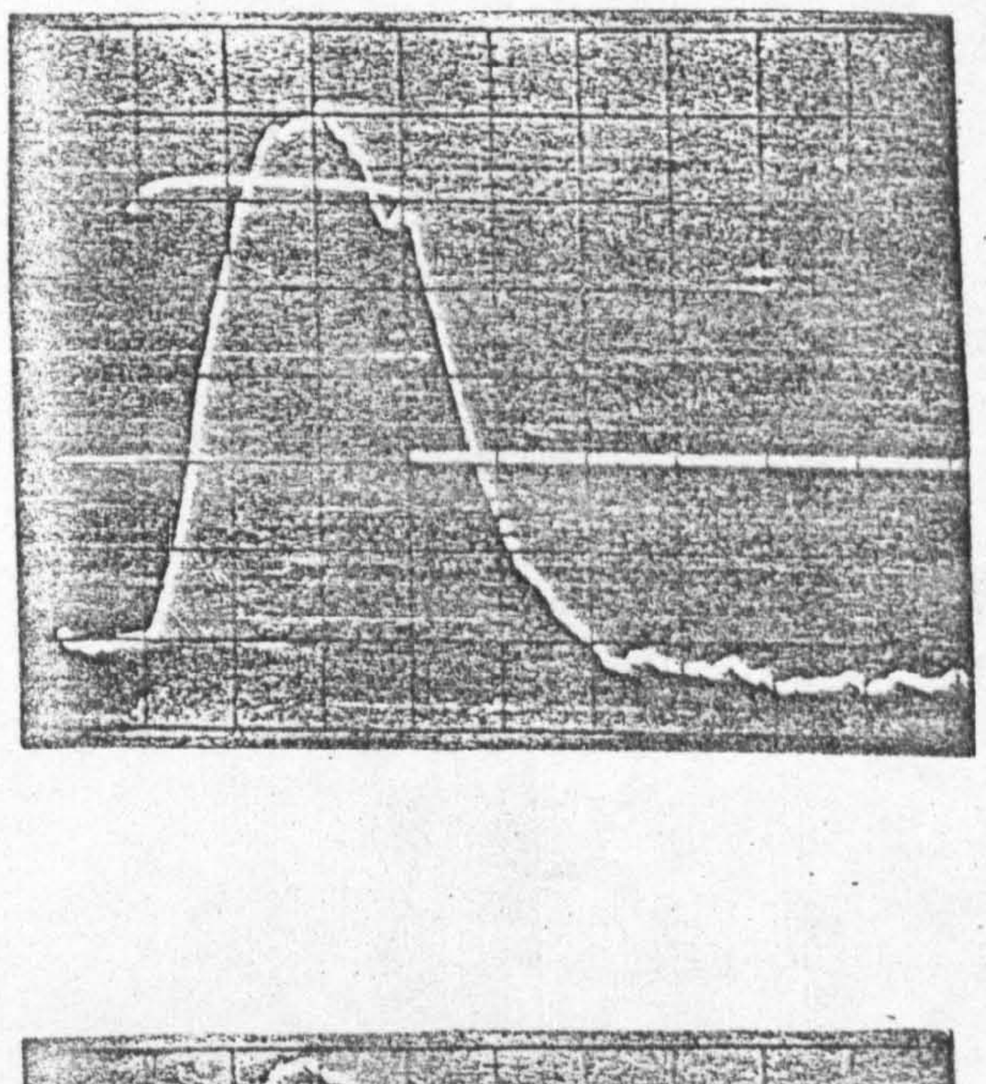

NO ADDED
HYALURONIC
ACID

HYALURONIC
ACID CONCENTRATION
SUFFICIENT TO
FORM AGGREGATE
(1% UA HA:PG)

Fig. 9.7
Transient responses of reduced and alkylated proteoglycans, both at same oscilloscope settings

preparations. The preparation of the reduced and alkylated form has not involved gross changes in the molecular geometry.

2. The addition of hyaluronic acid did not affect the transient birefringence response of the solution of this bastardised form of proteoglycans. This was true even up to an acid content corresponding to 1% of the total uronic acid content, the maximum concentration at which 'normal' proteoglycans were observed to be fully aggregated, in the earlier experiments. In Fig. 9.7, the traces for both zero and this maximal hyaluronic acid content are shown for the reduced and alkylated proteoglycan sample. It is instructive to compare Fig. 9.7 with Figs. 9.1 - 9.3.

3. With the addition of hyaluronic acid, both the molecular relaxation time, and the amplitude of the birefringence remain essentially constant. There is no gross reduction in the birefringence, no rapid growth in relaxation time, no change in optical density and no appearance of a 'slow', negative contribution. All of these factors indicate that, in the presence of hyaluronic acid, the reduced and alkylated molecules form neither the specific radial aggregate detected earlier, nor indeed do they appear to form any other type of aggregate.

4. The 'free' hyaluronic acid in this case does not contribute noticeably to the observed overall birefringence. This confirms the suggestion that the 'slow' component encountered with experiments on 'normal' proteoglycans (Figs. 9.2 and 9.3) was not due to free hyaluronic acid.

9.4 Conclusion

The work of this chapter has further substantiated the Hardingham-Muir proteoglycan-hyaluronic acid aggregate model. Moreover, the experiments have enabled the aggregate formation process to be followed stage by stage. The dimensional values calculated from the birefringence data offer really good agreement with those calculated from previous, more tedious techniques.

These factors therefore combine with the usual advantages of the birefringence technique, namely speed, small sample volume and simple sample preparation, to offer new horizons for the method in this vital area of research. Perhaps, ultimately, the key to the breakdown of these aggregates in cartilage tissue will lead to the solution of the osteoarthrosis problem and aleviate the suffering that it causes.

The work in this chapter has been accepted for publication in Volume 16 (1977) of 'Biopolymers', a copy appears in Appendix 2.

CHAPTER 10

The Thermal Denaturation of Collagen

10.1 Introduction

To complement the preceeding work on connective tissue constituents, it is logical to study the major constituent, collagen. Collagen has already been the object of electric birefringence studies by other workers,[101-104] but the author believes that this is the first time that thermal denaturation of collagen has been observed by the technique.

Collagen is the chief protein of bone, cartilage and connective tissue. Probably all animals have some collagen in them. It is thought that knowledge of collagen's molecular structure might lead to an understanding of how multicellular animals evolved from single cell ones. Of more immediate interest is the molecule's role in the ageing processes. There is a clear correlation between changes in collagen structures and ageing, when bones weaken and the skin becomes thin and wrinkled.[105]

10.11 Molecular Structure

(a) THE TRIPLE HELIX. Collagen is a right-handed super helix composed of three left-handed chains each formed from a sequence of amino acids. Every third amino acid is glycine. Just under half of the remaining units are approximately equal portions of alanine, proline and hydroxyproline. Assorted amino groups complete the molecule, details of which can be found elsewhere.[105,106] It is special sequences of these four above named amino acids, and in particular, the regular tertiary spacing of glycine, which are responsible for the triple helix conformation. At a particular temperature, the triple helix irreversibly dissociates into its three constituent chains. Typically, this occurs at around 37°C, but the temperature varies according to the collagen source and the physiological conditions. For example, Burge and Hynes[107] quote 11.4°C for a sample of cod swim bladder collagen.

(b) SIZE AND SHAPE. Original X-ray measurements by Ramachandran and Kartha[108] and Rich and Crick[109] established the conformation and size of individual molecules as rod like, just under 300 nm long and 1.5 nm diameter, with an approximate molecular weight of 300,000.

10.12 Collagen Fibrils

Native collagen forms filaments (microfibrils) of varying length and diameter. Wasserman[1010] has reported the diameter to vary with animal source and body location from 20 nm to 400 nm. Greenlee and Ross[1011] have noted an increase in diameter with age from 20 nm in foetal rats, up to 160 nm in fully mature specimens. Collagen fibrils have a very regular structure, the individual molecules staggered alongside each other every 66.8 nm. This gives rise to alternating regions having greater and smaller amounts of protein in them. This periodicity is associated with the amino acid sequences of individual molecules. It is thought that the relative displacement permits the greatest strength of bonding between the assorted amino acids not involved in super helix formation. The bonds form between the sidechains of the amino acids and are electrostatic or hydrophobic in nature. These bonds are relatively weak, but having held the molecules in contact, they allow strong covalent cross-links to form between the molecules' lysine amino acids.

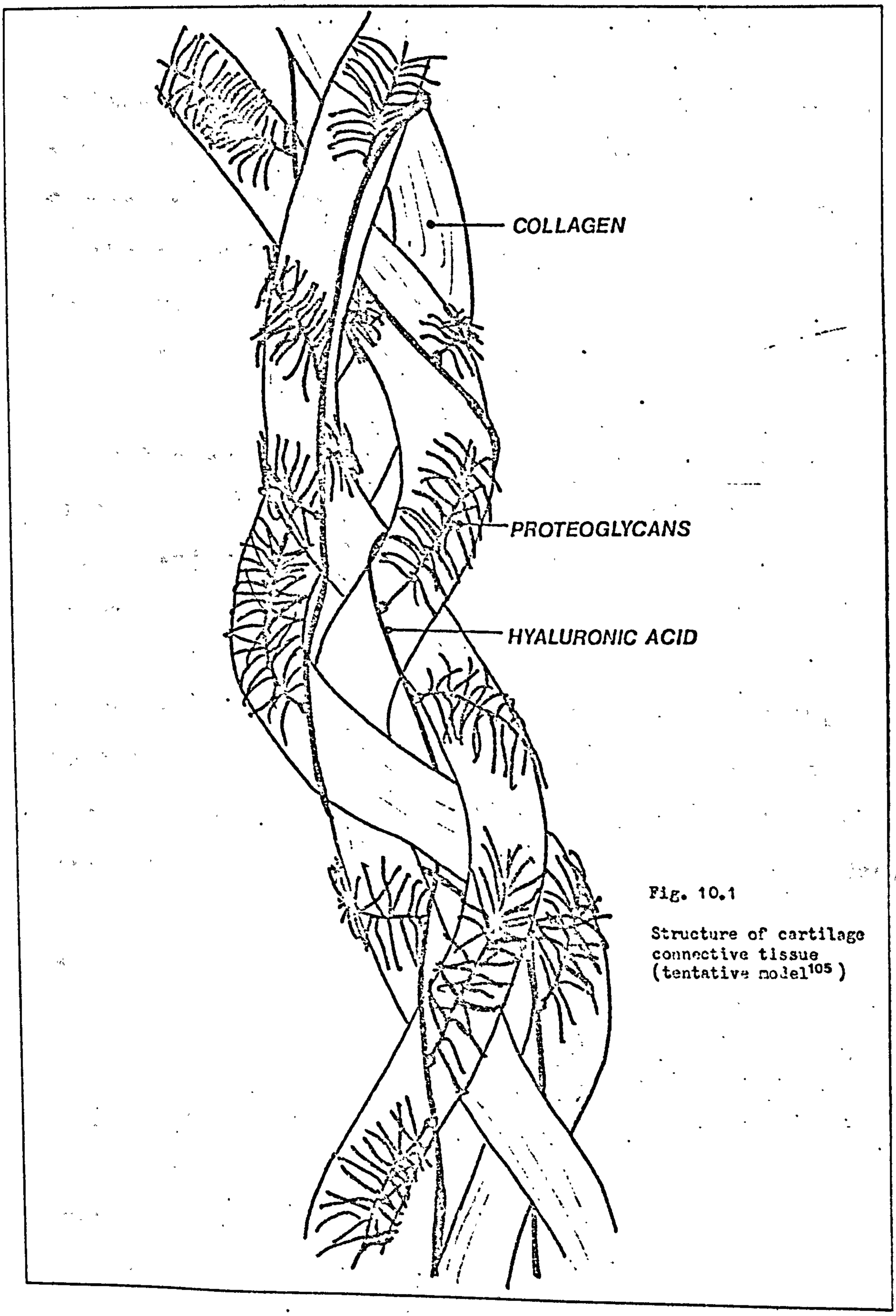

Fig. 10.1

Structure of cartilage connective tissue (tentative model[105])

10.13 Collagen Networks

Collagen fibrils form networks. Mucopolysaccharides affect the formation of these networks as well as forming part of them. In particular, chondroitin-6-sulphate has been shown to bind collagen molecules together. These measurements were performed using the electric birefringence technique.[1012]

The collagen - mucopolysaccharide networks are of prime importance in cartilage connective tissue and consequently in the associated problems of osteo-arthrosis.

Study of collagen fibrils, their formation and the building of networks with mucopolysaccharides may prove a rewarding exercise. In so far as electro-optic techniques are concerned, because of their size, the above systems are more suited to light scattering than electric birefringence.

10.14 Thermal Denaturation : The Present Study

Gelman and Blackwell[1013] have noted, using circular dichroism spectroscopy, that the denaturation temperature is affected by the presence of mucopolysaccharides. Therefore, this is an area in which electric birefringence may most usefully

contribute to the collagen related connective tissue studies. To this end, the work which follows seeks to demonstrate thermal denaturation of collagen by electric birefringence.

10.2 Experimental

10.21 Sample

The author is indebted to Dr A Bailey of the Meat Research Unit, Langford, Avon for kindly preparing and providing a sample of lathrytic rat tail tendon collagen. By special treatment of rats at an early stage in their development, collagen is prevented from cross-linking within their bodies, and consequently microfibrils do not form. The collagen then extracted from the rat's tail (a relatively abundant source) is soluble in dilute acetic acid. Cross-linked collagen, i.e. fibrils, are insoluble.

Dr Bailey's sample preparation involves dissecting tendons from tails of five month old rats, washing the tendons extensively in isotonic saline (0.9% NaCl, pH 7.4) and then dissolving them in 0.5% acetic acid maintained at $5^{o}C$ for two days. The insoluble residue is then removed by centrifugation and the

soluble collagen in the supernatant purified by precipitation at 0.9% NaCl, redissolution in acetic acid and centrifugation. The supernatant is thus treated three times, and throughout the temperature is kept at 5°C. The sample thus received was dissolved in 0.5 M acetic acid at a concentration of 0.307%. The pH of the solution has to be less than 4.8 to avoid reprecipitation of the collagen.

10.22 Apparatus

The plane polarised Coherent Radiation He Ne laser was used and a 500 kΩ load resistor on the photomultiplier. PG3, amplifying the output of the Lyons PG21 generator provided the DC field applied to the cell with fields of up to 400 V cm^{-1} and 2 ms duration. Initially the flow cell was used, but this was replaced by Cell B for measurements close to the temperature of denaturation.

Temperature regulation was achieved by keeping the body of the reservoir, associated with the flow cell, immersed in a water temperature bath controlled to ± 0.5°C. The temperature of the collagen was measured in the reservoir. A Watson-Marlow peristaltic pump constantly circulated the solution through the cell and reservoir. With Cell B, separate aliquots of solution were pre-heated by leaving sealed sample bottles to temperature

stabilise in the water bath. The solution was then transferred to the cell for measurement, since the denaturation process is irreversible, there was no need to worry if the temperature of the solution dropped at any time. The important thing was to observe the maximum temperature the sample had reached prior to any measurement.

10.23 Measurements

Before making thermal measurements, the field dependence was investigated, (Fig. 10.2). The thermal measurements were then undertaken at a constant applied field of 160 V cm^{-1} within the region of field dependent quadratic linearity, (Fig. 10.2). It was soon found that constant circulation of the solution mechanically degraded the collagen molecules. Therefore the flow cell system was used only until within two to three degrees of the denaturation temperature, with the circulatory pump being used as little as possible. Measurements close to the denaturation temperature used Cell B with aliquots as indicated previously.

It was not possible to determine behaviour below 20°C. This was the highest temperature the sample was expected to have reached in transit. Because of the irreversibility of the process measurements at lower temperatures would have been suspect.

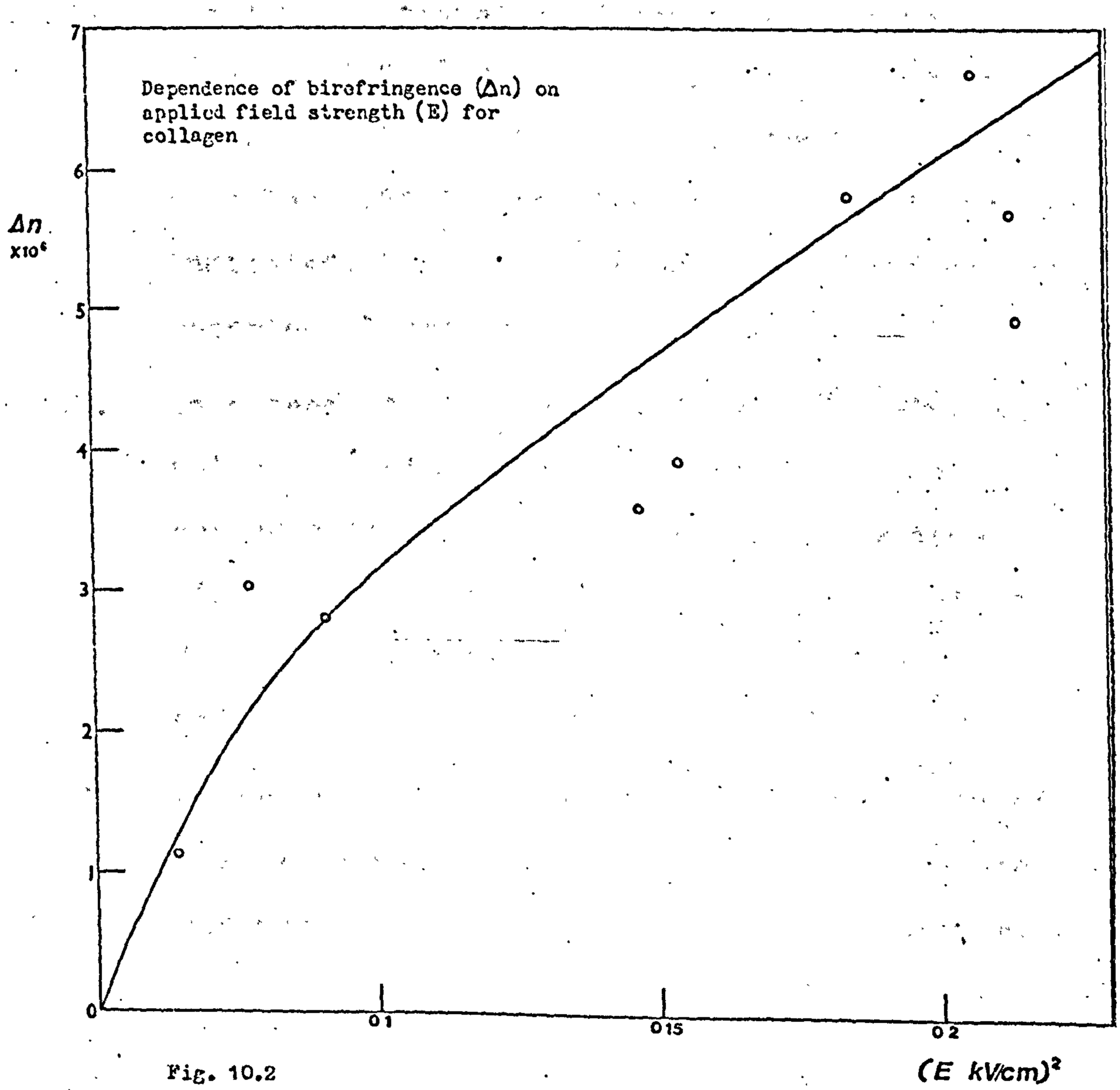
Dependence of birefringence (Δn) on applied field strength (E) for collagen
Δn x10⁶
7
6
5
4
3
2
1
0
0 1
0 15
0 2
(E kV/cm)²

Fig. 10.2

10.3 Results and Discussion

(A) The following points were noted in addition to observations directly related to the denaturation.

1. Analysis of transient decay times led to a value of 0.53 ± 0.06 ms for the relaxation time. Applying the Broersma rigid rod equation (section 2.811) a rod length of 350 ± 40 nm is indicated, in reasonable agreement with values reported elsewhere.[101-104,108,109]

2. In agreement with Bernengo's work,[104] single value relaxation times were found in decay analyses indicating a monodisperse system, (Fig. 10.3). From this it is clear that no fibrils were present in the solution and molecules were not aggregating in any way.

3. Observations supported the irreversibility of the denaturation process. Cooled solutions did not regain their original birefringence.

(B)

1. The process of thermal denaturation can be followed by changes in both the birefringence and relaxation time as shown in Fig. 10.4 and Fig. 10.5, respectively. The relaxation time curve clearly shows a temperature of thermal denaturation of 34.5 ± 0.7 °C defining this temperature as that at which the relaxation

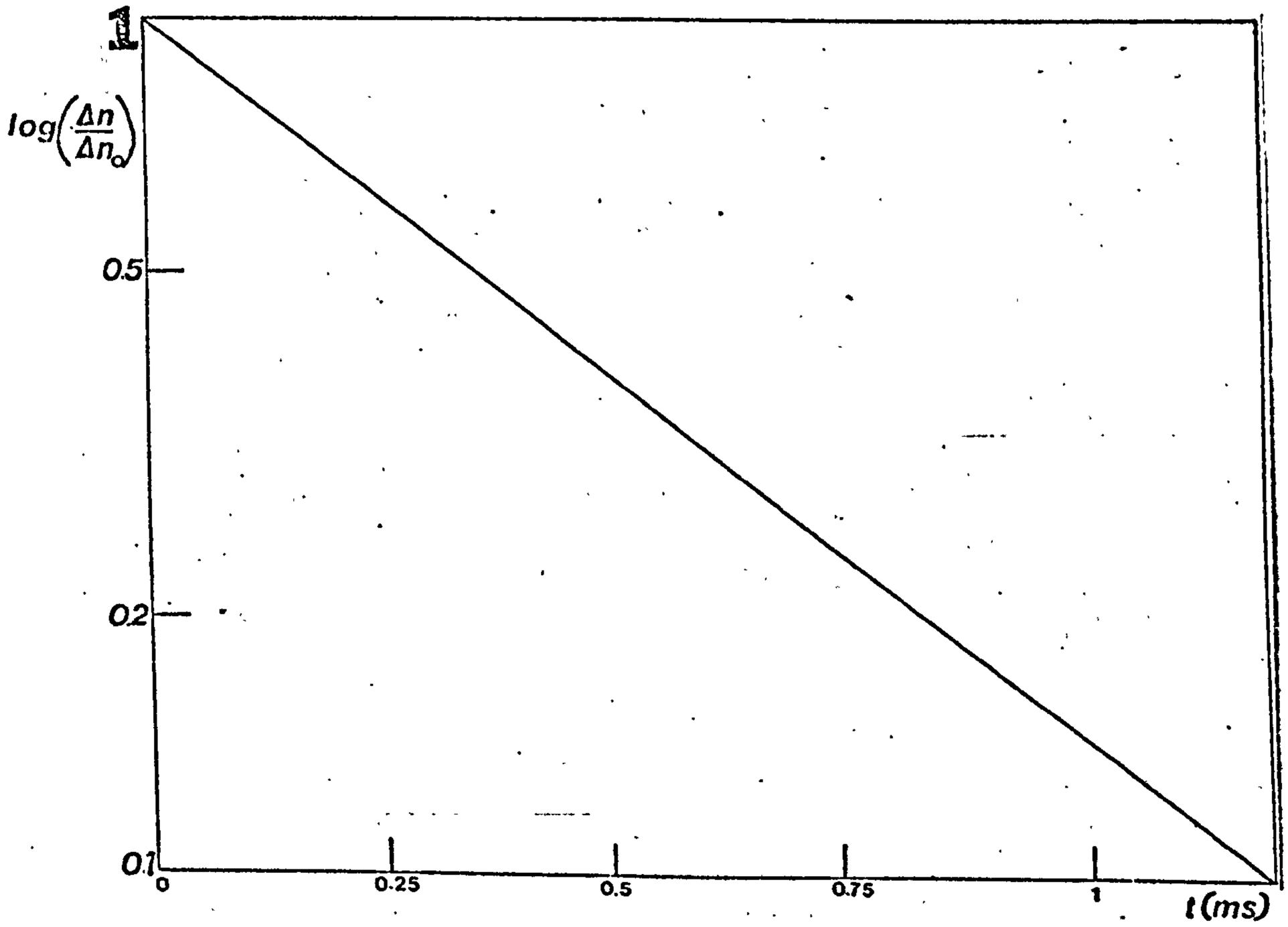

Fig. 10.3 Transient decay of birefringence $\left(\frac{\Delta n}{\Delta n_o}\right)$ against time (t) for collagen.

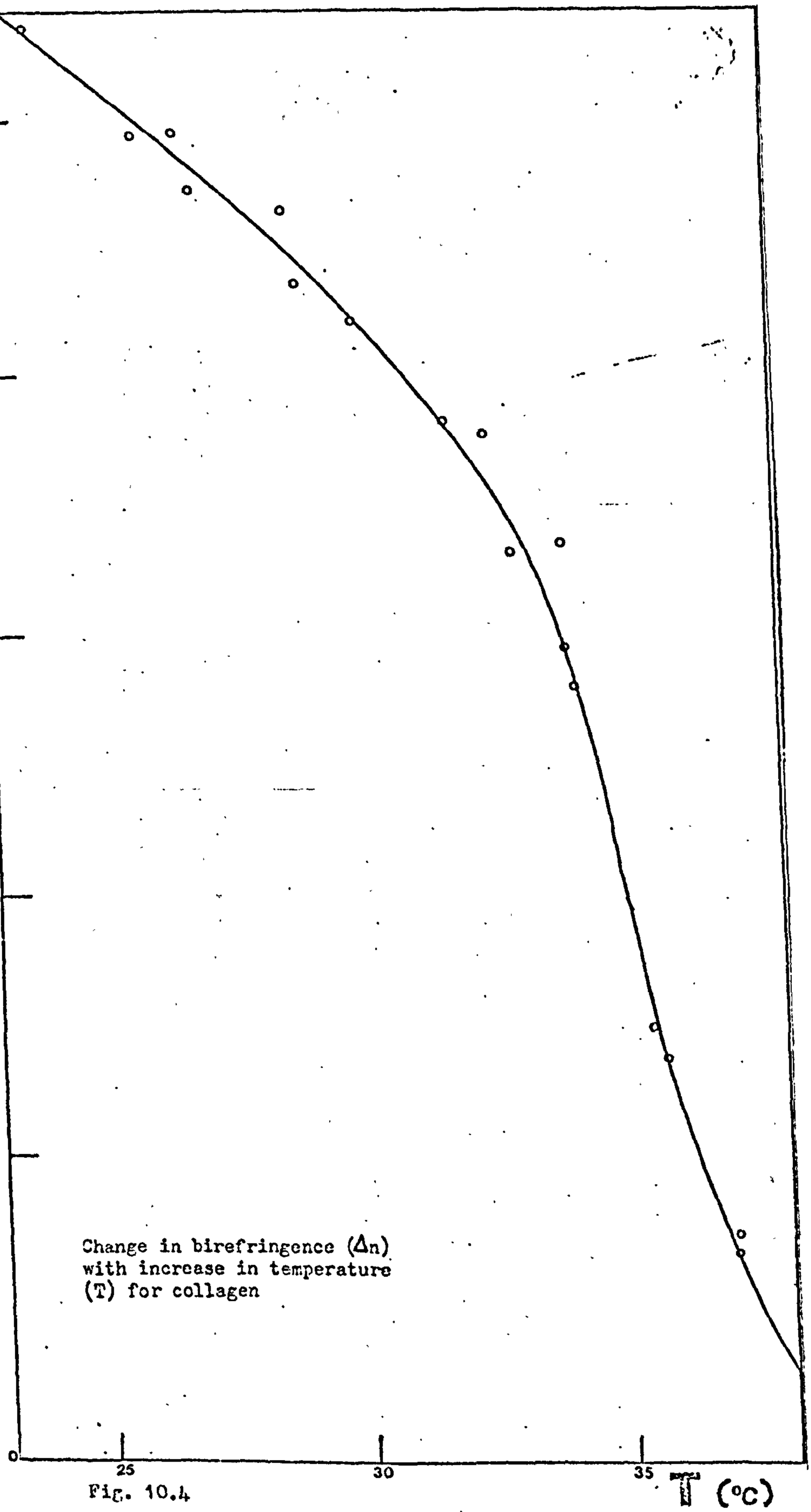

Change in birefringence (Δn) with increase in temperature (T) for collagen

Fig. 10.4

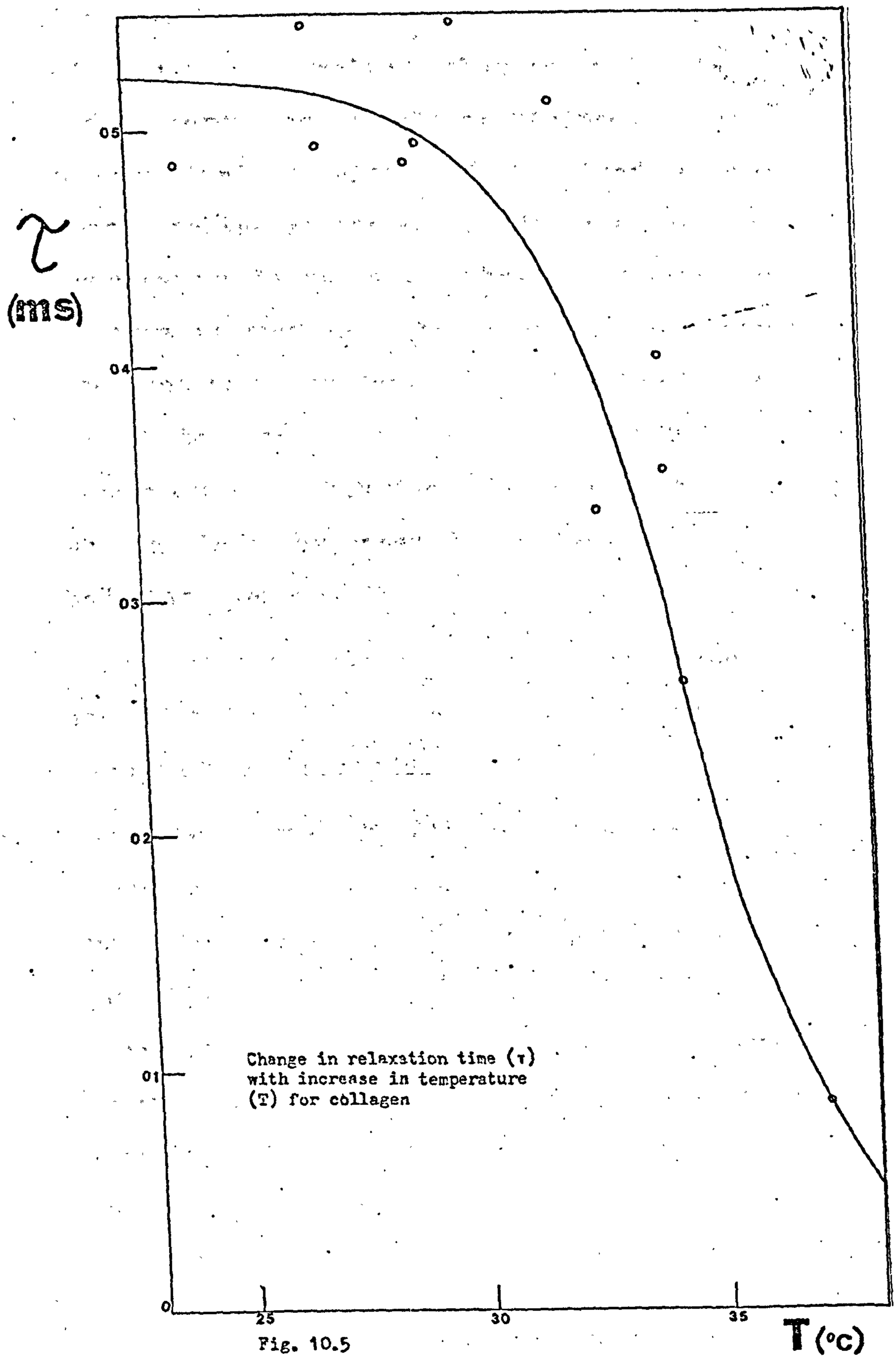

Change in relaxation time (τ) with increase in temperature (T) for collagen

Fig. 10.5

time has halved in value.[1014] The abruptness of this change implies that the molecule's rod conformation is well maintained. The more gradual transition of the birefringence curve implies an increasing disorder as the temperature is raised. These birefringence changes suggest that the denaturation process does not occur suddenly, and that the helix begins to denature quite steadily with temperature. This fact would be better substantiated by measurements below 20°C had this been possible.

2. No evidence of gel formation was observed prior to denaturation at the concentration used in these experiments.

3. Denatured solutions were subjected to fields of up to 40 kV cm^{-1} and some 10 μs duration to see if the orientation of the individual helical strands was possible. No birefringence was observed. This was somewhat surprising, though it may suggest that individual strands adopt a very random conformation, particularly at the low pH of the solution studied.

10.4 Conclusions

Electric birefringence provides another physical technique for studying the thermal denaturation of collagen, alongside the techniques of optical rotation, viscosity,[107] etc.. The technique's inherent superiority of speed and small sample volume are noted again.

This initial study, planned partly to gain experience of the material within our research group, has now opened the way for deeper studies of collagen interactions with the mucopolysaccharides. It should be possible to determine their relative bonding strengths to collagen from thermal measurements, and also the initial formation of collagen - mucopolysaccharide networks. The influence of heparin and DNA on microfibril formation may also prove a possible and interesting study.[1015]

The author recommends, however, that for thermal measurements a purpose built cell for altering and monitoring the temperature of the sample be employed in any earnest study. The temperature control on this experiment could have been much improved with some form of water jacketed cell and utilising a single sample of the solution in the cell throughout the range of thermal measurements.

CHAPTER 11

Conclusions and Suggestions for Further Work

In discussing the achievements of this work, it is best to deal with the matter section by section, and for the convenience of presentation, the first section on apparatus is left until last.

The work in Section 2 highlighted the problems of current research. Firstly, the question of flexible molecules and their kinetics is a theoretical problem waiting to be solved. Whilst there have been attempts to compare the flexibility of different molecular species on an experimental basis[111] it is readily apparent that a major break through might be possible once a definitive theoretical study of the problem has been made. Nonetheless, the work on the flexible polymer, nitrocellulose in acetone was able to provide data indicating a permanent dipole moment of a few debye per monomer unit and exclude extreme models of molecular conformation. A very stiff and somewhat non-free draining, yet coiled polymer is suggested as the

most appropriate model.

The work in this section went on further to demonstrate the technique's acute sensitivity to supposed changes in the interfacial region, between solute and solvent. The interactions in this strongly ionic region present an area of fundamental research to further understanding of many chemical and biological processes, and clearly, here is an important tool to be used in these researches. Such problems as the mechanism of blood clotting and cell membrane permeability may ultimately be fully comprehended as a result of greater knowledge acquired by further research in this area, aided by the electric birefringence technique.

The final work in Section 2 produced a range of results for many different materials and compared their transient and dispersion derived rotary diffusion constants. Previous workers have normally accepted these values as the same, independent of the method of their determination. Discrepancies were however observed in their data and this is again similarly reported by the author. No good correlation could be found between the observed results and the known variable parameters. The author's results therefore await full interpretation by subsequent researchers, but definite suggestions for the possible origin of the discrepancies are reported. The author

meanwhile suggests that dispersion derived rotary diffusion constants be treated with some caution.

As a corollary to this work, measurements on the clay, halloysite, suggested a comparison of particle rotary diffusion constants at high frequency and DC might enable a distinction to be made between transverse and longitudinal dipole moments for rod like conformations.

The work in Section 3 shows how well the technique can be applied to the area of biomedical research. The ability to continuously follow the proteoglycan - hyaluronic acid complex formation as it actually takes place is unparalleled by methods used hitherto. The speed and ease with which *in vivo* results can be obtained should greatly aid the researches into the causes of the onset of osteo-arthrosis. Indeed, the initial investigation, conducted by the author and Dr A R Foweraker is now being persued in depth within this research group on a grant provided by the Arthritis and Rheumatism Council.

Whilst the proteoglycan - hyaluronic acid complex formation was the most spectacular part of this section of the work, the parallel experiments should not be underestimated. The method proved itself capable of responding to small conformation changes with pH typifying the polyelectrolytic behaviour of

the hyaluronic acid salt. The ease with which enzymic degradation of hyaluronate could be followed with time opens the way to yet another application of the technique as a laboratory tool for the biochemist. Then, to complete both the range of materials involved and the diversity of conformational changes which electric birefringence can be used to observe, the thermal denaturation of collagen provides a means to gauge the relative bonding strengths of the cartilage mucopolysaccharide constituents.

The complete study of mucopolysaccharides and their interactions will, it is hoped, lead to wider recognition of the method and its wider application to problems, as yet unsolved, which it can so readily lend itself to.

To assist in this aim the development of the *MINEO-1* apparatus described in Section 1 is of prime importance. Being able to provide electric birefringence as a standard laboratory tool may soon be a reality coupled with suitable pulse generators which are now on the market. It is also important to note the high sensitivity which the new cell design attains, enabling measurement of birefringences down to 10^{-9}. This should permit the study of small biological polymers, such as heparin, which are on the limits of present apparatus.

Besides offering a compact, sensitive and easy to use machine, the concept of the *MINEO-1* instrument is such that it can be manufactured on a modular basis. Different photo-detectors and generators could be supplied according to the main study area of interest to the researchers involved. For example, clays which give large birefringences for small applied fields would require low voltage AC/DC generators and a photo-diode detector would suffice. For looking at coiled polymers, globular proteins and other instances where maximum sensitivity is required, a high gain photomultiplier and the windowless birefringence cell would be used.

The possibility of converting the apparatus to other forms of electro-optic methods has been considered. A suitable cell based on the Poweraker and Jennings[112] design for electric linear dichroism has been discussed (Fig. 11.1), together with the provision of a rotatable arm at the detection end of the apparatus for light scattering and floresence studies. Already the basic box design of *MINEO-1* has spawned similar apparatus for both magnetic birefringence and electric dichroism within this research group.

Basic design for linear dichroism cell for use in MINEO-1 style apparatus: vacuum deposited electrodes on prism faces.

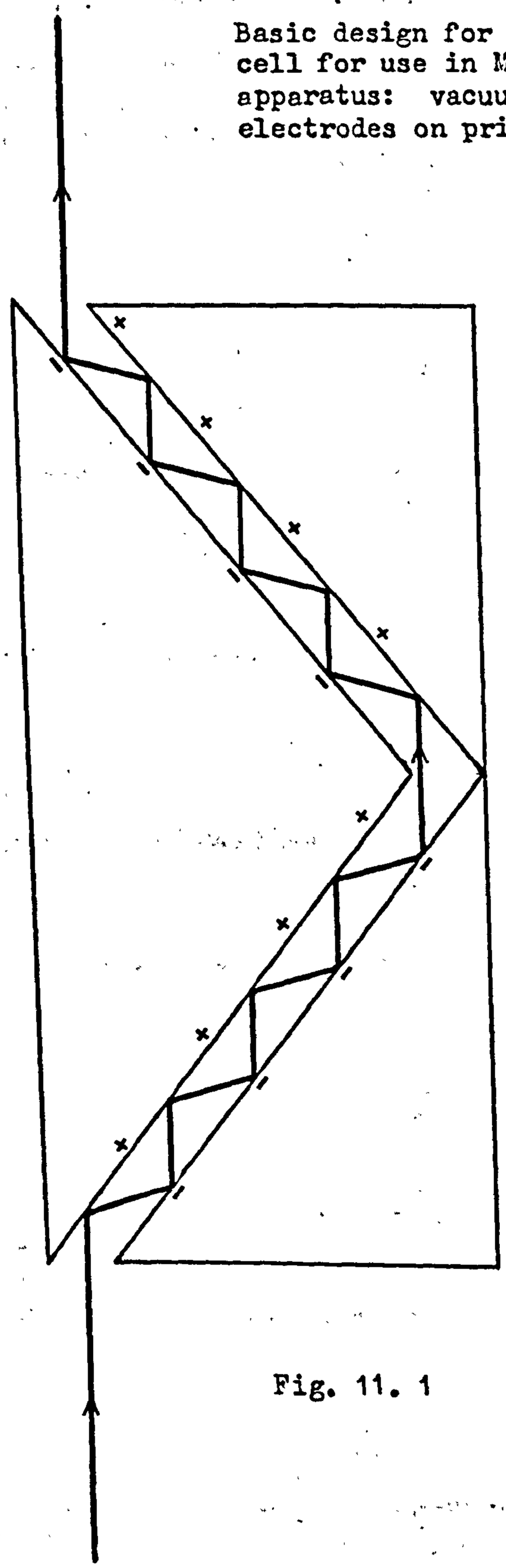

Fig. 11. 1

It is thus that this work concludes with the author's hopes and aspirations that the future for the technique will be assured and that as a result, the future for humanity will in some small way be improved.

ACKNOWLEDGEMENTS

The author is extremely grateful for all the help, encouragement and support provided by colleagues, friends and family during the course of this work. These classisfications are not necessarily mutually exclusive! Where appropriate individuals have been mentioned in the text and acknowledgement is additionally made in respect of specific assistance in the list below. Nonetheless, the author feels impelled to single out Dr Barry Jennings, his supervisor, as a constant source of encouragement, friendship, inspiration - and information - throughout. Thanks are also due to Dr Alan Foweraker who frequently performed a similar role and whose enthusiasm and energy can be refreshingly contagious!

The author is grateful to:

Prof C A Hogarth for the excellent laboratory facilities provided and his personal interest in the author's progress at both undergraduate and postgraduate levels.

The Science Research Council for financial support in conjunction with.....

Messrs. Unilever Ltd., Port Sunlight, and in particular.....

Dr Ian Robb of Unilever, for two interesting and informative stays at the Unilever laboratories.

Stan Woodise, Les Lighthowler and Richard Preston of the department's workshops for their expertise in transforming many of the author's designs into reality and for valuable discussion at the design stages.

Dave Buley for photographic illustrations (developing by Boots)

Robin Brown for access to a Rank-Xerox photocopier.

The Electro-Optics Research Group for companionship, amusement and encouragement for the last few years: Vic, Geoff, Harry, Pete, Hiroshi, Mano, Paul, Ken, Yvonne - and of course, Barry and Al, who have already been mentioned.

REFERENCES

Note that the final letters and digits after the date which appears in brackets, refer to Brunel Electro-Optics Group Library Numbers.

Chapter 1

11 J. Kerr, Phil. Mag. 50 337 (1875) KB15

12 H. Benoit, Ann. de Phys. (Paris) 6 561 (1951) KA11

13 A. Peterlin and H.A. Stuart, "Hand und Jahrbuch der Chemischen Physik," 8(IB) Ed. A. Eucken and K.L. Wolf, Akademische Verlagsgesellschaft, Leipzig. (1943) KB1

14 C.T. O'Konski and B.H. Zimm, Science, 111 113 (1950) KC39

15 H.J. Coles and B.R. Jennings, Phil. Mag. 32 1051 (1975) LC68

References

Chapter 2

21 J. Kerr, Phil. Mag. (5) 2 157 (1880)

22 P. Debye, "Handbuch der Radiologie" VI 597 Ed. E. Marx, Akad. Verlagsges, Leipzig. (1925)

23 V.G. Otterbein, Phys. Z. 35 249 (1934) KB59

24 A. Peterlin and H.A. Stuart, Z. Physik 112 129 (1939) KB28

25 C.T. O'Konski, K. Yoshioka and W.H. Orttung, J. Phys. Chem. 63 1558 (1959) KB10

26 M.J. Shah, J. Phys. Chem. 67 2215 (1963) MC2

27 D.N. Holcomb and I. Tinoco, J. Phys. Chem. 67 2215 (1963) KB26

28 H. Plummer and B.R. Jennings, J. Chem. Phys. 50 1033 (1969) SH52

29 G.B. Thurston and D.I. Bowling, J. Coll. Interface Sci. 30 34 (1969) KC45

210 I. Tinoko and K. Yamaoka, J. Phys. Chem. 63 423 (1959) KB42

211 H. Benoit, Ann. de Phys. (Paris) 6 561 (1951) KA11

212 D. Ridgeway, J. Am. Chem. Soc. 88 1104 (1966) KB13

213 K. Yoshioka and H. Watanabe, "Physical Principles and Techniques of Protein Chemistry" Part A Chapter 7 346 Ed. S. Leach, Academic Press, N.Y. (1969) KA7

214 J.F. Schweitzer and B.R. Jennings, Biopolymers 11 1077 (1972) SH63

215 J.F. Schweitzer and B.R. Jennings, Biopolymers 12 2439 (1973) R36

216 A.R. Foweraker, B.R. Jennings and V.J. Morris: a number of papers in preparation (1977).

217 S. Broersma, J. Chem. Phys. 32 1626 (1959) R8

218 C.W. Oseen, "Hydrodynamik" 35 Akademische Verlagsg. m.b.H., Leipzig. (1927)

219 J.M. Burgers, Verk. Kon. Ned. Akad. Wet. (1) 16 113 (1938) VA32

Chapter 2, contd.

220 F. Perrin, J. de Phys. 5 497 (1934) R29

221 A. Peterlin and H.A. Stuart, "Hand und Jahrbuch der Chemischen Physik" 8(IB) Ed. A. Eucken and K.L. Wolf, Akad. Verlagsges., Leipzig (1943) KB1

222 B.H. Zimm, J. Chem. Phys. 24 269 (1956) KC102

223 W.H. Stockmayer and M.E. Baur, J. Am. Chem. Soc. 86 3485 (1964) R6

224 J.E. Hearst, J. Chem. Phys. 38 1062 (1963) R15

225 J.E. Hearst and W.H. Stockmayer, J. Chem. Phys. 37 1425 (1962) U84

226 D.A. Dows, J. Chem. Phys. 41 2656 (1964) KB6

227 A. Peterlin and H.A. Stuart, J. Polym. Sci. 5 551 (1950)

228 V.N. Tsvetkov, Soviet Physics Uspekhi 6 639 (1964) XC44

229 E. Fredericq and C. Houssier, "Electric Birefringence and Electric Dichroism" 87 Clarendon Press, Oxford. (1973)

230 C.T. O'Konski and B.H. Zimm, Science 111 113 (1959) KC39

Chapter 3

31 B.W. Brown, Ph.D. Thesis, Queen Elizabeth College, University of London (1970) T7

32 P.J. Rudd, Ph.D. Thesis, Brunel University (1974) T11

33 W.H. Orttung and J.A. Mayers, J. Phys. Chem. 67 1905 (1963) KC64 or KD14

34 E.M.I. Photomultiplier Handbook, E.M.I., Hayes (1973)

References

Chapter 4

41 R.M. Badger and R.H. Blaker, J. Phys Colloid Chem. 53 1056 (1949) ML12 or SG48

42 T.E. Timmell, Svensk. Papperstidn 57 777 (1954) ML13

43 A.M. Holtzer, H. Benoit and P. Doty, J. Phys. Chem. 58 624 (1954) ML5 or SD6

44 C. Wippler, J. Chim. Phys. 53 346 (1956) SH6

45 M.L. Wallach and H. Benoit, J. Polym. Sci. A2,4 491 (1966) ML7 or SH12

46 B.R. Jennings and J.F. Schweitzer, Eur. Polym. J. 10 459 (1974) ML11 or SH79

47 P. Debye, "Polar Molecules" Dover, N.Y. (1958)

48 J.F. Schweitzer and B.R. Jennings, Biopolymers 12 2439 (1973) R36 or KB48

49 "Polymer Handbook" Ed. J. Bandrup and E.H. Immergut, Interscience, N.Y. (1966)

410 W.R. Moore and G.D. Edge, J. Polym. Sci. 47 469 (1960)

411 C. Tanford, "Physical Chemistry of Macromolecules" Wiley, N.Y. (1961)

412 G.W.C. Kaye and T.H. Laby, "Tables of Physical and Chemical Constants" 1966 Edition Longmans, London (1911)

413 H. Mosimann, Helv. Chim. Acta 26 61 (1943)

414 A.R. Foweraker and B.R. Jennings, Adv. Mol. Relxn. Process. 6 241 (1974) AB59 or MM44

415 A.R. Foweraker and B.R. Jennings, Polymer 16 720 (1975) ML29

416 S.K.K. Jatkar and D.S. Sastry, Univ. Poona. Sci. Technol. 4 55 (1953) ML6

417 V.N. Tsvetkov, Soviet Physics Uspekhi 6 639 (1964) XC44

References

Chapter 5

51 S.P. Stoylov, Advan. Colloid Interface Sci. 3 45 (1971) SH44

52 B.R. Jennings and V.J. Morris, J. Colloid Interface Sci. 49 87 (1974) MB75

53 B.R. Jennings and V.J. Morris, J. Colloid Interface Sci. 50 352 (1975) MB89

54 V.J. Morris and B.R. Jennings, Biochim Biophys. Acta 392 328 (1975) MB100

55 V.J. Morris and B.R. Jennings, J. Chem. Soc., Faraday Trans. II 71 1948 (1975) MB117

56 A. Albert, "Selective Toxicity" Chapman and Hall, London. (1973)

57 V.J. Morris, H.J. Coles and B.R. Jennings, Nature 249 240 (1974) SB78 or MB56

58 B.R. Jennings, "Light Scattering from Polymer Solutions" 13 529 Acad. Press, N.Y. (1972) SH61

59 P.J. Rudd, V.J. Morris and B.R. Jennings, J. Phys. D 8 170 (1975) MB90

510 V.J. Morris, P.J. Rudd and B.R. Jennings, J. Colloid Interface Sci. 50 379 (1975) MB91

511 P.J. Rudd, Ph.D. Thesis, Chapter 7, Brunel University (1974) T11

512 S. Gladston and D. Lewis, "Elements of Physical Chemistry" 561 McMillan, N.Y. (1963)

513 V.J. Morris and B.R. Jennings, J. Colloid Interface Sci. 55 143 (1976) MB118

514 A.R. Foweraker and B.R. Jennings, "Addition of Flexible Polymers to a PTFE Suspension" Private Communication to I.C.I. Ltd (1975)

Chapter 6

61 B.R. Jennings, B.L. Brown and H. Plummer, J. Colloid Interface Sci. 32 606 (1970) MC5

62 R.E. Grim, "Clay Mineralogy" 171 McGraw-Hill, N.Y. (1968)

63 T.F. Bates, F.A. Hildebrand and A. Swineford, Am. Mineralogist 35 463 (1950)

64 R.D. Harrison and R.D. Woods, Virology 28 610 (1966) MP5

65 A.R. Foweraker and B.R. Jennings, Spectrochimica Acta 31A 1075 (1975) AB65

66 H. Benoit, Ann. de Phys. (Paris) 12 36 (1951) KA11

67 B.R. Jennings, Ph.D. Thesis, University of Southampton (1964) T1

68 P.J. Rudd, V.J. Morris and B.R. Jennings, J. Phys. D 8 170 (1975) MB90

69 V.J. Morris, P.J. Rudd and B.R. Jennings, J. Colloid Interface Sci. 50 379 (1975) MB91

610 M.L. Bhanot, Unpublished work, these laboratories (1975)

611 H. Plummer and B.R. Jennings, Brit. J. Appl. Phys. D 1 1753 (1968) SH51

612 J.F. Schweitzer and B.R. Jennings, J. Phys. D: Appl. Phys. 5 297 (1972) SH59

613 H.J. Coles, Private Communication to the author (1976)

614 H.J. Coles, B.R. Jennings and V.J. Morris, Phys. Med. Biol. 20 225 (1975) SB81

615 L. Rosenberg, W. Hellman and A.K. Kleinschmidt, J. Biol. Chem. 245 4123 (1970) MU59

616 V.J. Morris and B.R. Jennings, J. Chem. Soc. Faraday Trans. II 71 1948 (1975) MB117

617 J.F. Schweitzer and B.R. Jennings, Biopolymers 13 12 2439 (1973) R36

618 M.L. Bhanot and B.R. Jennings, J. Colloid Interface Sci. 56 92 (1976) SH56

References

Chapter 7

71 K. Meyer and J.W. Palmer, J. Biol. Chem. 107 629 (1934) MU65

72 K. Meyer and J.W. Palmer, J. Biol. Chem. 114 689 (1936) MU64

73 J.H. Fessler and L.I. Fessler, Proc. Nat. Acad. Sci. 56 141 (1966) MU60

74 D.A. Rees, "Biochemistry Series One" 5 Chapter 1 Ed. W.J. Whelan, Butterworths, London. (1975) MU33

75 T.C. Laurent, Biochem. J. 93 106 (1964) MU3

76 D.A. Rees, Advan. Carbohyd. Chem. Biochem. 24 267 (1969) MU67

77 E.A. Balazs, Fed. Proc. 25 1817 (1966) MU66

78 D.A. Gibbs, E.W. Merrill, K.A. Smith and E.A. Balazs, Biopolymers 6 777 (1968) MU48

79 A.G. Ogston and J.E. Stainer, Biochem. J. 49 585 (1951) MU11

710 A.G. Ogston and J.E. Stainer, Disc. Faraday Soc. 13 275 (1953) MU53

711 T.C. Laurent and J. Gergely, J. Biol. Chem. 212 325 (1955) MU51

712 B.N. Preston, M. Davies and A.G. Ogston, Biochem. J. 96 449 (1965) MU2

713 E.D.T. Atkins and J.K. Sheehan, Nature New Biol. 235 253 (1972) MU6

714 I.C.M. Dea, R. Moorhouse, D.A. Rees, S. Arnott; J.M. Guss and E.A. Balazs, Science 179 560 (1973) MU7

715 E.D.T. Atkins and J.K. Sheehan, Science 179 562 (1973) MU7

716 J.M. Guss, D.W.L. Hukins, P.J.C. Smith, W.T. Winter, S. Arnott, R. Moorhouse and D.A. Rees, J. Mol. Biol. 95 359 (1975) MU10

Chapter 7, contd.

717 A. Darke, E.G. Finer, R. Moorhouse and D.A. Rees, J. Mol. Biol. 99 477 (1975) MU32

718 C.L. Riddiford and B.R. Jennings, J. Am. Chem. Soc. 88 4359 (1966) C2

719 C.L. Riddiford and B.R. Jennings, Biopolymers 5 757 (1967) KC101

720 R.L. Cleland and J.L. Wang, Biopolymers 9 799 (1970) MU25

721 H.J. Coles and B.R. Jennings, Biopolymers 14 2567 (1975) LC69

722 H.J. Coles, Private Communication to the author.

723 D. McClean and C.W. Hale, Biochem. J. 35 159 (1941) MU72

724 Z. Hadidian and N.W. Pirie, Biochem. J. 42 260 (1948) MU56

725 S.D. Gorham and A.H. Olavesen, Conn. Tiss. Res. 3 17 (1975) MU13

726 J.R. Polansky, B.P. Toole and J. Gross, Science 183 862 (1974) MU42

727 O. Hecliter, S.K. Dopkeen and M.H. Yudell, J. Pediat. 30 645 (1947) MU63

728 G. Asboe-Hansen, Acta Dermato.-Venereol. 30 27 (1950) MU62

729 M.H. Cottle, J.A. Weiss, E. Pottorf and E. Herzon, Arch. Otolaryngol. 52 369 (1950) MU68

730 C. Rhodes, K.S. Dodgson, A.H. Olavesen and B. Hogberg, Biochem. J. 122 575 (1971) MU49

731 K. Meyer and M.M. Rapport, Adv. Enzymol. 13 199 (1952) MU12

732 M.M. Rapport, K. Meyer and A. Linker, J. Biol. Chem. 186 615 (1950) MU52

Chapter 8

81 T.E. Hardingham and H. Muir, "Normal and Osteoarthrotic Articular Cartilage" 51 Ed. S.Y. Ali, M.W. Elves and D.H. Leaback, Inst. of Orthopaedics, London. (1973) MU31

82 T.E. Hardingham and H. Muir, Biochem. J.. 139 565 (1974) MU28

83 L.D. Kahn and L.P. Witnauer, Biochim. Biophys. Acta 243 388 (1971) MU44

84 H.J. Coles and B.R. Jennings, Molec. Phys. 31 (4) 1225 (1976) MO72

85 L. Rosenberg, W. Hellman and A.K. Kleinschmidt, J. Biol. Chem. 245 4123 (1970) MU59

86 P.J. Wells and A. Serafini-Fracasini, Nature New Biol. 243 268 (1973) MU58

87 T.E. Hardingham, Kennedy Institute of Rheumatology, Private Communication to the author (1976) .

88 T.C. Laurent, "Colston Papers No. 26 - 'Structure of Fibrous Biopolymers'" Ed. E.D.T. Atkins and E.A. Keller, Butterworth, London. (1975) MU4

Chapter 9

91 C.P. Tsiganos and H. Muir, "Connective Tissue and Ageing Workshop Conference, Hoechst" 1 132 Ed. H.G. Vogel, Excerpta Medica, Amsterdam (1973) MU61

92 Z. Simunek and H. Muir, Biochem. J. 126 515 (1972) MU50

93 C.A. McDevitt and H. Muir, Biochem. Soc. Trans. 1 287 (1973) MU47

94 C.A. McDevitt and H. Muir, Ann. Rheum. Dis. 34 suppl. 2 137 (1975) MU87

95 T.E. Hardingham and H. Muir, Biochim. Biophys. Acta 279 401 (1972) MU29

96 L. Rosenberg, W. Hellman and A.K. Kleinschmidt, J. Biol. Chem. 250 1877 (1975) MU54

97 E.D.T. Atkins, T.E. Hardingham, D.H. Isaacs and H. Muir, Biochem. J. 141 919 (1974) MU30

98 T.E. Hardingham and H. Muir, Biochem. J. 135 905 (1973) MU27

99 T.E. Hardingham and H. Muir, "Normal and Osteoarthrotic Articular Cartilage" 51 Ed. S.Y. Ali, M.W. Elves and D.H. Leaback, Inst. of Orthopaedics, London (1973) MU31

910 V.C. Hascall and D. Heinegård, J. Biol. Chem. 249 4242 (1974) MU84

911 V.C. Hascall and S.W. Sajdera, J. Biol. Chem. 244 2384 (1969) MU82

References

Chapter 10

101 K. Yoshioka and C.T. O'Konski, Biopolymers 4 499 (1966) MU88

102 S. Ananthanarayanan and A. Veis, Biopolymers 11 1365 (1972) MU90

103 L.D. Kahn and L.P. Witnauer, J. Amer. Leather Chem. Soc. 64 12 (1969) KC35

104 J.C. Bernengo, B. Roux and D. Herbage, Biopolymers 13 641 (1974) MU35

105 J. Woodhead-Galloway, New Scientist 67 582 (1975) MU41

106 N.S. Andreeva, N.G. Esipova, M.I. Millionova, V.N. Rogulenkova and V.A. Shibnev, Conf.-Biopolym., Pap. Int. Symp., Madras 2 469 (1967) MU71

107 R.E. Burge and R.D. Hynes, J. Mol. Biol. 1 155 (1959) MU36

108 G.N. Ramachandran and G. Kartha, Nature 174 269 (1954) MU92

109 A. Rich and F.H.C. Crick, Nature 176 915 (1955) MU89

1010 F. Wasserman, Ergebn. Anat. Entw. Gesch. 35 240 (1956) MU94

1011 T.K. Greenlee and R. Ross, J. Ultrastruct. Res. 18 354 (1967) MU91

1012 J.C. Bernengo, B. Roux and D. Herbage, Berichte der Bunsen Gesellscaht Bd80 Nr 3 246 (1976) MU45

1013 R.A. Gelman and J. Blackwell, Biochim. Biophys. Acta 342 254 (1974) MU40

1014 H. Boedtker and P. Doty, J. Am. Chem. Soc. 78 4267 (1956) MU93

1015 T.R. Oegema Jnr., J. Laidlaw, V.C. Hascall and D.D. Dziewiatkowski, Arch Biochem. Biophys. 170 (2) 698 (1975) MU81

Chapter 11

111 A.R. Foweraker and B.R. Jennings, Polymer 16 720 (1975) ML29

112 A.R. Foweraker and B.R. Jennings, Lab. Practice May (1976) AB67

APPENDIX

Published Work

1 "Electric Birefringence of Cellulose Trinitrate in Acetone"
M. ISLES & B.R. JENNINGS
British Polymer Journal MARCH 1976

2 "Electric Birefringence Studies of Cartilage Proteoglycan Aggregation"
A.R. FOWERAKER, M. ISLES, B.R. JENNINGS,
T.E. HARDINGHAM & H. MUIR.
Biopolymers Vol 16 1977

Electric Birefringence of Cellulose Trinitrate in Acetone

M. Isles* and Barry R. Jennings*

Electric birefringence studies have been made on a sample of high molecular weight cellulose trinitrate in acetone. The molecule is shown to have only a permanent dipole moment and no significant anisotropic polarisability in this solvent. Both the rotary relaxation times obtained from transient time dependent effects and the amplitudes of the observed birefringence have been analysed in terms of theories for rigid rods, weakly bending rods, worm-like chains and both flexible and stiff random coils. The study indicates that (a) electric birefringence data are sensitive to molecular flexibility and (b) that in this solvent, nitrocellulose of 12% nitrogen content appears to be a stiff, non free draining coil with a dipole moment of the order of a few debye (i.e. $\simeq 10^{-29}$ C m) per monomer unit.

1. INTRODUCTION

Electro-optical techniques are becoming increasingly popular for the study of macromolecules in solution since they lead to the evaluation of both conformational and electrical parameters. The most sensitive method is probably that of electric birefringence. It has been widely used on rigid macromolecules but is now being successfully applied to more flexible molecular structures.[1-4]

If individual solute macromolecules are optically anisotropic, in dilute solution they can be made to orientate under an applied electric field. The overall solution then becomes birefringent. This is generally detected by light transmission through a crossed polariser and analyser assembly. When the field is applied at 45° azimuth to the polariser transmission axis, the observed birefringence (Δn) is given by

$$\Delta n = \frac{\delta\lambda}{2\pi l} \qquad (1)$$

where δ is the optical phase difference between the light components which are polarised parallel and perpendicular to the field direction; l is the length of the electrodes to which the field is applied and λ the wavelength of the incident light. The electric fields are conveniently applied in the form of short duration, single shot, square wave pulses of direct or alternating current. When the field is actuated the molecules start to orientate until they reach the degree of orientation which corresponds to an equilibrium between the electrical torque on the one hand and the disruptive influence of Brownian motion on the other. In the viscous medium, this requires a finite time interval. The Brownian forces restore the system to a random array once the field has switched off. This field-free relaxation is characterised by the equation [5]

$$\frac{\Delta n}{\Delta n_0} = \exp\left(-\frac{t}{\tau}\right) \qquad (2)$$

where Δn_0 is the value of the birefringence at time t=o when the field is switched off. The relaxation time τ can be related to a rotary diffusion constant for a rigid particle by the expression $\tau = 1/6D$.

*Physics Department, Brunel University, Uxbridge, UB8 3PH

(Manuscript received 5 June 1975 and accepted 3 October 1975)

Nitrocellulose has been the subject of many studies by various techniques [6-8] in attempts to better understand the properties of cellulose and its derivatives. Recent electric field light scattering studies [9-11] have shown the relatively large response of suitable solutions to electro-optic effects. The objects of the present work were to study the electrical properties of the polymer and to see to what extent theories and experiments for electric birefringence, although scant at the present time, might be used to indicate molecular flexibility.

2. EXPERIMENTAL AND RESULTS

2.1. Sample

The sample of nitrocellulose used was donated by Mr. R. Stadden of ICI Ltd. The weight average molecular weight ($\bar{M}_W$) was 460,000 as was previously determined by electric field light scattering. The sample was the manufacturer's batch No. 245 stated to have a 12–12.3% nitrogen content, equivalent to 4.6 nitro groups per cellobiose unit. Solutions were prepared by stirring for several hours in spectroscopically pure acetone prior to filtration through Mitex 5 μm Millipore filters. A solution of concentration 7.68 mg.cm^{-3} determined by evaporation to dry weight, was used for the birefringence studies.

2.2 Apparatus

A conventional Kerr-effect optical system was used. The light source was a Coherent Radiation Model 80 HeNe Laser operating at a wavelength of 633 nm. This light was directed through a Kerr Cell which had a PTFE body and held stainless steel electrodes of length 4.98 cm. The electrodes were separated by 0.26 cm. The cell was positioned between a crossed polariser and analyser so that the incident light upon it was polarised at 45° to the direction of the applied field. The transmitted optical signal was received on an EMI type 9816KB photo-multiplier whose output was displayed directly on an oscilloscope and either photographed for analysis [3] at leisure or passed through a transient recorder and on to punched tape ready for direct computational analysis.[12] Pulsed electric fields of durations up to 0.3s, field strengths to a maximum of 10 kV.cm^{-1} and field frequencies from zero to 35 kHz were used. The short nature of the pulses and speed of recording make this method one of the most rapid for the analysis of polymer solutions.

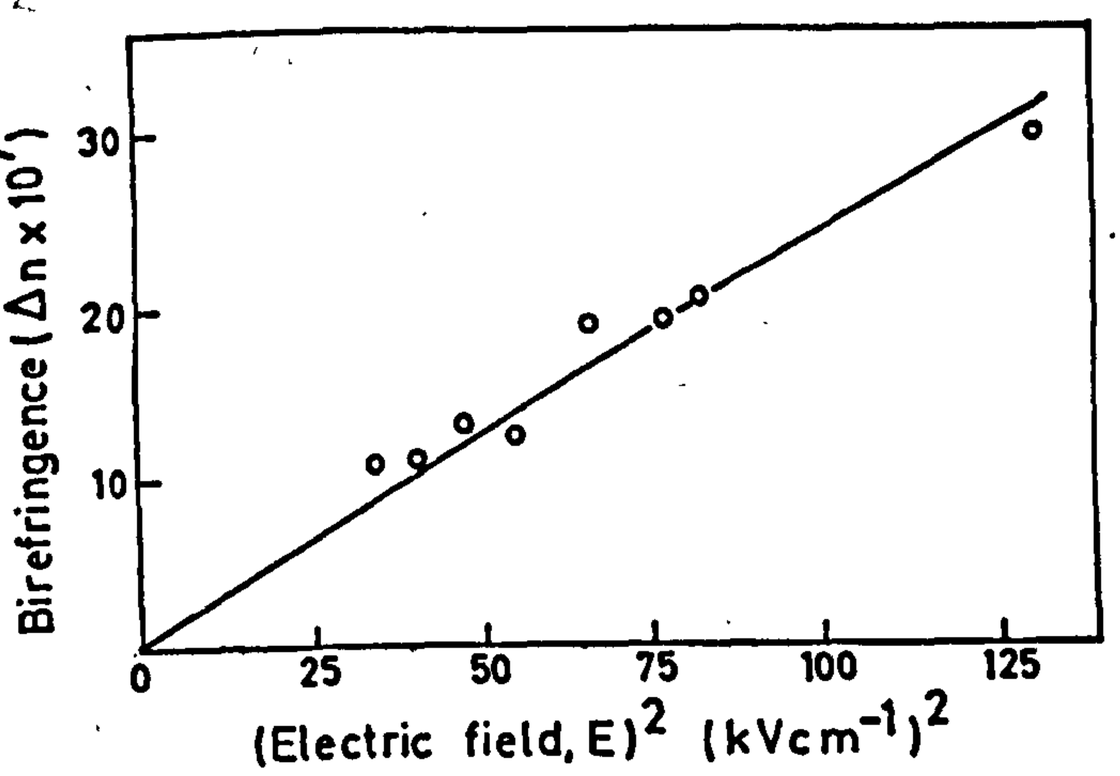

Fig.1 Quadratic dependence of the birefringence on the electric field strength. Solution concentration of 7.7 mg. cm^{-3}, λ = 633 nm.

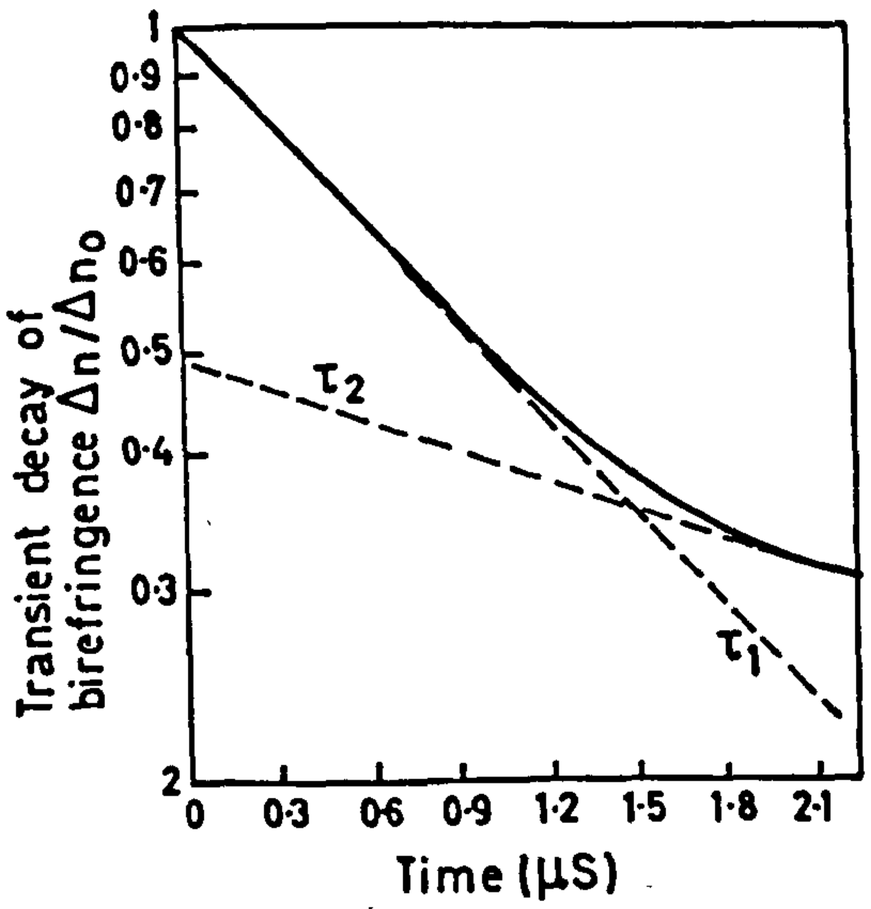

Fig.2 Analysis of the transient decay of the birefringence. Data for c = 7.7 mg. cm^{-3} and E = 8.8 kV. cm^{-1} Tangents correspond to τ_1 = 1.6 μs and τ_2 = 5.0 μs respectively.

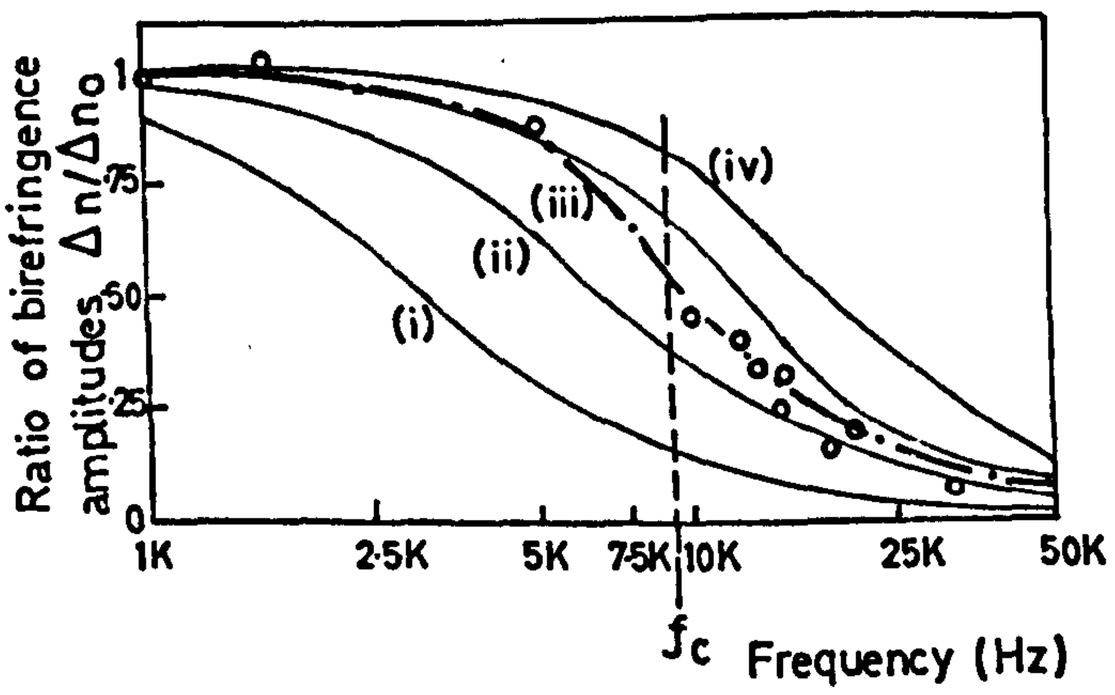

Fig.3 Frequency dispersion of the birefringence amplitudes. Experimental data are for fields of root mean square strength 380 V. cm^{-1}. Theoretical curves are for single values of the rotary diffusion constant, D = 1, 2, 4 and 6x10^4 s^{-1} indicated by (i), (ii), (iii) and (iv) respectively. The critical frequency is indicated by f_c.

As with all photoelectronic methods of signal recording, noise on the signal must be reduced to a minimum. The data were recorded through two sets of measurements. When the amplitudes of the response were of prime interest, a large load resistor (500 kΩ) was used across the photomultiplier. This improved the signal gain and smoothed out much of the noise, but also increased the time constant of the detection system causing it to be comparable to that of the molecular orientation times. For accurate recording of the relaxation times, this resistor was reduced (to 50Ω) so that the time constant of the detector was well below τ.

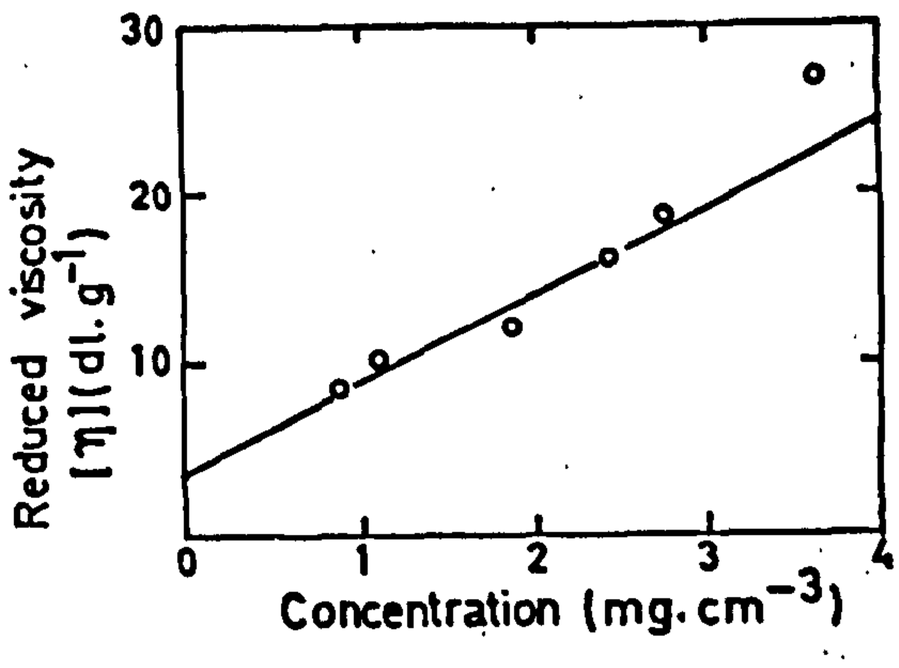

Fig.4 Variation of the reduced viscosity with concentration. T = 25 (± 0.5)°C.

The solutions exhibited electrically induced birefringence which obeyed Kerr's law (Fig.1). The solvent contribution to the observed birefringence was negligible. From Fig.1 a value of the specific Kerr constant

$$K_{sp} = \frac{\Delta n}{cn\,E^2\,\bar{\nu}} = 4.5 \times 10^{-16}\ V^{-2}\ m^2$$

was obtained. Here, c is the concentration in g.cm^{-3}, $\bar{\nu}$ the partial specific volume in cm^3.g^{-1}, n the refractive index of the medium and E the applied field strength in Vm^{-1}. The transient decay curves did not correspond to single component exponential decays (Fig.2) but rather reflected the polydisperse nature of the sample. From Fig.2, analysis of the decay data in terms of two contributions indicates values of τ_1 = 1.6 μs and τ_2 = 5.0 μs, corresponding to 3.3 x 10^4 s^{-1} and 10.4 x 10^4 s^{-1} for the rotary diffusion constants respectively.

From the pulsed alternating frequency field experiments, the amplitudes of the induced birefringence could be analysed as a function of the frequency (Fig.3) in much the same way as is customary in dielectric dispersion measurements. The critical frequency of such a dispersion is taken as the frequency at which the dispersion is at half its total amplitude (Fig.3). Analysing this critical frequency and treating the dispersion as a Debye [13] type leads to a value of τ = 5.7 μs (D = 2.9 x 10^4 s^{-1}). This corresponds closely to the longer time component of the decay curve analysis. Whereas the breadth of the dispersion in Fig.3 may display the polydisperse nature of the sample – as indicated by the theoretical Debye curves for single D values, encompassing the experimental data – the transient may indicate the polydisperse nature of the sample. The transient decay semi-logarithmic plot appears to be the more useful method for quantitative data on the polydispersity. Care should be taken not to treat τ_2 and τ_1 as representative of the largest and smallest particles present.[14]

Finally, in the evaluation of molecular parameters from the electro-optic data, the solution intrinsic viscosity was needed. Rather than rely on the multitude of different values (see below) implied in Mark–Houwinck type equations, $[\eta]$ was measured directly. A value of 3.5 dl g^{-1} was obtained (Fig.4) from measurements using an Ubbelhöde flow tube whose capillary diameter was 580 μm corres-

ponding to flow times from 80s to 500s. The temperature was controlled to 25.0 (± 0.5)°C.

3. DISCUSSION

3.1 Viscosity data

The Mark-Houwinck equation

$$[\eta] = KM^{\alpha} \tag{3}$$

is often used to evaluate M from measured values of $[\eta]$ and tabulations of the constants K and α. There are over 30 different sets of these constants for nitrocellulose in acetone; the majority are listed in the 'Polymer Handbook'.[15] They yield values over the complete range $20,600 < M < 269,000$ for our measured intrinsic viscosity. After restricting our consideration to those sets for which the original authors state the degree of nitration of their samples to be similar to that of the present material, the values quoted by Moore & Edge [16] appeared to be the most reliable, well documented and representative of the majority of determinations. Their equation involves a number average molecular weight and with our experimental value of $[\eta]$ leads to $\bar{M}_N = 160,000$. Light scattering data from this laboratory have already established that $\bar{M}_W = 460,000$ for this sample. A polydispersity of 2.9:1 is indicated for the $\bar{M}_W$: $\bar{M}_N$ ratio, which is not unreasonable.

We wish to make three observations from these viscosity data. Firstly, had we accepted the parameters for K and α suggested by Holtzer *et al.*, [8] a weight average molecular weight of 230,000, half the true value, would have been indicated for polymer samples of the same nitrogen content as ours. Thus their equation does not have the universal applicability that they claim. Secondly, in the earlier electro-optic study on our sample,[11] the measured value of $\bar{M}_W$ was used with the Holtzer *et al.*,[8] data to obtain $[\eta]$ and use it in the analysis of τ values. The viscosity so used was approximately twice the true value as measured in this work: the implications of this are discussed below. Thirdly, the exponent $\alpha = 0.80$, as determined by Moore & Edge [16] is neither that expected for a rigid helix or rod ($\alpha = 2$) nor for a freely flexible random coil ($\alpha = 0.5$). Some form of stiff coil is therefore indicated.

3.2 Relaxation times

Broersma's equation [17] for a rigid rod molecule relates τ to the half rod length (a_1), the axial ratio r, the absolute temperature T and the solvent viscosity η_0, through the expression

$$a_1^3 = \frac{9kT\tau}{4\pi\eta_0}(\ln 2r - A) \tag{4}$$

where k is the Boltzmann constant, $\eta_0 = 0.324$ cP [18] and

$$A = 1.57 - 7\left\{(\ln 2r)^{-1} - 0.28\right\} \tag{5}$$

This equation is not very sensitive to variations in r. Rod half lengths are found by approximating an initial value for a_1, using a value of 0.35 nm for the rod diameter (see below), inserting these data into r (and hence Equation 4) so as to obtain a better estimate for a_1. This procedure is reiterated until consistency is obtained. An initial value of 100 nm was used. Using the fact that

$$M = \frac{VN_A}{\bar{\nu}}$$

where V is the rod volume, N_A the Avogadro number and $\bar{\nu}$ the partial specific volume, which for this system [19] has the value 0.51 $cm^3.g^{-1}$, the largest relaxation time (or smallest D) in the present study is equivalent to $a_1 = 61$ nm and M = 14,000. This is clearly inappropriate and excludes this model for nitrocellulose in acetone. For a free, flexible, polar random coil, Stockmayer & Baur [20] quote an equation from Zimm;[21] namely

$$M = \frac{RT\tau}{f[\eta]\eta_0} \tag{6}$$

where f has the values of 1.21 and 0.85 for a free draining and non-free draining coil respectively. The exponent of the Mark-Houwinck equation suggests a non-free draining coil model as the most appropriate. Values of 5.0 μs and 1.6 μs for τ correspond to molecular weights of 128,000 and 41,000 respectively. Whereas these results are closer to the molecular weights ($\bar{M}_W = 460,000$ and $\bar{M}_N = 160,000$) of this sample than those obtained from the rod-model equation, they are too small to be considered as appropriate. In addition, we wish to point out that the apparent good agreement between experimental values of τ and the coil Equation 6, obtained in a previous electric field scattering study,[11] was based on data obtained from the Holtzer *et al.*[8] viscosity equation. This has been shown, in the previous section, to lead to values of $[\eta]$ and hence of M in Equation 6 which are too large by a factor of 2. It was therefore thought appropriate to study theories for models which are intermediate between the rigid rod and flexible coil.

Hearst [22] and Hearst & Stockmayer [23] have developed equations for two such models. One is the 'Worm-like Chain' (WLC) for which the rotary diffusion constant is given by

$$D = \frac{2kT\rho^2}{\eta_0 qM^2}\left\{0.126\sqrt{\frac{M}{q\rho}} + 0.159\ln\left(\frac{2q}{b}\right) - 0.387 + 0.16\left(\frac{b}{a}\right)\right\} \tag{7}$$

whilst the other is the 'weakly bending rod' (WBR) where

$$D = \frac{kT\rho^3}{\pi\eta_0 M^3}\left\{3\ln\left(\frac{M}{2\rho b}\right) - 4.92 + 4\left(\frac{b}{a}\right) + \frac{M}{4\rho q}\left[4.5\ln\left(\frac{M}{2\rho b}\right) - 10.2 + 4\left(\frac{b}{a}\right)\right]\right\} \tag{8}$$

In these equations,

$$\rho = \frac{M}{L},$$

the mass per unit length with L the extended chain length

of the polymer. For nitrocellulose, $\rho = 5.56 \times 10^{11}$ cm^{-1}.[6] Following Hearst & Stockmayer, the parameters a and b are assumed to be equal to the radius of the polymer backbone. This has been estimated to be 0.175 nm for nitrocellulose.[11] The interesting parameter in these equations is q, the 'persistence length' of the chain. This is defined as the projection of a chain, as if it were infinitely long, on the direction defined by the first bond. It varies between the extremes of zero and infinity for the random coil and rigid rod respectively. Substituting the appropriate experimental data into Equations 7 and 8 gave values as follows.

For the 'worm like chain', q = 10.7 nm or 12 nm depending on whether $\bar{M}_W$ or $\bar{M}_N$ was used in the equations. The 'weakly bending rod' gave values of 1.5 nm and 11.2 nm using $\bar{M}_W$ and $\bar{M}_N$ respectively. It has not been possible to distinguish between these two models for nitrocellulose but it has been noted that such values are always very low. Similar studies on other polysaccharides which are known to be stiff but not rigid coils, give q values of the same order of magnitude.[24,25]

It would appear that the relaxation times obtained from electro-optic experiments yield sensitive criteria which, in this particular study, enable one to reject the extreme assignments of the rigid rod on the one hand and the freely flexible coil on the other to nitrocellulose of this molecular weight in acetone. Furthermore, they confirm the viscosity data and indicate that the conformation of nitrocellulose in acetone is that of a stiff coil.

3.3 Dipole moments

From Fig.3, the birefringence amplitude reduces to zero at high frequency. This indicates that the molecules have a permanent dipole moment which at the lower frequencies tries to follow the field oscillations through a molecular tumbling motion. At sufficiently high frequency, the viscosity of the medium and the molecular size prevent this. There is no significant induced dipolar mechanism as this would give rise to a non zero higher frequency asymptote.

From Courtauld models and the esterification of the cellobiose unit, it would appear that any resultant dipole moment from the nitro groups will act predominantly along the polymer backbone; the net dipole moment being greater the higher the degree of nitration.

Evaluating the magnitude of the molecular dipole moment is more difficult however as a model and its related theory must be assumed. Three representative theories are conveniently available. These are for rigid cylinders or ellipsoids (Peterlin & Stuart [26]), polar, flexible coils (Dows [27] and Peterlin & Stuart [28]) and rigid, 'frozen' coils (Dows [27]) respectively.

Jatkar & Sastry [29] have reported dielectric measurements on nitrocellulose of different degrees of nitration in a variety of solvents. They list monomer dipole moments, that is of the cellobiose unit, of 4.0 and 4.7 debye (i.e. 13.2×10^{-30} and 15.5×10^{-30} C m respectively) for polymer with 11.8% nitrogen content. The availability of these dielectric data provide us with an opportunity to evaluate the suitability of these three models for this system.

For rigid, insulating, ellipsoidal particles, Peterlin & Stuart [26] predicted that

$$K_{sp} = \frac{2\pi\bar{\nu}(g_1 - g_2)\mu^2}{15\, n^2 k^2 T^2} \qquad (9)$$

where n is the refractive index of the solvent (1.362 for acetone [18]) and $(g_1 - g_2)$ is the anisotropy of the optical volume polarisabilities (g) between the major (subscript 1) and minor (subscript 2) molecular axes, for cylindrically symmetric or ellipsoidal molecules.

Tsvetkov [30] gives values of a segmental anisotropy factor $(a_{11} - a_\perp)$ which he relates to $(g_1 - g_2)$ by the expression

$$(g_1 - g_2) = (a_{11} - a_\perp)\frac{N_A}{M_0\bar{\nu}} \qquad (10)$$

where M_0 is the monomer molecular weight. From our experimental Kerr constant, this gives a value of 2.7×10^{-27} C m (815 debye) for the molecular dipole moment. For a linear, extended, or rod molecule, this corresponds to a monomer dipole moment μ_0 of 7.7×10^{-30} C m (2.3 debye) or 2.6×10^{-30} C m (0.8 debye) when $\bar{M}_N$ and $\bar{M}_W$ are used respectively. These are of the same order of magnitude as the dielectric values.

Dows [27] theory for flexible, polar random coils in non polar solvents was based on a dilute gas model. He assumed that the constituent polymer segments (taken herein to be monomer units in the first instance) experience uncorrelated freedom of rotation. His expression for the molar Kerr constant, neglecting contributions from induced dipole moments, is

$$K_m = \frac{4\pi N_A}{405k^2T^2}\,\mu_0^2\left(\frac{M}{M_0}\right)(a_{11} - a_\perp) \qquad (11)$$

where [31]

$$K_m = \frac{2}{27}\left(\frac{\Delta n}{E^2}\right) M\bar{\nu} \qquad (12)$$

Hence, for such a flexible system, the theory predicts an observed birefringence which should be independent of concentration (within the limitations of the 'dilute gas' concept), molecular weight and polydispersity. The equation is essentially the same as that derived by Peterlin & Stuart [28] for flexible polymers. Using 457 for M_0, this leads to a value of 1.5×10^{-28} C m (44 debye) for μ_0. This is far too large for nitrocellulose.

Dows' alternative expression for a 'rigid' coil in which all the dipolar segments were considered as being orientated parallel to each other, has the form

$$K_m = \frac{4\pi N_A}{405k^2T^2}\,\mu_0^2\left(\frac{M}{M_0}\right)^3(a_{11} - a_\perp) \qquad (13)$$

Using $\bar{M}_N$ for M, a value of $\mu_0 = 4 \times 10^{-31}$ C m (0.13 debye) is obtained, whilst $\bar{M}_W$ would give a monomer dipole moment as small as 0.014 debye. Both of these results are far too small when compared with the dielectric data. It would therefore appear that the Peterlin & Stuart theory for rigid ellipsoidal particles leads to values in closest agreement with the dielectric experiments and is best able to account for the observed electric birefringence amplitudes when a number average molecular weight is

used in their equation. A dipole moment per monomer unit of a few debye units is in agreement with previous dielectric and electric field scattering data.[11]

4. CONCLUSION

It is concluded that electric birefringence data indicate that nitrocellulose of high molecular weight and 12% nitrogen content, when dissolved in acetone, behaves as a very stiff, somewhat non free draining, coiled polymer, whose monomer dipole moment is of the order of a few debye units. Transient electric birefringence measurements yield data on both the electric and geometric molecular data and appear to be able to differentiate between rigid and flexible molecular systems. Whereas the experimental method is fast and sensitive, there is a need for theories better able to account for the region of intermediate flexibility between the rigid rod and flexible chain extremes.

5. ACKNOWLEDGEMENTS

Both authors thank the Physics Department of Brunel University for the facilities provided whilst one of us (MI) thanks the Science Research Council for a CAPS award research studentship with Messrs. Unilever Ltd.

References

1 Le Fevre, C. G.; & Le Fevre, R. J. in '*Technique of Organic Chemistry*', 1960, Vol. I part 3, p 2459; Ed. A. Weissberger, Interscience, New York
2 Golub, E. L. *Biopolymers*, 1964, 2, 113
3 Jennings, B. R.; & Brown, B. L. *Eur. Polym. J.* 1971, 7, 805
4 Tsvetkov, V. N.; Rjumtsev, E. L.; Pogodina, N. V.; & Shtennikova, I. N. *Eur. Polym. J.* 1975, 11, 37
5 Benoit, H. *Ann. Phys. (Paris)* 1951, 6, 561
6 Badger, R. M.; & Blaker, R. H. *J. Phys. Colloid Chem.* 1949, 53, 1056
7 Timmell, T. E. *Svensk. Papperstidn* 1954, 57, 777
8 Holtzer, A. M.; Benoit, H.; & Doty, P. *J. Phys. Chem.* 1954, 58, 624
9 Wippler, C. *J. Chim. Phys.* 1956, 53, 346
10 Wallach, M. L.; & Benoit, H. *J. Polym. Sci.* 1966, A2, 4, 491
11 Jennings, B. R.; & Schweitzer, J. F. *Eur. Polym. J.* 1974, 10, 459
12 Rudd, P.; & Jennings, B. R. *Lab. Practice*, 1973, p 535
13 Debye, P. '*Polar Molecules*', 1958, Dover, New York
14 Schweitzer, J. F.; & Jennings, B. R. *Biopolymers*, 1973, 12, 2439
15 '*Polymer Handbook*'; Eds. Brandrup, J.; & Immergut, E. H., 1966, Interscience, New York
16 Moore, W. R.; & Edge, G. D. *J. Polym. Sci.* 1960, 47, 469
17 Broersma, S. *J. chem. Phys.* 1960, 32, 1626
18 Kaye, G. W. C.; & Laby, T. H. '*Tables of Physical and Chemical Constants*' 1911, Longmans, London (1966 Edition)
19 Mosimann, H. *Helv. Chim. Acta.* 1943, 26, 61
20 Stockmayer, W.; & Baur, M. *J. Am. Chem. Soc.* 1964, 86, 3485
21 Zimm, B. H. *J. chem. Phys.* 1956, 24, 269
22 Hearst, J. E. *J. chem. Phys.* 1963, 38, 1062
23 Hearst, J. E.; & Stockmayer, W. H. *J. chem. Phys.* 1962, 37, 1425
24 Foweraker, A. R.; & Jennings, B. R. *Adv. Mol. Relxn. Process* 1974, 6, 241
25 Foweraker, A. R.; & Jennings, B. R. *Polymer*, 1975, 16, 720
26 Peterlin, A.; & Stuart, H. A. '*Hand und Jahrbuch der Chemischen Physik*' 1943, 8 (1B), Eds. A. Eucken, & K. L. Wolf; Akademische Verlaggesellschaft, Leipzig
27 Dows, D. A. *J. chem. Phys.* 1964, 41, 2656
28 Peterlin, A.; & Stuart, H. A. *J. Polym. Sci.* 1950, 5, 551
29 Jatkar, S. K. K.; & Sastry, D. S. *J. Univ. Poona Sci. Technol.* 1953, 4, 55
30 Tsvetkov, V. N. *Soviet Physics Uspekhi.* 1964, 6, 639
31 Buckingham, A. D.; & Pople, J. A. *Proc. Phys. Soc. (London)*, 1955, A68, 905

COMMUNICATION TO THE EDITOR

Electric Birefringence Studies of Cartilage Proteoglycan Aggregation

During the past ten years there has been an increasing interest in the use of electro-optical methods for the characterization of macromolecules in dilute solution. The most prominent effect to be utilized is that of electric birefringence or the Kerr effect.[1] With biopolymer solutions, this has its origin in the orientation of the solute molecules as the solution is subjected to an applied electric field.[2,3] It is advantageous to use pulsed electric fields. Then, the accompanying birefringence induced in the molecular solution becomes transient in nature, with the rates of change an indication of the rates of molecular orientation within the solvent environment. The decay rate of the transient birefringence is usually analyzed to give a direct measure of the molecular rotary relaxation time (τ). As this parameter is approximately a function of the third power of the greatest dimension of compact molecules,[4] it is an extremely sensitive indicator of molecular conformation changes and associations.

In this communication we draw attention to the potential of the method in the field of biophysics and medical physics through some electric birefringence measurements which, we believe, provide rapid confirmation of a model recently proposed[5] for the complexing of cartilage proteoglycans to hyaluronic acid chains.

Cartilage proteoglycans consist of a protein backbone about 400 nm long, with approximately 100 sidechains, each about 40 nm in length, of predominantly chondroitin sulphate [Fig. 1(a)]. Additional shorter side chains of keratan sulphate also occur. The proteoglycans are found in cartilage, mainly as large aggregates involving hyaluronic acid. From gel chromatographic, viscosimetric,[5] and electron microscopic[6] data the aggregate is thought to consist of an extended hyaluronic acid chain to which the proteoglycans are regularly attached (up to one per 10,000 molecular weight unit) in a radial manner [Fig. 1(c)]. Each proteoglycan molecule has a globular protein head which binds to the hyaluronic acid molecule.[7] The exact biological role of the aggregate in unknown. However, it has been noted that in severely fibrillated human cartilage, the amount of aggregate is markedly less than in regular, healthy cartilage connective tissue.[8]

Electric birefringence measurements were made on a sample of pig laryngeal proteoglycan, prepared in the manner outlined elsewhere.[9] Electric fields of up to 600 V cm^{-1} and for pulse durations of up to 160 msec were applied to solutions of proteoglycans in distilled water containing 209 μg uronic acid per ml (approx 0.8 mg ml^{-1} proteoglycan). The optical response of Figure 1(b) indicates the large birefringence of the sample and a rotary relaxation time of 3.6 (±0.3) msec. A hyaluronic acid solution of 20 μg uronic acid per ml (approximately 60 μg ml^{-1} of hyaluronic acid) was added in steps of 0.1 ml to 10 ml of the proteoglycans solution and successive optical transients were recorded. In Figure 1(d) we present a trace for the stable condition after effective saturation with hyaluronic acid.

Two observations are immediately apparent. First, the birefringence amplitude has changed significantly and has possibly changed sign. Although the effect of light scattering has not been allowed for in this initial study, a change in birefringence sign is consistent with the reversal of the optical anisotropy from the proteoglycan to the aggregated molecules. The refractive index associated with the major dimension of the proteoglycan molecule becomes that of the transverse axes of the aggregate. Second, the relaxation time of the complex is of the order of 650 (±30) msec, some 180 times that of the constituent proteoglycan molecules.

Treating the individual proteoglycan molecules as prolate ellipsoids of 40-nm semiminor axes,[5] a rotary relaxation time of 3.6 (±0.3) msec corresponds to a molecular length of 390 (±20) nm from the relevant Perrin[4] equation. This is in reasonable agreement with a previous estimate of 300–400 nm for this material[10] and suggests that the molecule was maximally extended under the conditions of low ionic strength used in this study.

Previous viscosity measurements on the hyaluronic acid sample indicated a viscosity average molecular weight of 670×10^4 from which an approximate extended chain length of 1.6 μm

is estimated. It is interesting to compare this with the length of the proteoglycan–hyaluronic acid complex. If the model of Figure 1(c) is realistic, then the aggregate can also be represented by a prolate ellipsoid but with semiminor axes equal to 380 nm, the length of an individual proteoglycan molecule. Inserting this in the Perrin equation with $\tau = 650$ msec leads to an aggregate length of 1.8 (±0.1) μm. This is in remarkably close agreement with the estimated length of the extended hyaluronic acid chain which forms the aggregate core and suggests that the aggregate is maximally extended in solution.

It would appear that transient electric birefringence provides a rapid means of sizing macromolecules in solution. Experimental data on proteoglycans both in isolation and as a complex aggregate with hyaluronic acid are consistent with previous determinations using more laborious methods for both the nature and the size of the aggregated and individual molecules. Extension of the method to the study of other associating systems of biomedical interest should prove beneficial.

One of us (M.I.) thanks the Science Research Council for a research studentship.

References

1. Kerr, J. (1875) *Philos. Mag.* **50**, 337–348.
2. Fredericq, E. & Houssier, C. (1973) *Electric Dichroism and Electric Birefringence*, Oxford University, London.
3. Benoit, H. (1951) *Ann. Phys. (Paris)* **6**, 561–609.
4. Perrin, F. J. (1934) *J. Phys. Radium (Paris)* **5**, 497–511.
5. Hardingham, T. E. & Muir, H. (1972) *Biochim. Biophys. Acta.* **279**, 401–405.
6. Rosenberg, L., Hellmann, W. & Kleinschmidt, A. K. (1975) *J. Biol. Chem.* **250**, 1877–1883.
7. Heinegård, D. & Hascall, V. C. (1974) *J. Biol. Chem.* **249**, 4250–4256.
8. McDevitt, C. A. & Muir, H. (1975) *Ann. Rheum. Dis.* **34**, Suppl. 2, 137–138.
9. Hardingham, T. E. & Muir, H. (1974) *Biochem. J.* **139**, 565–581.
10. Rosenberg, L., Hellman W. & Kleinschmidt, A. K. (1970) *J. Biol. Chem.* **245**, 4123–4130.

A. R. FOWERAKER
M. ISLES
B. R. JENNINGS

Physics Department
Brunel University
Uxbridge, Middlesex, U.K.

T. E. HARDINGHAM
H. MUIR

Kennedy Institute of Rheumatology
Bute Gardens
Hammersmith, London, U.K.

Fig. 1. Proteoglycan and its aggregation with hyaluronic acid. Frames a) and c) are schematic diagrams of the structure of a proteoglycan molecule and of the aggregate, respectively. Frames b) and d) are the transient electric birefringence responses for each system. In both cases the applied field was of 360 V cm^{-1} amplitude. Note the difference in time scales.